UNIVERSIDADE FEDERAL DE MINAS GERAIS
Escola de Engenharia
Programa de Pós-Graduação em Saneamento, Meio Ambiente e Recursos Hídricos

Thiago Bressani Ribeiro

SPONGE-BED TRICKLING FILTERS FOR NITROGEN REMOVAL FROM ANAEROBICALLY TREATED SEWAGE: MECHANISTIC INSIGHTS AND PRACTICAL EXPERIENCES

Belo Horizonte
2022

Thiago Bressani Ribeiro

SPONGE-BED TRICKLING FILTERS FOR NITROGEN REMOVAL FROM ANAEROBICALLY TREATED SEWAGE: MECHANISTIC INSIGHTS AND PRACTICAL EXPERIENCES

Tese apresentada ao Programa de Pós-graduação em Saneamento, Meio Ambiente e Recursos Hídricos da Universidade Federal de Minas Gerais, como requisito parcial à obtenção da dupla titulação de Doutor em Saneamento, Meio Ambiente e Recursos Hídricos, e Doutor em Engenharia de Bioprocessos: Ciências Ambientais e Tecnologia.

Área de concentração: Saneamento

Linha de pesquisa: Tratamento de Águas Residuárias

Orientador: Carlos Augusto de Lemos Chernicharo

Coorientador: Eveline Irma Paula Volcke (Ghent University)

Belo Horizonte

2022

Ribeiro, Thiago Bressani.
R484s Sponge-bed trickling filters for nitrogen removal from anaerobically treated sewage [recurso eletrônico] : mechanistic insights and practical experiences / Thiago Bressani Ribeiro. – 2022.
1 recurso online (214 f.: il., color.) : pdf.

Orientador: Carlos Augusto de Lemos Chernicharo.
Coorientadora: Eveline Irma Paula Volcke.

Tese (doutorado) - Universidade Federal de Minas Gerais, Escola de Engenharia.

Bibliografia: f. 200-214.
Exigências do sistema: Adobe Acrobat Reader.

1. Engenharia sanitária - Teses. 2. Saneamento - Teses. 3. Reator UASB - Teses. 4. Nitrogênio - Teses. 5. Modelagem matemática - Teses. 6. Esgotos - Tratamento - Teses. 7. Digestão anaeróbia - Teses. I. Chernicharo, Carlos Augusto de Lemos. II. Volcke, Eveline Irma Paula. III. Universidade Federal de Minas Gerais. Escola de Engenharia. IV. Título.
CDU: 628(043)

Ficha catalográfica elaborada pela Bibliotecária Roseli Alves de Oliveira CRB/6 2121
Biblioteca Prof. Mário Werneck, Escola de Engenharia da UFMG

UNIVERSIDADE FEDERAL DE MINAS GERAIS
[ESCOLA DE ENGENHARIA]
COLEGIADO DO CURSO DE GRADUAÇÃO / PÓS-GRADUAÇÃO EM [SANEAMENTO, MEIO AMBIENTE E RECURSOS HÍDRICOS]

FOLHA DE APROVAÇÃO

["Sponge-bed trickling filters for nitrogen removal from anaerobically treated sewage: mechanistic insights and practical experiences"]

[Thiago Bressani Ribeiro]

Tese de Doutorado] defendida e aprovada, no dia **[** 25 de janeiro de 2022**]**, pela Banca Examinadora designada pelo [Colegiado do Programa de Pós-Graduação **EM SANEAMENTO, MEIO AMBIENTE E RECURSOS HÍDRICOS**] da Universidade Federal de Minas Gerais constituída pelos seguintes professores:

[Profa. Dra. Kimberly Solon**] - Membro Externo]**

[Ghent University]

[Profa. Dra. Jules van Lier**] - Membro Externo]**

[TU Delf]

[Prof. Dr. Siegfried Vlaeminck**] - Membro Externo]**

[University of Antwerp]

[Prof. Dr. Wu Di **] - Membro Externo]**

[Ghent University]

[Prof. Dr. Stijn Van Hulle**] - Membro Externo]**

[Ghent University]

[Prof. Dr. Korneel Rabaey**] - Membro Externo]**

[Ghent University]

[Prof. Dr. Marcos von Sperling**] - Membro Interno]**

[UFMG]

[Profa. Dra. Eveline I. P. Volcke **- Co-tutela]**

[Ghent University]

[Prof. Dr. Carlos Augusto de Lemos Chernicharo **- Orientador]**

[UFMG]

APROVADA PELO COLEGIADO DO PPG SMARH

Sonaly Cristina Rezende Borges de Lima - Coordenadora

Belo Horizonte, 25 de janeiro de 2022.

Documento assinado eletronicamente por **Kimberly Tumlos Solon**, **Usuária Externa**, em 30/06/2022, às 05:17, conforme horário oficial de Brasília, com fundamento no art. 5º do Decreto nº 10.543, de 13 de novembro de 2020.

Documento assinado eletronicamente por **Eveline Irma Volcke**, **Usuária Externa**, em 03/08/2022, às 03:31, conforme horário oficial de Brasília, com fundamento no art. 5º do Decreto nº 10.543, de 13 de novembro de 2020.

Documento assinado eletronicamente por **Carlos Augusto de Lemos Chernicharo**, **Professor do Magistério Superior**, em 10/08/2022, às 15:14, conforme horário oficial de Brasília, com fundamento no art. 5º do Decreto nº 10.543, de 13 de novembro de 2020.

Documento assinado eletronicamente por **Marcos Von Sperling**, **Professor do Magistério Superior**, em 24/08/2022, às 15:08, conforme horário oficial de Brasília, com fundamento no art. 5º do Decreto nº 10.543, de 13 de novembro de 2020.

Documento assinado eletronicamente por **Julius Bernardus Van Lier**, **Usuário Externo**, em 30/08/2022, às 08:29, conforme horário oficial de Brasília, com fundamento no art. 5º do Decreto nº 10.543, de 13 de novembro de 2020.

Documento assinado eletronicamente por **Stijn Van Hulle**, **Usuário Externo**, em 30/08/2022, às 08:37, conforme horário oficial de Brasília, com fundamento no art. 5º do Decreto nº 10.543, de 13 de novembro de 2020.

Documento assinado eletronicamente por **Korneel Pieter Rabaey**, **Usuário Externo**, em 30/08/2022, às 11:23, conforme horário oficial de Brasília, com fundamento no art. 5º do Decreto nº 10.543, de 13 de novembro de 2020.

Documento assinado eletronicamente por **Siegfried Elias Vlaeminck**, **Usuário Externo**, em 15/09/2022, às 05:22, conforme horário oficial de Brasília, com fundamento no art. 5º do Decreto nº 10.543, de 13 de novembro de 2020.

Documento assinado eletronicamente por **Di Wu**, **Usuário Externo**, em 17/09/2022, às 22:16, conforme horário oficial de Brasília, com fundamento no art. 5º do Decreto nº 10.543, de 13 de novembro de 2020.

A autenticidade deste documento pode ser conferida no site https://sei.ufmg.br/sei/controlador_externo.php?acao=documento_conferir&id_orgao_acesso_externo=0, informando o código verificador **1209432** e o código CRC **2DD9E627**.

Referência: Processo nº 23072.204025/2022-56 SEI nº 1209432

No roots, no fruits.

Gatze Lettinga

ACKNOWLEDGEMENTS

There is a famous speech called “I have a dream”. Maybe the most appropriate sentence to phrase what this PhD represented to me, which now comes true. I vividly remember the moment I got an email from prof. Carlos saying that prof. Eveline had contacted him concerning the BOF call opening. It was great news, even better on the day the result of the scholarship application was announced.

Being enrolled in the BioCo research group was a life-changing, eye-opening experience. My deepest gratitude to prof. Eveline, who has a sharp ability to bring research to a high level. Thank you, prof. Eveline, for the faith you had in me (back in 2016), and the availability for the PhD guidance since 2017. I have learned a lot from your goal-oriented and critical view. Several times I find myself reflecting on “Why am I doing this?”, “What is the goal of that?” or even saying to someone that little Saint-Exupéry quote “a goal without a plan is just a wish”. Besides, I also had the opportunity to keep working in the group of prof. Carlos, to whom I heartfully thank for all the support since my master’s. This invaluable long-term partnership helped me coin a critical view on the sanitation needs for developing countries.

The vast expertise of jury members on different topics led to broad questions, which were deeply appreciated, ranging from modelling-specific aspects and experimental-related issues, to reflections on full-scale implementation and operation. The quality of this thesis has been improved following those comments.

Navigating the PhD research paths demands resilience. For this, I counted so much on the strength of a wonderful partner, Marina. We shared every single moment of this journey, and without her support, this would not have been possible. In the past years, we have been living in a pendular way between Belgium and Brazil (moving from six houses in total), and she always brought lovely daily ‘recharging’ moments that helped me bounce back to work.

I had the support of many people in Brazil and Belgium. Some of them were cornerstones in this PhD endeavour. When I returned to Belgium after the second research stay in Brazil, Lariza (a friend and PhD colleague from UFMG), carried out the whole sampling and lab work, which was a tremendous effort considering two

demo-scale reactors operated far away from the university campus. Gabriel Tadeu was also my eyes and hands on the field when I was not there. Besides that, a friend who is always available for a good talk. I also had invaluable lab support from Ana and Regiane, and thanks to Luis, Guilherme, and Fernanda for their help during the system start-up. I had the privilege to be in touch with brilliant people from the BioCo research group, like Annelies, Amr, Chris, David, Farhang, Janis, Kimberly, Laurance, Luis, Mingsheng, Paula, Quan, Stijn, Tinne, Xinyu, and the colleagues from the TCCB group. I am glad to have worked with Griet, who was essential for modelling the fate of CH_4 and H_2S. I thank Lut, Aïsja, Bjorn and Ann for all the help with administrative issues.

The list of people to whom I owe a lot goes beyond. Lucas Chamhum, Lucas Vassalle, and Lívia for always being willing to help (and sharing endless online meetings). Ayana, Bel, Rafael, Morandi, for the nice work at the INCT. Paulo Almeida, who has introduced me to sponge filters back in 2013, and I have the pleasure to keep working in close collaboration. Cocó (Ricardo), for the good friendship and essential help with the experimental apparatus. Natália, for the fieldwork on tracer tests. Luiz (Art Técnica) and Faria (Fibrasa) for their support in building the SBTF.

I thank Ghent University for the BOF funding, which made possible this PhD. I also thank the funding from the Brazilian institutions, such as the CNPq and FAPEMIG for the scholarship and financing of the research via the National Institute of Science and Technology (INCT) in Sustainable Sewage Treatment Plants.

Coming back to the day the BOF call result was announced, I remember my parents prepared a surprise dinner to celebrate. They always gave me full support to pursue my studies, besides the always encouraging words of my young brother Gabriel, whom I miss a lot.

Writing this, I realize how lucky I am to have all these people connected with me in different ways. My most sincere gratitude.

May all beings everywhere be happy and free, and may the thoughts, words, and actions of my own life contribute in some way to that happiness and to that freedom for all

Thiago 17 January 2022 in Ghent

RESUMO

O tratamento anaeróbio de esgoto cumpre um papel importante no controle da poluição hídrica na América Latina. Não obstante, existem limitações intrínsecas quanto à remoção de compostos nitrogenados. Em que pese a ampla utilização de filtros biológicos percoladores (FBP) como alternativa de pós-tratamento, o fato de serem tipicamente preenchidos com pedra britada restringe a remoção de nitrogênio. Como solução, tem-se pesquisado o meio suporte baseado em espuma de poliuretano, designando-se os FBP como *sponge-bed trickling filters* (SBTFs). Esta tese de doutorado se concentra no uso de SBTFs para o pós-tratamento de efluentes anaeróbios. O objetivo global é aprimorar a remoção de nitrogênio, considerando a presença de carbono orgânico residual, e integrado com a remoção de gases dissolvidos presentes no efluente anaeróbio. O Capítulo 1 apresenta uma introdução geral, sumarizando os desafios de pesquisa. No Capítulo 2 faz-se uma revisão crítica da literatura sobre o projeto e a operação de filtros biológicos percoladores pós-reatores UASB, provendo subsídios para a construção e operação de um SBTF em escala de demonstração, no âmbito do Capítulo 3. Após 300 dias de monitoramento notou-se o impacto à nitrificação pela falta de carbono inorgânico, a qual afetou em menor escala as bactérias oxidadoras de nitrito. Um modelo matemático foi desenvolvido e validado, demonstrando a necessidade de inserção de bicarbonato como variável para descrever a limitação de carbono inorgânico. No Capítulo 4, o referido modelo foi empregado para avaliar mecanisticamente, a longo prazo, os principais aspectos que governam as conversões de nitrogênio em SBTFs. Em síntese, os resultados mostram que a interação entre coeficientes cinéticos e de transferência de massa, em consonância com a área superficial específica da espuma, influencia a concentração ótima de oxigênio para sustentar a atividade das bactérias oxidadoras de amônia sem comprometer o crescimento de bactérias anammox. No Capítulo 5, um estudo comparativo experimental de longo prazo foi realizado em dois SBTFs operando em paralelo pós-reator UASB, tratando esgoto real. A recirculação do efluente para o compartimento superior do SBTF mostrou um rápido aumento na eficiência de remoção de nitrogênio. Estratégias de controle de ventilação não foram eficazes em reprimir a atividade de bactérias oxidadoras de nitrito, inviabilizando o crescimento de bactérias anammox. No Capítulo 6, o modelo desenvolvido foi expandido para agregar os processos de dessorção e conversão biológica do metano e H_2S dissolvidos no efluente anaeróbio. As simulações demonstraram a relevância da competição por oxigênio entre os microrganismos oxidadores de amônia, metano e H_2S. Ademais, a ocorrência de processos de desnitrificação via metano ou H_2S não se sustentam. A tese se encerra no Capítulo 7, destacando as principais lições aprendidas: *i)* a nitrificação plena em efluentes anaeróbios é impactada pela limitação de carbono inorgânico; *ii)* a recirculação do efluente estimula a desnitrificação heterotrófica, todavia o processo é passível de otimização; *iii)* rotas alternativas de remoção de nitrogênio baseadas em nitrificação parcial e/ou anammox são impraticáveis em SBTFs sob ventilação natural; e *iv)* a presença de metano e H_2S dissolvidos no efluente anaeróbio impacta a remoção de nitrogênio, devendo serem preferencialmente removidos a montante do SBTF.

Palavras-chave: Filtros biológicos percoladores. Pós-tratamento de efluentes anaeróbios. Reatores UASB. Nitrogênio. Modelagem matemática.

ABSTRACT

Anaerobic sewage treatment plays an important role in controlling water pollution in Latin America. However, there are intrinsic limitations regarding the removal of nitrogenous compounds. Although the wide use of trickling filters (TF) as a post-treatment alternative, the fact that they are typically filled with crushed stones restricts nitrogen removal. As a solution, support media based on polyurethane sponge has been researched, the so-named *sponge-bed trickling filters* (SBTFs). This doctoral thesis focuses on the use of SBTFs for the post-treatment of anaerobic effluents. The overall goal is to establish highly efficient nitrogen removal, dealing with residual organic carbon and integrated with the abatement of dissolved gases in the anaerobic effluent. Chapter 1 presents a general introduction, summarizing the research challenges. In Chapter 2, a literature review is performed on the design and operation of trickling filters post-UASB reactors, providing support for the construction and operation of a demonstration-scale SBTF, within the scope of Chapter 3. After 300 days monitoring, the impact on nitrification due to the lack of inorganic carbon was noted, which affected nitrite-oxidizing bacteria to a lesser extent. A mathematical model was developed and validated, demonstrating the need to include bicarbonate as a state variable to describe inorganic carbon limitation. In Chapter 4, the model was used to mechanistically assess, in the long term, the main aspects that govern nitrogen conversions in SBTFs. In summary, the results show that the interaction between kinetic and mass transfer coefficients, alongside the sponge specific surface area, influences the optimal oxygen concentration to sustain the activity of ammonia-oxidizing bacteria without compromising the growth of anammox bacteria. In Chapter 5, a long-term experimental comparative study was conducted on two SBTFs operating in parallel post-UASB reactor, treating real sewage. Effluent recirculation to the upper compartment of the SBTF showed a sharp increase in nitrogen removal efficiency. Ventilation control strategies were not effective in repressing the activity of nitrite-oxidizing bacteria, preventing the growth of anammox bacteria. In Chapter 6, the developed model was expanded to include the desorption and biological conversion processes of methane and H_2S dissolved in the anaerobic effluent. The simulations demonstrated the relevance of competition for oxygen between ammonia-, methane- and H_2S-oxidizing microorganisms. Furthermore, the occurrence of denitrification processes via methane or H_2S is not feasible. The thesis ends in Chapter 7, highlighting the main lessons learned: *i)* full ammonium conversion in anaerobically treated sewage is hampered by inorganic carbon limitation; *ii)* effluent recirculation stimulates heterotrophic denitrification. However, achieving higher total nitrogen removal efficiencies requires process optimization; *iii)* alternative nitrogen removal pathways based on partial ammonium conversion and/or anammox are hard to realize in naturally ventilated SBTFs; and *iv)* the presence of methane and H2S in anaerobic effluents negatively affects nitrogen removal; these compounds should therefore preferentially be removed upfront.

Keywords: Trickling filters. Post-treatment of anaerobic effluents. UASB reactors. Nitrogen. Mathematical modelling.

NOTATION INDEX

Abbreviation	Description
ANAMMOX	Anaerobic Ammonium Oxidation
AOB	Ammonia-Oxidizing Bacteria
AN	Anammox Bacteria
ASM	Activated Sludge Model
BNR	Biological Nitrogen Removal
BOD	Biochemical Oxygen Demand
COD	Chemical Oxygen Demand
DAMO-A	Denitrifying Anaerobic Methane Oxidation-Archaea
DAMO-B	Denitrifying Anaerobic Methane Oxidation-bacteria
DO	Dissolved Oxygen
FNA	Free Nitrous Acid
FR	Sponge Filling Ratio
HET	Heterotrophs
HLR	Hydraulic Loading Rate *(same as Surface Hydraulic Loading Rate - HLRs)*
HRT	Hydraulic Retention Time
MOB	Methane Oxidizing Bacteria
NLR	Nitrogen Loading Rate
NOB	Nitrite-Oxidizing Bacteria
OLR	Volumetric Organic Loading Rate
PN/A	Partial Nitritation-Anammox
SBDN	Sulfide Based Denitrification
SBR	Sequencing Batch Reactor
SBTF	Sponge-bed Trickling Filter
SEM	Scanning Electron Microscopy
SOB	Sulfide Oxidizing Bacteria
SRT	Solids Retention Time
Sset	Secondary settler
TF	Trickling Filter
TN	Total Nitrogen
TSS	Total Suspended Solid
STP	Sewage Treatment Plant
UASB	Upflow Anaerobic Sludge Blanket

Symbols	Characterization	Unit
a_s	Specific surface area of the sponge	$m^2\ m^{-3}$
b	Decay rate	d^{-1}
COD/N	The ratio of COD to nitrogen	g COD g N^{-1}
D_{NH4}	Diffusion coefficient of NH_4^+	$m^2\ d^{-1}$
D_{NO2}	Diffusion coefficient of NO_2^-	$m^2\ d^{-1}$
D_{NO3}	Diffusion coefficient of NO_3^-	$m^2\ d^{-1}$
D_{O2}	Diffusion coefficient of O_2	$m^2\ d^{-1}$
D_{CH4}	Diffusion coefficient of CH_4	$m^2\ d^{-1}$
D_{H2S}	Diffusion coefficient of H_2S	$m^2\ d^{-1}$
D_S	Diffusion coefficient of COD	$m^2\ d^{-1}$
ε_{Xi}	Volume fraction of particulate component X_i	-
f_{XI}	Inert fraction in biomass	g COD g COD^{-1}
i_{NXB}	Nitrogen fraction in biomass	g N g COD^{-1}
i_{NXI}	Nitrogen fraction in particulate inert components	g N g COD^{-1}
k_La	Volumetric oxygen transfer coefficient	d^{-1}
K_{NH}	Affinity constant for ammonium	g NH_4^+-N m^{-3}
K_{NO2}	Affinity constant for nitrite	g NO_2^--N m^{-3}
K_{NO3}	Affinity constant for nitrate	g NO_3^--N m^{-3}
K_{O2}	Affinity constant for oxygen	g O_2 m^{-3}
K_S	Affinity constant for COD	g COD m^{-3}
K_{IC}	Affinity constant for inorganic carbon	g $CaCO_3$ m^{-3}
L_{Bi}	Biofilm-liquid interface	-
L_L	External mass transfer boundary layer thickness	µm
L_F	Biofilm thickness	µm
μ_{max}	Maximum growth rate	d^{-1}
η	Anoxic reduction factor	-
Q_{in}	Inflow rate	$m^3\ d^{-1}$
r_i	Conversion rate of component i	g m^{-3} d^{-1}
S_{ini}	Initial concentration of soluble component i	g m^{-3}
S_{N2}	N_2 concentration	g N m^{-3}
S_{NH}	Ammonium concentration	g N m^{-3}
S_{ND}	Soluble biodegradable organic nitrogen concentration	g N m^{-3}
S_{NO2}	Nitrite concentration	g N m^{-3}
S_{NO3}	Nitrate concentration	g N m^{-3}
S_{O2}	Oxygen concentration (DO)	g O_2 m^{-3}
S_S	Soluble biodegradable organic carbon concentration	g COD m^{-3}
S_{IC}	Inorganic carbon concentration	g $CaCO_3$ m^{-3}
X_i	Particulate component i	g COD m^{-3}
Y	Yield coefficient	g COD g N^{-1} or COD^{-1}

Table of Contents

Chapter 1

General introduction

This chapter comprises the context, research challenges, and outline of this doctoral research work. The sanitation framework in Latin America and the crucial role of mainstream anaerobic sewage treatment in the region, notably in Brazil, is introduced first. Next, the need for nitrogen removal from anaerobic effluents is discussed, followed by critical aspects of sponge-bed trickling filters. A number of research challenges are identified. Finally, an outline of the chapters of this thesis is provided, along with the research objectives.

1.1 Sewage treatment in Latin America and the role of the anaerobic technology

Water resources in Latin America are historically undervalued. River pollution has worsened since the 1990s, mainly attributed to the discharge of untreated sewage (UNEP, 2016). The average wastewater treatment percentage in the region remains below 40% (United Nations, 2021). While the primary challenges of sanitation infrastructure and environmental protection are overcome in developed countries, Latin America struggles to achieve general sewage collection and treatment. Historical financial constraints and the lack of skilled personnel for process operation hamper further implementation of sewage treatment facilities. In most cases, political instabilities outweigh sound technical approaches. Therefore, whereas the developed countries further restrict discharge standards and focus on controlling emerging pollutants, the basic control of organic matter release is still a priority in Latin America.

A stepwise approach for this region is needed to tackle the sanitation hurdle. This means first improving organic carbon removal, followed by nutrients (nitrogen and phosphorus) removal, as was the case for European countries and the USA during the second half of the 20th century (Chen et al., 2020). Moreover, technologies that meet the historical financial and operational constraints should be prioritized. This approach would ensure minimum safe sewage treatment for all rather than providing higher sanitation standards for fewer, thus tackling the United Nations Sustainable Development Goal 6 (SDG 6 – ‘clean water and sanitation for all’).

Substantial progress has been made in some Latin American countries (e.g., Brazil) considering anaerobic processes for organic carbon removal. The upflow anaerobic sludge blanket (UASB) reactors were introduced in the 1980s for sewage treatment when projects were initiated by several national research groups and engineers working in the sector. Prompted by investments in research and development and favourable climate conditions, Brazil, Colombia, and Mexico became leaders in the field. Furthermore, the Brazilian Research Programme on Basic Sanitation from 1997 to 2007 contributed to the consolidation and dissemination of the anaerobic technology for mainstream (direct) sewage treatment in the country (Chernicharo et al., 2019). UASB reactors are currently the most applied in terms of the number of treatment plants in operation (Figure 1.1) (ANA, 2020). Worth mentioning that a pre-

concentration step is not required prior to the UASB reactor, as it is suggested for carbon redirection schemes derived from conventional activated sludge (Jia et al., 2020). Therefore, biogas can be directly recovered from the mainstream anaerobic treatment rather than from a sidestream sludge digester.

In general, most sewage treatment plants (STPs) implemented in Latin America still only aim to remove organic carbon. In other words, those facilities were not designed to incorporate the removal of ammonium or total nitrogen. Therefore, this has been causing systematic problems such as algal blooms in sensitive (lentic) water bodies and even in river streams (lotic environments).

This doctoral research work relies on the concept of organic carbon removal through anaerobic treatment (i.e., UASB reactors) as the core of the sanitation infrastructure in Latin America. The goal is to expand the current sanitation concept by focusing on a post-treatment stage for nitrogen removal from anaerobic effluents.

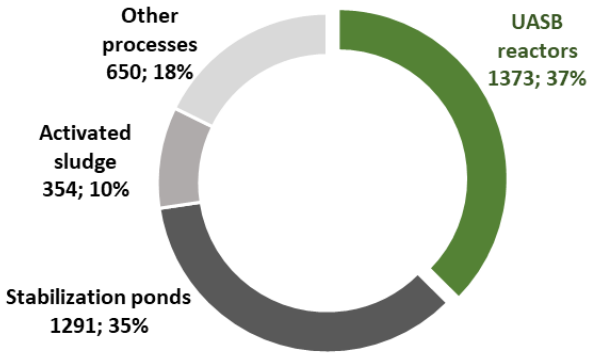

Figure 1.1 Sewage treatment technologies applied in Brazil. *The number of facilities currently in operation and prevalence (%) is presented.* (source: ANA, 2020)

1.2 Nitrogen removal from anaerobic effluents

In order to control environmental pollution, most regulations in Europe comprise discharge limits for total nitrogen instead of merely specifying standards for ammonium (Preisner et al., 2020). The same applies to the USA and Canada (e.g., The Great Lakes Water Quality Agreement). The European Urban Wastewater Treatment Directive (91/271/EEC) imposes effluent total nitrogen limits for areas sensitive to eutrophication based on the population equivalent (p.e.) of the treatment facility, i.e., 15 mg N L^{-1} (10,000 – 100,000 p.e.) and 10 mg N L^{-1} (> 100 000 p.e.). An exception is

made for Germany, where ammonium concentrations should be below 10 mg NH_4^+-N L^{-1} for treatment plants larger than 5,000 p.e. Total nitrogen concentrations should be below 18 mg N L^{-1} (> 100,000 p.e.) and 13 mg N L^{-1} (< 100,000 p.e.), regardless of whether the areas are sensitive or not. As for Brazil, generally, there are neither discharge limits for ammonium nor total nitrogen from sewage treatment plants, with few exceptions among Brazilian states (Morais and Santos, 2019). Nevertheless, the treated effluent must comply with maximum total nitrogen concentrations specified for the receiving water body, which can differ according to the national classification of water streams based on their intended uses. Usually, nitrite and nitrate concentrations should be lower than 1 and 10 mg N L^{-1}, respectively. Besides, ammonium concentrations are pH-dependent; however, values should be below 3.7 mg N L^{-1} for water streams intended for, e.g., drinking supply after treatment and crops irrigation. Furthermore, in case nitrogen is a rate-limiting compound for eutrophication, maximum concentrations in the water stream should be lower than 1.27 and 2.18 mg N L^{-1} for lentic and lotic aquatic bodies, respectively. The apparent dichotomy between the absence of discharge parameters, and the need to fit the effluent according to the specified water quality of the receiving body, may hamper environmental control. Therefore, there has been an increasing push from Brazilian environmental agencies to at least set discharge limits for ammonium, if not for total nitrogen.

The performance of currently established full-scale post-treatment processes for anaerobic effluents is limited in terms of ammonium removal, which is typically up to 70% (Figure 1.2a). However, the total nitrogen removal efficiency is still significantly low in most cases, around 30% (Figure 1.2b). The nitrification rates in post-treatment systems for anaerobic effluent are lower compared with systems treating raw or settled sewage, which has been hypothesized to be due to toxicity by hydrogen sulfide (H_2S) dissolved in the anaerobic effluent (Azevedo et al., 2021).

As for total nitrogen removal, an activated sludge process performs significantly better (> 70% TN removal efficiency) than the other post-treatment technologies, provided that a by-pass line around the UASB reactor is implemented (von Sperling et al., 2019), supplying raw sewage directly to the anoxic zones of the activated sludge in order to provide sufficient organic carbon for heterotrophic denitrification. Even though the activated sludge process for the treatment of anaerobic effluent is characterized by

smaller aeration tanks and more straightforward sludge handling than for direct sewage treatment, and even if biogas is recovered for electricity generation in the anaerobic step, the overall flowsheet (UASB + activated sludge) remains energy-intensive. Moreover, the latter also requires skilled personnel for operation, which is challenging for developing countries. As an alternative post-treatment technology for UASB reactors, rock-bed trickling filters achieve low ammonium and total nitrogen removal efficiency (see Figures 1.2a,b) but have a remarkable operational simplicity and entail much lower operating costs, even though less operational flexibility. The ammonium removal efficiency of trickling filters can be improved by replacing rock-based support material by sponges, as was first proposed by Agrawal et al. (1997); they are then termed sponge-bed trickling filters (SBTFs) (see section 1.3). The SBTFs have helped overcome the nitrification limitation of conventional trickling filters, yet total nitrogen removal is still an issue.

The prevalence of UASB reactors in Brazil (i.e., 37% out of the total number of STPs) poses challenges for realizing the desired total nitrogen removal standards for the country, considering the current level of maturity of post-treatment technologies. Nevertheless, the concept of an anaerobic-based sewage treatment plant should not be abandoned prior to its full possibilities have been explored. Before considering the possibility of adopting novel, well-developed sewage treatment processes currently in place in Europe and the USA (e.g., aerobic granular sludge), comprehensive efforts should be realized towards optimizing the anaerobic-based treatment schemes in place by optimizing heterotrophic denitrification or even establishing alternative metabolic pathways for nitrogen removal (see section 1.4.4). Otherwise, the vital sanitation progresses achieved so far could be jeopardized, as well as an unnecessary burden imposed for the new generation of sewage treatment plants in Brazil, acknowledging the historical financial and operational constraints.

Given the importance of preserving the anaerobic-based treatment schemes for sewage treatment in Brazil and the distinct advantages and optimization potential of sponge-bed trickling filters, the latter technology was put forward as the central research topic of this doctoral research work.

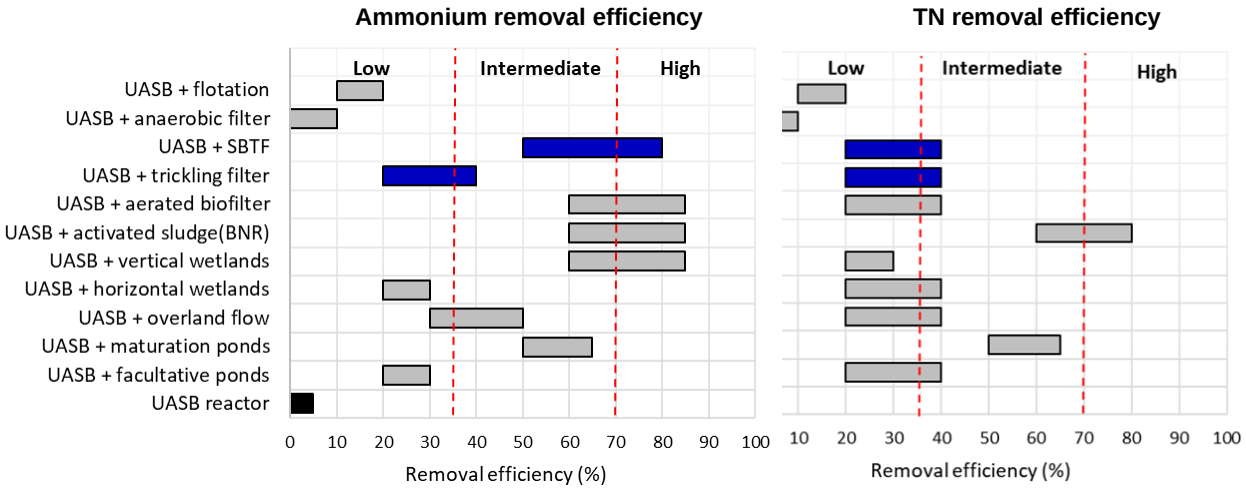

Figure 1.2 Removal efficiencies of ammonium (a) and total nitrogen (b) for various post-treatment technologies of anaerobic effluents. *BNR: activated sludge designed for biological nutrient removal. The black bar refers to UASB reactors without a post-treatment step. Gray bars refer to different combinations of UASB reactors and post-treatment technologies, with trickling (filled with rocks) and sponge-bed trickling filters (SBTF) highlighted in blue* (adapted from von Sperling et al. (2019)

1.3 Sponge-bed trickling filters

Following an extensive research period during the nineties, in the so-called Brazilian Research Program on Basic Sanitation (PROSAB), trickling filters were pointed out as one of the most prominent technologies for the post-treatment of anaerobic effluents (Chernicharo, 2006). Advantages compared to other systems refer to the passive aeration, low area requirement (similar to activated sludge post-UASB reactors; 0.1 – 0.2 m^2 PE^{-1}; von sperling et al., 2019), low sludge production (see Chapter 2, section 2.4.1), and relative operational and maintenance simplicity. This has motivated the widespread installation of those reactors at the expense of other biofilm-based systems (e.g., rotating biological contactors or wetlands), as further addressed in Chapter 2.

A trickling filter is basically a tank filled with a highly permeable material, allowing air circulation. A schematic representation is shown in Figure 1.3. The wastewater is applied mainly through rotary distribution arms, and the liquid percolates (trickles) downward. Temperature differences between the air and the liquid are the main driving force for convective airflows and consequent oxygen transfer to the liquid phase. As for tropical countries, a positive temperature gradient over 2 ^oC usually occurs, entailing an ideally downward airflow (WEF, 2000). The medium is hydraulically

unsaturated, meaning that the water level is restrained at the bottom of the reactor. Biofilm grows attached to the surface of the packing (support) material. The use of different support materials (e.g., gravel (75 – 100 mm), blast furnace slag, plastic rings, plastic sheets) has been widely covered in the literature (Metcalf & Eddy, 2013; Almeida et al., 2011), mostly for trickling filters following primary settlers. Nonetheless, as for the post-treatment of anaerobic effluents, rock- and plastic-based reactors are usually applied, as detailed in Chapter 2. The use of polyurethane sponge as a support medium in trickling filters (sponge-bed trickling filters; SBTFs) has emerged from the invention of the 'Downflow Hanging Sponge (DHS)' reactor (see Chapter 2). Further developments led to a self-structured sponge-based packing medium (see Figure 1.3), in which the sponge is contained into rectangular plastic frames allowing easy assembly in the field. Therefore, construction is further simplified compared to rock- or plastic-bed trickling filters.

Among the outstanding characteristics of the SBTFs are the high sludge retention time (> 100 days) and consequently low excess sludge production (even motivating the operation without secondary settlers) (see Chapter 2, section 2.4.1), improved air circulation (void ratio higher than 96%), and resistance to clogging. Moreover, a higher hydraulic retention time (HRT) has been reported for SBTFs compared to conventional rock and plastic-bed trickling filters. Although the medium is hydraulically unsaturated in a trickling filter, the HRT should be interpreted as the percolation time. A peculiar behaviour is noticed for SBTFs colonized with biomass, as the theoretical HRT calculation (V_{sponge}/Q) is reported close to the actual liquid retention time determined from tracer tests (Onodera et al., 2014; Tandukar et al., 2006b).

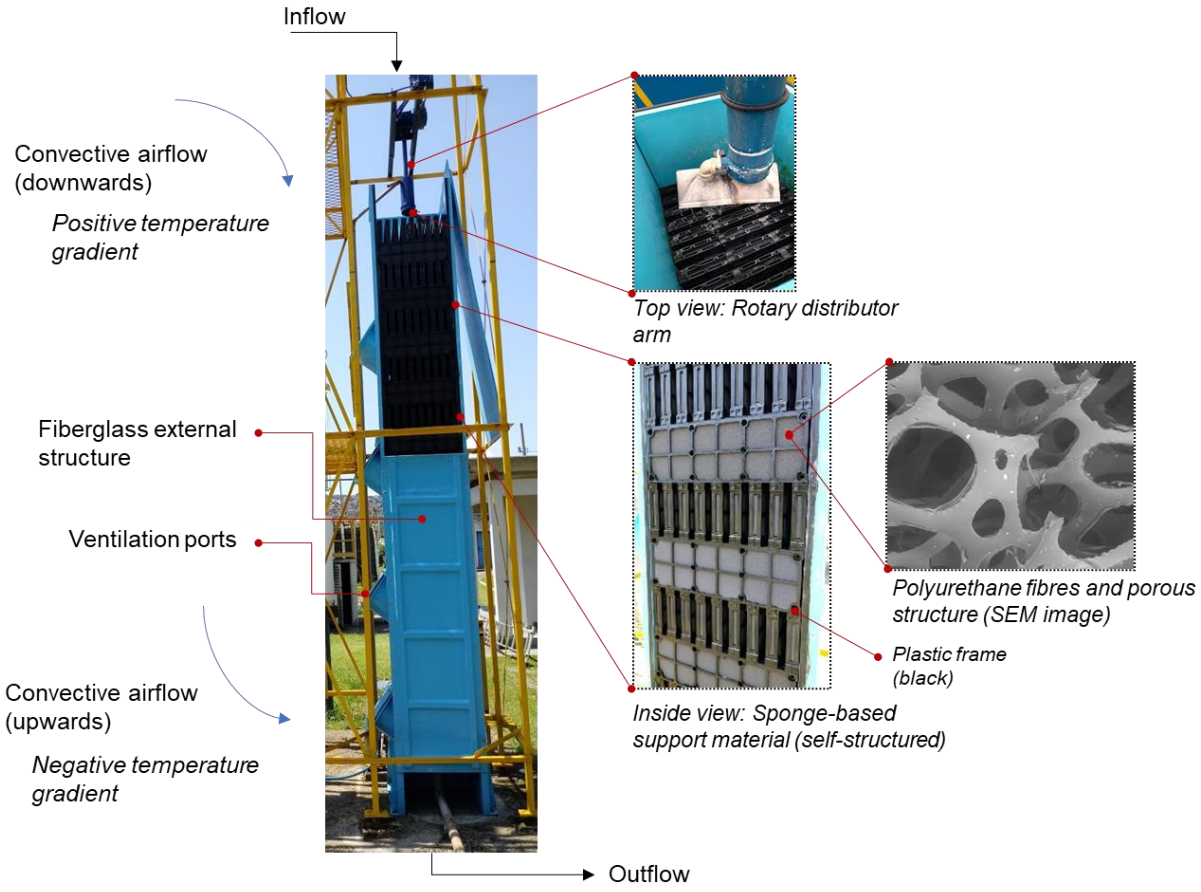

Figure 1.3 Schematic representation of a sponge-bed tricking filter and its main constituents

1.4 Summary of the research challenges

Improving total nitrogen removal in SBTFs following UASB reactors for sewage treatment involves a set of research challenges, which are summarized in this section.

1.4.1 Design of SBTFs following anaerobic sewage treatment

The design of trickling filters following UASB reactors has been typically based on surface hydraulic loading rates and volumetric organic loads. The concept was first derived from trickling filters preceded by primary settlers (Metcalf & Eddy, 2013). Concerning SBTFs, various attempts have been made to establish design criteria (Bressani-Ribeiro et al., 2017; Okubo et al., 2015; Tandukar et al., 2006b). Besides, empirical models have been used to predict trickling filter performance for organic matter removal based on practical experiences with rock-bed reactors following primary settlers (Daigger and Boltz, 2011). Still, similar operational conditions have led

to different process performance, e.g., in terms of ammonium removal efficiency. There is a lack of mechanistic understanding of microbial interactions in trickling filters post-UASB reactors, especially SBTFs.

1.4.2 Relevance of influent characteristics

While a relatively high ammonium removal efficiency (> 70%) is typically expected in SBTFs treating anaerobic effluents (Tandukar et al., 2007), this is not yet the case for total nitrogen removal. Further process optimization is hampered by a lack of knowledge regarding the influence of influent characteristics and operating conditions on total nitrogen removal. For instance, higher ammonium and bicarbonate concentrations in the UASB reactor effluent are expected compared with raw or settled sewage. This is ascribed to the ammonification process, i.e., the conversion of organic nitrogen into ammonium. Additionally, a low biodegradability is expected for the remaining organic content in the anaerobic effluent (Aquino et al., 2009), as the readily available COD is mainly converted into methane at the UASB reactor.

Furthermore, the influence of dissolved gases (methane and H_2S) present in the anaerobic effluent is often overlooked. Those gases are related to greenhouse effects and odour complaints, respectively. They can also hamper ammonium oxidation due to increased microbial competition for oxygen or even be toxic, as is the case for H_2S. On the other hand, dissolved gases abatement could be integrated into autotrophic nitrogen removal, as further discussed (see section 1.4.4).

1.4.3 Long-term SBTF performance

Currently, there is only one report of a long-term, full-scale monitoring campaign (> 1000 d) of an SBTF post-UASB reactor treating sewage (Onodera et al., 2016). Short operation periods do not detect key microbial changes when dealing with slow-growing microorganisms (e.g., anammox bacteria). In a lab-scale setup, Sánchez-Guillén et al. (2015a) observed high total nitrogen removal performance (> 80%) in a closed SBTF after more than 400 days of operation, primarily ascribed to anammox bacteria.

A mechanistic modelling approach can be a valuable tool to identify microbial changes in the long run. This has been demonstrated for autotrophic nitrogen removal in biofilm

reactors (Picioreanu et al., 1997; Volcke et al., 2010). Nonetheless, no SBTF models have been published so far.

1.4.4 Nitrogen removal pathways

This thesis focuses on two main biological nitrogen removal pathways: conventional nitrification-denitrification and partial nitritation-anammox (PN/A). Additionally, coupling denitrifying anaerobic methane oxidation (DAMO) and sulfur-based denitrification (SBDN) is addressed. The stoichiometry of those biological nitrogen removal processes is summarized in Table 1.1.

The major drawbacks of the conventional nitrification-denitrification (Eq. 1.1, Table 1.1) pathway are the aeration costs and the need for organic carbon. Nevertheless, there is still an appeal to foster heterotrophic denitrification in SBTFs following UASB reactors from a practical standpoint. As for aeration costs, no forced (mechanical) air supply is provided to SBTFs, as oxygen naturally diffuses in the percolating liquid. Hence, preventing nitrite oxidation to nitrate (nitratation) would not save energy (i.e., reduced aeration costs). Regarding organic carbon supply, it could be hypothesized that a simple recirculation of the SBTF effluent (containing nitrate) to its top layer (inlet) would enhance total nitrogen removal. The rationale is that the remaining COD fraction in the anaerobically treated sewage could be used as the electron donor for reducing nitrate to dinitrogen gas (N_2). Moreover, retained solids inside the sponge pores can be hydrolysed, releasing soluble products that can eventually be available as organic substrates (Almeida et al., 2013; Tandukar et al., 2006b). However, the effective contribution of the heterotrophic pathway in SBTFs following UASB reactors has not yet been fully quantified.

If external carbon addition is required for enhancing denitrification, diverting the organics present in influent sewage from the UASB reactor to the SBTF can be an approach (Bundy et al., 2017). Nonetheless, less COD would be available at the anaerobic step for biogas production, which can compromise the energy exportation potential of the treatment plant or even its energy autarky.

Table 1.1 Stoichiometry of the biological nitrogen removal processes of interest in this thesis. Only catabolic reactions are considered. The theoretical oxygen demand (g O_2 g N^{-1}) and organic carbon demand (g COD g N^{-1}) per nitrogen converted are also given.

Process	Reaction	Theoretical oxygen demand (g O_2 g N^{-1})	Organic carbon demand (g COD g N^{-1})
Nitrification-Denitrification (Eq. 1.1)	$\mathbf{NH_4^+}$ + 2 O_2 + 5/8 CH_3COO^- → 1/2 $\mathbf{N_2}$ + 5/8 CO_2 + 5/8 HCO_3^- + 17/8 H_2O + H^+	4.57	2.86
Partial nitrification-anammox (PNA) (Eq. 1.2)	$\mathbf{NH_4^+}$ + 3/4 O_2 → 1/2 $\mathbf{N_2}$ + 3/2 H_2O + H^+	1.71	0
Denitrifying anaerobic methane oxidation (DAMO)* (Eq. 1.3)	3 CH_4 + 8 $\mathbf{NO_2^-}$ + 8 H^+ → 3 CO_2 + 4 $\mathbf{N_2}$ + 10 H_2O	0	0
Sulfide-based denitrification (SBDN)** (Eq. 1.4)	S^{2-} + 1.6 $\mathbf{NO_3^-}$ + 1.6 H^+ → SO_4^{2-} + 0.8 $\mathbf{N_2}$ + 0.8 H_2O	0	0

*DAMO archaea reaction. DAMO bacteria reaction was also included for modelling (Chapter 6), referring to the conversion of nitrate to nitrite using methane as an electron donor; **SBDN was implemented for modelling (Chapter 6) considering intermediate products, distinguishing between electron donors (H_2S and S_0) and electron acceptors (NO_2^- and NO_3^-).

Saving organic carbon for the anaerobic step would thus be the most compelling reason for establishing autotrophic nitrogen removal through partial nitritation-anammox (Eq. 1.2, Table 1.1) in SBTFs post-UASB reactors. Essential factors to be considered in this respect are the residual organic carbon in the anaerobic effluent and the control of oxygen transfer in SBTFs. Lab-scale studies (with sequencing batch-reactors) have shown that the residual organic matter content in UASB reactor effluents (C/N ~ 5) does not negatively affect anammox activity (Leal et al., 2016), which is likely due to the low biodegradability of anaerobic effluents. As far as oxygen control is concerned, the proof of concept was already provided in lab-scale STBFs fed with synthetic effluents in controlled temperature rooms (Sánchez-Guillén et al., 2015b). Partial nitritation-anammox was achieved; however, the total nitrogen removal efficiencies remained relatively low (< 60%), attributed to a lack of oxygen transfer control. Reliable partial nitritation remains a significant challenge for upscaling autotrophic nitrogen removal in SBTFs.

Alternative autotrophic nitrogen removal pathways may also be stimulated in SBTFs post-UASB reactors, considering that the dissolved methane and H_2S in the anaerobic effluent could serve as electron donors for denitrification. Simultaneous methane abatement and nitrogen removal (i.e., denitrifying anaerobic methane oxidation – DAMO; Eq. 1.3, Table 1.1) has been demonstrated in a closed SBTF (Hatamoto et al.,

2017), treating synthetic wastewater deprived of organics and supplemented with nitrite. As for the simultaneous removal of H_2S and nitrogen (i.e., sulfide-based denitrification – SBDN; Eq. 1.4, Table 1.1), a high total nitrogen removal efficiency (> 90%) was reported in anaerobic/anoxic fixed bed reactor treating H_2S augmented synthetic effluents (bubbled-through with biogas) (Guerrero and Zaiat, 2018). However, process feasibility for sewage treatment has not yet been demonstrated and may only be achievable with high sulfide-containing streams (van den Hove et al., 2020).

Establishing highly efficient nitrogen removal, be it heterotrophic and/or autotrophic, dealing with residual organic carbon and combined with the abatement of dissolved methane and/or H_2S, thus forms a central challenge in the operation of SBTF reactors following anaerobic sewage treatment.

1.5 Outline of the thesis

Based on the presented research challenges, three main methodological tools were complementarily implemented in this doctoral research work, as illustrated in Figure 1.4, namely: literature review, experiments (i.e., demo-scale studies), and mathematical modelling and simulations.

Chapter 2 reviews the application of trickling filters following UASB reactors for mainstream sewage treatment. Design criteria for SBTFs treating anaerobic effluents are compiled. The aim is to get an overview of the state of the art and perspectives, mainly addressing the possibility of process optimization for total nitrogen removal. **Chapter 3** discusses the relevance of influent characteristics on nitrogen conversions based on experimental evidence and mathematical modelling. **Chapter 4** further explores the developed model to get mechanistic insights into the key parameters affecting total nitrogen removal in the long run of SBTFs. Promising strategies for enhancing process performance are put forward in a simulation study. **Chapter 5** compares the long-term behaviour of two demo-scale SBTFs operated in parallel fed with real anaerobically treated sewage. Previously identified operational approaches for enhancing total nitrogen removal (Chapter 4) are experimentally tested. Modelling and simulations are used to gain fundamental insights on nitrogen conversions. **Chapter 6** assesses the fate of dissolved methane and H_2S during nitrogen

conversions in SBTFs, considering an extension of the developed model (Chapter 3) and experiments. **Chapter 7** concludes this thesis by summarizing the main findings and providing perspectives for future research and developments.

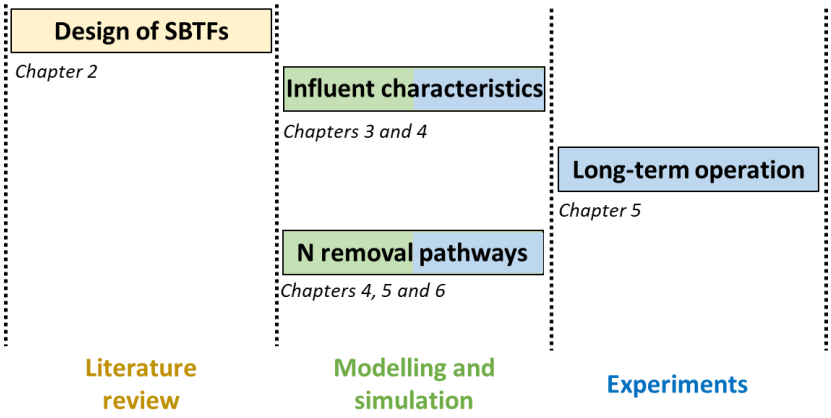

Figure 1.4 Schematic overview of the research challenges (in rows) and the methodology applied (in columns; according to three colour codes) in this thesis. *Influent characteristics and N removal pathways were assessed using modelling/simulation and experiments. References are made to the Chapters*

Chapter 2

Trickling filters following anaerobic sewage treatment: state of the art and perspectives

2.0 Abstract

High-rate anaerobic treatment of sewage using upflow anaerobic sludge blanket (UASB) reactors is a consolidated technology in warm climate countries. Nevertheless, since anaerobic treatment only removes organic carbon, post-treatment is required to remove nitrogen, besides residual organic carbon. Trickling filters (TFs) constitute a cost-effective post-treatment option, assuring a low sludge production, low operational costs, and maintenance simplicity compared to other post-treatment technologies (e.g., activated sludge). This chapter reviews the experience of the last 20 years of research, design, and operation of UASB/TF systems. Three main topics are addressed: (i) the development of trickling filters for UASB reactor effluent treatment, building on first experiences with TFs preceded by primary settlers; (ii) design criteria, performance, and empirical models for predicting the efficiency of TF post-UASB reactors; and (iii) future challenges associated with the elimination of secondary settlers and nitrogen removal in sponge-bed trickling filters (SBTFs).

This chapter has been published as

Bressani-Ribeiro, T., Almeida, P.G.S., Volcke, E.I.P. and Chernicharo, C.A.L. (2018) Trickling filters following anaerobic sewage treatment: state of the art and perspectives. Environmental Science: Water Research & Technology 4, 1721–1738.

2.1 Introduction

Adequate climate conditions and significant investments in research and development made Latin America (notably Brazil, Colombia, and Mexico) and India becoming frontrunners using UASB reactors for sewage treatment (Chernicharo et al., 2015). The application of such reactors for sewage treatment at lower temperatures has not yet been fully demonstrated but looks promising (Petropoulos et al., 2017). Nevertheless, given that anaerobic treatment only removes organic carbon, post-treatment to remove nitrogen and residual organic carbon is typically required to meet effluent discharge standards. Such post-treatment facilities typically comprise an aerobic stage. The resulting combined anaerobic/aerobic systems constitute an alternative to traditional sewage treatment systems, such as activated sludge and land-based pond systems.

The costs of a treatment plant comprising a UASB reactor followed by aerobic biological treatment usually allow capital expenditures (CAPEX) savings in the range of 20 – 50% and operational expenditures (OPEX) savings above 50%, in comparison with a conventional activated sludge plant (von Sperling and Chernicharo, 2005; Chernicharo, 2006). This is considered one of the reasons for increasing sewage treatment coverage in Latin America (Chernicharo et al., 2015).

Post-treatment options for anaerobically treated sewage are well covered in the literature (Chernicharo, 2006; Foresti et al., 2006; Chan et al., 2009; Kassab et al., 2010; Khan et al., 2011; Chong et al., 2012), addressing the available technologies and discussing the advantages and disadvantages of each alternative. In summary, combined anaerobic/aerobic systems allow the achievement of the necessary efficiencies to comply with discharge standards in terms of carbon and ammonium removal, mainly in developing countries (Chernicharo et al., 2015). A recent survey in Brazil (Chernicharo et al., 2018) has shown that amongst 333 investigated sewage treatment plants comprised of UASB reactors followed by post-treatment units, trickling filters accounted for 25% (82 plants), as shown in Figure 2.1. In terms of installed capacity, the population equivalent (PE) that can be served by the existing UASB/TF systems accounts for approximately 3.6 million inhabitants, which represents 29% of the total surveyed population.

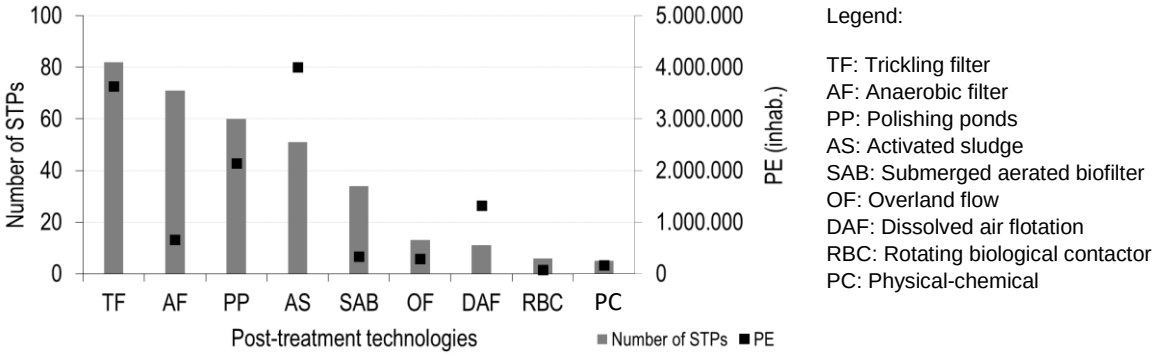

Figure 2.1 Post-treatment technologies for UASB reactors commonly applied in Brazil

Trickling filters (TFs) are non-submerged aerobic biofilm reactors, which were applied for sewage treatment for the first time in England in 1893 (Rittmann and McCarty, 2001). In Brazil, the first application was recorded in 1910 (Jordão and Pessoa, 2005). A trickling filter consists basically of a tank filled with a highly-permeable material, onto which wastewater is applied through a distribution system. The liquid trickles downward, allowing bacterial growth (biofilm) on the surface of the packing material, and air naturally moves upward or downward (Chernicharo, 2006; Metcalf & Eddy, 2013). The TFs operational simplicity and performance stability are key aspects to their worldwide application, especially in developing countries.

Indeed, the possibility of using trickling filters post-UASB reactors has shown remarkable advantages compared to other post-treatment options of anaerobically treated sewage (Chernicharo, 2006; Gonçalves et al., 2001). The technological choice of TFs as post-treatment units of UASB reactors ensures a low sludge production and relative operational and maintenance simplicity. Additionally, such a combined system has a low operating cost due to the reduced electricity consumption and no need for chemical products dosing (Chernicharo, 2006) (unless P removal is a target). In this context, the UASB/TF system can play an important role in universalizing sewage treatment coverage in developing regions. Specifically, in the case of Brazil, only 42.7% of the produced sewage is currently treated (SNIS, 2018); nevertheless, there is a national target of full sewerage coverage and treatment until 2033.

While a comprehensive state-of-the-art review on design and operation of trickling filters preceded by primary settlers was published by Daigger and Boltz (Daigger and Boltz, 2011), the experiences of the last 20 years of research, design, and operation

of trickling filters following UASB reactors still need to be consolidated. Therefore, the structure of this Chapter comprises three main topics: (i) the development of trickling filters for UASB reactor effluent treatment, building on first experiences with TFs preceded by primary settlers; (ii) design criteria, performance, and empirical models for predicting the efficiency of TF post-UASB reactors; and (iii) future challenges associated with the elimination of secondary settlers and nitrogen removal in sponge-bed trickling filters (SBTFs).

2.2 Development of trickling filters following UASB reactors for sewage treatment

Trickling filters for sewage treatment were originally applied following primary settlers. The primary settlers were later replaced by UASB reactors. Over the last approximately ten years, particular attention was paid to the use of sponge-based support media. These three stages of development are detailed below.

2.2.1 Trickling filters preceded by primary settlers

Trickling filters for sewage treatment were initially conceived with rock-based support media and preceded by a primary sedimentation tank. A secondary settler following the TF was included to reduce the concentration of effluent suspended solids and total BOD. The resulting flowsheet (Figure 2.2) was typically applied for rural and small sewage treatment plants in cold climate regions (e.g., in the United Kingdom and Germany) and remains in use nowadays. Additional primary and secondary sludge handling units are required, typically for thickening, digestion, and dewatering.

In this flowsheet (Figure 2.2), a portion of the final effluent is typically recycled to the top of the trickling filter to dampen BOD-loading fluctuations and consequent problems of BOD overload and dissolved oxygen depletion (Rittmann and McCarty, 2001). As BOD removal in primary settlers is typically low (< 35%), effluent recycling for feeding trickling filters in this flowsheet seeks to ensure an influent BOD concentration to the filter around 100 mg L^{-1} (von Sperling and Chernicharo, 2005). Additionally, recirculation tends to improve support media wetting efficiency.

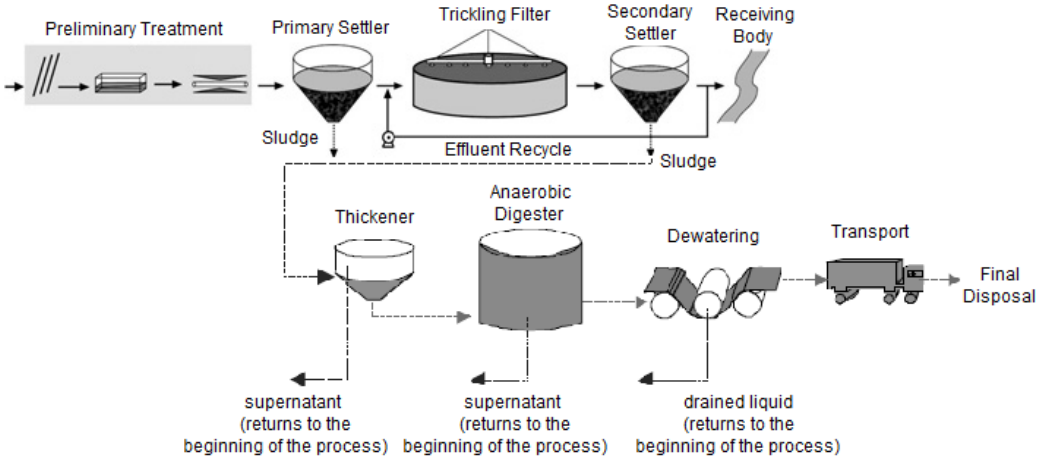

Figure 2.2 Sewage treatment flowsheet based on trickling filter preceded by a primary settler. *Reproduced and adapted from von Sperling and Chernicharo (2005) with permission from IWA Publishing, copyright 2005*

2.2.2 Trickling filters following UASB reactors

Driven by the success of anaerobic sewage treatment in warm climate regions, primary settlers were often replaced by UASB reactors, mostly in developing countries. The resulting UASB/TF flowsheet (Figure 2.3) is simpler than trickling filters preceded by primary settlers. The excess aerobic sludge from secondary settlers is returned to the UASB reactor such that separate units for sludge thickening and digestion are not required. Additionally, as BOD removal in UASB reactors is typically higher than that of primary settlers (> 60%), effluent recycling for feeding TFs is usually unnecessary (von Sperling and Chernicharo, 2005), setting the admissible ranges recommended for design. In the case of well-operated UASB reactors, even secondary settlers may turn out unnecessary (see further) depending on the operational conditions being imposed on the trickling filters.

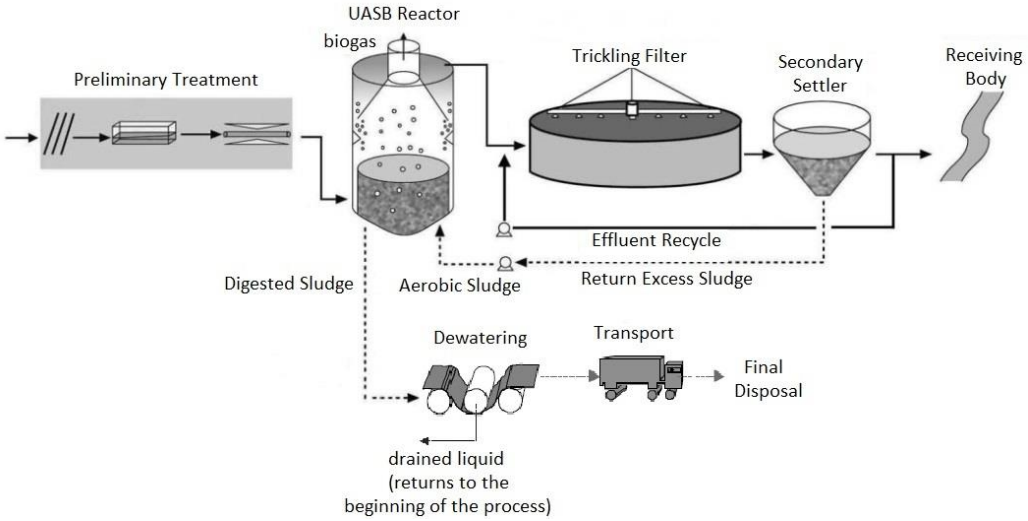

Figure 2.3 Sewage treatment flowsheet based on trickling filter following UASB reactor. *Reproduced and adapted from von Sperling and Chernicharo (2005) with permission from IWA Publishing, copyright 2005*

2.2.3 Trickling filter improvements through plastic- and sponge-based support media

The performance and operation of trickling filters can be improved with plastic packing and, more recently, sponges instead of the conventional rock-based support media. From the biological standpoint, higher surface area for biofilm development and the ability to retain biomass for longer periods within the system are key points for performance improvements. Other relevant aspects are the high hydraulic capacity, better air circulation (high void ratio), and resistance to clogging.

Because the application of low hydraulic loading rates (10 – 20 $m^3\ m^{-2}\ d^{-1}$; based on surface area) may lead to an ineffective wetting of the filter packing with high specific surface area, the use of plastic-based support media (i.e., plastic rings or cross-flow) does not guarantee performance improvements, as observed in trickling filters preceded by primary settlers (Grady et al., 1999). Experiments with random plastic rings indicated that when the organic loading is lower than 1.0 kgBOD $m^{-3}\ d^{-1}$ (hydraulic loading rates: 10 – 20 $m^3\ m^{-2}\ d^{-1}$), the performance of rock- and plastic-based trickling filters for organic matter removal following UASB reactors is similar (Almeida et al., 2011). Whether or not recirculation could be an operational strategy improving the performance of plastic-bed trickling filters following UASB reactors is still a matter of further research. Interestingly, the experiences with plastic packing reactors are seldom reported in the literature. More frequent application of rock medium as filling

material is related to the trade-offs between costs and benefits under the perspective of more flexible legal discharge standards for carbon and nitrogen.

A promising alternative to improve trickling filters performance considers using sponge-based support media, as discussed in Kassab (Kassab et al., 2010). The use of polyurethane sponge as a support media in TFs following UASB reactors has begun with the development of a system so-called 'Downflow Hanging Sponge (DHS)' by the research group of Professor Hideki Harada at the Universities of Tohoku and Nagaoka (Japan) (Agrawal et al., 1997). A comprehensive report on the steps through the development and evolution of the DHS system can be found on Uemura and Harada (2010). From the research outcomes, a Brazilian research group of Universidade Federal de Minas Gerais (UFMG, Brazil) has been developing a self-structured sponge-based packing medium since 2012.

The first study with the DHS system in Brazil was implemented considering the comparison with other types of packing material, such as blast furnace slag, plastic rings, and corrugated plastic tubings (Almeida et al., 2011). At the same operational conditions, DHS performance tended to be superior for organic matter removal, and the possibility to operate the system without secondary settlers was preliminarily verified. In fact, plastic-based packing media did not attribute any performance improvements, considering the operational conditions imposed on the systems. In sequence, another study was developed to verify the benefits of using sponge-based packing media (Almeida et al., 2013). The results clearly demonstrated the benefits provided by sponges, improving the effluent quality in terms of organic matter, also indicating a noticeable increase in ammonium removal. Additionally, a molecular investigation was implemented to observe the bacterial community composition by pyrosequencing (Mac Conell et al., 2015). The results suggested that denitrifiers, nitrifiers, and even anammox bacteria coexisted in the reactor. Considering this finding and the observed potential to retain slow-growing organisms within sponge-bed trickling filters (Tandukar et al., 2006b; Kubota et al., 2014), future improvements could also be directed for total nitrogen removal (see further).

From the results obtained in Japan and Brazil, a self-structured sponge-based packing medium was industrially prototyped and tested on a demonstration-scale under a typical full-scale flow regime (Bressani-Ribeiro et al., 2017). The justification for

adopting a self-structured design is because intermediate underdrains are needed when random sponge-based packing media is used, avoiding excessive compression of the elements. As expected, nitrification activity was low because the system was designed to operate at high organic loadings (0.45 kgBOD $m^{-3}_{reactor}$ d^{-1}). Nevertheless, 50% ammonium removal was observed using the prototyped sponge-based support media, whereas it could only be achieved in rock-bed trickling filters with applied volumetric loading rates of around 0.22 kgBOD $m^{-3}_{reactor}$ d^{-1} (Metcalf & Eddy, 2013). The main steps for developing the sponge-based packing medium at UFMG are summarized in Table 2.1.

Table 2.1 Development of sponge-based packing medium for the improvement of trickling filters following UASB reactors: lessons learned from the UFMG experience.

Reference (focus of the research)	Scale	Operational conditions (Trickling filter)		Main lessons learned
		HLR (m^3 m^{-2} d^{-1})	OLR (kgBOD m^{-3} d^{-1})	
Almeida et al. (2011, 2009) *(Perspective of using sponge-based packing media; operation without secondary settlers)*	Demo-scale (V = 8.7 m^3 H = 2.5 m)	10-20	0.25-0.45	▪ From a comparison study with different media, the benefits of using sponges were demonstrated in terms of organic matter removal, indicating the perspective to operate UASB/TF systems without secondary settlers. ▪ The overall performance for the DHS system (a sponge-based medium) was above 80% for BOD, COD, and TSS. However, the operational conditions seemed inappropriate when ammonium removal above 50% was required.
Almeida (2012); Almeida et al. (2013) *(Effective influence of sponges improving UASB/TF system performance; operation without secondary settlers)*	Demo-scale (V = 1.9 m^3 H = 4.1 m)	10-12	0.12-0.20	▪ Considering the previous outcomes, the influence of sponges enhancing the performance of low-rate trickling filters following UASB reactors was investigated. ▪ A sponge-based packing medium was significantly more effective for organic matter removal than a plastic-based packing medium. For ammonium removal, 50% was achieved using a plastic-based medium, whereas 80-95% was observed using sponges. ▪ The sponges notably increased the system's reliability to operate without secondary settlers.

Reference (focus of the research)	Scale	Operational conditions (Trickling filter)		Main lessons learned
		HLR ($m^3\ m^{-2}\ d^{-1}$)	OLR ($kgBOD\ m^{-3}\ d^{-1}$)	
Mac Conell et al. (2015) *(Microorganisms involved in nitrogen cycle within the sponge-bed trickling filter)*	Demo (V = 1.9 m^3 H = 4.1 m)	10-12	0.12-0.20	▪ The bacterial community composition involved in N-cycle within a sponge-bed trickling filter treating UASB effluent was investigated by pyrosequencing. ▪ The results revealed that denitrifiers, nitrifiers, and anammox bacteria coexisted in the reactor, suggesting that different metabolic pathways were involved in nitrogen removal within the system, including the activity of anammox bacteria.
Bressani-Ribeiro (2015); Bressani-Ribeiro et al. (2017) *(Performance of UASB-SBTF system without secondary settler, considering realistic conditions in terms of flow regime; testing of a sponge-based packing medium industrially prototyped)*	Demo (V = 4.4 m^3 H = 3.5 m)	11.5	0.45	▪ The performance of the UASB/TF system considering the use of a sponge-based packing medium industrially prototyped was evaluated. A typical full-scale flow regime was imposed on the system for a more realistic investigation. High organic loadings were applied to the trickling filter to observe the system's performance under limiting operational conditions. ▪ Even under limiting operational conditions, the possibility of operating the system without a secondary settler was confirmed. Organic matter removal was around 85-90%. As observed in previous studies, the results confirmed that ammonium removal above 50% should not be expected.

HLR: hydraulic loading rate (same as surface hydraulic loading rate - HLRs); OLR: volumetric organic loading rate; H: height of the trickling filter bed.

Fundamental aspects related to the improvements provided by sponge-based packing media. Interstitial biomass retention within the sponge-based media leads to a high HRT (≈ 1.5 – 2.5h) and sludge retention time (SRT) (> 100 days), which ensures a significant improvement for the removal of organic matter and ammonium in the post-treatment step. In addition, long interstitial retention of biomass favours lysis/hydrolysis of inactive cells, resulting in low excess of sludge production (around 0.10 $gTSS\ gBOD^{-1}_{removed}$). High sludge concentration, sufficient oxygen supply, adequate endogenous respiration rate, and a high density and diversity of microfauna are also relevant factors highlighted by Onodera et al. (2013), explaining why the sludge accumulation was in near balance with the degradation of sludge within the reactor. Tandukar et al. (2006b)

also correlated sludge degradation with heterotrophic denitrification within anoxic zones of the sponges (see further). It is important to point out that larger SRT tends to reduce the start-up period in a sponge-bed trickling filter.

In a DHS post-UASB reactor, the outer portion of the sponges tends to be predominantly aerobic (Araki et al., 1999). Worth mentioning that Araki et al. (1999) and Machdar et al. (2000) reported concentrations of 1.0 mgDO L^{-1} even at inner portions of the sponge (e.g., 6 mm in depth). This finding suggests increased aerobic niches within a sponge-bed bioreactor where slow-growers, such as nitrifiers, could also be active. High DO concentration tends to increase the presence of macrofauna, which contributes to the predation of bacteria and protozoa (Onodera et al., 2013; Hendrickx et al., 2009). However, because macrofauna overgrazing is only prominently observed on the surface of the sponge media (smaller pores tend to physically protect biomass from the snails), the presence of the related organisms does not lead to significant impacts on the process performance (Onodera et al., 2014; Onodera et al., 2015). Thus, the ability of the sponge-based medium to protect biomass from snail overgrazing is a crucial aspect maintaining the activity of microorganisms, especially the activity of slow-growers (e.g., nitrifiers).

A DO gradient occurs within the sponge pores and the biofilm developed on sponge fibres, creating anoxic niches and a proper environment for heterotrophic denitrification. Thus, hydrolysed biomass could be utilized as an additional source of substrate in the presence of oxidized forms of nitrogen. Because of the anoxic zones within the sponges and longer SRT, we cannot eliminate the hypothesis that the activity of anaerobic ammonium-oxidizing bacteria (anammox bacteria) could also be a factor for nitrogen removal. In fact, anammox bacteria were detected in several samples within a sponge-bed trickling filter following a UASB reactor, as discussed in Mac Conell et al. (2015). However, nitrogen removal tends to be more relevant (≈ 65%) within fully ventilated systems only when effluent recycling is practiced, as observed in Okubo et al. (2015). It indicates that the presence of readily biodegradable organic matter and oxidized forms of nitrogen in anoxic zones is essential for a high heterotrophic denitrification activity.

2.3 Design and performance of trickling filters following UASB reactors

2.3.1 Main design criteria for TFs following UASB reactors

The main design criteria associated with trickling filters concern the surface hydraulic loading rate (HLR) and the volumetric organic loading rate (OLR), primarily originated from the experience of TFs preceded by primary settlers for sewage treatment (Metcalf & Eddy, 2013; WEF, 1996). In this case, five categories of TFs based on the imposed HLR were reported in the classic literature: low rate (1.0 to 4.0 $m^3\ m^{-2}\ d^{-1}$), intermediate rate (3.5 to 10.0 $m^3\ m^{-2}\ d^{-1}$), high rate (10.0 to 40.0 $m^3\ m^{-2}\ d^{-1}$), super high rate (12.0 to 70.0 $m^3\ m^{-2}\ d^{-1}$) and rough (45.0 to 185.0 $m^3\ m^{-2}\ d^{-1}$) (Metcalf & Eddy, 2013; WEF, 1992; WEF, 2000).

Design of rock-bed trickling filters following UASB reactors. In general, most of the full-scale units have been designed as a high-rate trickling filter, adopting organic loading rates between 0.5 to 1.0 kgBOD $m^{-3}\ d^{-1}$. The reason for adopting such high organic loading rates is based on the less stringent discharge standards considered in developing countries to progressively accomplish the goals for sewage treatment expansion. Under these conditions, satisfactory removal of organic matter is expected, with very low NH_4^+-N removal. The listed criteria and parameters for designing rock-bed trickling filters as a post-treatment of UASB reactor effluents (Table 2.2) are based on the outputs of the Brazilian Research Program on Basic Sanitation (PROSAB) (Chernicharo, 2001). The expected performance of rock-bed trickling filters following UASB reactors is currently based on practical experiences, as the empirical models predicting organic matter and ammonium removal are not well established, as further discussed.

Table 2.2 Criteria and parameters currently adopted for the design of high-rate rock-bed trickling filters following UASB reactors.

Parameter	Operational range		
	Average flow	Maximum daily flow	Maximum hourly flow
Organic loading rate (kgBOD m^{-3} d^{-1})	0.5 – 1.0	0.5 – 1.0	0.5 – 1.0
Hydraulic loading rate (m^3 m^{-2} d^{-1})	15 – 30	18 – 22	25 – 30
Height (m)	2.0 – 3.0	2.0 – 3.0	2.0 – 3.0

Note: For rock-bed trickling filters following UASB reactors, the adopted sludge production rate is 0.8 – 1.0 kg SS $kgBOD^{-1}_{removed}$.

Designing trickling filters, regardless of the selected support media, should take place through the following subsequent steps: (i) determine the volumetric organic loading rate (OLR) to be applied, taking into account the BOD and COD concentrations of UASB reactor effluent; (ii) calculate the support media volume, considering a recommended OLR value; (iii) select a support media height, which will be typically between 2.0 and 3.0 m; (iv) calculate the surface area of the biofilter, considering the predefined volume and support media height; (v) verify the applied surface hydraulic loading rate.

For UASB reactors treating sewage (typically diluted – BOD < 400 mg L^{-1}), the organic matter concentration in the anaerobic effluent is typically low (< 100 mgBOD L^{-1}), implying a low OLR to the post-treatment step. As a result, the following designs steps of calculating support media volume, determining height, and calculating surface area are intrinsically correlated. After obtaining a rock-media volume for an applied OLR, choosing heights between 2.0 and 3.0 m is sufficient to ensure a minimum surface area required for a proper HLR condition. Therefore, the HLR, and consequently the surface area, is usually the limiting factor for designing rock-bed trickling filters post-treating anaerobic effluents.

Design of sponge-bed trickling filters following UASB reactors. Important efforts have been directed to establish the design criteria based on practical experiences with sponge-bed trickling filters (SBTF) following UASB reactors (Tandukar et al., 2006b; Bressani-Ribeiro et al., 2017; Onodera et al., 2014; Okubo et al., 2015; Onodera et al., 2016). The Down-flow Hanging Sponge (DHS) system is generally designed for carbon and ammonium removal in a single reactor volume as a low-rate bioreactor. Effluent recycling has also been practiced in full-scale systems (Okubo et al., 2015). Table 2.3

summarizes some experiences and the observed operational conditions and performances related to sponge-bed trickling filters treating anaerobic effluents.

Table 2.3 Summary of operational conditions and performances for BOD and ammonium removal observed for sponge-bed trickling filters following UASB reactors (lab-, demo- and full-scale experiences).

Reference	Operational conditions					SBTF performance		Scale
	OLR (kgBOD m^3 d^{-1})	HLR (m^3 m^{-2} d^{-1})	HRT (h)	Sponge filling ratio - FR (%)	Effluent recycle	BOD removal (%)	NH_4^+-N removal (%)	
Okubo et al.(2015); Onodera et al.(2016)	0.23	21	1.5	25	1:1	90	80	Full
Onodera et al. (2014)	0.40	12	2.0	40	none	85	80	Lab
Bressani-Ribeiro et al. (2017)	0.40	11.5	2.5	40	none	72	44	Demo

OLR: volumetric organic loading rate; HLR: surface hydraulic loading rate; HRT: hydraulic retention time (calculated as V_{sponge}/Q). FR: Ratio between sponge volume and reactor volume.
Note: the reported results related to Bressani-Ribeiro et al. (2017) consider the operation of the UASB/SBTF system under a typical flow regime, as observed in full-scale sewage treatment plants.

From a full-scale experience (Okubo et al., 2015), the organic load applied to the DHS system was around 2.80 kgCOD m^{-3}_{sponge} d^{-1} (0.23 kgBOD $m^{-3}_{reactor}$ d^{-1}), considering a theoretical hydraulic retention time (HRT) of 1.5 h. The sponge filling ratio was around 25% of the reactor, with 5 meters of useful height. The trickling filter performance for BOD and ammonium removal was around 90% and 80%, respectively, considering 100% effluent recirculation. In a lab-experience (Onodera et al., 2014), a high organic loading rate was applied to the DHS system (0.40 kgBOD $m^{-3}_{reactor}$ d^{-1}), with removal efficiencies of 85% for BOD and around 80% for ammonium, similar to those reported for the full-scale experience. Sponge filling ratio and HRT were 40% and 2 hours, respectively, and 3 meters for useful height was adopted. No effluent recycling was practiced during the experimental period. For similar design and operational conditions, Bressani-Ribeiro et al. (2017) reported removal efficiencies of 72% for BOD and 44% for ammonium. The demo-scale UASB/SBTF system operated under a typical flow regime, as observed in full-scale sewage treatment plants, with no effluent recycle and no secondary settlers. The useful reactor height was 3.5 m.

The observed differences in terms of performance can probably be related to the choice of operational conditions and the intrinsic characteristics of the support media used to perform each experiment. For the design of the full-scale DHS system, a

curtain-type packing medium was used, whereas for the lab- and demo-scale, random and vertical self-structured packing media were used, respectively. The pore size used for the random packing medium was 1.6 mm, larger than the pore size of the polyurethane media previously used (Onodera et al., 2014). The pore size tends to affect HRT and solids retention in sponge-bed trickling filters. As reported in Tawfik et al. (2006b), an increase in HRT for sponges with 0.56 mm pores compared to those with pores ranging from 0.63 to 1.92 m was observed. In addition, considering the similar operational conditions observed on lab- and demo-scale operation (Table 2.3), deeper penetration of oxygen (despite no systematic evaluations being performed) within the sponges and influent flow regime could explain the observed differences in terms of BOD and NH_4^+-N performance.

Adopting a loading criterion (0.20 – 0.40 kgBOD $m^{-3}_{reactor}$ d^{-1}) to design sponge-bed trickling filters, the hydraulic retention time needs to be verified for the usual range. In general, most of the experiences related to sponge-bed trickling filters following UASB reactors indicate HRT ranging from 1.5 to 2.5 h. Because of the uncertainties regarding operational conditions and the system's performance, the design of sponge-bed trickling filters following UASB reactors should be currently based on practical experiences (e.g., as observed in Table 2.3).

Detailed trickling filter design aspects associated with the effluent distribution system (rotating distributor arms), underdrains, and natural ventilation systems fall beyond the scope of this Chapter – they are described in classic textbooks (Rittmann and McCarty, 2001; Metcalf & Eddy, 2013).

2.3.2 Performance of rock-, plastic- and sponge-bed trickling filters post-UASB reactors for carbon and ammonium removal

Experiences of trickling filters using conventional support media (rock and plastic) following UASB reactors are summarized in Table 2.4, including typical OLR, and HLR ranges applied and corresponding carbon and ammonium removal efficiencies. The UASB-trickling filter systems considered the operation with secondary clarifiers.

The BOD removal efficiencies of trickling filters fed with effluent from UASB reactors (median of 65%; Table 2.3) are typically lower than those for traditional TFs following primary settlers (65 – 80%; Metcalf & Eddy, 2013). This was expected since most

readily biodegradable organic matter is consumed in the anaerobic step. Nevertheless, overall BOD removal efficiency (UASB + trickling filter) is likely to remain similar to the traditional combination of primary settlers and trickling filters. From the operational results indicated in Table 2.3, it was observed that the UASB-trickling filter systems produced effluents with BOD and TSS concentrations below 40 mgBOD L^{-1} and 30 mgTSS L^{-1}, respectively (OLR 0.45 – 0.90 kgBOD m^{-3} d^{-1}; HLR 10 – 30 m^3 m^{-2} d^{-1}). From additional practical experiences with high-rate rock-bed trickling filters as post-treatment of UASB reactors effluents, maximum OLR and HLR values should be between 0.5 – 1.0 kgBOD m^{-3} d^{-1} and 20 and 30 m^3 m^{-2} d^{-1} for BOD and TSS concentrations lower than 60 mg L^{-1} (Chernicharo, 2001). In terms of ammonium removal, it can be noticed that for OLR above 0.20 kgBOD m^{-3} d^{-1} (OLR ranging from 0.20-0.70 kgBOD m^{-3} d^{-1}), ammonium removal around 10 – 42% is observed.

Typical BOD/NH_4^+-N ratios fed to trickling filters following primary settlers are approximately 6.5 (WEF, 2000). Due to the relatively higher removal of readily biodegradable organic matter (especially soluble BOD fractions) in UASB reactors, the UASB effluent BOD/NH_4^+-N ratio is lower, approximately 2 (Bressani-Ribeiro et al., 2017). This gives more opportunities for the nitrifying bacteria, because relatively less oxygen is consumed by heterotrophs. Denitrification could also occur by implementing recirculation of the final effluent to the inlet trickling filter (see section 2.4.2.1).

Table 2.4 Main characteristics and performance of rock and plastic-bed trickling filters following UASB reactors (and followed by secondary settlers).

Scale	Operational conditions		TF characteristics			UASB reactor effluent concentrations (mg L^{-1})			Trickling filter effluent concentrations (mg L^{-1}) [removal efficiency - %]			Ammonium-N removal rate (kgN m^{-3} d^{-1})	Reference
	Flow (m^3 d^{-1})	OLR (kgBOD m^{-3} d^{-1})	HLR (m^3 m^{-2} d^{-1})	Height (m)	Volume (m^3)	Media	BOD	TSS	NH_4^+-N	BOD	TSS	NH_4^+-N		
Pilot	0.54	0.07	3.1	2.1	0.2	Plastic	-	-	35	-	-	10 [71]	0.04	Victoria (2006)
Pilot	0.54	0.13	5.6	2.1	0.2	Plastic	-	-	30	-	-	15 [50]	0.04	Victoria (2006)
Full	- [c]	0.09 – 0.22	-	-	-	Plastic	-	-	12-25	-	-	0.8-1.6	-	Pearce et al. (2011)
Demo	20.0	0.24	10.0	3.0	3.0	Plastic	105	39	37	44 [58]	13 [67]	28 [25]	0.06	Fonseca (2009)
Demo	69.0	0.31	13.6	1.9	9.7	Slag	44	35	23	23 [48]	14 [60]	19 [17]	0.03	Frade (2003)
Pilot	6.0	0.33	32.1	4.0	1.1	Rock	40	50	21	18 [55]	23 [54]	17 [19]	0.03	Aisse (2002)
Pilot	6.0	0.42	21.2	4.0	1.1	Rock	78	64	21	37 [53]	26 [59]	18 [14]	0.02	Aisse (2002)
Full	7,402	0.45	8.7	2.7	2,309	Rock	~140	140	36	30 [79]	-	21 [42]	0.05	Sanepar (*apud* Almeida, 2012)
Demo	69.1	0.50	-	1.9	11.5	Slag	88	42	-	31 [65]	19 [55]	-	-	Pontes and Chernicharo (2011)[a]
Full	155.52	0.56	13.3	2.5	3,30	Rock	106	181	-	37 [65]	53 [71]	-	-	Moraes et al. (2011)
Demo	69.0	0.68	13.6	1.9	9.7	Slag	96	75	30	42 [56]	34 [55]	26 [13]	0.03	Frade (2003)
Demo	69.0	0.68	13.6	1.9	9.7	Slag	96	48	29	32 [67]	22 [54]	28 [3]	0.01	Frade (2003)
Demo	72.0	0.89	63.7	7.0	7.9	Plastic	99	-	30	32 [68]	-	21 [10]	0.03	Collivignarelli et al. (1990)
Full	155.52	< 1.0	16.8	2.5	3,29	Rock	-	-	-	85-89[b]	86-89[b]	-	-	Chernicharo et al. (2014)[a]
Full	14.69	-	18.5	2.5	994	Rock	114	38	-	18 [84]	11 [53]	-	--	Lobato et al. (2011)[a]
-		**0.07 – 1.0**	**3.1 – 63.7**	**1.9 – 7.0**	-	-	**40 – 140**	**35 – 181**	**19 - 37**	**18 – 44 [32]**	**11 – 53 [22]**	**1.2 – 28 [19]**	**0.01 – 0.06**	Observed ranges (efficiency
		[0.42]	**[13.6]**	**[2.5]**			**[96]**	**[49]**	**[30]**	***48 – 84 [65]***	***53 - 71 [55]***	***3 – 90 [19]***	**[0.03]**	in italic) [median]

[a] Flowsheet with secondary sludge returns for digestion and thickening in the UASB reactor. [b] Overall STP removal efficiencies (PE ≈ 1,000,000) not considered for the observed ranges. [c] Population equivalents between 2,500 and 80,000 inhabitants.

The experiences with sponge-bed trickling filters following UASB reactors for sewage treatment are summarized in Table 2.5. Typical combined UASB/SBTF removal efficiencies are 95% for BOD, 85 – 90% for COD and 70 – 90% for TSS. Ammonium removal efficiencies above 70% are obtained for OLR up to 2.0 kgCOD m^{-3}_{sponge} d^{-1} (around 0.76 kgCOD $m^{-3}_{reactor}$ d^{-1}), which is higher than would be expected for rock and plastic-based TFs (ammonium removal efficiencies lower than 50% at an OLR of 0.50 kgCOD $m^{-3}_{reactor}$ d^{-1}). This could be due to the relatively better retention of nitrifying biomass in sponge-bed trickling filters due to the greater sludge retention time (SRT), HRT, and oxygen availability (Tandukar et al., 2006b; Machdar et al., 1997).

Ammonium removal efficiency increases with decreasing OLR only down to a certain limit. Tawfik et al. (2008) observed that an OLR reduction from 2.6 to 1.6 kgCOD m^{-3}_{sponge} d^{-1} resulted in a 29% increase in NH_4^+-N removal efficiency. However, a further OLR decrease to 1.3 kgCOD m^{-3}_{sponge} d^{-1} did not improve nitrification efficiency. This could be explained by substrate limitation (NH_4^+-N and inorganic carbon) in the bottom compartment of the SBTF (below 3 meters height). Mac Conell et al. (2013) observed a population reduction of ammonia oxidizing bacteria and, consequently, low nitrification rates at the bottom compartment of an SBTF operated at OLR between 0.45 – 0.55 kgCOD m^{-3}_{sponge} d^{-1}.

Low specific sponge volumes (m^3_{sponge} $m^{-3}_{reactor}$) may result in lower organic matter and ammonium removal efficiencies considering the same applied OLR. Tawfik et al. (2010) determined a reduction of COD and NH_4^+-N removal efficiencies from 80 to 62% and 86 to 38%, respectively, when the sponge volume changed from 38 to 19% under the same applied OLR (2.0 kgCOD m^{-3}_{sponge} d^{-1}). Such effect can be associated with a reduction in the specific surface area and consequently surface adsorption, which is the first step in the sequence of organic matter degradation in sponge-bed trickling filters.

Finally, it is worth noting that significant coliforms removal occurs in SBTF systems (up to 4.2 log units in a demo-scale set-up, see Bressani-Ribeiro et al. (2017)). This is probably associated with the mechanism of adsorption followed by predation in the SBTF (Tawfik et al., 2006a).

Table 2.5 Main characteristics and performance of sponge-bed trickling filters following UASB reactors (and followed by secondary settlers)

Scale	TF characteristics			Operational conditions			TF influent concentrations				TF effluent concentrations [removal efficiencies - %]				Removal rate of NH_4^+-N	References
				Applied loads												
	Support media [pore (mm)]	Sponge volume (m^3) [Sponge filling ratio - %]	Height (m)	kgCOD m^{-3}_{sponge} d^{-1}	kgTKN m^{-3} d^{-1}	HLR (m^3 m^{-2} d^{-1})	COD (mg L^{-1})	TSS (mg L^{-1})	BOD (mg L^{-1})	NH_4^+ (mg L^{-1})	COD (mg L^{-1})	TSS (mg L^{-1})	BOD (mg L^{-1})	NH_4^+ (m L^{-1})	gNH_4^+-N m^{-3} d^{-1}	
Pilot	Cylinders [0.3-1.0]	-	0.5	0.2	-	-	172	-	-	30	46 [73%]	-	-	2 [93%]	-	Bundy et al. (2017)
Demo	*Spongepacking* [1.0]	4.0 [40%]	3.5	2.0	0.37	11.5	218	79	123	26	83 [62%]	30 [62%]	35 [72%]	17 [44%]	84	Bressani-Ribeiro et al. (2017)[a]
Full	DHS-G3 [0.46]	27.7 [22.3%]	5.31	1.1	-	40.8	168	51	62	26	40 [76%]	11 [78%]	10 [91%]	12 [54%]	-	Okubo et al. (2016)
Full	DHS-G2	31.1 [24.7%]	5.31	2.84	-	21.0	177	53	56	-	37 [79%]	19 [64%]	6 [89%]	-	-	Okubo et al. (2015)
Pilot	DHS – G3	0.102 [53%]	4.8	1.34	-	-	63	33	15	6.9	25 [60%]	1 [97%]	2 [87%]	0.1 [99%]	81	Yoochatchaval et al. (2014)[b]
Pilot	DHS – G6 [1.6]	0.046 [33.8%]	4.0	2.03	0.41	12.2	169	44	93	25	48 [68%]	17 [51%]	12 [87%]	4 [84%]	252	Onodera et al. (2014)
Pilot	DHS – G3 [0.63]	0.86 [53%]	4.0	0.9	0.10	-	113	33	53	27	36 [68%]	12 [64%]	7 [87%]	3 [89%]	180	Onodera et al. (2013)
Demo	*Rotosponge*	1.85 [49%]	4.0	0.36	-	10	160	60	60	40	50 [69%]	20 [67%]	15 [75%]	8 [80%]		Almeida et al. (2013)
Demo	DHS – G3/G5 [0.89]	0.93-1.62 [31-54%]	-	1.4	-	14.0	147	54	-	-	78 [47%]	34 [37%]	-	-	-	Tanaka et al. (2012)[c]
Pilot	DHS – G1	2.4 E-4 [30%]	2.0	1.24	-	7.0	106	-	-	19	14 [87%]	-	-	1 [95%]	203	Uemura et al. (2012)
Pilot	DHS – G3 [0.63]	0.024 [18%]	3.5	1.84	-	7.6	169	49	84	-	50 [70%]	13 [73%]	11 [87%]	4 [83%]	115	Mahmoud et al. (2011)[d]
Pilot	DHS – G3 [0.63]	0.024 [18%]	3.5	3.2	-	10.1	-	-	-	-	74 [61%]	-	-	~15 [49%]	-	Mahmoud et al. (2011)
Pilot	DHS – G3 [0.63]	0.024 [18%]	3.5	4.8	-	15.2	-	-	-	-	94 [52%]	-	-	~20 [27%]	-	Mahmoud et al. (2011)
Pilot	DHS – G3 [0.63]	0.024 [18%]	3.5	6.2	-	30.3	-	-	-	-	128 [34%]	-	-	~25 [13%]	-	Mahmoud et al. (2011)
Demo	DHS – G3	4.3 [31%]	3.0	-	-	-	94	37	41	-	68 [28%]	45 [-21%]	8 [80%]	-	-	Takahashi et al. (2011)[c]

Scale	TF characteristics			Operational conditions			TF influent concentrations				TF effluent concentrations [removal efficiencies - %]				Removal rate of NH_4^+-N	References
				Applied loads												
	Support media [pore (mm)]	Sponge volume (m^3) [Sponge filling ratio - %]	Height (m)	kgCOD m^{-3}_{sponge} d^{-1}	kgTKN m^{-3} d^{-1}	HLR (m^3 m^{-2} d^{-1})	COD (mg L^{-1})	TSS (mg L^{-1})	BOD (mg L^{-1})	NH_4^+ (mg L^{-1})	COD (mg L^{-1})	TSS (mg L^{-1})	BOD (mg L^{-1})	NH_4^+ (m L^{-1})	gNH_4^+-N m^{-3} d^{-1}	
Pilot	DHS – G3	0.05 [38.2%]	3.5	2.0	0.29	14.6	226	50	-	28	41 [82%]	33 [67%]	-	4 [86%]	199	Tawfik et al. (2010)
Pilot	DHS – G3 [0.63]	0.133 [18%]	3.5	3.4	-	7.6	287	-	-	21	121 [58%]	-	-	6 [72%]	180	Mahmoud et al. (2010)
Full	DHS – G2	31.1 [24.7%]	5.31	-	-	-	166	66	53	26	33 [80%]	8 [88%]	6 [89%]	5 [81%]	-	Uemura and Harada (2010)[e]
Demo	*Rotosponge*	1.90 [49%]	4.20	0.11-0.37	-	10-12	170	40	58	-	80 [53%]	10 [75%]	20 [66%]	-		Chernicharo and Almeida (2011)
Pilot	DHS – G3 [0.63]	0.0516 [38%]	3.5	1.6	0.27	12.1	-	-	-	-	-	-	8	3 [88%]	196	Tawfik et al. (2008)
Pilot	DHS – G3 [0.63]	0.0516 [38%]	3.5	2.6	0.36	16.3	-	-	-	-	63	[88%]	21	8 [59%]	204	Tawfik et al. (2008)
Pilot	DHS – G5 [0.63]	0.480 [55%]	4.0	2.17	0.28	11.0	227	41	136	23	62 [73%]	18 [56%]	17 [88%]	9 [61%]	117	Tandukar et al. (2007)
Pilot	DHS – G3[0.63]	0.0516 [38%]	3.5	1.6	0.13	12.1	178	47	67	21	43 [75%]	12 [75%]	2.3 [97%]	3 [86%]	180	Tawfik et al. (2006a)
Pilot	DHS – G2	0.051	2.0	2.03	-	14.6	167	71	55	40	65 [61%]	28 [61%]	4 [93%]	20 [50%]	240	Tandukar et al. (2006a)
Pilot	DHS – G2	0.051	4.0	3.15	-	20.9	173	75	68	37	69 [60%]	40 [47%]	9 [87%]	10 [73%]	498	Tandukar et al. (2006a)
Pilot	DHS – G4	0.38 [39%]	4.0	2.40	0.49	18.0	-	-	-	-	46 [76%]	17 [74%]	8	[28%]	-	Tandukar et al. (2006b)
Pilot	DHS – G4	0.375 [39%]	4.0	2.34	0.48	18.0	195	66	78	25	46 [76%]	17 [74%]	9 [88%]	18 [28%]	84	Tandukar et al. (2005)
Pilot	DHS – G2	-	-	-	-	-	161	56	51	39	68 [62%]	46 [39%]	10 [83%]	15 [61%]	-	Machdar et al. (2000)
-	-	**18%-55% [34%]**	**2.0-5.3 [3.5]**	**0.9-6.2 [2.1]**	**0.1-0.49 [0.29]**	**7-30.3 [14.6]**	**63-227 [169]**	**33-75 [50]**	**15-136 [56]**	**6.9-40 [26]**	**14-128 [56]** ***[68%]***	***[67%]***	***[87%]***	***[73%]***	**81-498 [188]**	Observed ranges (efficiency in italic) [median]

*G1 to G6 are different configurations of the Downflow Hanging Sponge. [a] Operation under a typical full-scale flow regime, without secondary settler; [b] TF directly receiving diluted sewage (BOD between 20 and 50 mg L^{-1}); [c] Operation with mechanical ventilation; [d] Polyurethane sponge was placed in the settler compartment of the UASB reactor, improving TSS removal; [e] Operation with recirculation (R=1).

2.3.3 Empirical models for predicting the performance of trickling filters following UASB reactors

BOD removal estimation. Empirical models predicting effluent BOD concentrations or BOD removal efficiencies are available for trickling filters preceded by primary settlers (Daigger et al., 2011; WEF, 2010). However, because UASB effluents tend to present lower readily biodegradable organic matter, such models should be handled with caution when dealing with UASB reactor effluents (Chernicharo, 2001). In any case, extrapolations outside the operational range should be avoided (Rittmann and McCarty, 2001).

The classic empirical models available for the prediction of rock-bed trickling filter performance following primary settlers are: (i) National Research Council (NRC) model for BOD removal efficiency; (ii) Galler-Gotaas model for BOD effluent concentration; and (iii) Eckenfelder model for BOD effluent concentration. Detailed descriptions and evaluations of these and other equations for TFs performance prediction are presented in the Manual of Practice n. 868. Some of the developed equations consider a number of empirical coefficients related to trickling filters preceded by primary settlers, using plastic-based support media. However, most of the trickling filters following UASB reactors are currently filled with crushed stones, and operational data from plastic-bed trickling filters are seldom available, as previously discussed. Table 2.6 presents the equations typically used to design rock-bed trickling filters preceded by primary settlers and the parameters considered for the empirical relations.

Table 2.6 Equations typically considered to estimate rock-bed trickling filters performance following UASB reactors.

Empirical model	Equation	Comments
NRC formula *Currently used to estimate the performance of BOD removal in TFs following UASB reactors	$E = \frac{1}{1+0.4432\sqrt{\frac{OLR}{F}}}$ *E* = BOD removal efficiency ratio at 20 °C OLR = Organic loading rate (kgBOD m^{-3} d^{-1}) *F* = recirculation factor (1 + $Q_{recycle}/Q_{influent}$), where F = 1, if $Q_{recycle}$ = 0	▪ For the model development, several operational data from rock-bed trickling filters were statistically analysed. The systems operated essentially treating relatively high concentrated sewage from military bases. ▪ Basically developed to estimate the BOD removal efficiency as a function of organic loading rate and effluent recirculation. ▪ The formula does consider the effect of secondary clarifiers.
Galler-Gotaas formula	$E = \frac{K(v \cdot S_{in} + v^r \cdot S_{efl})^{1.19}}{(v+v^r)^{0.78} \cdot (0.305+h)^{0.67} \cdot r^{0.25}}$ $K = \frac{0.57}{v^{0.28} \cdot T^{0.15}}$ *E* = BOD removal efficiency ratio at 20 °C *v* = hydraulic loading rate (m^3 m^{-2} d^{-1}) v^r = recycle loading rate (m^3 m^{-2} d^{-1}) S_{in} = influent BOD concentration (mg L^{-1}) S_{efl} = effluent BOD concentration (mg L^{-1}) *h* = filter height (m) *r* = radius of the filter (m) *T* = temperature (°C)	▪ Developed from multiple regression analysis based on an extensive database of sewage treatment plants. ▪ The formula allows the inclusion of geometry effect, hydraulic and organic loadings, and effluent recycling. ▪ Include intrinsic exponents not easily handled for analytical calibrations.
Eckenfelder formula *Proposed formula to estimate BOD concentration	$S_{efl} = S_{in}{}^0 \, exp\left[\frac{-k \, . \, h^{(1-m)}}{(Q/A)^n}\right]$ S_{in} = influent BOD concentration (g m^{-3}) S_{efl} = effluent BOD concentration (g m^{-3}) A = plan-view area (ft^2) *h* = packing height (ft) Q = flow rate (gallons.min^{-1}) *k* = factor for effluent treatability *n* = filter media exponent *m* = slime distribution factor (*m* = 0 if evenly distributed)	▪ The semi-empirical formula considering BOD removal as a first-order function along the tricking filter. ▪ The equation considers the effect of the wastewater treatability, also including the effect of geometry, hydraulic and flow rates. ▪ **Because wastewater treatability (*k*) and filter medium (*n*) are variables directly included, when properly calibrated, the equation might be potentially applied to design trickling filters following UASB reactors, even when innovative support media are considered (e.g., sponge-based media).**

Figure 2.4 presents a comparison of predicted final effluent BOD concentrations considering the usual operative range for trickling filters following UASB reactors. Typical values (Bressani-Ribeiro et al., 2017) of effluent BOD_{UASB} concentrations (105 mg BOD L^{-1}), organic loading rate (0.58 kg BOD m^{-3} d^{-1}), hydraulic loading rate (13.6 m^3 m^{-2} d^{-1}), and reactor height (2.5 m) were used to implement the graphical representation. It was assumed that the UASB effluent and biofilm formation was evenly distributed (slime distribution factor - m = 0).

The empirical relation from Galler-Gotaas seems to considerably underpredict the final BOD effluent concentrations, whereas NRC and Eckenfelder equations tend to

overpredict the trickling filter performance. The low adherence of the model results to the expected effluent BOD concentration (based on practical experiences) is possibly related to the fact that the models have been developed for trickling filters preceded by primary settlers. However, the largest portion of readily biodegradable organic matter is consumed in the anaerobic step, which may reflect on the performance of trickling filters following UASB reactors.

The Eckenfelder formula seems to provide a good estimation for BOD concentration in the final effluent, provided a simple calibration for the effluent treatability factor (*k*) is performed. When properly calibrated, the equation might be potentially applied to the design of trickling filters after UASB reactors, as observed in a preliminary fitting plant data from a full-scale UASB-trickling filter system (data not shown). As the Eckenfelder semi-empirical equation considers an exponent related to the support media used, it could be applied even when innovative support media is adopted (e.g., sponge-based media). Although the NRC formula may provide a reasonable approximation for final BOD concentrations, more efforts should be directed to determine a typical range for filter media (*n*) and effluent treatability factor (*k*) related to trickling filters treating UASB reactors effluents.

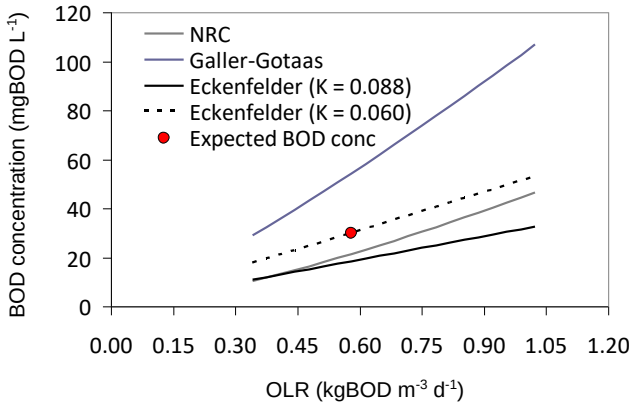

Figure 2.4 Graphical representation of empirical and semi-empirical relations for a typical organic loading range applied to trickling filters following UASB reactors. *The expected effluent BOD concentration (in red) is based on practical experiences*

2.4 Sponge-bed trickling filters post-UASB reactors: future challenges

The future challenges regarding effluent quality improvement and further simplification of construction, operation, and maintenance of SBTFs post-UASB reactors seem to be

related to two main topics: (i) elimination of secondary settlers; and (ii) establishing the best design and operational condition for innovative nitrogen removal. These aspects are addressed below.

2.4.1 Flowsheet simplification via elimination of secondary settlers

One of the main advantages of using sponge-based packing media relates to less stringent construction requirements of the TF tank compared to rock-based systems, achieved by implementing a self-structured medium. From the treatment process standpoint, the use of sponges allows the retention of microorganisms for longer periods at higher hydraulic retention time for the same bed volume compared with rock or plastic-bed TFs (Almeida et al., 2013). Moreover, no additional operational strategies (e.g., recirculation of the final effluent) are needed to meet the discharge standards generally adopted in developing countries or even additional procedures to overcome clogging issues or improve the wetting efficiency.

Furthermore, the increase in solids retention time (SRT) provided by the sponge media leads to high levels of endogenous respiration rate, which contributes to a low total suspended solids (TSS) load in the effluent (Table 2.7). In fact, TSS removals around 70 – 90% are reported from full-scale experiences (Okubo et al., 2015). Excess sludge produced in SBTFs following UASB reactors reported in the literature is shown in Table 2.7.

Low excess sludge production in SBTFs post-UASB reactors can be observed. Additionally, even for simplified UASB/SBTF flowsheets (without secondary settlers), low median values have been reported (0.28 kgTSS $kgCOD^{-1}_{removed}$). In fact, a relatively low excess of sludge is produced in SBTF systems when compared to the typical range of 0.25 – 0.88 kgTSS $kgCOD^{-1}_{removed}$ for aerobic processes (activated sludge, rotating biological contactors, submerged aerated biofilters, high-rate trickling filters) following UASB reactors (Metcalf & Eddy, 2013; Gonçalves et al., 2001; Tandukar et al., 2007; Gonçalves et al., 1998). Moreover, the typical yield of excess sludge from the conventional suspended growth process (i.e., activated sludge) ranges from 0.4 to 1.7 kgTSS $kgCOD^{-1}_{removed}$ (Metcalf & Eddy, 2013).

Table 2.7 Excess sludge production and effluent TSS loads in UASB/SBTF systems with and without secondary settlers.

SRT (d)	HRT (h)	OLR (kgCOD m^3_{sponge} d^{-1})	Excess sludge production (kgTSS $kgCOD^{-1}_{removed}$)	Effluent TSS load (kgTSS $m^{-3}_{reactor}$ d^{-1})	Secondary settler (Sset)	Reference
-	1.2	0.8	0.16	0.09	Without Sset	Bressani-Ribeiro (2015)
-	2.0	0.82-1.33	0.06-0.20[a]	0.05		Almeida et al. (2013)
-	-	0.76[b]	0.38	-		Almeida et al. (2011)
168	2.7	1.6	0.09	0.04		Tawfik et al. (2006a)
47	2.0	2.03	0.08	0.07	With Sset	Onodera et al. (2014)
> 135	3.2	0.85	0.18	0.05		Onodera et al. (2013)
38	2.9	6.8	0.39	-		Tawfik et al. (2011)[c]
64	5.8	3.6	0.26	-		Tawfik et al. (2011)[c]
109	11.7	1.9	0.19	-		Tawfik et al. (2011)[c]
69	-	-	0.06	-		Uemura and Harada (2010)
-	-	0.43	0.45	1.49		Almeida (2007)
-	-	0.24	0.26	0.61		Almeida (2007)
90-125	2.5	2.17	0.10	0.09		Tandukar et al. (2007)
90-100	1.3-4.0	2.03-3.15	0.27-0.4[d]	0.07-0.30		Tandukar et al. (2006a)
38-135 [82]	**1.3-11.7 [3.1]**	**0.24-6.80 [2.03]**	**0.06-0.45 [0.19]**	**0.05-1.49 [0.07]**	Typical range: flowsheet with Sset [median]	
-	**2.0-2.7 [2.4]**	**0.82-1.60 [1.47]**	**0.09-0.38 [0.28]**	**0.04-0.50 [0.05]**	Typical range: flowsheet without Sset [median]	

[a] kgVSS $kgCOD^{-1}_{removed}$; [b] kgBOD m^{-3}_{sponge} d^{-1}; [c] DHS system treating grey water (similar to a concentrated sewage); [d] kgVSS $kgBOD^{-1}_{removed}$.

Such results could support the elimination of secondary settlers, an important advancement towards simplifying UASB/SBTF systems, as schematically shown in Figure 2.5. Studies at demonstration scale (population equivalent: 300-500 inhabitants) indicate that the conditions to design a UASB-trickling filter system without secondary settlers are compatible with the organic loadings required to improve nitrification in the post-treatment step (Almeida et al., 2009). In this case, the use of sponge-based support media tends to significantly improve the reliability of the system complying with discharge standards (Almeida, 2012). Thus, for less stringent discharge standards and low-skilled personnel for operation, the design of UASB/SBTF systems without secondary settlers is a very promising alternative. Furthermore, no additional sidestream units are required for sludge thickening and digestion.

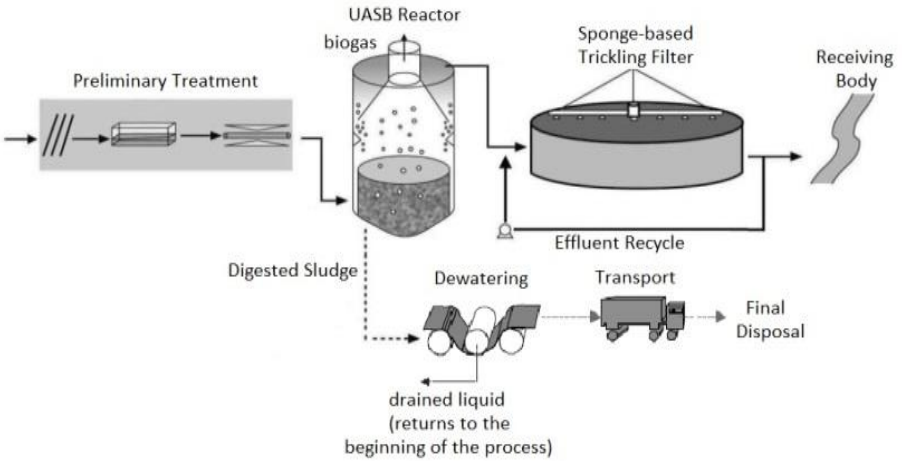

Figure 2.5 UASB/SBTF system without secondary settlers. *Reproduced and adapted from von Sperling and Chernicharo (2005) with permission from IWA Publishing, copyright 2005*

In order to effectively implement such a proposed flow-sheet simplification, the aforementioned design criteria (section 2.3.1) should be taken into account. In addition, effluent TSS_{UASB} concentration should be kept below 100 mg L^{-1} avoiding solids overload in the post-treatment step (Almeida et al., 2013; Bressani-Ribeiro et al., 2017). Thus, to operate UASB-sponge-bed trickling filters without secondary clarifiers, the anaerobic sludge management needs to be very established to avoid solids washout. For UASB/SBTF systems without secondary settlers, typical overall removal efficiencies obtained are 88 – 97% for BOD, 80 – 87% for COD, 78 – 91% for TSS, and 44 – 95% for NH_4^+-N (Almeida et al., 2013; Bressani-Ribeiro et al., 2017; Chernicharo and Almeida, 2011). Corresponding effluent concentrations are less than 90 mg L^{-1} for COD, less than 40 mg L^{-1} for BOD and TSS, and less than 20 mg L^{-1} for NH_4^+-N. These average values tend to meet environmental discharge standards in developing countries (e.g., in Brazil).

UASB/SBTF systems without secondary settlers could be made even more compact by implementing the UASB reactor and the SBTF in a single treatment module (i.e., the SBTF is installed right next to the anaerobic reactor, profiting its walls, as in Bressani-Ribeiro *et al.*, 2017). Such an option is mainly suitable either for sewage treatment in small communities or as a decentralized option in densely populated regions, since its area requirement is less than 0.05 m^2 $inhabitant^{-1}$. To manage the solid phase (i.e., anaerobic excess sludge), simplified dewatering units (i.e., drying beds) can be implemented.

2.4.2 Mainstream nitrogen removal considering heterotrophic denitrification or anammox process

The effective and reliable establishment of simultaneous removal of residual organic carbon and nitrogen in the post-treatment step preceded by UASB reactors has been contextualized as a possibility (Ikeda et al., 2013; Sánchez-Guillén et al., 2015a; Leal et al., 2016). Promising strategies have been reported in literature considering two different metabolic pathways for nitrogen removal: denitrification and/or anammox process. The main operational aspects of each process are summarized in Table 2.8.

2.4.2.1 N-removal via heterotrophic denitrification

Nitrogen removal in fully ventilated sponge-bed trickling filters (SBTFs) without effluent recirculation is typically between 25 and 35% (Tandukar et al., 2006b; Onodera et al., 2014). Such conditions have also been observed by Almeida et al. (2013) and Bressani-Ribeiro (2017), in which an increase in organic loadings led to greater N-removal. It could be associated with a substrate input (residual carbon from the UASB reactor) which may increase the activity of heterotrophs in anoxic zones of the biofilm in the presence of oxidized forms of nitrogen. When applying final effluent recirculation, N-removal could be enhanced up to values between 60 and 65% (Onodera et al., 2016; Ikeda et al., 2013), since it promotes the contact of residual carbon from the UASB reactor with the nitrate produced at the nitrifying portion of the SBTF. N-removal efficiencies around 75% have been reported, considering the by-pass of a fraction of pre-settled sewage (which contains readily biodegradable COD) to anoxic compartments of SBTFs (Bundy et al., 2017). The heterotrophic denitrification was reported to be the predominant process in all these studies. Considering the inner sponge anoxic conditions (Machdar et al., 2000), as well as the typical low F/M ratio (0.032 gCOD gVSS d^{-1}) and high sludge retention time (~100 d), the endogenous respiration might be related to heterotrophic denitrification within the DHS system (Tandukar et al., 2006b; Araki et al., 1999). Thus, the use of an additional source of organic matter by heterotrophs in anoxic zones could also contribute to explaining how a sponge-bed trickling filter produces effluents with low solids concentration, even operating without secondary settlers (Onodera et al., 2013), as previously discussed in Tandukar et al. (2006a). However, because of the anoxic zones within the sponges, and long SRT, the hypothesis that the activity of anaerobic ammonium oxidizing

bacteria (anammox bacteria) was a factor for nitrogen removal cannot be eliminated, as discussed in Almeida et al. (2013).

2.4.2.2 N-removal via anammox process

The partial nitritation in SBTFs under controlled ventilation conditions was proposed by Chuang et al. (2007). The purpose was to further provide a proper environment for anammox bacteria colonization. High N-removal efficiencies were obtained (70 – 95%), and effluent recirculation (1:3) was applied to ensure proper support media wetting (Chuang et al., 2008). Aiming at establishing the cultivation of anammox bacteria in SBTFs, Sánchez Guillén et al. (2015a) developed a study following a methodological approach similar to that used by Chuang et al. (2008). In this case, the performance for N-removal stayed around 75 – 80% for temperatures between 20 – 30 ºC (effluent recirculation 1:1). Considering these promising results, research aiming at establishing simultaneous partial nitritation-anammox was developed (Sánchez-Guillén et al., 2015b). Nevertheless, the N-removal was limited to 54%. In this proof-of-concept experiment, uncontrolled oxygen supply from passive aeration was probably a factor lowering TN removal efficiency. Therefore, it seems that in this case, ammonium oxidizers could not out-compete nitrite oxidizers. Regardless of such performance obtained by Sánchez-Guillén et al. (2015b), the study clearly showed the potential of sponge-bed trickling filters for TN removal via anammox process.

Table 2.8 Nitrogen removal in SBTFs: heterotrophic denitrification and anammox process.

Reference	Effluent	HRT (h)	Influent to the SBTF (mg L^{-1})	N loads (kgN m^{-3} d^{-1})		N removal (%)	Main aspects
				Applied	Removed		
Conventional nitrogen removal through (autotrophic) nitrification and heterotrophic denitrification							
Machdar et al. (2000) *Pilot-scale*	Anaerobic (UASB reactor)	2.0	COD:161 TN: 51	-	-	25-31	• System designed for C and NH_4^+-N removal post-UASB reactor.
Onodera et al. (2013) *Pilot-scale*	Anaerobic (UASB reactor)	3.2	COD:113 TN: 30	0.23	0.07	30	• DHS post-UASB reactor (without recirculation). Heterotrophic denitrification was associated with biomass decay (endogenous respiration).
Almeida et al. (2013) *Demo-scale*	Anaerobic (UASB reactor)	2.0	COD: 200 TN:45	0.44	0.11-0.31	25-70	• System designed for C and NH_4^+-N removal post-UASB reactor. Higher performance for N-removal with increased OLR or effluent recirculation.
Ikeda et al. (2013) *Pilot-scale*	Synthetic	12.0 (4/reactor)	COD: 600-1800 TN: 500	1.00	0.20-0.60	20-60	• Unusual configuration for sewage treatment, due to the high HRT.
Bundy et al. (2017) *Pilot-scale*	Pre-settled sewage	0.6-1.2	COD: 170-220 TN: 40-48	-	-	40-74	• Reactor with an aerobic volume followed by a submerged anoxic compartment and effluent recirculation. Part of the pre-settled sewage was sent to the anoxic compartment.
Onodera et al. (2016) *Full scale*	Anaerobic (UASB reactor)	1.5	COD: 177 TN: 26	0.42	0.33	65	• Full-scale DHS system post-UASB reactor, with effluent recirculation (1:1).
Innovative nitrogen removal predominantly based on the anammox conversion							
Chuang et al. (2008) *Pilot-scale*	Synthetic	0.7-2.0	COD: non-applied TN: 40	1.94-2.98	1.84-2.01	68-95	• Operation with anammox process (with recirculation), receiving NH_4^+-N and NO_2^--N.
Sánchez-Guillén et al. (2015a) *Pilot-scale*	Synthetic	1.14-2.23	COD: non-applied TN: 100	2.10-2.15	1.52-1.60	74-78	• Operation with anammox process (with recirculation), receiving NH_4^+-N and NO_2^--N.
Sánchez-Guillén et al. (2015b) *Pilot-scale*	Synthetic	1.71-2.96	COD: non applied TN: 100-110	1.68-0.95	0.77-0.88	52-54	• Operation with partial nitritation and anammox process (without recirculation).

2.5 Conclusions and perspectives

The replacement of primary settlers by UASB reactors in the technological flowsheet of trickling filters for sewage treatment has brought remarkable advantages, mainly in terms of construction simplification and operational requirements associated with sludge handling. Following this important step, improving the performance of trickling filters by implementing sponge-based support media has shown to be an interesting strategy. In this case, better system performance is associated with greater biomass retention and higher hydraulic retention time compared to conventional rock and plastic-bed trickling filters. Additionally, a self-structured support media can further simplify the construction, operation, and maintenance of SBTFs.

The design of sponge-bed trickling filters following UASB reactors for simultaneous removal of residual carbon and ammonium should be currently based on practical experiences due to the uncertainties regarding operational conditions and the system's performance. Therefore, adopting a loading criterion (0.20 – 0.40 kgBOD $m^{-3}_{reactor}$ d^{-1}), the hydraulic retention time needs to be verified for the usual range (1.5 to 2.5 h). In terms of predicting effluent BOD concentrations or BOD removal efficiencies for TFs post-UASB reactors, the available models still have to be properly adjusted to allow direct application. In this case, the Eckenfelder model could be further improved, taking into account data from full-scale trickling filters following UASB reactors.

Future efforts to improve UASB/SBTF technology should consider heterotrophic denitrification as a possible strategy for N removal, considering final effluent recirculation. On the other hand, since the sponge-based media tends to increase the SRT to more than 100 days, the use of anammox process might be a promising alternative if the interaction of heterotrophic and autotrophic microorganisms can be managed by simply controlling the oxygen supply within the SBTF.

Additionally, to the best of our knowledge, the conditions for UASB/SBTF operating without secondary settlers are not yet fully established, mainly because it requires rigorous sludge management control in the anaerobic reactor. Hence, low anaerobic reactor performance, typically ascribed to poor operation and management, can jeopardize the advantages of the integrated UASB/SBTF system, especially

considering the proposed simplified flowsheet, in which secondary settlers are not implemented.

Acknowledgements

The authors acknowledge the support obtained from Ghent University Special Research Fund (BOF UGent - Funding for joint doctorate) and from the following Brazilian institutions: Conselho Nacional de Desenvolvimento Científico e Tecnológico – CNPq; Fundação de Amparo à Pesquisa de Minas Gerais – FAPEMIG; Instituto Nacional de Ciência e Tecnologia em Estações Sustentáveis de Tratamento de Esgoto – INCT ETEs Sustentáveis.

Chapter 3

Inorganic carbon limitation during nitrogen conversions in sponge-bed trickling filters for mainstream treatment of anaerobic effluent

3.0 Abstract

Anaerobic sewage treatment is a proven technology in warm climate regions, and sponge-bed trickling filters (SBTFs) are an important post-treatment technology to remove residual organic carbon and nitrogen. Even though SBTFs can achieve a reasonably good effluent quality, further process optimization is hampered by a lack of mechanistic understanding of the factors influencing nitrogen removal, notably when it comes to mainstream anaerobically treated sewage. In this study, the factors that control the performance of SBTFs following anaerobic (i.e., UASB) reactors for sewage treatment were investigated. A demo-scale SBTF fed with anaerobically pre-treated sewage was monitored for 300 days, showing a median nitrification efficiency of 79% and a median total nitrogen removal efficiency of 26%. Heterotrophic denitrification was limited by the low organic carbon content of the anaerobic effluent. It was demonstrated that nitrification was impaired by a lack of inorganic carbon rather than alkalinity limitation. To properly describe inorganic carbon limitation in models, bicarbonate was added as a state variable, and sigmoidal kinetics were applied. The resulting model was able to capture the overall long-term experimental behaviour. There was no nitrite accumulation, which indicated that nitrite oxidizing bacteria were little or less affected by the inorganic carbon limitation. Overall, this study indicated the vital role of influent characteristics and operating conditions concerning nitrogen conversions in SBTFs treating anaerobic effluent, thus facilitating further process optimization.

This chapter has been published as

Bressani-Ribeiro, T., Almeida, P.G.S., Chernicharo, C.A.L. and Volcke, E.I.P. (2021) Inorganic carbon limitation during nitrogen conversions in sponge-bed trickling filters for mainstream treatment of anaerobic effluent. Water Research 201, 117337.

3.1 Introduction

Anaerobic sewage treatment using Upflow Anaerobic Sludge Blanket (UASB) reactors has been widely implemented in warm climate regions (Chernicharo et al., 2015). For instance, such technology comprises approximately 40% of the 2,300 sewage treatment plants currently in operation in Brazil (ANA, 2020). This refers to mainstream anaerobic treatment (i.e., directly applied to the main flow of sewage) rather than more common applications of anaerobic digestion for sidestream process (i.e., sludge digestion). UASB reactors remove organic components from sewage and turn them into biogas, a renewable energy source. The amount of excess sludge produced is low compared to aerobic processes. While anaerobic treatment converts organic carbon, it does not remove nitrogen, which leaves the UASB reactor mainly in the form of ammonium. Additional (aerobic) treatment is thus required to remove nitrogen from the anaerobic effluent. Sponge-bed trickling filters (SBTFs) have been successfully applied for this purpose, mostly at pilot and demo-scales (Bressani-Ribeiro et al., 2017; Onodera et al., 2013), but also at full-scale (Okubo et al., 2016). SBTFs can be regarded as trickling filters packed with polyurethane sponge as a support media for biomass growth and were first proposed in the late ’90s (Agrawal et al., 1997). Such reactors can achieve an excellent effluent quality in terms of residual organic carbon and ammonium removal, with little or very low energy consumption and involving simple equipment, operation, and maintenance (Tandukar et al., 2007). Still, there is a lack of knowledge regarding the influence of influent characteristics and operating conditions on nitrogen removal in SBTFs treating anaerobic effluent, which hampers further process optimization.

Mathematical modelling could help unravel the governing factors driving the nitrogen removal pathways in SBTFs. Modelling and simulation have proven to be powerful tools to assess the most critical parameters influencing autotrophic nitrogen removal in biofilm reactors (Picioreanu et al., 1997; Hubaux et al., 2015; Volcke et al., 2010). However, the latter simulation studies deal with sidestream conditions associated with high-strength nitrogenous wastewater (> 1000 mg N L^{-1}). Only a few studies relate to mainstream autotrophic nitrogen removal, considering the interaction among ordinary heterotrophs (OHO), ammonium- and nitrite-oxidizing bacteria (AOB and NOB), and anaerobic ammonium-oxidizing bacteria (Al-Omari et al., 2015; Trojanowicz et al.,

2019). Other studies dealing with biofilm reactors for mainstream sewage treatment are mostly connected with aerobic processes such as high-rate activated sludge (Roots et al., 2020), sequencing batch reactors (SBR) (Drewnowski et al., 2021), and moving-bed biofilm reactors (MBBR) (Laureni et al., 2019). To the best of our knowledge, no models have been applied so far to describe nitrogen conversions from mainstream anaerobically treated effluents.

Inorganic carbon is an important factor influencing nitrogen removal in sewage treatment plants. It is directly associated with alkalinity, as most of the total inorganic carbon is in the form of bicarbonate, given the typical neutral pH conditions in anaerobically treated effluents. The dynamics of AOB have been reported to change significantly under inorganic carbon limitation while NOB activity remains stable (Guisasola et al., 2007; Ma et al., 2015; Zhang et al., 2016). Biesterfeld et al., 2003 showed that nitrification rates are affected by an inorganic carbon shortage (below 45 mg $CaCO_3$ L^{-1}) independently from pH. Alkalinity, expressed as bicarbonate, is typically introduced in models to predict possible pH changes and to close charge balances (Rieger; et al., 2012). This is also the case for the Activated Sludge Models (from ASM1 to ASM3) (Henze et al., 2006), in which alkalinity limitation on (single-step) nitrification is described by Monod kinetics. It is important to note that the alkalinity limitation considered in these models refers to unfavourable pH conditions rather than inorganic carbon limitation. Modelling approaches considering inorganic carbon limitation effects on autotrophs have also been proposed, described with Monod or sigmoidal kinetics (Wett and Rauch, 2003; Guisasola et al., 2007; Seuntjens et al., 2018). However, the different behaviour of AOB and NOB under inorganic carbon depleted conditions is typically neglected in models. Moreover, mainstream process models typically assume that influent inorganic carbon content is sufficiently high, meaning hardly any limitation (Sin et al., 2008).

This contribution deals with mainstream nitrogen conversions in sponge-bed trickling filters (SBTF) following UASB reactors treating sewage. Long-term experimental data of a demo-scale UASB/SBTF system were gathered, indicating inorganic carbon limitation for ammonium removal. Based on these insights and available literature, a mechanistic model for mainstream nitrogen removal of anaerobically treated sewage

was developed. The model was subsequently calibrated and validated to dynamic data.

3.2 Materials and methods

3.2.1 Experimental setup – system under study

A sponge-bed trickling filter (SBTF) was operated as a post-treatment step of a UASB reactor (V: 14.1 m^3; hydraulic retention time (HRT): 8.5 h), receiving part of the anaerobic effluent. The UASB/SBTF system (Figure 3.1) was fed continuously (constant flow rate) with real sewage from a full-scale treatment plant (about 2 million population equivalent) in Belo Horizonte city (19° 54' S, 43° 56' W), Brazil, after preliminary treatment (removal of coarse solids and grit).

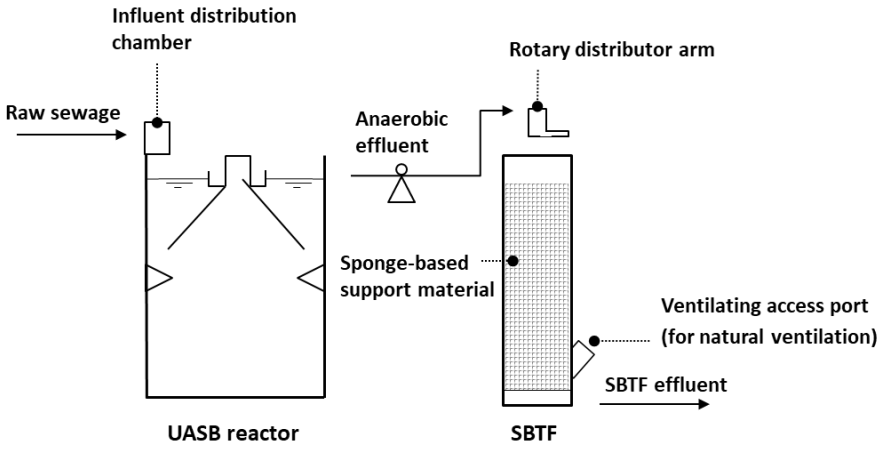

Figure 3.1 Schematic representation of the experimental UASB/SBTF set-up

The main SBTF design characteristics are summarized in Table 3.1. No inoculation was performed for the reactor start-up, and the support material consisted of a clean polyurethane sponge. The surface area of the polyurethane sponge available for biofilm growth was determined using the method proposed by Moon et al., 2010, which relies on the number and diameter of sponge fibres assessed through scanning electron microscopy (FEI Quanta 200 FEG) (detailed in Appendix, Section A.3.2).

The SBTF operation resembled a classical operation of a low- to intermediate-rate trickling filter following a UASB reactor, in which the effluent was distributed on top of the unit by rotary arms and trickled down to the bottom. Nevertheless, the UASB/SBTF system under study operated without a secondary settler, resulting in a compact system as proposed previously (Almeida et al., 2009; Onodera et al., 2016). For

oxygen supply, the bottom ventilating access port of the SBTF (see Figure 3.1) was kept fully open. The vent area was equivalent to the total required area for natural-draft trickling filters (Metcalf & Eddy, 2013).

Table 3.1 Design parameters of the sponge-bed trickling filter under study

Parameter	Value	Unit
Useful height (H)	3.91	m
Cross-section area (A)	0.25	m^2
Reactor volume (V)	0.98	m^3
Influent flow rate (Q)	2.5	$m^3\ d^{-1}$
Surface hydraulic loading rate (HLR_s)[a]	10	$m^3\ m^{-2}\ d^{-1}$
Sponge filling ratio (FR)[b]	40	%
Total sponge volume (V_{sponge})	0.39	m^3
Specific surface area of the sponge (a_s)[c]	6,600	$m^2\ m^{-3}$

[a] HLRs = Q/A; [b] Ratio between sponge volume and reactor volume; [c] Determined as detailed in Section A.3.2.

Additionally, five different sewage treatment plants (STPs) with full-scale UASB reactors (population equivalent from 10,000 up to 1,000,000 inhabitants) in the state of Minas Gerais, Brazil, were intensively monitored between July and September 2018. Composite samples were collected twice weekly. Bicarbonate alkalinity (as $CaCO_3$) and NH_4^+-N concentrations were determined according to the Standard Methods for the Examination of Water and Wastewater (Baird and Bridgewater, 2017).

3.2.2 Influent characteristics

The UASB/SBTF system was monitored for 300 days. Weekly grab samples were collected, and the following parameters were measured according to the Standard Methods for the Examination of Water and Wastewater (Baird and Bridgewater, 2017): COD_{total}, $COD_{filtered}$ (0.45 µm), TSS, VSS, bicarbonate alkalinity (as $CaCO_3$), NH_4^+-N, NO_2^--N, and NO_3^--N. Total nitrogen (TN) was determined using a TOC/TN analyser (Shimadzu TOC-VCPH-TNM-1). Field analysis of dissolved oxygen (DO), pH, and temperature were carried out using a multiparametric sensor (Hach HQ 40D).

A spreadsheet is provided concerning the dynamic effluent dataset of the monitored UASB/SBTF system (detailed in Appendix - section A.3.8).

3.2.3 Model development

3.2.3.1 Biological conversions

A mechanistic one-dimensional biofilm model was developed to describe the behaviour of an SBTF following a UASB reactor treating real sewage. Biological conversion reactions were based on the model of Mozumder et al. (2014) (detailed in Appendix, Section A.3.1). Given the indication for inorganic carbon limitation in this study, bicarbonate was included as a limitation term in the kinetic expressions for the growth of autotrophs. Therefore, bicarbonate accounted for neutralizing protons generated during the nitritation process, as well as a source of inorganic carbon for cell synthesis and growth (see further). Ammonification was added to the model accounting for the conversion of organic nitrogen present in the anaerobic effluent fed to the SBTF. Biomass decay was modelled to lead directly to soluble ammonium instead of soluble organic nitrogen, which is a reasonable assumption given that hydrolysis is not the rate-limiting step (Henze et al., 2006). The key catabolic processes implemented in the model are depicted in Figure 3.2. The stoichiometric matrix, kinetic expressions, and model parameter values are detailed in Tables A.3.1 – A.3.4 (Section A.3.1).

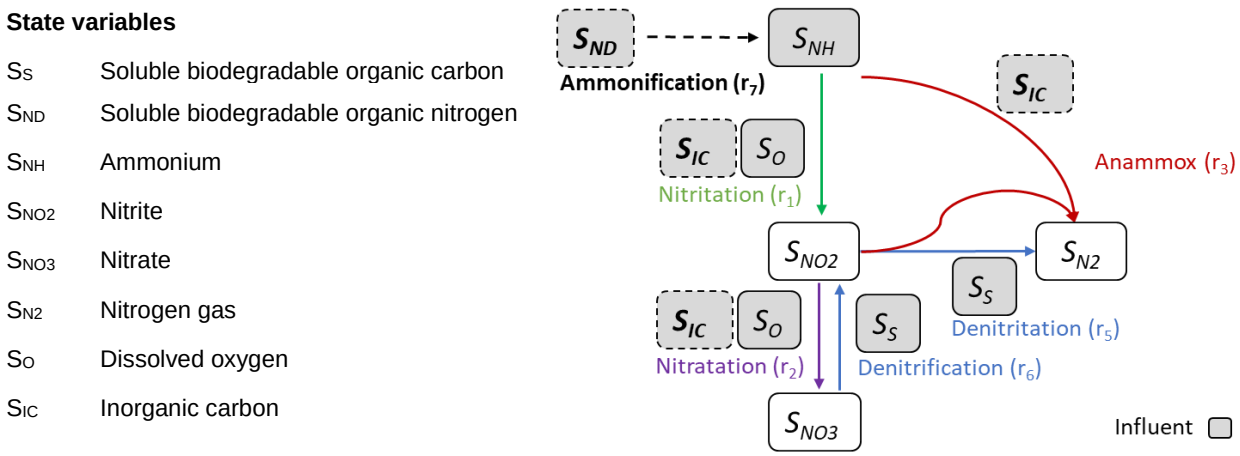

Figure 3.2 Schematic representation of the catabolic reactions related to nitrogen conversions in an SBTF reactor. *The state variables (S_{IC}, S_{ND}) and process (r_7) indicated in bold and with dashed lines denote additions to the model of Mozumder et al. (2014). Expressions for the kinetic rates r_j are given in Table A.3.2 – Section A.3.1. The grey boxes indicate variables present in the influent*

pH was not included as a state variable in the model. Indeed, for the system under study, pH stayed relatively constant, between 7.1 and 7.4 (10 – 90th percentile) (see

results – section 3.3.1). In this range, the effect of pH on nitrification rates can be neglected. The latter was confirmed by Biesterfeld et al. (2003), who showed that pH (between 7.0 and 7.5) did not correlate with nitrification rates in different full-scale nitrifying trickling filters. Similar ammonia removal rates in biofilms were reported by Zhang and Bishop, 1996 despite a pH ranging from 6.6 to 7.2. In case significant pH changes occur, pH would need to be included as a state variable in the model and could be calculated at every time instant from the charge balance in the reactor, involving all components involved in chemical equilibria. The latter include total inorganic carbon (with equilibrium forms CO_2, HCO_3^- and CO_3^{2-}), the concentration of which would then be calculated from a carbon balance. This pH calculation approach has been described in detail by Volcke (2006).

Particulate organic carbon present in the anaerobically treated sewage fed to the SBTF was assumed non-biodegradable. In addition, decayed biomass was assumed to be directly converted into S_S rather than particulate organic substrate (X_S). This assumption is supported by practical observations indicating that the hydrolysis of X_S to S_S is not a rate-limiting step in SBTFs (Tandukar et al., 2006a) as solids retention time is considerably large in the system. In mathematical terms, X_S was not taken up as a state variable in the model.

3.2.3.2 Modelling inorganic carbon limitation

Different saturation models (Monod, sigmoidal, Tessier, and Haldane kinetics – Table 3.2) have been applied in the literature to describe inorganic carbon limitation on AOB, NOB and anammox bacteria, with various parameter values (Table 3.3). The alkalinity limitation term considered in the ASM models (Henze et al., 2006) was included in the overview for reasons of completeness, even though it serves as a placeholder to indicate a threat of dropping pH rather than to describe inorganic carbon limitation. In this study, the description of inorganic carbon limitation in the model has been scrutinized following its experimental observation (see section 3.3.4).

Table 3.2 Mathematical expressions of inorganic carbon kinetic terms according to different saturation models

Saturation model	Mathematical expression	
Monod kinetics	$S_{IC}/(K_{IC} + S_{IC})$	Eq. 3.1
Sigmoidal kinetics	$e^{(SIC-k)/a}/(1+e^{(SIC-k)/a})$	Eq. 3.2
Haldane kinetics	$S_{IC}/(S_{IC} + K_{IC} + K_{IC}^2)/K_I$	Eq. 3.3
Tessier kinetics	$1-e^{(-SIC.KIC)}$	Eq. 3.4

S_{IC}: inorganic carbon; K_{IC}: inorganic carbon half-saturation coefficient (Monod kinetics); *k*: inorganic carbon saturation coefficient (Sigmoidal kinetics); *a*: sigmoidal kinetics non-dimensional parameter; K_I: inorganic carbon inhibition constant (Haldane kinetics).

Table 3.3 Coefficients of inorganic carbon limitation (expressed as mg $CaCO_3$ L^{-1}), according to different saturation models

AOB	NOB	Anammox	Reference
Monod K_{IC} = 12.5	Same as AOB	n.a.	Henze et al. (2006)[1]
Monod K_{IC} = 21.4	x	n.a.	Guisasola et al. (2007)[2]
Monod K_{IC} = 10.0	Same as AOB	n.a.	Boltz et al. (2011)[1]
n.a.	n.a.	Monod K_{IC} = 1.2	Kimura et al. (2011)[2]
Monod K_{IC} = 18.0	Monod K_{IC} = 1.2	Monod K_{IC} = 1.2	Al-Omari et al. (2015)[2]
Monod K_{IC} = 21.4	Monod K_{IC} = 1.2	n.a.	Seuntjens et al. (2018)[3]
Haldane K_{IC} = 19.3 K_I = 1,617	Same as AOB	n.a.	Denecke and Liebig (2003)[1]
Tessier K_{IC} = 7.7	x	n.a.	Guisasola et al. (2007)[2]
Sigmoidal *k* = 50.0 *a* = 10.0	Same as AOB	n.a.	Wett and Rauch (2003)[2]
Sigmoidal *k* = 13.3 *a* = 6.8	x	n.a.	Guisasola et al. (2007)[2]
Sigmoidal *k* = 13.3 – 50.0 *a* = 6.8 – 10.0	Sigmoidal *k* = 1.2 *a* = 6.8	n.a.	Seuntjens et al. (2018)[3]
Sigmoidal *k* = 31 *a* = 5	Monod K_{IC} = 1.2	Monod K_{IC} = 1.2	This study

n.a.: not applicable (species was not considered in the model); x: no inhibition

[1]Values originally expressed as mol equiv HCO_3 m^{-3}. Converted to mg $CaCO_3$ m^{-3} considering a conversion factor of 50 g (mol equiv)$^{-1}$.

[2]Values originally referred to total inorganic carbon concentrations as mg C L^{-1} (or mmol C L^{-1}). Assumed, therefore, to equal the total inorganic carbon concentration expressed as mg $CaCO_3$ m^{-3}.

[3]Seuntjens et al. (2018) considered values for AOB derived from Guisasola et al. (2007) and Wett and Rauch (2003). Values declared for NOB were assumed by Seuntjens et al. (2018) as being similar to Guisasola et al. (2007), although this original reference explicitly mentioned that nitratation was not influenced by inorganic carbon.

3.2.4 Biofilm reactor modelling

The SBTF reactor was described using the biofilm compartment of the AQUASIM software (Reichert, 1995), in which the biological conversions were implemented.

As biofilm was considered to be rigid, particulate components were displaced only due to the expansion or shrinking of the biofilm solid matrix. In all simulations, a planar biofilm was grown from an initial thickness of 1 µm to a predefined steady-state thickness of 60 µm, as nitrifying biofilms are reported to be relatively thin (20 to 250 µm thick) (Boller et al., 1994; Siegrist and Gujer, 1987).

The biofilm porosity was considered constant ($\varepsilon W = 0.80$), and in all simulations the initial fractions of particulate components were set at $\varepsilon_{ini}X_{AOB} = 0.10$, $\varepsilon_{ini}X_{NOB} = 0.05$ and $\varepsilon_{ini}X_{I} = 0$, as in Mozumder et al. (2014). The initial anammox fraction ($\varepsilon_{ini}X_{AN}$) was assumed as 0.005. This low initial active biomass fractioning for anammox (2.5% of the total particulate components) was set as no inoculum was used in the start-up of the monitored SBTF. Consequently, the initial fraction of heterotrophs ($\varepsilon_{ini}X_{H}$) was set at 0.045. The density of autotrophic biomass and particulate inert material in the biofilm was set to 60,000 g VSS m^{-3} (van Benthum et al., 1995). For heterotrophic biomass, the density was defined as 20,000 g VSS m^{-3} (van Benthum et al., 1995). A typical conversion factor of 0.75 g VSS g^{-1} COD (Henze et al., 2006) was considered for all particulate material.

The biofilm model was defined as ‘confined’, which means that the reactor volume stays constant independent of biofilm growth. The SBTF reactor under study had a plug-flow hydrodynamic behaviour, as demonstrated by preliminary tracer tests in the SBTF with fluorescent dyes (data not shown). The plug flow behaviour is supported by substrate concentration gradients, usually observed along with the SBTF height (Mac Conell et al., 2015). The reactor was modelled as a sequence of four completely mixed biofilm reactor compartments (0.25 m^3 each) to mimic plug-flow hydraulic conditions.

Oxygen supply was introduced in the model as a dynamic process from the bulk liquid phase, as follows

$$dSO_2/dt = k_La \,.(SO_{2,sat} - SO_2) \qquad \text{Eq. 3.5}$$

in which $SO_{2,sat}$ and SO_2 represent the oxygen saturation level and the bulk liquid dissolved oxygen, respectively. The volumetric oxygen mass transfer coefficient (k_La) was estimated during model calibration.

An external mass transfer boundary layer thickness (L_L) of 1500 µm was adopted in all simulations as a typical value for low-rate trickling filters (Henze et al., 2008). As diffusion is assumed to occur over the entire biofilm compartment, diffusion coefficients were corrected by a factor of 0.8. This accounts for additional mass transport limitations caused by the presence of the solid phase (Eberl et al., 2006).

Concerning possible model limitations, the simplified hydrodynamic modelling approach allows for a focus on the biokinetics of SBTFs following UASB reactors. The visually observed heterogeneity in effluent percolation and the possible existence of dead zones in the porous media are assumed to be simply lumped in other parameters.

3.2.5 Simulation set-up

Dynamic simulations were performed with the experimental data of the UASB reactor effluent over the considered 300-day period (Section A.3.8) as model input. The soluble biodegradable COD fraction of the anaerobic effluent was assumed as 50% of the measured filtered COD. This is supported by extensive measurements in UASB reactors effluents, in which 40 – 60% of the soluble COD was biodegradable (Aquino et al., 2009).

3.2.6 Model calibration and validation

Model calibration was performed through extensive simulations considering the dynamic effluent dataset. Most model parameters were adopted from literature (see Table A.3.3, Section A.3.1). Several parameters were adjusted to match the simulation results with the dynamic experimental data (i.e., DO, inorganic carbon, NH_4^+-N, NO_2^--N, and NO_3^--N in the SBTF) gathered in this study. Two independent calibration procedures were assessed. First, the simulated residual ammonium concentration was matched to the observed one by adjusting parameters related to AOB growth, as they are known to significantly influence nitrogen profiles (de Kreuk et al., 2007; Vannecke and Volcke, 2015). More specifically, the maximum growth rate AOB (μ_{max}^{AOB}) and the half-saturation coefficient for ammonium (KNH) were selected, given that the observed

dissolved oxygen and ammonium concentrations were non-limiting for nitrification (see results – section 3.3.2). Inorganic carbon limitation was not considered in the rate expressions.

Secondly, the calibration considered the simulated bulk effluent concentrations (i.e., DO, inorganic carbon, NH_4^+-N, and NO_3^--N) fitted to the experimental results by assessing the impact of inorganic carbon limitation in the two-step nitrification process. This was performed iteratively with proper k_La values set to reproduce the measured bulk effluent DO concentration in the SBTF, as DO cannot be calibrated independently from ammonium conversion rates.

For the simulations considering the Monod approach for inorganic carbon limitation of AOB, the affinity constant (K_{IC}^{AOB}) was stepwise tested from 10 to 25 mg $CaCO_3$ L^{-1}. For the sigmoidal kinetics approach for AOB, simulations with an incremental variation of the parameters *k* and *a* were performed, considering a range between 15 and 35 mg $CaCO_3$ L^{-1}, and 3 and 5, respectively. These ranges of values for both approaches (Monod and sigmoidal kinetics) are anchored in the reported coefficients in the literature (see Table 3.3). For all the simulations performed, k_La values were varied according to previously reported values (106 and 373 d^{-1} - Watari et al. (2020)) to adjust bioconversion rates of NH_4^+-N, NO_2^--N, and NO_3^--N (and thus effluent concentrations) to observed experimental data.

The goodness-of-fit between model predictions and bulk liquid concentrations was assessed by applying the Nash-Sutcliffe criterion, based on the calculated model efficiency (E) according to Eq. 3.6 (Nash and Sutcliffe, 1970). A similar approach can be found in the literature (Vannecke and Volcke, 2015).

$$E = 1 - \frac{\sum_{i=1}^{n}(y_i^m - y_i)^2}{\sum_{i=1}^{n}(y_i^m - \bar{y}_m)^2} \qquad \text{Eq. 3.6}$$

where y_i^m denotes the experimentally observed value of the i^{th} output variable, y_i is the corresponding simulated value and $\bar{y}_m$ is the mean value of the observations.

In this case, *E* should be preferably larger than 0 and close to the maximum of 1. The higher model efficiency, the better the fit between simulations and measured values. When no good representation of data by modelling was achieved (i.e., $E \leq 0$), the

difference between medians from experimental data and modelling outputs was statistically assessed. Non-parametric statistical tests were applied (Wilcoxon Matched Pairs Test), as data distribution typically followed a non-normal behaviour in all cases. Statistical significance was defined by 95% confidence limits (i.e., $p < 0.05$). Analyses were performed in SPSS Statistics software (IBM Corp., v27). Retaining the null hypothesis from statistical tests (i.e., no difference between experimental and simulated medians) was set as a final criterion for required accuracy after calibration.

Following calibration, model validation was performed based on two independent datasets. The first one was a dynamic dataset from a different SBTF following a UASB reactor. This SBTF was operated under a similar HLR (10 m^3 m^{-2} d^{-1}) and median OLR (1.0 kg COD m^{-3}_{sponge} d^{-1}) (Almeida et al., 2013), compared to the currently monitored SBTF. Although also based on polyurethane sponge, the specific surface area of the packing medium was not reported. It was therefore assumed equal to the determined value in the present study (detailed in Appendix, Section A.3.2). The second independent experimental dataset applied for model validation concerned an SBTF operated in parallel with the experimental set-up under study, which was first subject to a prolonged period (> 300 days) of limited oxygen supply and then operated under similar oxygen supply conditions as the SBTF considered for model calibration. This reactor was also fed with real anaerobically treated sewage and subjected to similar operating conditions (HLR of 10 m^3 m^{-2} d^{-1} and median OLR of 1.0 kg COD m^{-3}_{sponge} d^{-1}). The goodness-of-fit between model predictions and bulk liquid concentrations during validation was also assessed by applying the Nash-Sutcliffe criterion.

3.3 Results and discussion

3.3.1 Overall performance of the combined UASB/SBTF system

The UASB/SBTF system performance over the 300 day monitoring period is summarized in Table 3.4. The median COD removal efficiency of the anaerobic reactor was 68%, which is typical of well-operated UASB reactors treating sewage under mesophilic temperatures (Chernicharo et al., 2015). The remaining median total COD (153 mg L^{-1}) was removed in the SBTF with an efficiency of 60%. Overall, the COD removal efficiency of the UASB/SBTF system was 89%, resulting in a median effluent COD concentration of 62 mg L^{-1}. Note that filtered COD removal in the SBTF was

limited to approximately 40%. Most probably, the remaining filtered COD content in the final effluent (43 mg L^{-1}) was non-biodegradable, which is supported by previous reports on the low biodegradability (40 – 60%) of the total effluent soluble COD from UASB reactors treating sewage (Aquino et al., 2009).

A remarkably high overall TSS removal efficiency (94%) was obtained, even though operating without a secondary settler after the SBTF. The excess sludge production of the SBTF amounted to 0.12 kg TSS kg $COD_{removed}^{-1}$, which is considerably lower than typical ranges reported for aerobic processes following UASB reactors (0.25 – 0.88 kg TSS kg $COD_{removed}^{-1}$ – Gonçalves et al. (1998); Tandukar et al. (2007)). Longer sludge retention time (SRT) due to the interstitial biomass retention has been indicated to be a key mechanism contributing to low effluent TSS concentrations from SBTFs in contrast to conventional trickling filters filled with rock-based support media (Onodera et al., 2013; Tandukar et al., 2006a).

As expected, no nitrogen conversion occurred in the UASB reactor, supporting the need for a subsequent post-treatment step. The overall ammonium and total nitrogen removal efficiencies in the SBTF amounted to 79% and 26%, respectively.

Table 3.4 Summary of the UASB/SBTF system performance (median values) over the 300-days monitoring period

Variable (mg L^{-1})[a]	Influent sewage	UASB reactor effluent	SBTF effluent	Overall removal efficiency (%)
Total COD (COD_{total}) (n = 38)	514 (176)	153 (59)	62 (30)	89 (9)
Soluble (Filtered) COD ($COD_{filtered}$) (n = 25)	-	70 (25)	43 (33)	-
TSS (n = 37)	251 (110)	43 (29)	12 (15)	94 (8)
Total nitrogen (TN) (n = 26)	-	52 (9)	39 (5)	26 (14)
Ammonium nitrogen (NH_4^+-N) (n = 37)	30 (9)	30 (9)	6 (3)	79 (9)
Nitrite (NO_2^--N) (n = 25)	-	-	0.2 (1.0)	-
Nitrate (NO_3^--N) (n = 28)	-	0 (2)	27 (4)	-
Bicarbonate (as $CaCO_3$) (n = 29)	207 (43)	237 (38)	19 (15)	-
Average bulk liquid temperature (T) (n = 38)	25.4 (2.7)	25.5 (2.2)	24.3 (2.3)	-
pH (n = 38)	7.7 (0.2)	7.2 (0.2)	7.4 (0.4)	-
Dissolved oxygen (n = 38)	0.2 (1.4)	0.6 (0.5)	6.6 (0.5)	-

[a] pH: dimensionless; T: °C; -: not measured; Median values. Standard deviations in brackets; n: number of data

3.3.2 Dynamic nitrogen conversions in the SBTF

The ammonium concentrations and ammonium removal efficiency of the SBTF over the 300-day experimental period are displayed in Figure 3.3. The influent ammonium concentration to the SBTF ranged between 23 and 44 mg L^{-1} (10 – 90th percentile; median nitrogen loading rate - NLR: 0.33 kg N m^{-3}_{sponge} d^{-1}). Nitrification was observed soon after the start-up of the SBTF. The ammonium removal efficiency steadily increased, ranging between 73% and 84% (10 – 90th percentile) during the first 100 days of operation, and increased further up from day 175 to reach over 90% ammonium removal efficiency on days 220 – 255. From day 255 to 300, the median ammonium removal efficiency dropped to 79%. A noticeable increase in the influent ammonium concentration was recorded from day 182 onwards.

The median OLR applied to the monitored SBTF was 1.0 kg COD m^{-3}_{sponge} d^{-1}. Ammonium removal efficiencies in SBTFs post-UASB reactors typically reach 70% or higher values for OLR up to 2.0 kg COD m^{-3}_{sponge} d^{-1} (Bressani-Ribeiro et al., 2018). The observed median NH_4^+-N removal rate throughout the monitoring period amounted to 168 g NH_4^+-N m^{-3}_{sponge} d^{-1}, which is comparable to previously reported values of pilot-scale SBTFs operating under similar OLR (Onodera et al., 2013; Tawfik et al., 2006b; Uemura et al., 2012). Over the whole monitoring period, effluent ammonium concentrations remained stable below 10 mg L^{-1}, regardless of the dynamic behaviour of the influent ammonium concentration. Median effluent nitrite and nitrate concentrations were 0.2 mg L^{-1} and 27 mg L^{-1}, respectively (see Table 3.4). This clearly indicates NOB activity in the reactor.

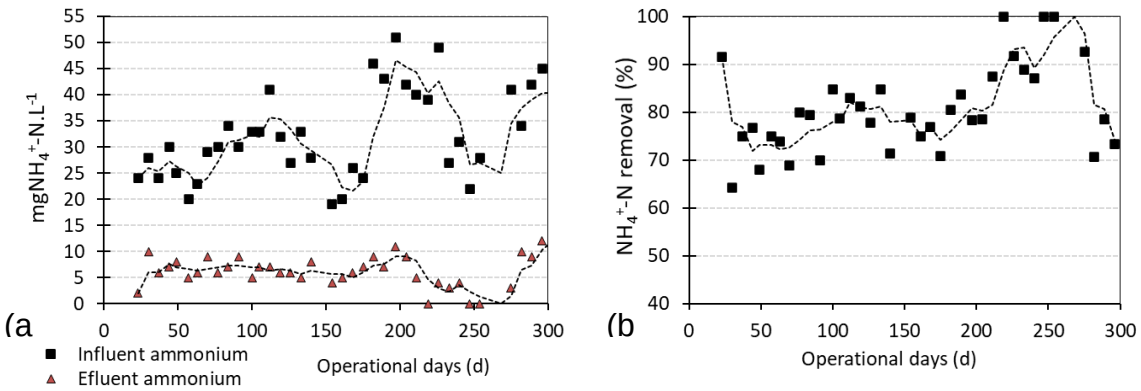

Figure 3.3 Evolution of (a) SBTF influent (= UASB reactor effluent) and SBTF effluent ammonium concentrations, and (b) ammonium removal efficiencies with moving averages (3 terms)

In contrast to the relatively high ammonium removal efficiency, the nitrogen removal efficiency was limited to 26% (median nitrogen removal rate – NRR: 0.09 kg N m^{-3}_{sponge} d^{-1}). This is in line with previously reported values for nitrogen removal efficiency in fully ventilated SBTFs without effluent recirculation, namely 25 and 35% (Onodera et al., 2014; Tandukar et al., 2006b). Due to the long SRT, retained solids inside the sponge pores can be hydrolysed, releasing soluble products that can eventually be available as organic substrate (Almeida et al., 2013). Endogenous respiration as a source of additional organic carbon for heterotrophic denitrification was first pointed out by Araki et al. (1999). This can also be related to the little excess sludge production in the monitored SBTF.

The remaining ammonium concentration in the effluent (median value: 6 mg L^{-1}) reflects that AOB could not convert all the influent ammonium, despite the DO concentrations in the effluent being close to the local saturation level (approximately 8 mg L^{-1}, see Figure 3.6b). Nitrite was hardly detected (0.2 mg L^{-1}) and definitely below inhibiting levels. The observed incomplete ammonium conversion could only be reproduced by simulation when increasing the affinity constant of AOB for nitrogen (K_{NH}) to over 45 g N m^{-3} (Figure A.3.3, Section A.3.4), which is unrealistically high compared with typical literature values (1.67 – 18.76 g N m^{-3}, i.e., the interquartile ranges reported by Vannecke and Volcke (2015)). Furthermore, the maximum growth rate of AOB (μ_{max}^{AOB}) had to be adjusted to unlikely values ($\mu_{max}^{AOB} \approx \mu_{max}^{NOB}$), as long as AOB tend to have a higher μ_{max} than NOB at temperatures close to the observed ones (24.3 °C (2.3 °C) – Table 3.4).

3.3.3 Inorganic carbon limitation - experimental indications

Bicarbonate was systematically depleted within the SBTF, from a median influent value of 237 mg $CaCO_3$ L^{-1} to values lower than 45 mg $CaCO_3$ L^{-1} (see Figure 3.6c), which is regarded as the threshold for impairing nitrification rates in biofilms (Biesterfeld et al., 2003). Inorganic carbon seemed to play a key role as a limiting substrate for AOB in the SBTF. Conversely, NOB activity was unaffected by the inorganic carbon limitation, as nitrite accumulation was negligible. NOB capability to adapt to limiting inorganic carbon concentrations has been reported in the literature, as previously addressed. It is interesting to note that the pH remained relatively constant (around 7.4 – see Table 3.4) over the monitored period, despite the inorganic carbon drop. This

supports that lack of inorganic carbon for cell synthesis is the rate-limiting step for nitritation, instead of pH inhibition, as similarly observed by Biesterfeld et al. (2003) considering a pH ranging from 6.9 to 8.0.

To unravel inorganic carbon limitation in post-treatment systems of anaerobic effluents, an overview was made on the effluent bicarbonate and ammonium concentrations of five full-scale UASB reactors (Figure 3.4). The median bicarbonate ranged between 300 and 350 mg $CaCO_3$ L^{-1}, except for the STP 5, which showed a much higher concentration (600 mg $CaCO_3$ L^{-1}) because of its location in a city whose water supply is drawn from carbonate sedimentary rock underground areas. The ammonium concentrations in the UASB reactor effluents ranged between 50 and 70 mg L^{-1}. Overall, a typical bicarbonate/ammonium ratio in the order of 5 to 6 mg $CaCO_3$ /mg NH_4^+-N was noticed, which is below the stoichiometric requirement for the complete oxidation of ammonium to nitrate (7.14 mg $CaCO_3$ consumed mg NH_4^+-$N^{-1}_{oxidized}$ – (Rittmann and McCarty, 2001). Therefore, complete nitrification in post-treatment systems following UASB reactors tends to be generally bicarbonate-limited.

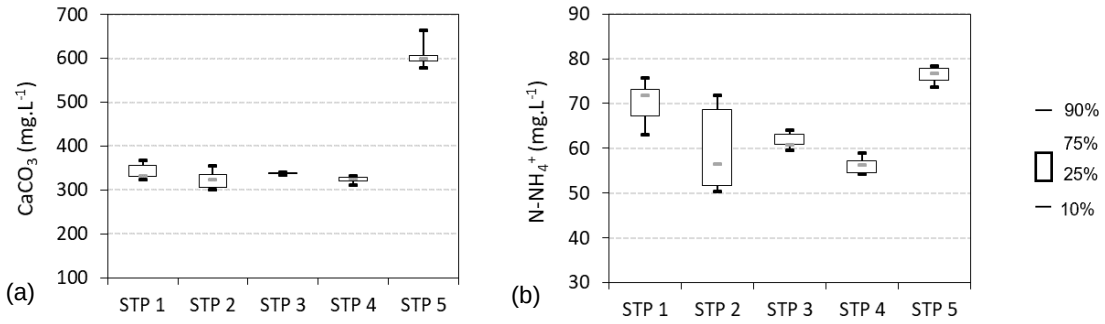

Figure 3.4 Box-plot graph of (a) effluent bicarbonate (as $CaCO_3$) and (b) effluent ammonium concentrations of five full-scale UASB reactors

In conventional aerobic processes (e.g., activated sludge), the degradation of organic matter by heterotrophic microorganisms supplies enough CO_2 as an inorganic carbon source for autotrophs (Guisasola et al., 2007). Conversely, systems comprised of UASB reactors followed by aerobic post-treatment units (e.g., trickling filters) experience a decoupling of organic matter degradation and further CO_2 supply for autotrophic growth. Indeed, organic carbon is mostly converted to biogas (mainly CH_4; as most of the CO_2 remains dissolved in the liquid phase) in the anaerobic stage, decreasing available readily biodegradable organic carbon (and associated CO_2 production) in the post-treatment step. Besides, depending on turbulent conditions

during influent distribution, dissolved CO_2 in the anaerobic effluent is stripped, as the mass transfer is liquid-phase controlled due to the low value of its Henry constant (K_H CO_2 (25 ºC) = 0.0338 mol L^{-1} atm^{-1} – (Perry and Chilton, 1973). This supports the hypothesis that nitrification in post-treatment systems following UASB reactors, notably trickling filters, tends to be limited by the influent inorganic carbon.

3.3.4 Model structure selection and calibration

A detailed analysis of the different saturation models for inorganic carbon was performed for AOB, NOB, and anammox (Figure 3.5). The Monod (Eq. 3.1) and sigmoidal approach (Eq. 3.2) to describe inorganic carbon limitation for AOB were compared, considering the range of coefficients from Table 3.3 (see section 3.2.3.2). Tessier kinetics for AOB (proposed by Guisasola et al. (2007)) was not included, as it renders a steep transition to a zero-order behaviour for inorganic carbon values less than 1.0 mg $CaCO_3$ L^{-1}. Likewise, process inhibition (Haldane kinetics approach) due to high inorganic carbon levels is unrealistic for mainstream sewage treatment. Furthermore, the values reported by Boltz et al. (2011) regarding AOB kinetics were not considered separately since they were based on Henze et al. (2006).

Care should be taken when adopting the same inorganic carbon limitation kinetics and associated parameter values from the literature, especially when modelling nitrification as a two-step process. Wett and Rauch (2003) assumed the same (sigmoidal) inorganic carbon limitation function for both AOB and NOB, leading to an unrealistic nitrite build-up in the SBTF effluent under limited inorganic carbon supply (Figure A.3.2, Section A.3.3). Guisasola et al. (2007) only reported (sigmoidal) inorganic carbon limitation of AOB and no inorganic carbon limitation of NOB. However, the sigmoidal expression (Eq. 3.2) is characterized by a non-zero value ($1/e^{(k/a)}+1$) at a null substrate concentration (S_{IC} = 0 mg $CaCO_3$ L^{-1}). For the parameter values of Guisasola et al. (2007), this led to a relatively high offset and associated positive growth rate of AOB ($1/e^{(k/a)}+1$) = 0.12 and $\mu_{max} > 0$ for S_{IC} = 0 mg $CaCO_3$ L^{-1}), which was found to cause numerical instabilities during simulation. In order to remedy this, a switching function could be applied to impose zero growth in the absence of inorganic carbon. This either comes down to implementing an IF-function (implying the introduction of discontinuous dynamics, which may again lead to numerical instabilities) or choosing a different saturation model (Eq. 3.1, Eq. 3.3, or Eq. 3.4). Alternatively, the sigmoidal model

structure could be applied with parameters values resulting in an almost-zero value at S_{IC} = 0.

	Experimental studies	Modelling and simulation studies
AOB	Guisasola et al. (2007) - Monod kinetics Guisasola et al. (2007) - Sigmoidal kinetics	Henze et al. (2006) - Monod kinetics [a] Wett and Rauch (2003) - Sigmoidal kinetics [b] This study
NOB		Al-Omari et al. (2015) - Monod kinetics
Anammox	Kimura et al. (2011) - Monod kinetics [c]	

[a] Henze et al. (2006) did not distinguish between AOB and NOB (single-step nitrification is assumed).

[b] Wett and Rauch (2003) reported the same half-saturation constant for AOB and NOB.

[c] Saturation models in Al-Omari et al. (2015) and Kimura et al. (2011) render the same curve due to the identical half-saturation constant determined for NOB and anammox (see Table 3).

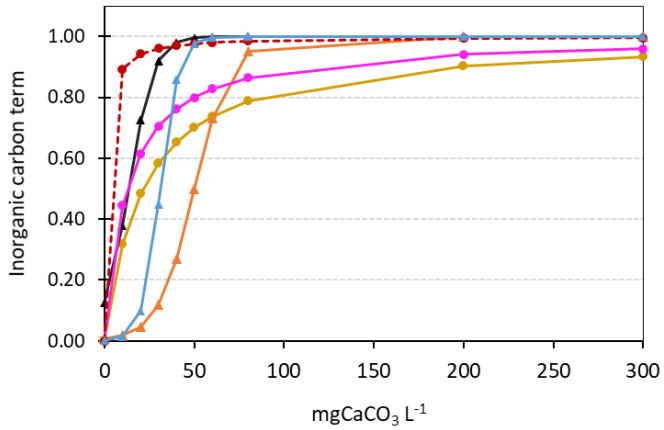

Figure 3.5 Inorganic carbon limitation term according to different saturation models (see Table 3.2 and Table 3.3)

Few examples are found in modelling nitrogen removal considering the significance of inorganic carbon as an assimilative carbon source (Al-Omari et al., 2015; Seuntjens et al., 2018). Even fewer references deal with the impact of inorganic carbon steering microbial competition among different autotrophic guilds. From a respirometric-titrimetric experiment, Guisasola et al. (2007) showed the inhibition of AOB activity at inorganic carbon concentrations lower than 36 mg L^{-1}, while no limitation for NOB was reported. Similar microbial dynamics were observed by Zhang et al. (2016) in a pilot-scale membrane bioreactor treating synthetic wastewater, where NOB prevailed, and AOB was suppressed under an inorganic carbon/N ratio less than 1.5. From a fundamental standpoint, it is supported that NOB are likely less limited than AOB regarding inorganic carbon, as NOB can up-regulate its anabolism mixotrophically from traces of organic matter (Bock, 1976; Ren et al., 2014). Some NOB (Nitrospira genus)

could use simple organic substrates (e.g., pyruvate) for carbon assimilation and likely simultaneously as energy sources in addition to CO_2 and nitrite (Daims et al., 2001; Gruber-Dorninger et al., 2015). Furthermore, AOB use bicarbonate preferably instead of gaseous CO_2 as a source of inorganic carbon (Jiang et al., 2015; Lücker et al., 2015; Mellbye et al., 2016). Low inorganic carbon levels were also stated to be limiting for anammox growth, as experimentally demonstrated by Ma et al. (2015). However, only one study reporting the affinity constant value (K_{IC}^{AN}) was found in the literature (Kimura et al., 2011).

Given that dissolved oxygen and ammonium were non-limiting for AOB activity in the monitored SBTF, the observed residual ammonium concentration in this reactor could only be simulated when inorganic carbon limitation was included in the model. The nitritation process was a sink of inorganic carbon, which was primarily consumed for buffering (Figure A.3.5, Section A.3.5). The best fit was obtained with sigmoidal kinetics for AOB (calibrated values k = 31 mg $CaCO_3$ L^{-1}; a = 5, see Figure 3.5) coupled with a k_La of 330 d^{-1}; the corresponding concentration dynamics of NH_4^+-N, DO, inorganic carbon, and NO_3^--N are displayed in Figure 3.6. The kinetics of inorganic carbon limitation for NOB and anammox bacteria were described by a Monod-type saturation, considering relatively low half-saturation constant values (1.2 mg $CaCO_3$ L^{-1}, as in Al-Omari et al. (2015), Table 3.3). This kinetic term thus serves as a mathematical switch to prevent bacterial growth in the absence of substrate (as recommended by (Hauduc et al. (2010)) rather than as an inorganic carbon limitation term. This is supported by the less pronounced effects of inorganic carbon limitation on NOB and anammox bacteria growth.

The overall trends for the SBTF performance could be captured, i.e., a residual ammonium concentration in the bulk liquid associated with the lack of influent inorganic carbon and nitrate production without nitrite accumulation. The model fit may have been influenced by the dynamic variations in the influent total nitrogen concentration (Figure 3.6a). Yet, the sigmoidal kinetics with calibrated parameters for inorganic carbon limitation of AOB did not lead to statistical differences (p < 0.05) between the median observed effluent ammonium concentration (6 mg L^{-1}) and the median simulated value (5 mg L^{-1}) (Table A.3.5, Section A.3.5). Such observation of residual ammonium concentrations is only possible when considering inorganic carbon

limitation, unless unrealistic kinetic parameter values (K_{NH} over 45 g N m^{-3} and $\mu_{max}^{AOB} \approx \mu_{max}^{NOB}$) are assumed, as previously discussed (Figure A.3.3, Section A.3.4). Besides, the model was able to describe the overall behaviour of effluent DO, inorganic carbon, and nitrate concentrations (Figure A.3.4, Section A.3.5).

A satisfactory goodness-of-fit for effluent ammonium concentrations could also be achieved considering the Monod approach for inorganic carbon kinetics of AOB (Table A.3.5, Section A.3.5). However, a poorer representation of the inorganic carbon dynamics was revealed compared to the sigmoidal approach. For all tested conditions, the Monod approach rendered remarkable differences between the median observed effluent inorganic carbon concentration (19 mg L^{-1}) and the median simulated value (< 5 mg L^{-1}). The best fit obtained with sigmoidal kinetics is in line with the literature (Guisasola et al., 2007; Seuntjens et al., 2018; Wett and Rauch, 2003).

The width of the transient range associated with data acquisition (i.e., approximately seven days between monitoring campaigns) is likely influencing the modelling outputs, corroborating for the low dynamic model efficiency ($E < 0$) (Table A.3.5, Section A.3.5). Moreover, the observed sensitivity of nitrification to the dynamic loading conditions is typical for the cases with low effluent bicarbonate alkalinity (< 50 mg $CaCO_3$ L^{-1}; Figure 3.6c) (Henze et al., 2008). Finally, pronounced peaks on the simulated effluents predictions could also be related to the less developed biofilm, as steady-state biofilm thickness and biomass profiles were not reached under the simulated time (300 days). Overall, considering parameter uncertainty, the model was found to satisfactorily describe the experimental data, capturing important trends for process understanding and further optimization.

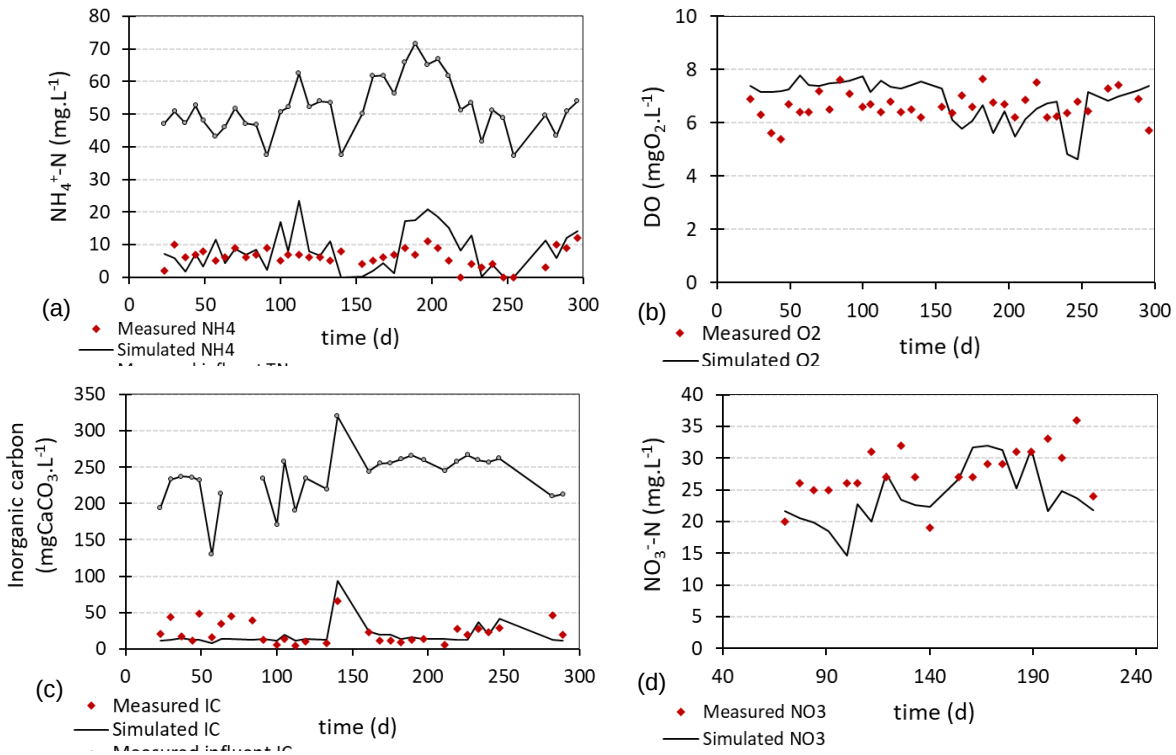

Figure 3.6 Comparison between simulated and experimental dynamic SBTF performance in terms of effluent concentrations of (a) ammonium, (b) dissolved oxygen (DO), (c) inorganic carbon, and (d) nitrate. *Measured influent total nitrogen concentrations are also displayed*

3.3.5 Model validation

The calibrated model was validated on two independent datasets. The first one was a dynamic dataset from a different SBTF following a UASB reactor, operated under a similar HLR (10 m^3 m^{-2} d^{-1}) and median OLR (1.0 kg COD m^{-3}_{sponge} d^{-1}), compared to the currently monitored SBTF. The second dataset concerned an SBTF operated in parallel with the experimental set-up under study, which was first subject to a prolonged period (> 300 days) of limited oxygen supply and then operated under similar conditions as the SBTF considered for model calibration. Concerning the first validation dataset, the model was able to capture the overall effluent behaviour in terms of ammonium, dissolved oxygen, and nitrate concentrations (Figure A.3.6, Section A.3.6), despite less accurate dynamic outputs (E < 0) (Figure A.3.7, Section A.3.6). Nevertheless, the simulation results present peaks of effluent inorganic carbon concentration, which did not correspond with the experimental observations (Figure A.3.7(c), Section A.3.6) and were related to less nitrate consumption via heterotrophic denitrification. The simulated behaviour could be explained by the lack of soluble

biodegradable COD, which was assumed in the model as a fraction (50%) of the anaerobic effluent filtered COD, as measured experimentally (see section 3.2.3). However, in reality, an additional organic carbon source could be present in the form of entrapped solids in the sponge carrier, which was not accounted for in the model. The characterization of solids entrapment and further COD release could be included in a more detailed model. However, this would also lead to the need to assess flow paths in porous media, requiring a more detailed (at least 2-dimensional, as proposed by Bottero et al. (2013) biofilm model and consequently increase the computational burden. Another aspect that may have affected a better fitting is that the specific surface area of the sponge-based support material was not reported by Almeida et al. (2013). This is a critical model parameter that directly affects the amount of biomass retained in the reactor and, as such, impacts biological conversion rates.

As for the validation on the SBTF following a prolonged period of oxygen limitation, again, the model was able to capture the overall effluent behaviour in terms of ammonium, dissolved oxygen, and nitrate concentrations (Figure A.3.8, Section A.3.6). The presented operational data was recorded straight after ceasing oxygen limitation, and a lag period (approximately the first 30 days) seemed to take place before the reactor regained its full oxygenation capacity. It is worth mentioning that oxygen transfer dynamics in trickling filters is not yet entirely clear (Logan, 1993)). During this period, less ammonium was converted due to the decreased dissolved oxygen availability, resulting in reduced inorganic carbon consumption and less nitrate formation (Figure A.3.9, Section A.3.6). Such dynamics could not be captured quantitatively through simulation, likely due to the modelling approach with a constant oxygen mass transfer coefficient.

To present further evidence of the need to include inorganic carbon limitation when modelling SBTFs treating anaerobic effluents, complementary simulations were performed on both validation datasets without inorganic carbon in the kinetic rate expression of AOB. Model outputs were remarkably impacted, as null effluent ammonium concentrations were predicted (Figure A.3.10, Section A.3.7). This highlights the validity of the model structure with sigmoidal kinetics for inorganic carbon limitation of AOB considering calibrated parameters (k = 31 mg $CaCO_3$ L^{-1}; a = 5, see Table 3.3)

3.4 Conclusions

The start-up and stable operation of a demo-scale sponge-bed trickling filter to remove nitrogen and residual organic carbon from anaerobically pre-treated sewage was monitored for 300 days. A mathematical model was developed, calibrated, and validated for the first time to describe mainstream nitrogen removal from anaerobically treated effluents.

- Nitrification was observed soon after the start-up of the SBTF. From the 20th day after the start-up onwards, the effluent ammonium concentrations remained stable below 10 mg N L^{-1}, despite variations in the influent ammonium concentration (23 – 44 mg L^{-1}; 10 – 90th percentile). The median ammonium removal efficiency amounted to 79%.

- Total nitrogen removal efficiency was limited to 26%, a low value which is typical for fully ventilated SBTFs without effluent recirculation. Heterotrophic denitrification was limited by the low organic carbon content of the anaerobic effluent.

- The limited ammonium conversion was ascribed to a lack of influent inorganic carbon, as the incoming concentration (median 237 mg $CaCO_3$ L^{-1}) was systematically depleted to values below the required minimum (45 mg $CaCO_3$ L^{-1}) to sustain nitrification in biofilms. Limitation was attributed to inorganic carbon rather than alkalinity, as the pH remained constant. Ammonium and oxygen limitation were excluded, as was inhibition by nitrite.

- To properly describe inorganic carbon limitation in models, bicarbonate as a state variable should be used to quantify inorganic carbon limitation, rather than to merely indicate pH changes. The need to include this state variable was confirmed through simulation, demonstrating the crucial role of inorganic carbon for both buffering and as an inorganic carbon source in calibrating nitrogen conversions.

- Nitrite accumulation was not observed during the monitored period, which indicates that NOB activity was little affected by the inorganic carbon limitation, or at least less than AOB activity. Considering a higher inorganic carbon

limitation for AOB than NOB is essential for modelling nitrogen conversions in SBTFs following UASB reactors for sewage treatment. Inorganic carbon limitation of AOB was best described using sigmoidal kinetics with calibrated values (k = 31 mg $CaCO_3$ L^{-1}; a = 5).

Acknowledgements

The authors acknowledge the support obtained from the Ghent University Special Research Fund (BOF UGent – funding for joint doctorate: BOF DCV 2017.0012.01) and from the following Brazilian institutions: Conselho Nacional de Desenvolvimento Científico e Tecnológico – CNPq; Fundação de Amparo à Pesquisa de Minas Gerais – FAPEMIG; Instituto Nacional de Ciência e Tecnologia em Estações Sustentáveis de Tratamento de Esgoto – INCT ETEs Sustentáveis.

Appendix

In this appendix, details of the developed one-dimensional biofilm model are given, along with the corresponding biological conversion reactions, stoichiometric matrix, and kinetics and parameter values (Section A.3.1). The procedure to determine the specific surface area of the sponge-based support media is addressed in Section A.3.2. The following sections contain detailed simulation results as follows: i) nitrite build-up in SBTFs when assuming the same half-saturation coefficients for inorganic carbon limitation for AOB and NOB (Section A.3.3); ii) model calibration attempts using other kinetic parameter values AOB (μ_{max}^{AOB}) and K_{NH} (Section A.3.4); and iii) various kinetic approaches to describe the observed inorganic carbon limitation of AOB (Section A.3.5). Model validation results with and without inorganic carbon limitation are presented in Section A.3.6 and Section A.3.7, respectively. Finally, the dynamic dataset of the monitored UASB reactor and SBTF is made available as an MS Excel spreadsheet (A.3.8).

A.3.1 Model description, stoichiometric matrix, kinetic expressions, and model parameter

Biological conversion reactions were based on the model of Mozumder et al., 2014. Nitrification was described as a two-step process: oxidation of ammonium (NH_4^+) to nitrite (NO_2^-) by AOB (X_{AOB}), followed by nitrite oxidation to nitrate (NO_3^-) by NOB (X_{NOB}). Anammox bacteria (X_{AN}) convert ammonium and nitrite to nitrogen gas (N_2). Heterotrophic growth reactions were described using dissolved oxygen, nitrite (NO_2^-), or nitrate (NO_3^-) as electron acceptors. The proposed artificial distinction among heterotrophic groups ($X_{H,O2}$, $X_{H,NO2}$, $X_{H,NO3}$) for tracking electron acceptors was kept. Still, all heterotrophic biomass was assumed equally capable of performing each conversion in practice, which was reflected by expressing the corresponding reaction rates in terms of total heterotrophs (X_H). Denitrification was modelled as a two-step process in which nitrate is converted to nitrite and subsequently to nitrogen gas (Sin et al., 2008). Therefore, the intermediate nitrite released is available for NOB and anammox bacteria, besides heterotrophs. The production of organic materials during biomass decay was simulated based on the death-regeneration concept, in which living cells become substrate, as well as a fraction of inert material through microorganisms' decay and/or hydrolysis (van Loosdrecht and Henze, 1999). Decay

was assumed to directly generate soluble organic substrate (S_S) rather than particulate organic substrate (X_S), which would be successively hydrolysed to S_S (as proposed by Mozumder et al., 2014). This approach implies that decay rather than hydrolysis of X_S is the rate-limiting step. Surface detachment was assumed to be a growth-associated phenomenon with detached biomass eluting with the bulk liquid.

Table A.3.1 Stoichiometric matrix and composition matrix

A_{ij} i component → / j process ↓	S_S [g COD m^{-3}]	S_{NH} [g N m^{-3}]	S_{ND} [gN m^{-3}]	S_{NO2} [g N m^{-3}]	S_{NO3} [g N m^{-3}]	S_{O2} [g O_2 m^{-3}]	S_{N2} [g N m^{-3}]		S_{IC} * [mol equiv HCO_3^- m^{-3}]	X_{AOB} [gCOD m^{-3}]	X_{NOB} [gCOD m^{-3}]	X_{AN} [gCOD m^{-3}]	X_H [g COD m^{-3}]			X_I [gCOD m^{-3}]
							S_{N2A} [gN m^{-3}]	S_{N2H} [g N m^{-3}]					$X_{H,A}$	$X_{H,NO2}$	$X_{H,NO3}$	
1. nitritation - growth of X_{AOB}		$-\frac{1}{Y_{AOB}} - i_{NXB}$		$\frac{1}{Y_{AOB}}$		$1-\frac{3.43}{Y_{AOB}}$			$\left(-\frac{i_{NXB}}{14} - \frac{1}{7Y_{AOB}}\right)$	1						
2. nitratation - growth of X_{NOB}		$-i_{NXB}$		$-\frac{1}{Y_{NOB}}$	$\frac{1}{Y_{NOB}}$	$1-\frac{1.14}{Y_{NOB}}$			$\left(-\frac{i_{NXB}}{14}\right)$		1					
3. anammox - growth of X_{AN}		$-\frac{1}{Y_{AN}} - i_{NXB}$		$-\left(\frac{1}{Y_{AN}}\right)$	$\frac{1}{1.14}$		$\left(\frac{2}{Y_{AN}}\right)$		$\left(-\frac{i_{NXB}}{14}\right)$			1				
4. aerobic growth of heterotrophs (X_H)	$-\frac{1}{Y_H}$	$-i_{NXB}+\frac{i_{NSS}}{Y_H}$				$1-\frac{1}{Y_H}$			$\left(-\frac{i_{NXB}}{14} + \frac{i_{NSS}}{14Y_H}\right)$				1			
5. denitritation - anoxic (on NO_2^-) growth of heterotrophs (X_H)	$-\frac{1}{Y_{H,NO_2}}$	$-i_{NXB}+\frac{i_{NSS}}{Y_{H,NO_2}}$		$-\frac{1-Y_{H,NO_2}}{1.71\,Y_{H,NO_2}}$				$\frac{1-Y_{H,NO_2}}{1.71\,Y_{H,NO_2}}$	$\left(-\frac{i_{NXB}}{14} + \frac{i_{NSS}}{14Y_{H,NO_2}}\right) + \left(\frac{1-Y_{H,NO_2}}{1.71\,Y_{H,NO_2}14}\right)$					1		
6. denitrification - anoxic (on NO_3^-) growth of heterotrophs (X_H)	$-\frac{1}{Y_{H,NO_3}}$	$-i_{NXB}+\frac{i_{NSS}}{Y_{H,NO_3}}$		$\frac{1-Y_{H,NO_3}}{1.14\,Y_{H,NO_3}}$	$-\frac{1-Y_{H,NO_3}}{1.14\,Y_{H,NO_3}}$				$\left(\frac{i_{NXB}}{14} - \frac{i_{NSS}}{14Y_{H,NO_3}}\right)$						1	
7. ammonification		1	-1						$\left(\frac{1}{14}\right)$							
8. decay of X_{AOB}	1-f_I	i_{NXB} - f_I i_{NXI} – (1-f_I) i_{NSS}								-1						f_I
9. decay of X_{NOB}	1-f_I	i_{NXB} - f_I i_{NXI} – (1-f_I) i_{NSS}									-1					f_I
10. decay of X_{AN}	1-f_I	i_{NXB} - f_I i_{NXI} – (1-f_I) i_{NSS}										-1				f_I
11. decay of X_H	1-f_I	i_{NXB} - f_I i_{NXI} – (1-f_I) i_{NSS}											-1			f_I
Composition matrix																
gCOD/unit comp	1			-3.43	-4.57	-1	-1.71			1	1	1	1			1
gN/unit comp	i_{NSS}	1	1	1	1		1			i_{NXB}	i_{NXB}	i_{NXB}	i_{NXB}			i_{NXI}
Charge (mol_{eq}/unit		1/14		-1/14	-1/14				-1							

*Coefficients for inorganic carbon (SIC), expressed as mol equiv HCO_3 m^{-3}, were determined from the charge balance. Conversion of inorganic carbon expressed as calcium carbonate (g CaCO3 m^{-3}, as experimentally measured) is performed taking into account a conversion factor of 50 g mol $equiv^{-1}$.

Table A.3.2 Kinetic rate expressions

j process ↓	Rate expression
1. nitritation - growth of X_{AOB}	$\rho G,AOB = \mu_{max}^{AOB}.\frac{S_{O2}}{K_{O2}^{AOB}+S_{O2}}.\frac{S_{NH}}{K_{NH}^{AOB}+S_{NH}}.\frac{e^{(S_{IC}-k)/a}}{1+e^{(S_{IC}-k)/a}}.X_{AOB}$
2. nitratation - growth of X_{NOB}	$\rho G,NOB = \mu_{max}^{NOB}.\frac{S_{O2}}{K_{O2}^{NOB}+S_{O2}}.\frac{S_{NO2}}{K_{NO2}^{NOB}+S_{NO2}}.\frac{S_{NH}}{K_{NH}^{NOBH}+S_{NH}}.\frac{S_{IC}}{K_{IC}^{NOB}+S_{IC}}.X_{NOB}$
3. anammox - growth of X_{AN}	$\rho G,AN = \mu_{max}^{AN}.\frac{K_{O2}^{AN}}{K_{O2}^{AN}+S_{O2}}.\frac{S_{NH}}{K_{NH}^{AN}+S_{NH}}.\frac{S_{NO2}}{K_{NO2}^{AN}+S_{NO2}}.\frac{S_{IC}}{K_{IC}^{AN}+S_{IC}}.X_{AN}$
4. aerobic growth of X_H	$\rho G,H = \mu_{max}^{H}.\frac{S_S}{K_S^H+S_S}.\frac{S_{O2}}{K_{O2}^H+S_{O2}}.\frac{S_{NH}}{K_{NH}^{NOBH}+S_{NH}}.X_H$
5. denitritation - anoxic growth (on NO_2^-) of X_H	$\rho G,H^{NO2} = \mu_{max}^{H}.\eta_{NO2}.\frac{K_{O2}^H}{K_{O2}^H+S_{O2}}.\frac{S_{NO2}}{K_{NO2}^H+S_{NO2}}.\frac{S_{NO2}}{S_{NO2}+S_{NO3}}.\frac{S_S}{K_S^H+S_S}.\frac{S_{NH}}{K_{NH}^{NOBH}+S_{NH}}.X_H$
6. denitrification - anoxic growth (on NO_3^-) of X_H	$\rho G,H^{NO3} = \mu_{max}^{H}.\eta_{NO3}.\frac{K_{O2}^H}{K_{O2}^H+S_{O2}}.\frac{S_{NO3}}{K_{NO3}^H+S_{NO3}}.\frac{S_{NO3}}{S_{NO2}+S_{NO3}}.\frac{S_S}{K_S^H+S_S}.\frac{S_{NH}}{K_{NH}^{NOBH}+S_{NH}}.X_H$
7. ammonification	$\rho a = k_a.S_{NH}.X_H$
8. decay of AOB	$\rho D,AOB = b_{AOB}.X_{AOB}$
9. decay of NOB	$\rho D,NOB = b_{NOB}.X_{NOB}$
10. decay of anammox	$\rho D,AN = b_{AN}.X_{AN}$
11. decay of heterotrophs	$\rho D,H = b_H.X_H$

Table A.3.3 Stoichiometric and kinetic parameter values. *Parameters estimated in this study are indicated in bold*

Parameter	Description	Value	Unit	Reference/Comments
Stoichiometric parameters				
Y_{AOB}	Yield coefficient of AOB	0.20	g COD g^{-1} N	Wiesmann, 1994[a]
Y_{NOB}	Yield coefficient of NOB	0.057	g COD g^{-1} N	Wiesmann, 1994[a]
Y_{AN}	Yield coefficient of AN	0.17	g COD g^{-1} N	Strous et al., 1998[b]
Y_H	Yield coefficient of heterotrophs (H)	0.67	g COD g^{-1} COD	Henze et al., 2006
$Y_{H,NO2}$	Yield coefficient of HNO_2	0.53	g COD g^{-1} COD	Muller et al., 2003
$Y_{H,NO3}$	Yield coefficient of HNO_3	0.53	g COD g^{-1} COD	Muller et al., 2003
i_{NXB}	N content of biomass	0.07	g N g^{-1} COD	Mozumder et al., 2014
i_{NXI}	N content of particulate inerts	0.07	g N g^{-1} COD	Mozumder et al., 2014
i_{NSS}	N content of soluble organic substrate	0.03	g N g^{-1} COD	Henze et al., 2006
f_I	Fraction of inert COD in biomass	0.08	g COD g^{-1} COD	Henze et al., 2006
Kinetic parameters (at 24.3°C)				
AOB				
μ_{max}^{AOB}	Growth rate of AOB	0.81	d^{-1}	Hellinga *et al.*, 1999[c]

b^{AOB}	Decay rate of AOB	0.054	d^{-1}	Assumed, such that ratio b^{AOB}: $\mu_{max}^{AOB} = b^{H}$: μ_{max}^{H} as proposed in Mozumder et al., 2014
$K_{O_2}^{AOB}$	DO half-saturation coefficient for AOB	0.6	g O_2 m^{-3}	Hao et al., 2002
K_{NH}^{AOB}	NH_4^+ half-saturation coefficient for AOB	1.1	g N m^{-3}	Wiesmann, 1994
k	**Inorganic carbon saturation coefficient for AOB (Sigmoidal kinetics)**	**31**	**g $CaCO_3$ m^{-3}**	**Estimated in this study**
a	**Inorganic carbon sigmoidal kinetics non-dimensional parameter**	**5**	**Dimensionless**	**Estimated in this study**
NOB				
μ_{max}^{NOB}	Growth rate of NOB	0.57	d^{-1}	Hellinga et al., 1999[c]
b^{NOB}	Decay rate of NOB	0.038	d^{-1}	Assumed, such that ratio b^{NOB}: $\mu_{max}^{NOB} = b^{H}$: μ_{max}^{H} as proposed in Mozumder et al., 2014
$K_{NO_2}^{NOB}$	NO_2^- half-saturation coefficient for NOB	0.51	g N m^{-3}	Wiesmann, 1994
$K_{O_2}^{NOB}$	DO half-saturation coefficient for NOB	1.1	g O_2 m^{-3}	Wiesmann, 1994
K_{NH}^{NOBH}	NH_4^+ half-saturation coefficient for NOB and heterotrophs	0.02	g N m^{-3}	Mozumder et al., 2014
K_{IC}^{NOB}	Inorganic carbon half-saturation coefficient for NOB	1.2	g $CaCO_3$ m^{-3}	Al-Omari et al., 2015
AN				
μ_{max}^{AN}	Growth rate of AN	0.03	d^{-1}	Strous *et al.*, 1998[c]
b^{AN}	Decay rate of AN	0.002	d^{-1}	Assumed, such that ratio b^{AN}: $\mu_{max}^{AN} = b^{H}$: μ_{max}^{H} as proposed in Mozumder et al., 2014
K_{NH}^{AN}	NH_4^+ half-saturation coefficient for AN	0.03	g N m^{-3}	Mozumder et al., 2014
$K_{O_2}^{AN}$	DO inhibition coefficient for AN	0.01	g O_2 m^{-3}	Strous et al., 1998
$K_{NO_2}^{AN}$	NO_2^- half-saturation coefficient for AN	0.005	g N m^{-3}	Mozumder et al., 2014
K_{IC}^{AN}	Inorganic carbon half-saturation coefficient for AN	1.2	g $CaCO_3$ m^{-3}	Kimura et al., 2011
Heterotrophs				
μ_{max}^{H}	Growth rate of heterotrophs	8.1	d^{-1}	Henze et al., 2006[d]
b^{H}	Decay rate of heterotrophs	0.54	d^{-1}	Hiatt and Grady, 2008[e]
$K_{NO_2}^{H}$	NO_2^- half-saturation coefficient for heterotrophs	0.3	g N m^{-3}	Alpkvist et al., 2006

$K_{NO_3}^H$	NO_3^- half-saturation coefficient for heterotrophs	0.3	g N m^{-3}	Alpkvist et al., 2006
K_S^H	COD half-saturation coefficient for heterotrophs	20	g COD m^{-3}	Henze et al., 2006
$K_{O_2}^H$	DO half-saturation coefficient for heterotrophs	0.2	g O_2 m^{-3}	Henze et al., 2006
$\eta_{NO2}=\eta_{NO3}$	Reduction factor for maximum growth rate under anoxic conditions	0.8	Dimensionless	Henze et al., 2006
k_a	Organic nitrogen hydrolysis rate constant	0.11	m^3COD (g d) $^{-1}$	Henze et al., 2006[d]
Mass transfer				
D_{NH4}	NH_4^+ diffusion coefficient in water	1.5x10^{-4}	m^2 d^{-1}	Williamson and McCarty, 1976
D_{NO2}	NO_2^- diffusion coefficient in water	1.4x10^{-4}	m^2 d^{-1}	Williamson and McCarty, 1976
D_{NO3}	NO_3^- diffusion coefficient in water	1.4x10^{-4}	m^2 d^{-1}	Williamson and McCarty, 1976
D_{O2}	O_2 diffusion coefficient in water	2.2x10^{-4}	m^2 d^{-1}	Picioreanu et al., 1997
D_{N2}	N_2 diffusion coefficient in water	2.2x10^{-4}	m^2 d^{-1}	Williamson and McCarty, 1976
D_{IC}	Inorganic carbon (as bicarbonate) diffusion coefficient in water	1.6x10^{-4}	m^2 d^{-1}	Williamson and McCarty, 1976
D_S	COD diffusion coefficient in water	1x10^{-4}	m^2 d^{-1}	Hao and van Loosdrecht, 2004
Df/Dw	Diffusion correction factor	0.8	Dimensionless	Eberl et al., 2006

[a] After unit conversion, using a typical biomass composition of $CH_{1.8}O_{0.5}N_{0.2}$, corresponding to 1.3659 g COD g^{-1} biomass

[b] After unit conversion, using an anammox biomass composition of $CH_2O_{0.5}N_{0.15}$ (Strous et al., 1998) corresponding to 36.4 g COD mol^{-1} or 1.51 g COD g^{-1} biomass

[c] Conversion of values given by Hellinga et al. (1999) at 35°C and by Strous et al. (1998) at 32.5°C to 24.3°C using the following relationship (written for X_{AOB}, analogous for X_{NOB} and X_{AN}) (Eq. A.3.1)

$$\mu_{max}^{AOB}(T) = \mu_{max}^{AOB}(T_{ref}) \exp\left(\frac{E_a^{AOB}.(T-T_{ref})}{R.\ T.\ T_{ref}}\right) \qquad \text{Eq. A.3.1}$$

with E_a^{AOB}= 68 kJ mol^{-1} ; E_a^{NOB}= 44 kJ mol^{-1}; E_a^{AN} = 70 kJ mol^{-1} (Strous et al., 1998); R = 8.31 J mol^{-1} K^{-1}.

[d] Conversion of ASM1-value (μ_{max}^H) given by Henze et al., 2006 at 10°C and 20°C to 24.3°C using the temperature relationship proposed by these authors (ASM3).

[e] Conversions of the decay rate of heterotrophs at 20 °C to 24.3°C through the equation Eq. A.3.2.

$$b(T) = b(T_{ref}) \exp\left(\frac{E_{act}(T - T_{ref})}{RTT_{ref}}\right) \qquad \text{Eq. A.3.2}$$

in which E_{act}^{Het} = 48 kJ mol^{-1} (calculated with maximum growth rate values at 283.15 K and 293.15 K according to Eq. A.3.2 (Henze et al., 2006).

Table A.3.4 Model parameters values

Parameter	Value	Unit
Reactor volume (V)	0.98	m^3
Number of reactor compartments (n)	4	-
Influent flow rate (Q)	2.5	$m^3\ d^{-1}$
Sponge filling ratio (FR) [a]	40.0	%
Sponge specific surface area (a_s)[b]	6,600	$m^2\ m^{-3}$

[a] Ratio between sponge volume and reactor volume
[b] Determined as indicated in Appendix A.3.2.

A.3.2 Determination of the specific surface area (a_s) of the polyurethane sponge

The specific surface area (a_s) (6,600 $m^2\ m^{-3}$ – Table A.3.4) of the polyurethane (PU) sponge was determined as proposed by Moon et al., 2010. A sequence of scanning electron microscopy - SEM (FEI Quanta 200 FEG) images (see a sample in Figure A.3.1) of the sponge-based support medium was processed with the free-software Image J.

Parallel transects were randomly put alongside the vertical axis of the SEM images. The length (L; m) and the number of PU fibres (n) in each transect were then determined. The fibre diameter (df; m) was assessed for each fiber identified in the transect. The specific surface area ($m^2\ m^{-3}$) of a cubic PU sponge sheet per unit volume was then calculated as follows (Eq. A.3.3):

$$a_s = \frac{3\,n^2\pi d_f(L-nd_f)}{L^3} \qquad \text{Eq. A.3.3}$$

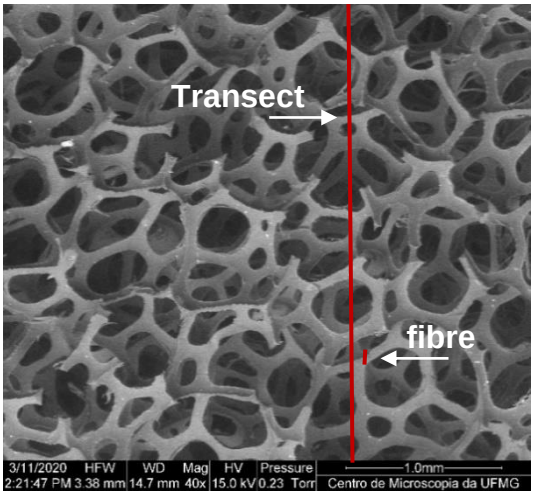

Figure A.3.1 Sample of an SEM image of the sponge-based support medium used to estimate the specific surface area. *A transect and polyurethane fibre is depicted*

A.3.3 Nitrite build-up in SBTFs considering the same AOB and NOB kinetics for inorganic carbon

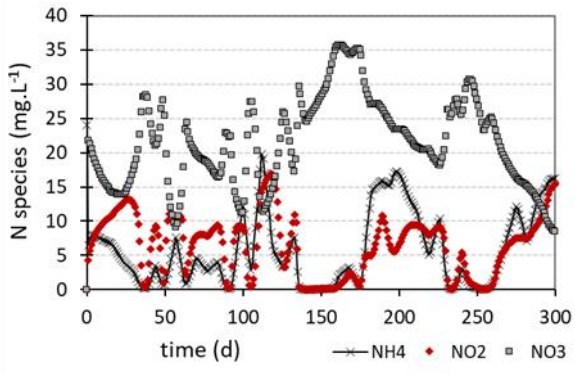

Figure A.3.2 Unrealistic nitrite build-up considering the same AOB and NOB inorganic carbon half-saturation coefficient (Sigmoidal kinetics as proposed by Wett and Rauch (2003))

A.3.4 Ammonium accumulation due to higher half-saturation ammonium coefficient (K_{NH}) and low maximum growth rate (μ_{max}^{AOB}) of AOB

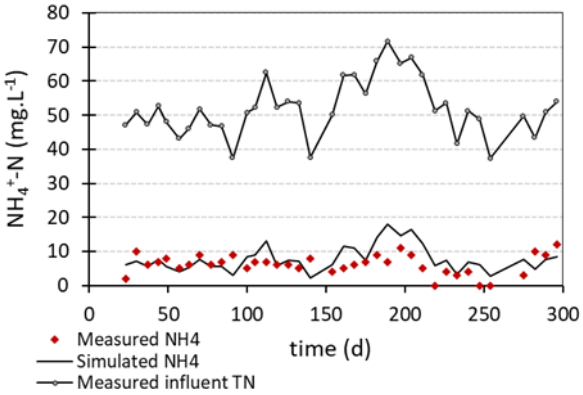

Figure A.3.3 Comparison between simulated and experimental dynamic SBTF performance in terms of effluent ammonium concentrations, based on K_{NH} and μ_{max}^{AOB} values of 50 g N m^{-3} and 0.60 d^{-1}, respectively. *Measured influent total nitrogen concentrations are taken up as well*

A.3.5 Model calibration considering inorganic carbon limitation

Table A.3.5: Overview of all tested approaches for Monod and sigmoidal kinetics description of inorganic carbon limitation for AOB, with the corresponding model efficiency (*E*), simulated median value (x_{md}), and *p*-value concerning the fit of effluent bulk liquid concentrations

Modelling approach	Coefficients for Monod kinetics (K_{IC}; mg L^{-1}) and sigmoidal kinetics (*k*; mg L^{-1} and *a*)	k_La (d^{-1})	Model efficiency (*E*), simulated median (x_{md}; mg L^{-1}) and *p-value*			
			NH_4^+-N	NO_3^--N	$CaCO_3$	DO
Monod	K_{IC} = 10	300	*E* = -2.2 x_{md} = 3 *p* > 0.05	*E* = -2.3 x_{md} = 32 *p* < 0.05	*E* = -1.1 x_{md} = 3 *p* < 0.05	*E* = -13.0 x_{md} = 6.2 *p* < 0.05
		310	*E* = -2.2 x_{md} = 3 *p* > 0.05	*E* = -2.3 x_{md} = 32 *p* < 0.05	*E* = -1.1 x_{md} = 3 *p* < 0.05	*E* = -9.6 x_{md} = 6.6 *p* < 0.05
	K_{IC} = 20	310	*E* = -2.1 x_{md} = 3 *p* > 0.05	*E* = -2.4 x_{md} = 32 *p* < 0.05	*E* = -1.0 x_{md} = 4 *p* < 0.05	*E* = -9.4 x_{md} = 6.6 *p* > 0.05
	K_{IC} =25	310	*E* = -2.1 x_{md} = 4 *p* > 0.05	*E* = -2.4 x_{md} = 32 *p* < 0.05	*E* = -0.9 x_{md} = 5 *p* < 0.05	*E* = -9.3 x_{md} = 6.5 *p* < 0.05
		320	*E* = -2.1	*E* = -2.4	*E* = -1.0	*E* = -7.0

Modelling approach	Coefficients for Monod kinetics (K_{IC}; mg L^{-1}) and sigmoidal kinetics (k; mg L^{-1} and a)	k_La (d^{-1})	Model efficiency (E), simulated median (x_{md}; mg L^{-1}) and *p-value*			
			NH_4^+-N	NO_3^--N	$CaCO_3$	DO
			x_{md} = 4 p > 0.05	x_{md} = 32 p < 0.05	x_{md} = 4 p < 0.05	x_{md} = 6.9 p < 0.05
		330	E = -2.1 x_{md} = 4 p > 0.05	E = -2.5 x_{md} = 32 p < 0.05	E = -1.0 x_{md} = 4 p < 0.05	E = -5.3 x_{md} = 7.0 p > 0.05
Sigmoidal	k = 15 a = 3	310	E = -2.2 x_{md} = 4 p > 0.05	E = -1.9 x_{md} = 31 p < 0.05	E = -0.7 x_{md} = 9 p > 0.05	E = -7.9 x_{md} = 6.7 p > 0.05
	k = 20 a = 4	310	E = -2.3 x_{md} = 4 p > 0.05	E = -1.7 x_{md} = 31 p < 0.05	E = -0.5 x_{md} = 11 p > 0.05	E = -7.2 x_{md} = 6.8 p > 0.05
		320	E = -2.2 x_{md} = 4 p > 0.05	E = -1.7 x_{md} = 31 p < 0.05	E = -0.5 x_{md} = 11 p > 0.05	E = -5.4 x_{md} = 7.1 p > 0.05
	k = 22 a = 4	310	E = -2.3 x_{md} = 4 p > 0.05	E = -1.6 x_{md} = 31 p < 0.05	E = -0.4 x_{md} = 13 p > 0.05	E = -6.8 x_{md} = 6.9 p < 0.05
		320	E = -2.3 x_{md} = 4 p > 0.05	E = -1.6 x_{md} = 31 p < 0.05	E = -0.4 x_{md} = 13 p > 0.05	E = -5.2 x_{md} = 7.1 p > 0.05
	k = 20 a = 5	310	E = -2.2 x_{md} = 4 p > 0.05	E = -1.7 x_{md} = 31 p < 0.05	E = -0.5 x_{md} = 11 p > 0.05	E = -5.4 x_{md} = 7.1 p > 0.05
	k = 25 a = 5	310	E = -2.2 x_{md} = 5 p > 0.05	E = -1.8 x_{md} = 31 p < 0.05	E = -0.6 x_{md} = 9 p > 0.05	E = -7.6 x_{md} = 6.7 p > 0.05
	k = 27 a = 5	310	E = -2.4 x_{md} = 5 p > 0.05	E = -1.5 x_{md} = 30 p < 0.05	E = -0.4 x_{md} = 14 p > 0.05	E = -6.6 x_{md} = 6.9 p > 0.05
		320	E = -2.4 x_{md} = 5 p > 0.05	E = -1.5 x_{md} = 30 p < 0.05	E = -0.3 x_{md} = 16 p > 0.05	E = -4.7 x_{md} = 7.1 p > 0.05
	k = 28 a = 5	320	E = -2.4 x_{md} = 5	E = -1.4 x_{md} = 30	E = -0.3 x_{md} = 17	E = -4.6 x_{md} = 7.1

Modelling approach	Coefficients for Monod kinetics (K_{IC}; mg L^{-1}) and sigmoidal kinetics (k; mg L^{-1} and a)	k_La (d^{-1})	Model efficiency (E), simulated median (x_{md}; mg L^{-1}) and *p-value*			
			NH_4^+-N	NO_3^--N	$CaCO_3$	DO
			$p > 0.05$	$p < 0.05$	$p > 0.05$	$p > 0.05$
		330	E = -2.4 x_{md} = 5 $p > 0.05$	E = -1.5 x_{md} = 30 $p < 0.05$	E = -0.3 x_{md} = 16 $p > 0.05$	E = -3.6 x_{md} = 7.2 $p > 0.05$
k = 30 a = 5		320	E = -2.5 x_{md} = 5 $p > 0.05$	E = -1.4 x_{md} = 30 $p < 0.05$	E = -0.3 x_{md} = 18 $p > 0.05$	E = -4.4 x_{md} = 7.1 $p > 0.05$
		330	E = -2.5 x_{md} = 5 $p > 0.05$	E = -1.4 x_{md} = 30 $p < 0.05$	E = -0.3 x_{md} = 18 $p > 0.05$	E = -3.5 x_{md} = 7.2 $p > 0.05$
k = 31 a = 5		320	E = -2.5 x_{md} = 5 $p > 0.05$	E = -1.3 x_{md} = 30 $p < 0.05$	E = -0.3 x_{md} = 19 $p > 0.05$	E = -4.2 x_{md} = 7.1 $p > 0.05$
		330	**E = -2.5 x_{md} = 5 $p > 0.05$**	**E = -1.3 x_{md} = 30 $p < 0.05$**	**E = -0.3 x_{md} = 19 $p > 0.05$**	**E = -3.4 x_{md} = 7.2 $p > 0.05$**
k = 32 a = 5		320	E = -2.6 x_{md} = 5 $p > 0.05$	E = -1.3 x_{md} = 30 $p < 0.05$	E = -0.3 x_{md} = 20 $p > 0.05$	E = -4.1 x_{md} = 7.1 $p > 0.05$
		330	E = -2.6 x_{md} = 5 $p > 0.05$	E = -1.3 x_{md} = 30 $p < 0.05$	E = -0.3 x_{md} = 20 $p > 0.05$	E = -3.3 x_{md} = 7.3 $p > 0.05$
		350	E = -2.5 x_{md} = 5 $p > 0.05$	E = -1.4 x_{md} = 30 $p < 0.05$	E = -0.3 x_{md} = 20 $p > 0.05$	E = -2.6 x_{md} = 7.4 $p < 0.05$
k = 33 a = 5		330	E = -2.5 x_{md} = 5 $p > 0.05$	E = -1.3 x_{md} = 30 $p < 0.05$	E = -0.3 x_{md} = 21 $p > 0.05$	E = -3.2 x_{md} = 7.3 $p > 0.05$
k = 35 a = 5		330	E = -2.8 x_{md} = 6 $p > 0.05$	E = -1.2 x_{md} = 30 $p < 0.05$	E = -0.3 x_{md} = 23 $p > 0.05$	E = -3.1 x_{md} = 7.3 $p > 0.05$

Bold and highlighted values refer to the calibrated approach (Sigmoidal k = 31 mg $CaCO_3$ L^{-1}; a = 5; k_La = 330 d^{-1}).
E: accuracy efficiency applying the Nash-Sutcliffe criterion (Nash and Sutcliffe, 1970); x_{md} = median values from simulation; p = p-value from Wilcoxon Signed Rank Test

Observed median values from experimental data: 6 mg NH_4^+-N L^{-1}; 27 mg NO_3^--N L^{-1}; 19 mg $CaCO_3$ L^{-1}; 6.6 mg O_2 L^{-1}

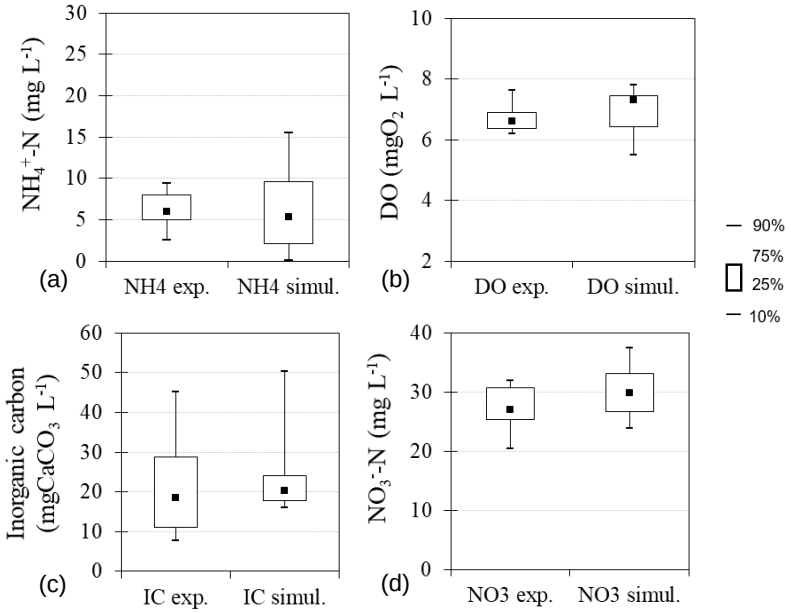

Figure A.3.4 Boxplot of simulated dynamic SBTF effluent concentrations of (a) ammonium, (b) dissolved oxygen (DO), (c) inorganic carbon, and (d) nitrate (Sigmoidal approach for inorganic carbon limitation of AOB – K = 31 mg $CaCO_3$ L^{-1}; a = 5; k_La = 330 d^{-1})

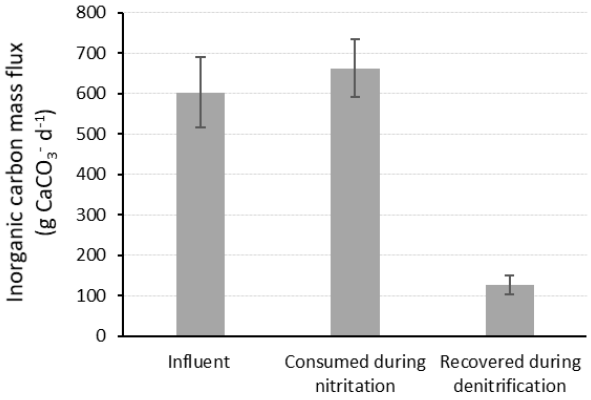

Figure A.3.5 Main mass fluxes of inorganic carbon (g $CaCO_3^-$ d^{-1}) in the modelled SBTF

A.3.6 Model validation results

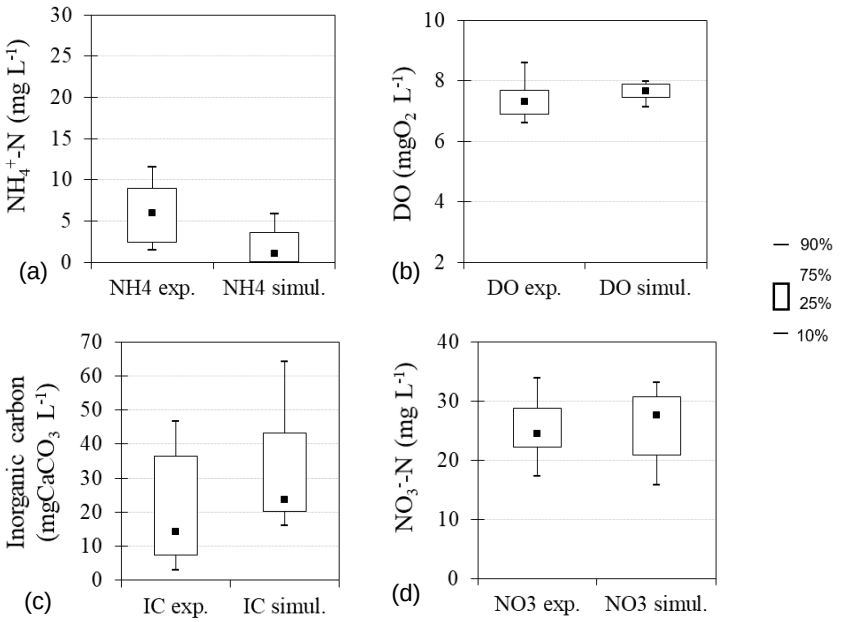

Figure A.3.6 Model validation on the dataset of Almeida et al. (2013): boxplot of simulated dynamic SBTF effluent concentrations of (a) ammonium, (b) dissolved oxygen (DO), (c) inorganic carbon, and (d) nitrate (Sigmoidal approach for inorganic carbon limitation of AOB – k = 31 mg $CaCO_3$ L^{-1}; a = 5)

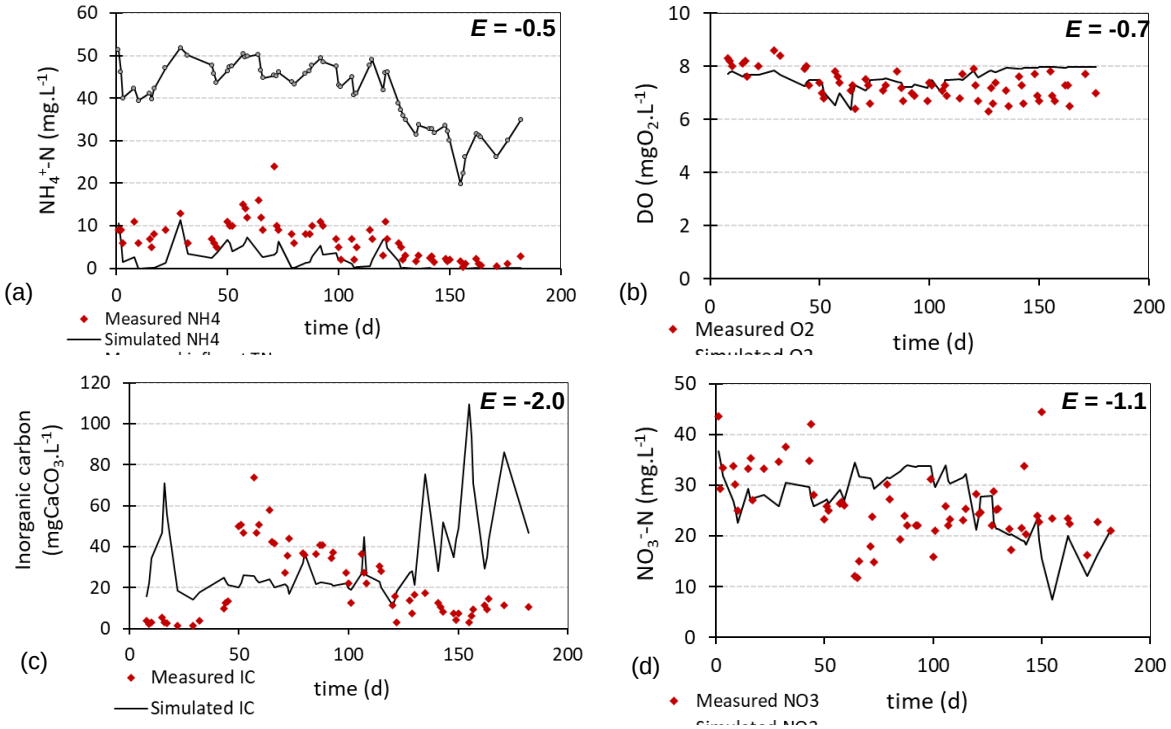

Figure A.3.7 Model validation on the dataset of Almeida et al. (2013): dynamic simulation results compared to experimental data of effluent (a) ammonium, (b) dissolved oxygen, (c) inorganic carbon, and (d) nitrate (Sigmoidal approach for inorganic carbon limitation of AOB – k = 31 mg $CaCO_3$ L^{-1}; a = 5). *Model efficiencies (E criteria) are shown as well*

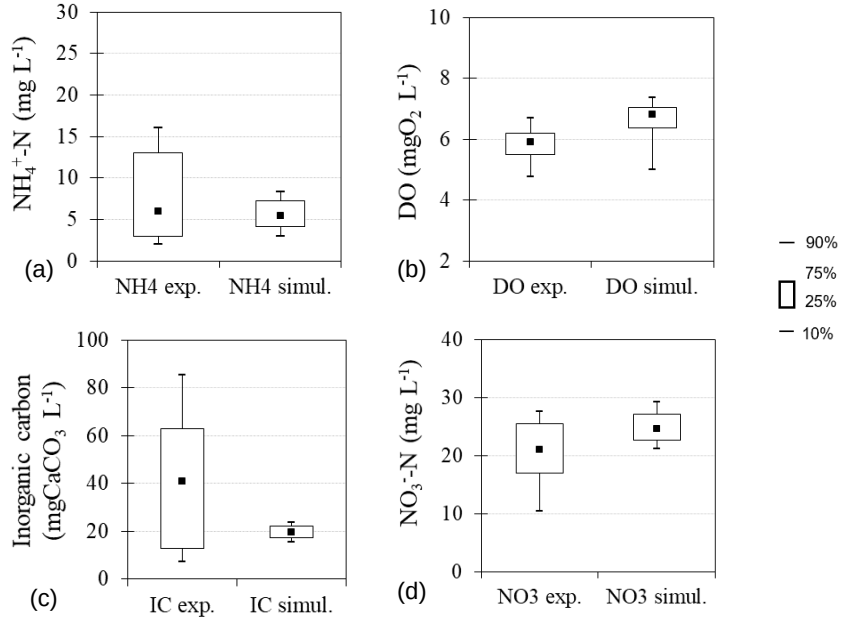

Figure A.3.8 Model validation on parallel SBTF dataset: boxplot of simulated dynamic effluent concentrations of (a) ammonium, (b) dissolved oxygen (DO), (c) inorganic carbon, and (d) nitrate (Sigmoidal approach for inorganic carbon limitation of AOB – k = 31 mg $CaCO_3$ L^{-1}; a = 5)

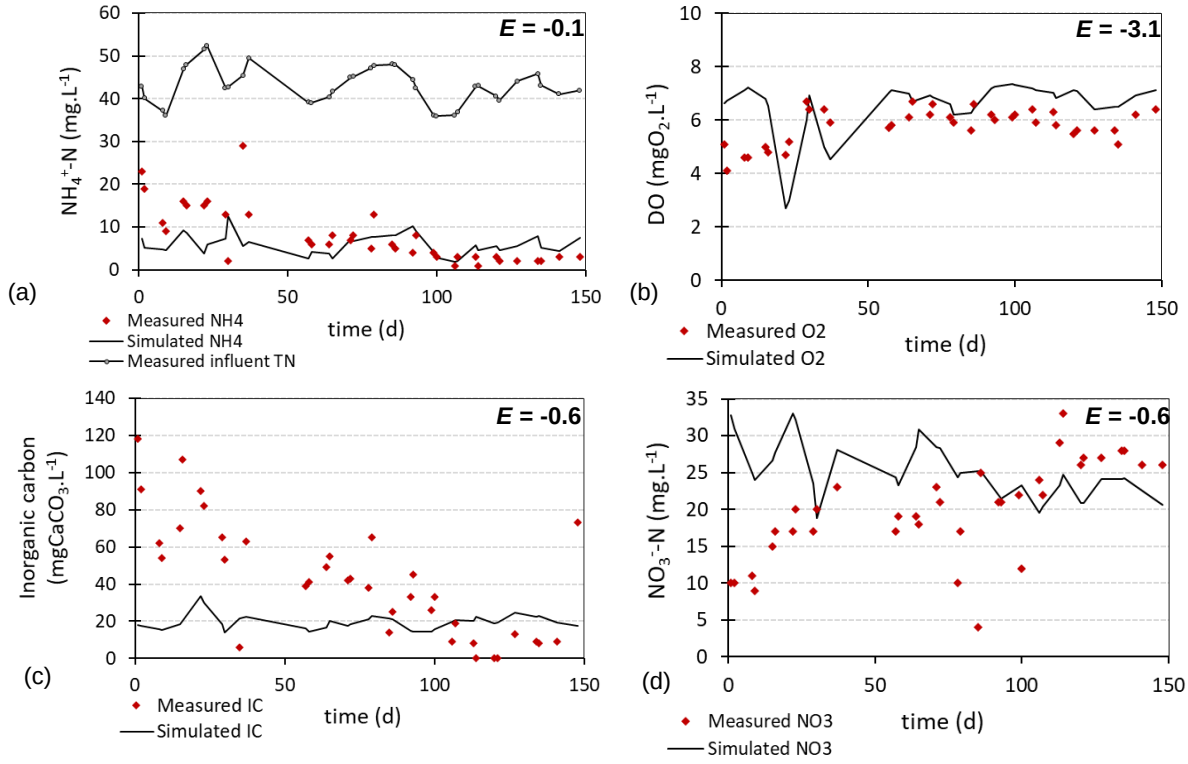

Figure A.3.9 Model validation on parallel SBTF dataset: dynamic simulation results compared to experimental data of effluent (a) ammonium, (b) dissolved oxygen, (c) inorganic carbon, and (d) nitrate (Sigmoidal approach for inorganic carbon limitation of AOB – k = 31 mg $CaCO_3$ L^{-1}; a = 5). *Model efficiencies (E criteria) are shown as well*

A.3.7 Alternative model validation results - without inorganic carbon limitation

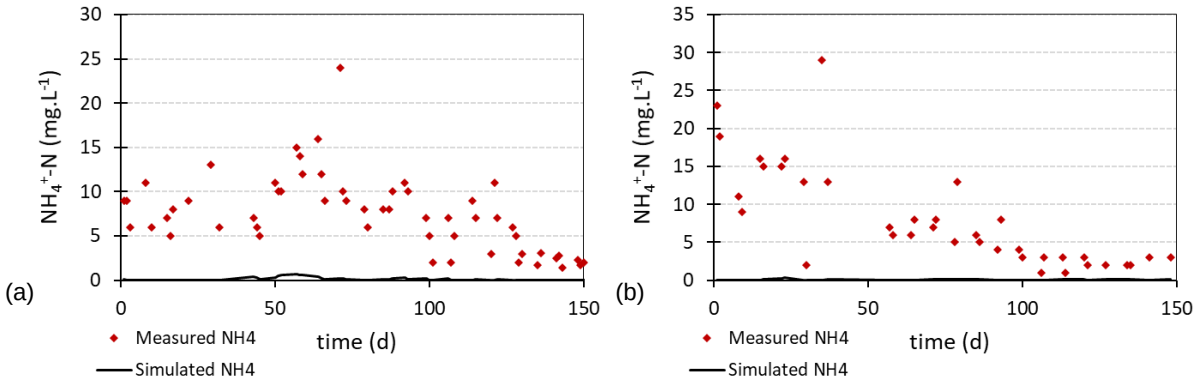

Figure A.3.10 Model validation results without including inorganic carbon limitation in the kinetic rate expression of AOB, considering the dataset of (a) Almeida et al. (2013) and (b) the parallel monitored SBTF

A.3.8 Dynamic effluent dataset of the monitored UASB reactor and SBTF

A spreadsheet is provided concerning the dynamic effluent dataset of the monitored UASB reactor and SBTF in terms of COD, filtered COD, NH_4^+-N, NO_2^--N, NO_3^--N, DO, and bicarbonate. It can be downloaded at

https://www.sciencedirect.com/science/article/pii/S0043135421005352?via%3Dihub#sec0020.

Chapter 4

Key parameters controlling nitrogen removal in sponge-bed trickling filters treating mainstream anaerobic effluents

4.0 Abstract

Efficient nitrogen removal following anaerobic sewage treatment is generally accomplished in mechanically aerated systems, which are energy-intensive compared to naturally ventilated processes, such as sponge-bed trickling filters (SBTFs). Promising configurations have been presented for total nitrogen removal in SBTFs treating anaerobic effluents. Nevertheless, there is a remaining knowledge gap on the main factors influencing process performance. This contribution mechanistically assesses the effect of key reactor and kinetic parameters controlling nitrogen conversions in SBTFs. Based on a sensitivity analysis, a simulation study was performed considering the key reactor-specific parameters that influence the formation of nitrogen gas via heterotrophic denitrification or anammox. The results support that the interplay between the oxygen transfer coefficient, external mass transfer resistance, biofilm thickness, and specific surface area of the sponge influences the optimum oxygen concentration to sustain AOB activity without compromising anammox bacteria growth. Furthermore, attention was paid to deriving strategies for enhancing process start-up for high total nitrogen removal, which was identified as a primary bottleneck. Standalone biomass inoculation strategies for promoting a fast partial-nitritation anammox are ineffective if inhibitory oxygen levels remain at the biofilm-liquid interface. Effluent recirculation coupled to sewage by-pass led to a quick establishment of heterotrophic denitrification; however, limited at approximately 55% total nitrogen removal. Overall, high performance for both processes (heterotrophic and autotrophic) relies on particular reactor-specific parameters.

4.1 Introduction

Anaerobic sewage treatment, typically through UASB reactors, is widely applied in Latin American countries such as Brazil. However, while anaerobic treatment removes the majority of organic carbon from wastewater, it does not remove nitrogen. The total nitrogen concentration of anaerobically treated sewage typically amounts to approximately 45 mg N L^{-1}. In order to protect receiving water bodies, there has been a growing momentum to set a maximum discharge target of, e.g., 20 mg N L^{-1}, which corresponds with a required minimum total nitrogen removal efficiency of 60%.

Currently achieved total nitrogen removal efficiencies during post-treatment of UASB-effluent are typically quite modest. The highest nitrogen removal efficiencies reported are less than 80% and are only achieved by mechanically aerated systems, such as the activated sludge process adapted for biological nutrient removal (see **Chapter 1**). Less energy-intensive technologies, such as sponge-bed trickling filters (SBTFs), have proven to achieve stable nitrification treating anaerobic effluents, albeit limited by a lack of inorganic carbon (see **Chapter 3**). The realization of efficient nitrogen removal is limited by the removal of organic carbon during the preceding anaerobic stage. Reported efficiencies are typically limited to approximately 35% (Onodera et al., 2014; Tandukar et al., 2006b).

Conventional nitrification-denitrification has been reported as the predominant pathway for nitrogen removal in SBTFs following UASB reactors for sewage treatment (Onodera et al., 2016; Tandukar et al., 2006b). The long solids retention time (SRT) in the reactor contributes to the release of soluble products (Almeida et al., 2013), which could be a significant additional source of electron donors for heterotrophic denitrification (Araki et al., 1999) - given that most of the organic carbon from the sewage has been removed in the preceding anaerobic treatment stage. Besides, the low biodegradability of the residual COD in the anaerobically treated sewage (Aquino et al., 2009) may favour the growth of slow-growing autotrophic organisms such as anammox bacteria in their competition with heterotrophs for nitrogen removal. The first report of partial nitritation in SBTFs by Chuang et al. (2007) paved the way to pilot-scale trials, which demonstrated the implementation of nitrogen removal through the partial nitritation-anammox process (PN/A) in a one-stage SBTF for synthetic wastewater (Sánchez-Guillén et al., 2015b). Still, the competition between anammox

bacteria and heterotrophic denitrifiers in SBTFs fed with anaerobically treated sewage has not yet been fully elucidated. Particular questions remain regarding the influence in the long term of residual organic carbon, dissolved oxygen concentrations and lack of inorganic carbon in the anaerobic effluent.

Overall, effective total nitrogen removal in SBTFs is limited by a lack of knowledge on the prevailing nitrogen removal pathways (nitrification-denitrification versus PN/A) and the main design and operating factors influencing process performance. Long-term assessments considering possible influencing factors are not available. Only one report of a long-term full-scale SBTF operation achieved 65% total nitrogen removal efficiency (Onodera et al., 2016). In this case, effluent recirculation was applied, and heterotrophic denitrification was assumed as the prevailing pathway, possibly assisted by biomass decay products. Nonetheless, the mechanisms were not clearly addressed, and the autotrophic process might have played a role based on the presence of anammox bacteria in other SBTFs treating anaerobic effluents (Mac Conell et al., 2015). Some experimental data is available on implementing PN/A in SBTFs by controlling natural ventilation (Sánchez-Guillén et al., 2015b). A fast process start-up was also suggested (< 100 days); however, the tested influent had no organic matter and ammonium concentrations far exceeded (> 100 mg L^{-1}) those typically found in anaerobically treated sewage. Therefore, insights are still lacking on influent conditions, process control, and start-up of SBTFs following UASB reactors for high nitrogen removal performance. Moreover, performing experiments is costly and time-consuming. Mathematical modelling and simulation constitute adequate complementary tools, allowing insight into the underlying nitrogen removal mechanisms that are hard to identify experimentally.

In this contribution, a mechanistic model was applied to assess the main design and operational factors influencing total nitrogen removal in SBTFs treating anaerobic effluents. The simulation results were validated against experimental results available from the literature, complemented with additional DO microsensor measurement data. A long-term simulation was performed to evaluate the SBTF at steady-state effluent conditions, complemented by a sensitivity analysis towards nitrogen gas formation. The key parameters influencing total nitrogen removal were then combined in different

scenarios which would realistically occur in full-scale plants. Possible operational strategies were simulated to circumvent the identified bottleneck of process start-up.

4.1 Materials and methods

4.1.1 SBTF model

A sponge-bed trickling filter was described by a previously developed mechanistic one-dimensional biofilm model, calibrated, and validated for SBTFs following UASB reactors treating sewage (**Chapter 3**). The model considers biological conversion reactions by ammonium oxidizing bacteria (AOB), nitrite oxidizing bacteria (NOB), anammox bacteria, and heterotrophs. The stoichiometric matrix, reaction rates, and parameter values were the same as for **Chapter 3** (detailed in Appendix, section A.3.1). The SBTF was modelled as a sequence of four completely mixed biofilm reactor compartments (0.25 m^3 each), considering a sponge filling ratio of 40%.

4.1.2 Sensitivity analysis

A steady-state sensitivity analysis was performed to determine the model parameters that most affect N_2 formation (i.e., total nitrogen removal) via heterotrophic denitrification and anammox process. The model structure features different state variables to trace nitrogen gas based on its origin, i.e., production through the anammox conversion (state variable S_{N2A}) or by heterotrophic denitrification (state variable S_{N2H}), as proposed in Mozumder et al. (2014). To this end, the absolute-relative sensitivity function available in the AQUASIM software was used (Reichert, 1995), which determines the absolute change in the output of a model variable for a 100% change in the parameter of interest.

The determined standard deviations from long-term experiments (from **Chapter 5**) were assigned to each input variable for the influence of uncertainty, and a relative uncertainty of 10% was ascribed to each model parameter. Minimum and maximum bounds were assigned to the input variables as measured experimentally, and value ranges reported in the literature were considered for model parameters, as detailed in Table A.4.1.

4.1.3 Simulation study

The SBTF operation described in **Chapter 3** was taken as the reference scenario. In contrast to the 300 days simulation presented in that chapter, the model was run sufficiently long (6000 days) to achieve steady-state, in the sense that less than 1% change was reached in terms of final effluent concentrations.

Seven additional scenarios were defined to assess the influence of influent characteristics, design parameters, and operating conditions (Table 4.1). For all scenarios, the temperature remained constant at 25^{o}C. The process settling time, i.e., the time required to reach 95% of the observed steady-state output in terms of the bulk liquid concentrations, was used to characterize process speed for comparison between scenarios. Scenarios 1 – 4 aimed at assessing the influence of critical parameters on the steady-state total nitrogen removal efficiency; scenarios 5 – 7 aimed at evaluating possible operational strategies to optimize process start-up, as this was identified as a bottleneck by the former group of simulations.

In scenario 1, the most reactor design parameters as identified through the sensitivity analysis (Section 4.1.2) were varied, i.e., k_La, L_L, L_F, and a_s. The oxygen transfer rate (k_La) and the external mass transfer boundary layer thickness (L_L) were varied from 10 to 1000 d^{-1} and 20 to 1500 µm, respectively. This is in line with reported values for k_La and L_L for trickling filters, with broad ranges between 106 and 7027 d^{-1} (Uemura et al., 2016; Watari et al., 2020), and 20 and 1,500 µm (Henze et al., 2008), respectively. An upper value of 100 µm was considered for the maximum biofilm thickness (L_F) as nitrifying biofilms in trickling filters are reported to be relatively thin (< 100 µm; Siegrist and Gujer, (1987). Concerning the specific surface area of the sponge-based support material (a_s), the assessed lower and upper values (5600 and 8500 m^2 m^{-3}) were derived from scanning electron microscopy determination (detailed in Appendix, section A.3.2 - **Chapter 3**).

Scenario 2 addressed the influence of the applied loading rates (hydraulic rate - HLR, organic loading rate - OLR, and nitrogen loading rate – NLR) by increasing the influent flow rate with a factor 2 to 4 compared to the reference scenario (from 2.5 to 5 - 10 m^3 d^{-1}). Conversely, Scenario 3 kept the reference influent flow rate (2.5 m^3 d^{-1}) but increased the influent COD concentration (from 30 to 45 - 135 g m^{-3}; soluble COD),

implying higher C/N ratios and OLR. Such a condition can occur in practice due to variations in the COD conversion efficiency in the preceding UASB reactor.

Scenario 4 considered the possible by-pass of raw sewage to the inlet of SBTFs as a way of increasing the SBTF influent COD content. Raw sewage was assumed to have a readily biodegradable COD content of 190 mg L^{-1} (**Chapter 3**); its flow rate was determined such that target COD concentrations of 45 and 90 g m^{-3} (C/N ratios of 1 and 2 g COD g N^{-1}, respectively) at the SBTF inlet were obtained by mixing the raw sewage and the anaerobic effluent (30 mg COD L^{-1}; Q_{in} = 2.5 m^3 d^{-1}). In addition, the impact of different k_La and L_L values was considered to study the combined effects.

In order to evaluate the possible optimization of process start-up, scenario 5 considered the impact of different initial active biomass fractioning of anammox (from 2.5 to 10% of the overall biomass fraction). This stands for different inoculum strategies at the start-up of the SBTF. As an alternative, scenario 6 implemented effluent recirculation to the top compartment of the SBTF, which leads to higher HLR (from 15 to 25 m^3 m^{-2} d^{-1}). In Scenario 7, sewage by-pass was implemented analogous to Scenario 4 but this time also applying effluent recirculation (at 2.5 m^3 d^{-1}). The resulting influent flow rate was determined based on the mixture of the anaerobic effluent and raw sewage for the target C/N ratios of 1 or 2 g COD g N^{-1}. In addition, Scenario 7 also considered the impact of different k_La and L_L values.

Table 4.1 Overview of scenario analysis to assess the influence of influent characteristics, design parameters, and operating conditions on the steady-state nitrogen removal efficiency and the process start-up. Bold indications refer to values differing from the reference scenario

	k_La (d^{-1})	L_L (µm)	L_F (µm)	a_s (m^2 m^{-3})	εX_{AN} (%)	Q (m^3 d^{-1})	HLR (m^3 m^{-2} d^{-1})	COD (g m^{-3})	Influent C/N ratio[a] (g COD g TN^{-1})	OLR (kg COD m^{-3}_{sponge} d^{-1})	NLR[a] (kg N m^{-3}_{sponge} d^{-1})
Reference scenario											
Reference scenario	330	1500	65	6600	0.1	2.5	10	30	0.7	0.19	0.28
Influence on steady-state nitrogen removal efficiency											
Scenario 1 *Influence of reactor parameters*	**10 – 1000**	**20 – 1500**	**65 – 100**	**5600 – 8500**	0.1	2.5	10	30	0.7	0.19	0.28
Scenario 2 *Influence of influent flow rate – impacting HLR, OLR, and NLR*	330	1500	65	6600	0.1	**5.0** **7.5** **10.0**	**20** **30** **40**	30	0.7	**0.38** **0.56** **0.75**	**0.56** **0.84** **1.13**
Scenario 3 *Effect of influent COD concentration – impacting influent C/N ratio and OLR*	330	1500	65	6600	0.1	2.5	10	**45** **90** **135**	**1.0** **2.0** **3.0**	**0.28** **0.56** **0.84**	0.28
Scenario 4 (raw sewage bypass) *Combined effects of OLR, NLR and C/N ratio – besides k_La, L_L*	**10 – 1000** **10 – 1000**	**20 – 1500** **20 – 1500**	65	6600	0.1	**2.8** **4.0**	**11** **16**	**45** **90**	**1.0** **2.0**	**0.31** **0.89**	**0.31** **0.45**
Possible operational strategies to optimize process start-up											
Scenario 5 *Effect of biomass inoculation*	330	1500	65	6600	**2.5 – 10**	2.5	10	30	0.7	0.19	0.28
Scenario 6 *Effect of effluent recirculation*	330	1500	65	6600	0.1	**3.8** **5.0** **6.3**	**15** **20** **25**	30[c]	0.7	**0.29**[c] **0.38**[c] **0.47**[c]	**0.43**[c] **0.56**[c] **0.71**[c]
Scenario 7 *Effect of sewage by-pass and effluent recirculation*	**10 – 1000** **10 – 1000**	**20 – 1500** **20 – 1500**	65	6600	0.1	**5.3**[b] **6.5**[b]	**21** **26**	**45**[c] **90**[c]	**1.0** **2.0**	**0.60**[c] **1.46**[c]	**0.60**[c] **0.73**[c]

[a] TN influent concentration set as 45 g m^{-3}; [b] Determined based on the mixture of the anaerobic effluent (30 g COD m^{-3}; Q_{in} = 2.5 m^3 d^{-1}) and raw sewage (193 g COD m^{-3}) for the target C/N ratios of 1 or 2 g COD g N^{-1}. Recirculation flow rate kept at 2.5 m^3 d^{-1}; [c] As recirculation is implemented, real values of influent C/N ratio, OLR, and NLR rely on the effluent concentrations of COD and TN. k_La: volumetric oxygen transfer coefficient; L_L: external mass transfer boundary layer thickness; L_F: biofilm thickness; a_s: specific surface area of the sponge; εX_{AN}: initial volume fraction of anammox bacteria.

4.1.4 Experimental microsensor DO measurements

Data on microsensor DO measurements at the top and bottom compartments of a previously monitored SBTF (**Chapter 3**) were gathered. Such a reactor was operated according to the present reference simulation scenario. The goal is to confront simulation outputs with experimental evidence concerning bulk liquid DO concentrations over the SBTF depth.

4.2 Results and Discussion

4.2.1 Total nitrogen removal in SBTFs: reference scenario

As for the first 1000 simulated days, total nitrogen removal was limited to approximately 35% (Figure 4.1). Heterotrophic denitrification was the primary process during this period, nearly accounting for the whole (97%) total nitrogen observed in the period and gradually decreasing at the expense of increasing anammox activity. A steep increase in total nitrogen removal efficiency was observed between day 1090 and 2020, from 35% to 79%. A shift in the primary metabolic conversion pathway occurred at day 1600, from heterotrophic denitrification to the anammox process. The process settling time amounted to 2347 days. At steady-state, total nitrogen removal reached approximately 95%, and the anammox reaction accounted for 95% of the total N_2 produced. This performance is slightly above the stoichiometric limit for the anammox process (89%), demonstrating the synergetic interaction with heterotrophic denitrification in the SBTF. Decay products likely contributed as electron donors for heterotrophs, as organic carbon was fully converted in the upper compartments of the reactor (see further), and nitrogen incorporation into biomass is negligible.

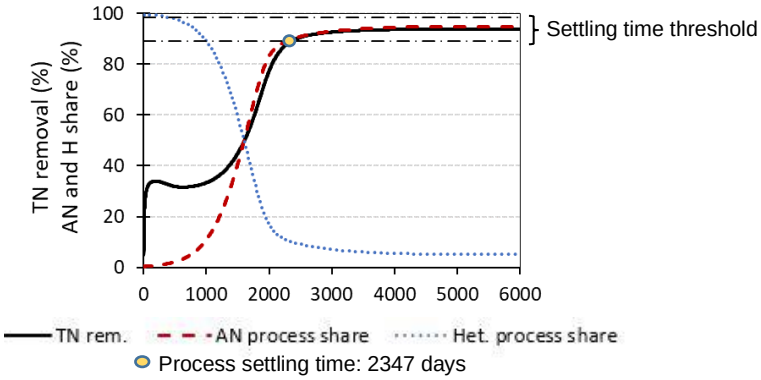

Figure 4.1 Total nitrogen removal efficiency - share of heterotrophic denitrification and anammox processes in the N_2 production

The corresponding microbial population distribution over the height of the trickling filter and over time is displayed in Figure 4.2. An arbitrary day (day 500) was selected prior to the observed metabolic change to highlight microbial variations compared to process settling time. As for the first 1000 simulated days, AOB colonized the entire SBTF depth, while NOB prevailed only in the reactor bottom compartments. Over time, AOB abundance in the bottom compartments decreased, and anammox bacteria grew in the top compartments (up to mid-depth). Such behaviour was also experimentally reported by Mac Conell et al. (2015) for an SBTF under a similar hydraulic loading rate (approximately 10 $m^3\ m^{-2}\ d^{-1}$), receiving anaerobic effluents.

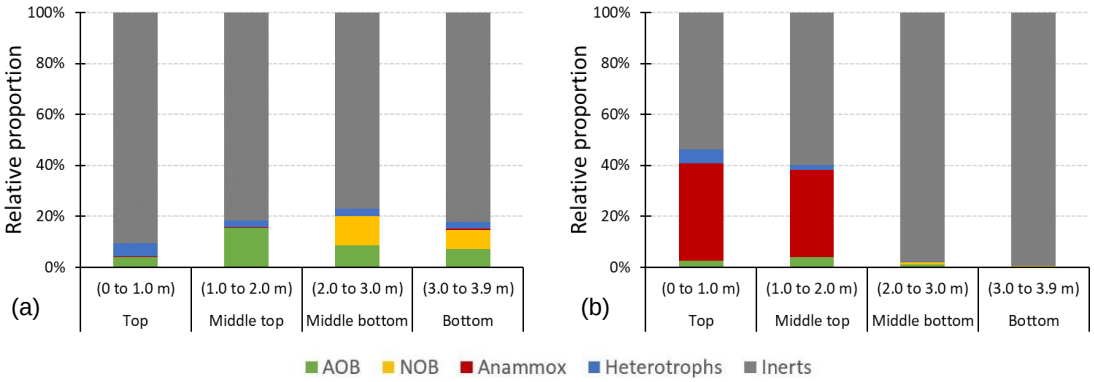

Figure 4.2 Relative biomass proportion in each SBTF compartment at (a) 500 days and at (b) the process settling time (2347 days)

From the substrate concentration profiles along with the SBTF depth (Figure 4.3), it is clear that the incoming COD is fully removed in the upper half of the reactor. This was experimentally demonstrated in SBTFs treating anaerobic effluents (Okubo et al., 2015). Ammonium is mostly removed at the top and middle top compartments. Nitrite accumulated in the middle top compartment at 500 days (Figure 4.3a) but was fully converted at steady-state (Figure 4.3b), along with increasing anammox activity. The middle top compartment of the SBTF is thus a nitrite sink.

Experimental results also showed nitrite accumulation at the middle layer of an SBTF post-UASB reactor (Almeida et al., 2013). The already low C/N ratio at the inlet (0.7 g COD g N^{-1}) further decreases downwards in the SBTF, restraining heterotrophic competition. Moreover, the incoming organic substrate is already depleted at the bottom of the reactor, but biofilm thickness steadily increases over time associated with the build-up of inerts from endogenous respiration. This tends to further limit substrate

transport (i.e., NO_3^--N) to the inner biofilm, thus decreasing heterotrophic denitrification.

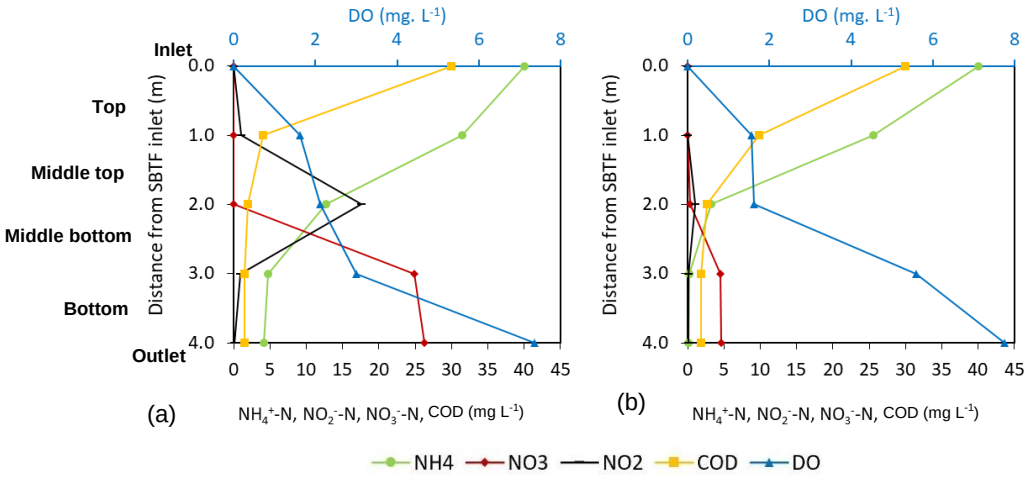

Figure 4.3 Substrate profiles of nitrogen species, DO and COD along with the SBTF depth at 500 days (a) and at the process settling time (2347 days) (b)

The simulated bulk liquid DO concentrations at the upper compartments (up to the middle top) are approximately 2 mg L^{-1} (see Figure 4.3). This is supported by experimental observations in which DO is mainly incorporated into the liquid phase from the middle top downwards (Hatamoto et al., 2018), where COD and ammonium were already depleted. Although the relatively high bulk-liquid DO concentrations at the biofilm-liquid interface are less than 0.06 (Figure 4.4a) and 0.12 mg L^{-1} (Figure 4.4b) at the top and middle top compartment, respectively, due to the external mass transfer resistance. Therefore, oxygen diffusion further decreases into the biofilm and NOB is outcompeted by AOB close to the biofilm surface due to the lower oxygen affinity of the former ($K_{O2,AOB}$ = 0.6 g m^{-3}; $K_{O2,NOB}$ = 1.1 g m^{-3}).

At steady-state, the maximum concentration of anammox bacteria in the biofilm is found just below a layer of heterotrophs at the top and middle top compartments of the SBTF. Close to the biofilm surface, AOB compete with heterotrophs for the limited available oxygen as electron acceptor. This potentially led to partial nitrification, also preventing NOB overgrowth. Therefore, anammox bacteria have easy access to the remaining non-oxidized ammonium (diffusing from the bulk liquid) and nitrite (produced by AOB) as their electron acceptor. Data from microsensor profile measurements of DO in a previously monitored SBTF (**Chapter 3**) confirm the existence of anoxic niches

at the upper compartments of the monitored SBTF (Figure A.4.1), thus supporting the prevalence of anammox in the long-term observed through simulations.

To further assess the relevance of partial denitrification for the nitrite build-up in the middle bottom compartment, a supplementary simulation was performed deactivating such a process (see process 6, Table A.3.1 – **Chapter 3**). Results confirm that partial denitrification was neither a relevant mechanism supporting the observed transition for short-curt total nitrogen removal nor a significant nitrite source for anammox bacteria in the long term. Under steady-state conditions, partial denitrification contributes to a slight increase in TN removal (from 85 to 94% - Figure A.4.2).

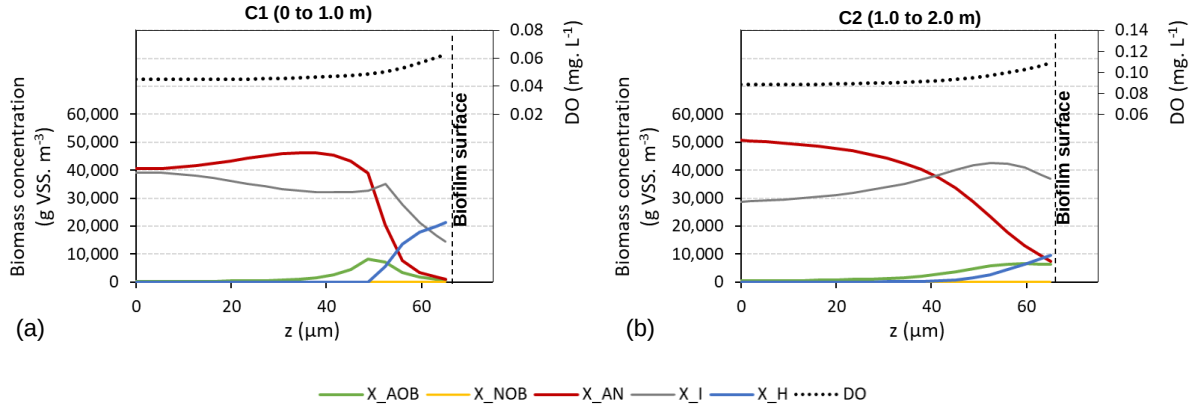

Figure 4.4 Biomass distribution and oxygen profile in the biofilm at the (a) top and (b) middle top SBTF compartments, at the process settling time

4.2.2 Sensitivity analysis: key parameters influencing total nitrogen removal in SBTFs

The absolute-relative sensitivity function (as g N m^{-3}) of model parameters towards N_2 formation (i.e., total nitrogen removal) is shown in Figure 4.5 for both the anammox process and heterotrophic denitrification. Only values higher than 1 g N m^{-3} are shown, as this was assumed as a threshold of significant effect. A similar approach was applied by Mburu et al. (2014), studying the organic matter and nitrogen transformations in a wetland system.

Concerning reactor-operation-specific parameters, N_2 formation is most influenced by the volumetric oxygen mass transfer coefficient (k_La), maximum biofilm thickness (L_F), and specific surface area of the sponge media (a_s). Besides, the external mass transfer boundary layer thickness (L_L) plays a role. N_2 formation is also remarkably sensitive to

the kinetic parameters of anammox bacteria, AOB, and heterotrophs. As for the influence of influent characteristics and initial conditions, the total nitrogen removal performance is susceptible to the influent nitrogen (mainly as ammonium) ($S_{in}\_NH_4$) and organic carbon concentrations (S_{in}_S). Influent concentrations of inorganic carbon (S_{in}_IC) and the initial volume fraction of anammox bacteria (εX_{AN}) play a role in nitrogen removal via the anammox process.

The results from section 4.2.1 showed that the SBTF could be assumed to be in its optimum performance in the reference scenario at steady-state (94% total nitrogen removal). However, the slow process start-up (> 1500 days) is a major drawback. Therefore, the performed sensitivity analysis substantiated further evaluation of mass-transfer related parameters, influent characteristics, and initial conditions, as those most impacted N_2 formation in the reactor. Although kinetic parameters showed to highly influence N_2 formation from both pathways (heterotrophic and autotrophic), their values were not changed during scenario analysis ahead, as they had been previously calibrated and validated for the system under study (see **Chapter 3**).

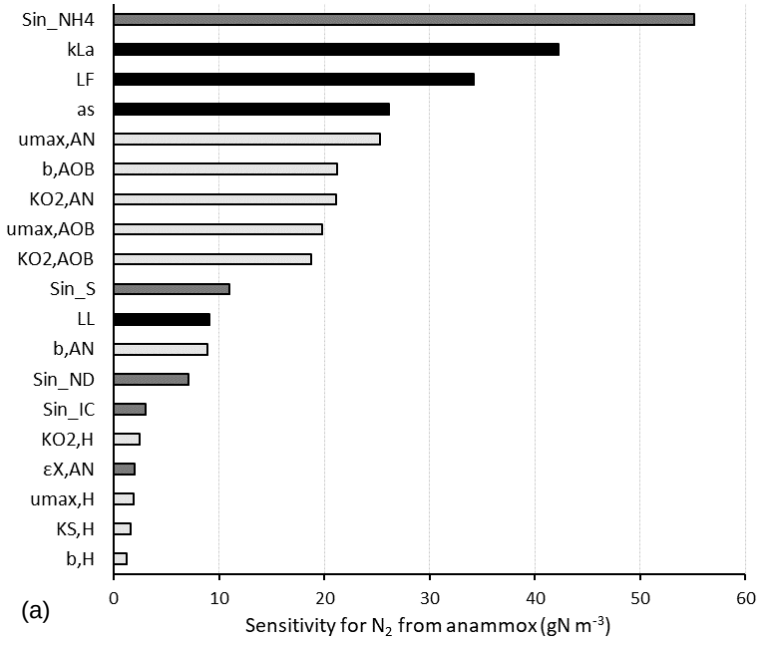

(a)

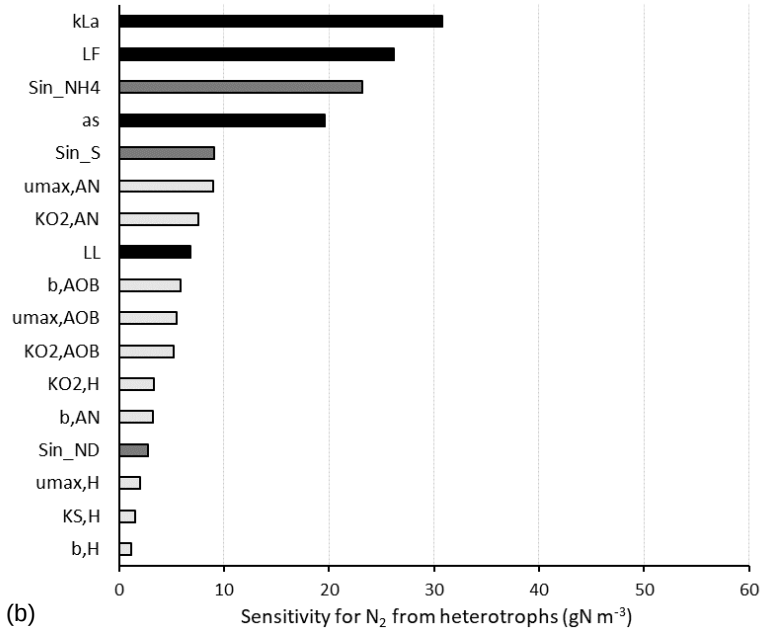

Figure 4.5 Sensitivity analysis towards N_2 formation via (a) anammox process and (b) heterotrophic denitrification. *In black: reactor-operation-specific parameters that can be operationally manipulated. In dark grey: influent concentrations or input conditions. In light grey: kinetic parameters that cannot be directly controlled by operation*

4.2.3 Influence of key parameters on steady-state total nitrogen removal efficiency

4.2.3.1 Mass-transfer related parameters

The effect of the oxygen transfer coefficient (k_La) and the external mass transfer boundary layer thickness (L_L) on the total nitrogen removal efficiency is displayed in Figure 4.6, for two different biofilm thicknesses (L_F = 65 µm (Figure 4.6a)) and 100 µm (Figure 4.6b)). As for thin biofilms (L_F = 65 µm, Figure 4.6a), an operational window with a total nitrogen removal efficiency higher than 60% is identified, considering k_La ranging from 100 d^{-1} to 660 d^{-1}, regardless of the prevailing external mass transfer boundary layer thickness (L_L). A high k_La (> 660 d^{-1}) resulted in a decreased total nitrogen removal unless there is a high external mass transfer (L_L > 1500 µm). Conversely, a k_La lower than 100 d^{-1} impaired total nitrogen removal irrespective of the adopted L_L. The maximum removal efficiency of 95% was achieved considering the simulation at a k_La and L_L of 330 d^{-1} and 1500 µm, respectively. This refers to a steady-state condition considering the default parameters (i.e., the reference scenario).

Overall, the higher the L_L for thin biofilms, the better the total nitrogen removal performance.

As for thick biofilms (L_F = 100 µm (Figure 4.6b), a broader operational window takes place for total nitrogen removal higher than 60%, considering k_La ranging from approximately 200 d^{-1} up to 1000 d^{-1}. The maximum removal efficiency of approximately 95% was achieved considering simulations at a k_La of 330 d^{-1} and L_L at 500 or 1500 µm. Moreover, efficiencies higher than 87% were reached under high k_La (1000 d^{-1}), except for the simulation at L_L 1500 µm. Overall, the beneficial effects of operation under high L_L observed for thin biofilms are less relevant for thick biofilms, especially at high k_La (> 600 d^{-1}) conditions.

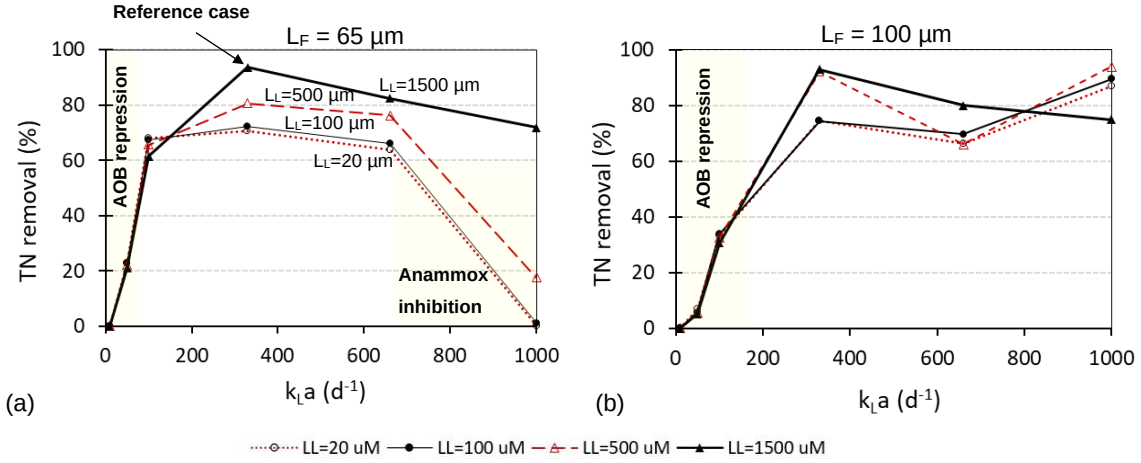

Figure 4.6 Total nitrogen removal considering the interaction between k_La and L_L at a fixed L_F of (a) 65 and (b) 100 µm. *Yellow shades refer to operational conditions that lead to AOB repression or anammox inhibition*

The higher the L_L, the lower the oxygen concentration at the biofilm-liquid interface at the top compartment of the SBTF, as shown in Figure 4.7a. The oxygen gradient as a function of L_L is even more evident for thin biofilms. For all the performed simulations, low k_La (< 100 d^{-1} and < 200 d^{-1}, for thin and thick biofilms, respectively) hampered ammonium conversion. This is due to the lack of oxygen in the bulk liquid (and consequently at the biofilm-liquid interface) compared to the operation under high k_La (e.g., 1000 d^{-1}), as shown in Figure 4.7b.

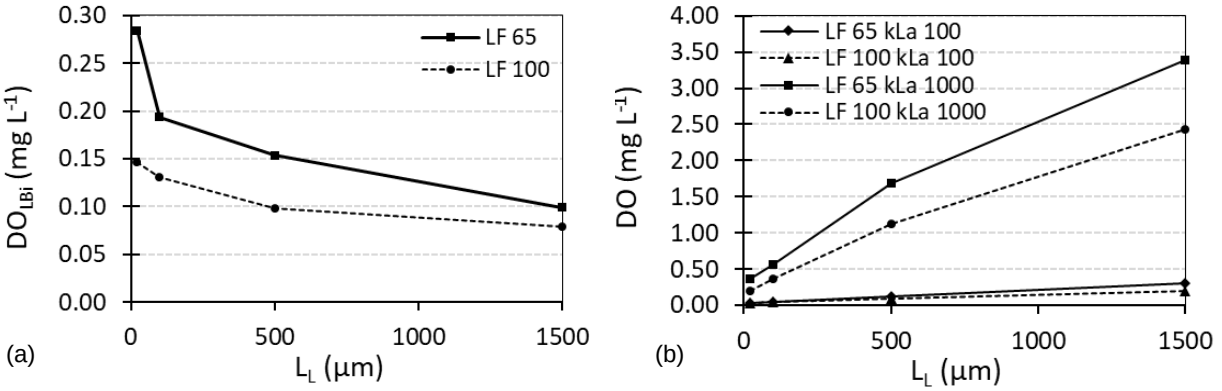

Figure 4.7 DO concentrations at the top compartment of the SBTF for thin and thick biofilms (a) at the biofilm-liquid interface for a k_La of 1000 d^{-1}, and (b) at the bulk liquid for a k_La of 100 and 1000 d^{-1}

The prevailing anammox process at steady-state is inhibited under high k_La (> 660 d^{-1}) and low L_L (< 1500 µm) for thinner biofilms (L_F = 65 µm). In such conditions, the oxygen inhibition term in the anammox growth reaction equation ($K\_O_{2,AN}/(K\_O_{2,AN}+S\_O_2)$) imposes rate limitations from 31% (L_L 500 µm) to 63% (L_L 20 µm) compared to the operation under high L_L (1500 µm). On the other hand, the oxygen concentration at the biofilm-liquid interface is less affected by L_L for thicker biofilms (L_F = 100 µm), which assures a niche for anammox bacteria in the biofilm even under high k_La. Therefore, biofilm thickness counteracts the effect of a thick LL protecting against oxygen inhibition, which was assumed as a less relevant parameter for other biofilm reactors such as MBBR (Pérez et al., 2020).

From the performed sensitivity analysis, the specific surface area (a_s) of the sponge-based support material appeared as another key reactor parameter influencing total nitrogen removal. Table 4.2 shows the variation of the total nitrogen removal efficiency considering the lower and upper values of a_s (5600 and 8500 $m^2\ m^{-3}$) for all k_La and L_L combinations, for both biofilms thicknesses. As for thin biofilms (65 µm), increasing a_s potentially enhances total nitrogen removal when k_La is higher than 100 d^{-1}, except for operation under thick external mass transfer boundary layer (L_L 1500 µm). A remarkable total nitrogen removal increase (from 18 to 63%) is noticed considering the operation at a k_La of 1000 d^{-1} and L_L of 500 µm. Conversely, decreasing a_s potentially decreases total nitrogen removal when k_La is higher than 100 d^{-1}. As for thick biofilms (100 µm), the opposite behaviour holds, namely: increasing a_s potentially diminishes

total nitrogen removal, and decreasing a_s tends to enhance total nitrogen removal for k_La lower than 1000 d^{-1}.

The specific surface area (a_s) directly impacts the amount of biomass retained in the SBTF, which affects the oxygen consumption at the top compartment of the SBTF. Hence, for a thin biofilm, increasing a_s (from the reference of 6600 to 8500 m^2 m^{-3}) reduces the oxygen concentration at the biofilm-liquid interface. Moreover, the oxygen penetration depth in the biofilm was approximately halved for concentrations higher than 0.06 mg L^{-1}, as shown in Figure 4.8. Conversely, for thick biofilms, increasing a_s (from the reference of 6600 to 8500 m^2 m^{-3}) tends to hinder total nitrogen removal performance as oxygen is depleted due to higher biomass concentration (and consequently decay), thus hampering AOB activity.

In all simulations, no nitrite accumulation was noticed in the effluent, and nitrate was completely removed. Therefore, nitrification was the limiting process for enhanced total nitrogen removal. These results support that the interplay between k_La, L_L, L_F, and a_s in SBTFs ultimately dictates optimum oxygen levels at the biofilm-liquid interface and oxygen penetration depth in the biofilm, which can sustain AOB activity without compromising anammox bacteria growth.

Worth mentioning that the timespan to reach a 60% total nitrogen removal target in all simulations remained higher than 1500 days (Figure A.4.3). After one year of simulation time, total nitrogen removal efficiency is limited to approximately 35%, as observed in experimental results (**Chapter 3**).

Table 4.2 Effects of the specific surface area (a_s) of the sponge-based support media on total nitrogen removal, considering the interaction between k_La and L_L for thin and thick biofilms (65 and 100 µm, respectively). *Green and red cells refer, respectively, to increased or decreased total nitrogen removal efficiency compared to the reference (a_s = 6600 m² m^{-3})*

		L_F 65 µm			L_F 100 µm		
L_L (µm)	k_La (d^{-1})	a_s 5600 m² m^{-3}	Reference a_s 6600 m² m^{-3}	a_s 8500 m² m^{-3}	a_s 5600 m² m^{-3}	Reference a_s 6600 m² m^{-3}	a_s 8500 m² m^{-3}
20	50	27	23	14	13	7	0
	100	79	68	49	47	33	5
	330	68	71	95	94	75	56
	660	37	64	94	94	66	64
	1000	0	0	24	54	87	94
100	50	27	23	14	13	6	0
	100	78	67	48	47	34	5
	330	68	72	94	93	74	56
	660	49	66	94	92	70	64
	1000	0	1	27	52	89	95
500	50	27	22	13	12	6	0
	100	75	66	47	46	32	2
	330	75	81	90	87	92	54
	660	62	76	88	82	66	61
	1000	12	18	63	75	94	91
1500	50	25	21	13	11	5	0
	100	69	61	46	43	31	3
	330	87	94	80	78	93	52
	660	83	82	72	66	80	85
	1000	64	72	88	85	75	81

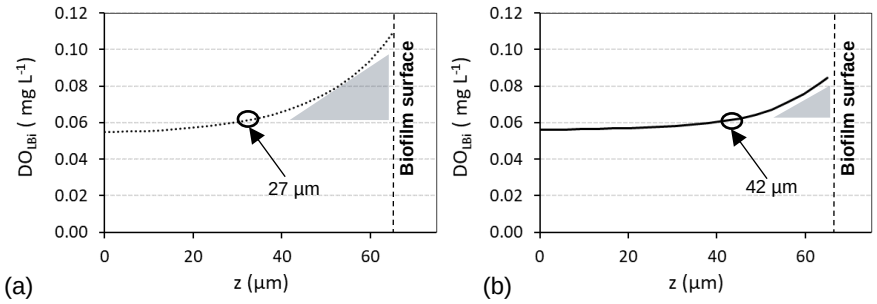

Figure 4.8 Biofilm-liquid interface concentrations of dissolved oxygen (DO_{LBi}) at the top compartment of the SBTF for thin biofilms (L_F 65 µm) at a_s of 5600 m² m^{-3} (a) and 8500 m² m^{-3} (b)

Overall, the SBTF performance for high total nitrogen removal relies on the oxygen level at the biofilm-liquid interface. This ultimately highlights the significance of the

anammox bacteria inhibition by oxygen, which could be depicted from the sensitivity analysis ($K_{O2,AN}$ – see Figure 4.5). A similar condition was reported by Corbalá-Robles et al. (2016) for modelling an SBR for ammonium-rich reject water (sidestream). To further assess the relevance of oxygen penetration depth in the biofilm, a complementary simulation was performed reducing the magnitude of the anammox process inhibition by oxygen (i.e., increasing $K_{O2,AN}$ from 0.01 to 0.05 g O_2 m^{-3}). This led to a slight improvement in total nitrogen removal at steady-state; however, a paramount decrease in process start-up (Figure A.4.4), supporting the critical role of oxygen penetration depth in anammox colonization in SBTFs.

Although a nitrite sink was identified at the middle bottom compartment of the SBTF, further decreasing k_La did not imply improved NOB repression and consequently fast anammox process start-up, as suggested in the literature (Pérez et al., 2014). Conversely, AOB activity is hampered, thus compromising nitrogen removal. The only PN/A experiment available so far in SBTFs showed reduced total nitrogen removal efficiency due to the lack of oxygen control (Sánchez-Guillén et al., 2015b).

From a process control standpoint, it is risky to rely on the coupling of k_La-L_L-L_F-a_s to ensure non-inhibitory oxygen levels at the biofilm-liquid interface and therefore enhance nitrogen removal through the anammox process in SBTFs. Such process was reported to be irreversibly inhibited at relatively low DO concentrations (>18% air saturation) (Egli et al., 2003) compared to some of the measured DO values in the SBTF (see Figure A.4.1).

4.2.3.2 Influent flow rate

The influence of the influent loading rate was examined by varying the influent flow rate, while keeping the influent COD and total nitrogen concentrations constant. The hydraulic loading rate, organic loading rate, and nitrogen loading rate thus varied proportionally. Figure 4.9 shows the effect on the total nitrogen removal efficiency in the SBTF.

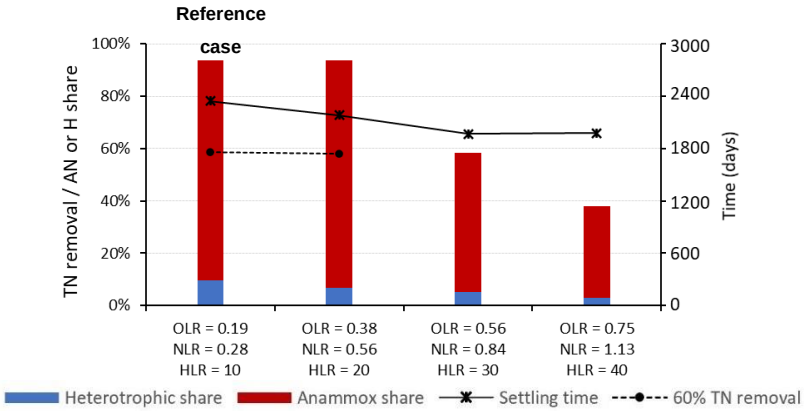

Figure 4.9 Total nitrogen removal and process share considering the effect of influent flow rate (OLR = 0.19 – 0.75 kg COD m^{-3}_{sponge} d^{-1}, NLR = 0.28 – 1.13 kg N m^{-3}_{sponge} d^{-1}, HLR = 10 – 40 m^3 m^{-2} d^{-1}).

Increasing the hydraulic loading rate from 10 to 20 m^3 m^{-2} d^{-1} marginally reduced the required time to achieve the targeted 60% total nitrogen removal. Nevertheless, a significant impact occurs when further increasing the hydraulic loading rate higher than 20 m^3 m^{-2} d^{-1}, as the steady-state total nitrogen removal sharply decreases (from approximately 95 to slightly less than 60%).

At a hydraulic loading rate higher than 20 m^3 m^{-2} d^{-1}, the resulting organic and nitrogen loading rates outweigh the oxygen supply to the SBTF, thus limiting AOB activity and hampering total nitrogen removal. From a process design standpoint, organic and nitrogen loading rates are defined as the hydraulic loading rate function, since the influent COD and ammonium concentrations are assumed constant. Therefore, the applied hydraulic loading rate dictates the threshold for a total nitrogen removal efficiency over 60%. Such an observed HLR upper value of 20 m^3 m^{-2} d^{-1} matches the recommended operational conditions for high nitrification efficiency in SBTFs, as discussed in Chapter 2 (see Table 2.3, section 2.3.1).

4.2.3.3 Influent organic carbon concentration

The influence of different influent C/N ratios was assessed by varying the influent COD concentration, while keeping influent concentrations of nitrogen and incoming flow rate constant. The applied organic loading rate thus varied accordingly. Figure 4.10 shows the effect on the total nitrogen removal in the SBTF.

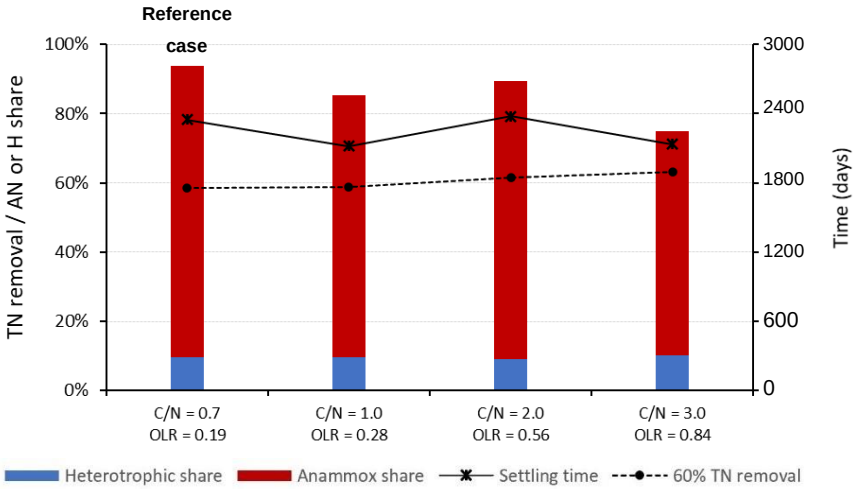

Figure 4.10 Total nitrogen removal and process share considering the effect of influent organic carbon concentration (C/N ratio = 0.7 – 3.0 g COD g N^{-1}, OLR = 0.19 – 0.84 kg COD m^{-3}_{sponge} d^{-1}).

Increasing the influent COD (i.e., operating at C/N ratio higher than 1 g COD g N^{-1}) neither significantly hampers total nitrogen removal efficiency at steady-state nor improves process-start up. The total nitrogen removal efficiency remains higher than 60% for all simulated conditions. However, more than 1500 days are still required to achieve such targeted efficiency. This is mainly because the organic carbon is degraded by ordinary heterotrophs rather than heterotrophic denitrifiers at the top compartment of the SBTF, as nitrate is only available further down in the SBTF (middle bottom and bottom; see Figure 4.3).

Interestingly, anammox bacteria are not washed out even under high C/N ratios (e.g., 3.0 g COD g N^{-1}). Conversely, high C/N ratios or organic loading rates (> 0.56 kg COD m^{-3}_{sponge} d^{-1}) push anammox bacteria towards the bottom of the SBTF (Figure A.4.5). This is supported by experimental reports in which anammox bacteria were detected in the bottommost compartments of an SBTF under periods of increased organic loading rate (Mac Conell et al., 2015). Therefore, SBTFs should have at least 3.0 m depth to sustain the anammox process in case of exposure to C/N ratios over 2.0 g COD g N^{-1}.

4.2.3.4 Combined effects

Increasing influent COD content can be practically implemented via a by-pass of raw sewage to the inlet of the SBTF, which also increases the influent flow rate. The combined effects of increasing the influent COD and flow rate were assessed. The

interference of k_La and L_L was also considered for a more comprehensive analysis. Figure 4.11 shows the impact on the total nitrogen removal in the SBTF.

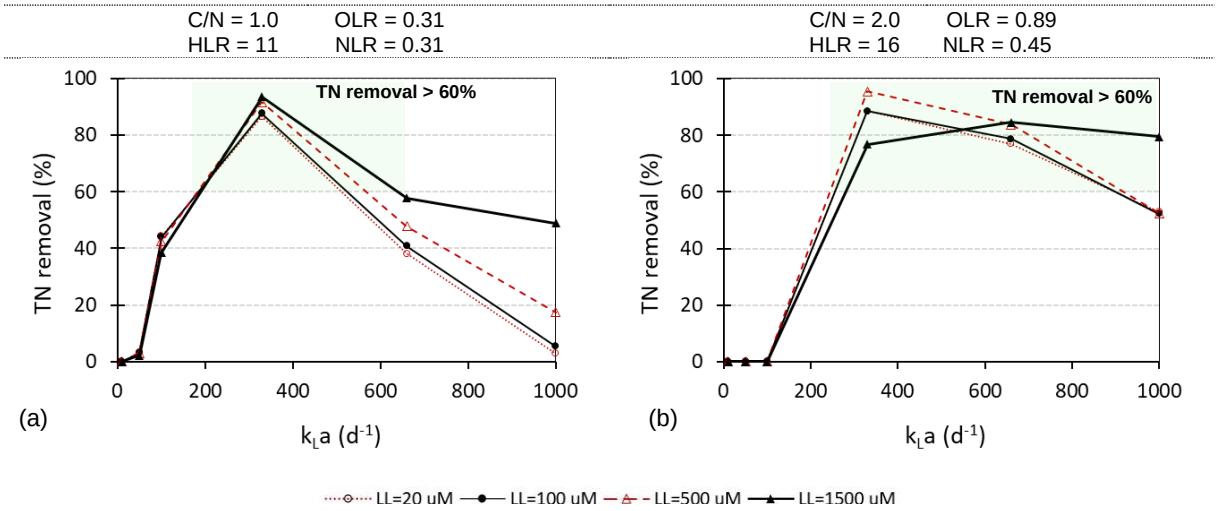

Figure 4.11 Total nitrogen removal considering the interaction between k_La and L_L for (a) C/N = 1.0 g COD g N^{-1}; HLR = 11 m^3 m^{-2} d^{-1} and (b) C/N = 2.0 g COD g N^{-1}; HLR = 16 m^3 m^{-2} d^{-1}. *Green shades refer to total nitrogen removal efficiency over 60%*

The higher the C/N ratio, the lower the influence of external mass transfer resistance on total nitrogen removal efficiency at steady-state. For instance, operating at a C/N ratio of 2 g COD g N^{-1} allows for total nitrogen removal efficiency higher than 60% even for L_L lower than 500 µm and k_La up to 800 d^{-1}, which is not feasible operating at a C/N ratio of 1 g COD g N^{-1}. The higher the C/N ratio, the higher the required k_La for achieving total nitrogen removal efficiency over 60%.

A broader operational window for total nitrogen removal performance over 60% is possible under a high C/N ratio. This enhances oxygen consumption at the top compartments of the SBTF (up to the middle top), thus decreasing anammox inhibition close to the biofilm surface. Simulation results are in line with experimental results for SBRs treating anaerobic effluents (Leal et al., 2016). These authors showed that a COD/N ratio of 5.0 g COD g N^{-1} (or approximately 3.0 g soluble biodegradable COD g N^{-1}) allowed the prevalence of anammox bacteria over heterotrophic denitrifiers.

More than 1500 days were still required for all the simulations performed to achieve a targeted 60% total nitrogen removal. Process optimization for enhancing process start-up is then urged.

4.2.4 Possible operational strategies to optimize process start-up

4.2.4.1 Biomass inoculation

Different inoculum strategies at the start-up of the SBTF were assessed. To this end, the active biomass fractioning of anammox was stepwise increased from 2.5 to 10% of the overall biomass fraction. Figure 4.12 shows the impact on the total nitrogen removal in the SBTF.

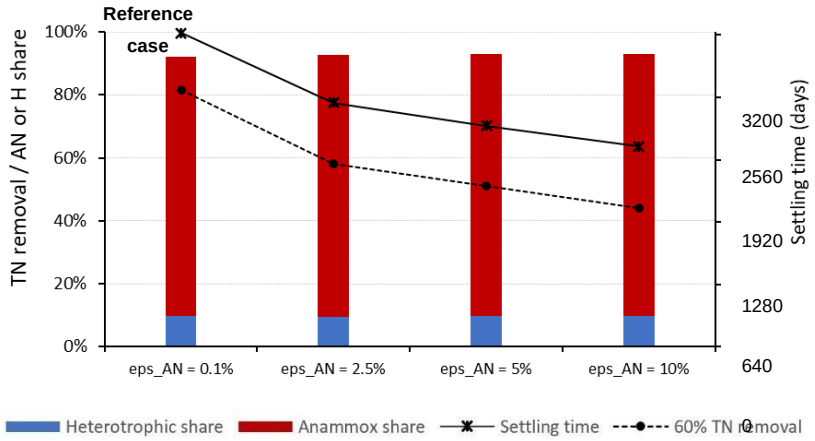

Figure 4.12 Total nitrogen removal and process share considering the effect of initial biomass fractioning (εX_{AN} = 0.1 – 10%). *Other parameters are retained as the reference condition, as indicated in Table 4.1*

The process settling time decreased as the initial anammox fraction increased, from c.a. 2500 days at the reference scenario to approximately 1900 days considering an initial fraction of 10%. The steady-state behaviour was retained, i.e., total nitrogen removal of approximately 90% and prevalence of autotrophic process. Same steady-state outputs regardless of initial conditions are expected from non-linear models, like the one used in the present study.

Process start-up ranging from 60 days (Ni and Zhang, 2013) up to 3.5 years (van der Star et al., 2007) have been reported in the literature. Relevant gains in shortened start-up period are attributed to the availability of anammox seed. Nevertheless, even if a high proportion (10%) of anammox bacteria is inoculated to the SBTF, the settling time for total nitrogen removal is reached after more than 1900 days. Therefore, unless the right conditions to ensure low oxygen levels at the biofilm-liquid interface are provided, standalone inoculation is an ineffective strategy for process optimization.

4.2.4.2 Effluent recirculation

Effluent nitrate concentrations observed during the first 1000 days of simulation could be recirculated to the top of the SBTF, where organic carbon is available. Based on that rationale, three different effluent recirculation rates (R = 0.5, 1.0, and 1.5) were assessed. Figure 4.13 shows the impact on total nitrogen removal in the SBTF.

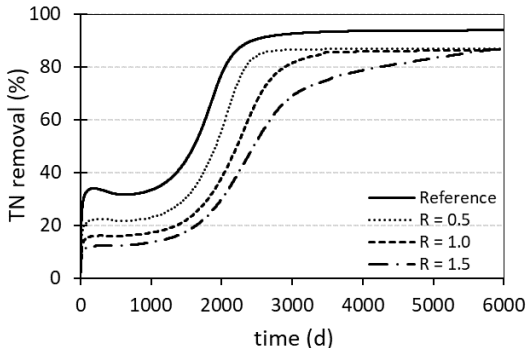

Figure 4.13 Total nitrogen removal efficiency for the reference case and the simulated effluent recirculation ratios (R = 0.5 – 1.5) to the top of the SBTF (therefore, HLR = 15 – 25 m^3 m^{-2} d^{-1}). *Other parameters are retained as the reference condition, as indicated in Table 4.1*

Interestingly, the higher the recirculation rate, the lower the total nitrogen removal at the SBTF start-up. In addition, the time to reach a targeted 60% removal performance is delayed. To further evaluate this behaviour, substrate profiles (ammonium, nitrite, nitrate, and organic carbon) along with the SBTF depth for the recirculation ratios of 0.5 and 1.5 are shown in Figure 4.14a-b. Complementary, Figure 4.14c shows the inorganic carbon content over the SBTF depth for all simulated recirculation ratios.

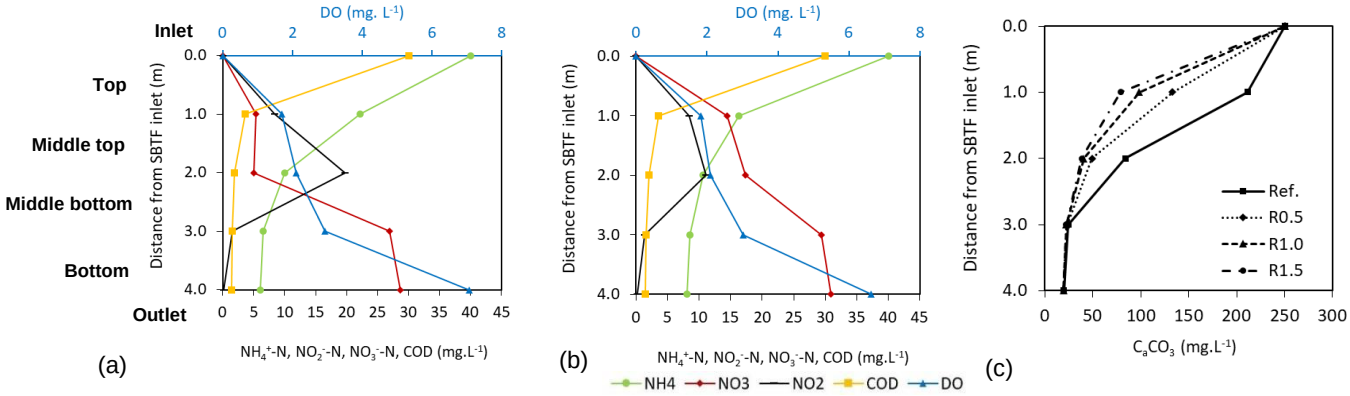

Figure 4.14 Substrate profiles over the SBTF compartments for nitrogen compounds, DO, and COD at 500 simulation days for the recirculation ratios of (a) 0.5 and (b) 1.5; (c) substrate profile of inorganic carbon for all simulated scenarios (R = 0.5 – 1.5). *Recirculated flow is mixed at the top compartment (refers to the point '1.0 m' in the y axis)*

Nitrate concentrations at the top compartment of the SBTF increased as the recirculation ratio rose. Conversely, less nitrite was accumulated in the middle top of the reactor. This is associated with less ammonium available at the middle compartment, as it is mainly consumed at the SBTF top layer as the recirculation ratio increases. Therefore, effluent recirculation was only effective for improving nitrification, which is optimized at the upper compartments of the SBTF. At a recirculation ratio of 1.5, the nitrogen loading rate increases 30% (from 0.25 to 0.33 kg N m^{-3}_{sponge} d^{-1}), and ammonium is mostly converted up to the middle top compartment, where inorganic carbon is not limiting. Nevertheless, total nitrogen removal remains impaired since it lacks organic carbon for heterotrophic denitrification. Moreover, effluent recirculation increases oxygen concentration at the biofilm-liquid interface at the top compartment of the SBTF (Figure A.4.6), which delays the transition to PN/A and hampers process performance at steady-state.

Adding inorganic carbon to increasing AOB activity over NOB does not significantly improve the transition for PN/A (Figure A.4.7), as hypothesized in the literature for activated sludge systems deprived of inorganic carbon (Seuntjens et al., 2018). Furthermore, inorganic carbon is not a drawback for ammonium removal in the long term, as residual ammonium concentrations due to reduced AOB activity are taken up by anammox bacteria. Therefore, the crucial aspect for short-cut nitrogen removal in SBTFs is NOB out-selection and oxygen control at the biofilm-liquid interface, rather than enhancing AOB activity.

4.2.4.3 Sewage by-pass combined with effluent recirculation

The lack of organic carbon during effluent recirculation motivated a final set of simulations. Sewage by-pass was implemented as before (section 4.2.3.4) but this time also applying effluent recirculation. Hydraulic loading rates are thus increased, besides the organic and nitrogen loading rates. The influence of different k_La and L_L values was also considered. Figure 4.15 shows the impact on total nitrogen removal in the SBTF.

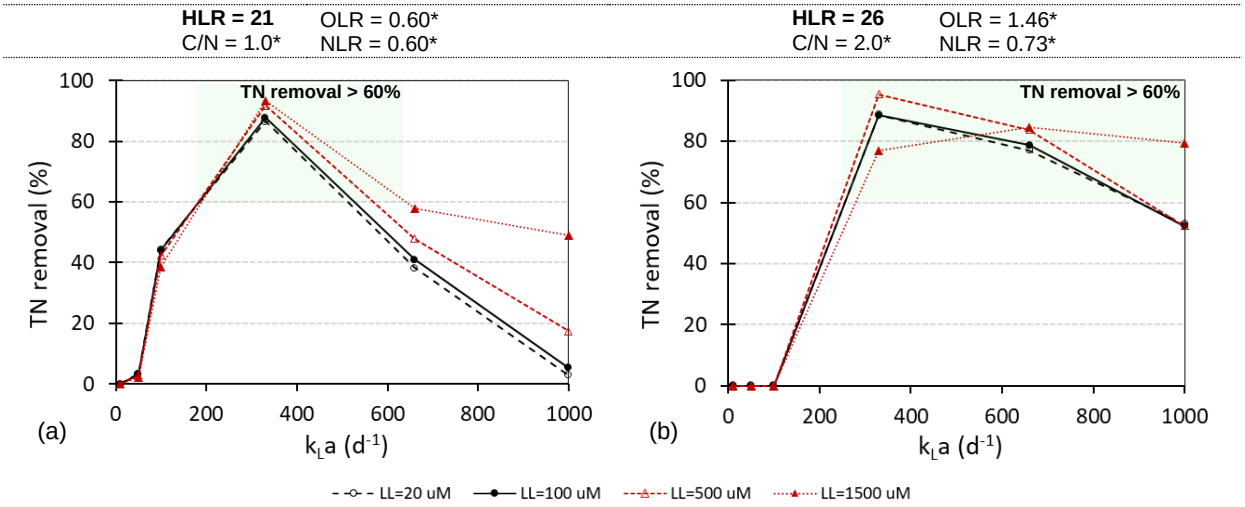

Figure 4.15 Total nitrogen removal efficiency considering the interaction between k_La and L_L for (a) HLR = 21 m^3 m^{-2} d^{-1} and (b) HLR = 26 m^3 m^{-2} d^{-1} **Values for C/N, OLR, and NLR are given prior to recirculated flow mixing Green shades refer to total nitrogen removal efficiency over 60%*

A similar pattern is observed compared with results from supplying raw sewage to the inlet of SBTFs, without effluent recirculation (section 4.2.3.4). In summary, the higher the OLR (or C/N ratio), the higher the required k_La for achieving a targeted total nitrogen removal efficiency (> 60%). Similar behaviour is noticed between the simulations with a higher hydraulic loading rate (26 m^3 m^{-2} d^{-1} (Figure 4.15b)) compared to section 4.2.3.4 (Figure 4.11b), meaning that a broad operational window for total nitrogen removal over 60% remained for k_La over 200 d^{-1}. Nonetheless, a remarkable reduced operational window for the targeted total nitrogen removal efficiency is observed under HLR of 21 m^3 m^{-2} d^{-1} (Figure 4.15a), compared to section 4.2.3.4 (Figure 4.11a). In this case, k_La values higher than 600 d^{-1} hamper the SBTF performance, regardless of the operating L_L.

The timespan to reach a 60% total nitrogen removal target for all simulations remained higher than 1500 days. An exception is made under conditions of increased sewage by-pass (HLR = 26 m^3 m^{-2} d^{-1}) and high k_La (660 d^{-1}), irrespective of the adopted L_L. This leads to process settling time before 100 days, mainly due to heterotrophic denitrification (Figure 4.16).

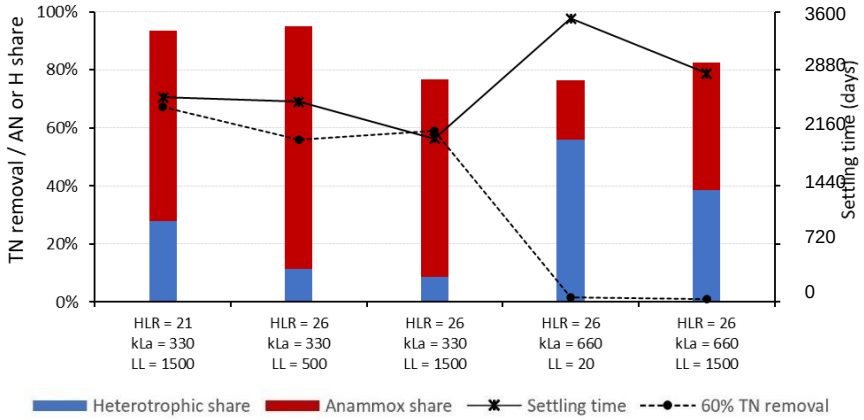

Figure 4.16 Total nitrogen removal and process share considering selected simulations for HLR = 21 m^3 m^{-2} d^{-1} (k_La = 330 d^{-1} and L_L = 1500 µm) and HLR = 26 m^3 m^{-2} d^{-1} (k_La = 330 and 660 d^{-1} and L_L = 500 and 1500 µm)

When organic carbon is provided via sewage by-pass and effluent recirculation is kept, two different behaviours are noticed: (i) at a low hydraulic loading rate, a reduced operational window occurs for total nitrogen removal. The increased nitrate availability at the top compartment prompts heterotrophic denitrifiers and hampers anammox bacteria, which do not thrive further down (from middle top) in the SBTF, as oxygen levels are inhibiting; and (ii) at a high hydraulic loading rate, anoxic conditions occur at the middle top of the SBTF, besides the top compartment, where anammox can be harboured. In other words, anammox is pushed downwards, whereas, under a low hydraulic loading rate, no anoxic niche is sustained apart from the top SBTF compartment.

Total nitrogen removal via heterotrophic denitrification in SBTFs is thus apparently limited to approximately 60%, provided that sewage by-pass (to ensure a C/N ratio above 2.0 g COD g N^{-1}; i.e., 26 m^3 m^{-2} d^{-1}) and effluent recirculation is implemented. However, it does not guarantee a fast process start-up unless an operation under improved ventilation conditions (high k_La) and a thin external mass transfer boundary layer (L_L) are in place. The latter is impractical to fine-tune under an actual SBTF operation.

To reach a high C/N ratio (2 g COD g N^{-1}) at the inlet of the SBTF, a significant raw sewage by-pass (ranging from approximately 20 to 60%, depending upon the incoming COD concentration) should be implemented to the SBTF. Hence, less biogas would be produced in the preceding UASB reactor. A trade-off analysis should thus consider

a fast-process start-up for total nitrogen removal at the expense of reduced energy potential at the anaerobic treatment step.

4.3 Conclusions

In this chapter, modelling and simulation were applied to gain insight into the mechanisms and influencing factors regarding total nitrogen removal in SBTFs treating anaerobic effluents. Besides the long-term (steady-state) behaviour, particular attention was paid to the process start-up.

- High total nitrogen removal (> 60%) in SBTFs can potentially be realized through partial nitritation-anammox. Simulated microbial profiles were consistent with published experimental data on microbial distribution along with the SBTF depth. Nevertheless, the long start-up period jeopardizes the process.

- Low dissolved oxygen concentrations at the biofilm-liquid interface ensure nitrite build-up in the middle bottom compartment of the SBTF, thus favouring anammox growth in the long run.

- Partial denitrification was a less relevant mechanism supplying nitrite for the anammox process in the SBTF.

- Implementing the partial nitritation-anammox in SBTFs highly relies on the coupling between oxygen transfer coefficient, external mass transfer resistance, biofilm thickness, and sponge specific surface area. The interaction of those parameters dictates oxygen levels at the biofilm-liquid interface.

- Decreasing oxygen transfer did not benefit partial nitritation-anammox, as AOB activity was impaired.

- Total nitrogen removal efficiency via heterotrophic denitrification was limited to approximately 60%, provided effluent recirculation and sewage by-pass for carbon supply are implemented.

- Under low organic loading rates, the anammox process thrived at the top compartment of the SBTF. Conversely, a high organic loading rate pushes

anammox bacteria to the bottom compartment. Therefore, SBTFs should have at least 3.0 m depth to safely ensure high total nitrogen removal.

- Biomass inoculation is ineffective as a standalone strategy for process start-up optimization if non-inhibitory oxygen levels at the biofilm-liquid interface are not guaranteed.

- A fast start-up can be achieved via heterotrophic denitrification under high C/N, thin external mass transfer boundary layer, and high volumetric oxygen transfer. Therefore, effluent recirculation coupled to sewage by-pass seems to be a relevant strategy.

Appendix

A.4.1 Supplementary experimental data

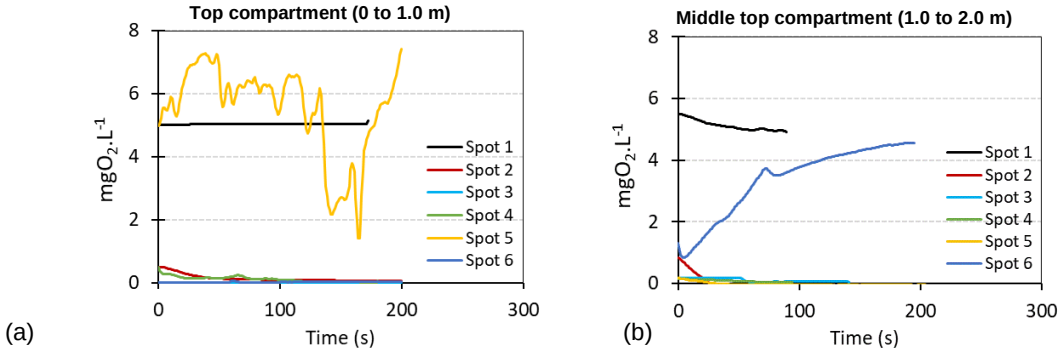

Figure A.4.1 Microsensor DO profiles measured at different spots at the top (a) and middle top (b) compartments of the monitored SBTF. *The spots refer to randomly selected positions for the insertion of the microsensor in different sponge sheets, however at the same compartment – top or middle top*

A.4.2 Supplementary simulation results

Table A.4.1 Value ranges assigned to influent composition and model parameters for the sensitivity analysis

Parameter	Definition	Unit	Range
$S_{in,NH4}$	Influent ammonium concentration	g NH_4^+-N m^{-3}	20 – 60
$S_{in,ND}$	Influent soluble organic nitrogen concentration	g N m^{-3}	1 – 10
$S_{in,S}$	Influent COD concentration	g COD m^{-3}	3 – 90
$S_{in,IC}$	Influent inorganic carbon concentration	g $CaCO_3$ m^{-3}	130 – 330
μ_{max}^{AN}	Growth rate of AN	d^{-1}	0.016 – 0.225
μ_{max}^{H}	Growth rate of heterotrophs	d^{-1}	1.5 – 24
μ_{max}^{AOB}	Growth rate of AOB	d^{-1}	0.2 – 2.03
$b_{,AN}$	Decay rate of AN	d^{-1}	0.0011 – 0.0151
$b_{,H}$	Decay rate of heterotrophs	d^{-1}	0.1 – 1.44
$b_{,AOB}$	Decay rate of AOB	d^{-1}	0.013 – 0.136
$K_{O2,AN}$	DO inhibition coefficient for AN	g O_2 m^{-3}	0.001 – 0.1
$K_{O2,H}$	DO half-saturation coefficient for heterotrophs	g O_2 m^{-3}	0.02 – 2.0
$K_{O2,AOB}$	DO half-saturation coefficient for AOB	g O_2 m^{-3}	0.07 – 3.0
$K_{S,H}$	COD half-saturation coefficient for heterotrophs	g COD m^{-3}	0.1 – 100
$\varepsilon X_{,AN}$	Volume fraction of AN	-	0.001 – 0.16
L_L	External mass transfer boundary layer	µm	20 – 1500
k_La	Volumetric oxygen mass transfer coefficient	d^{-1}	5 – 1000
L_F	Biofilm thickness	µm	20 – 250
a_s	Specific surface area of the sponge	m^2 m^{-3}	5600 – 8500

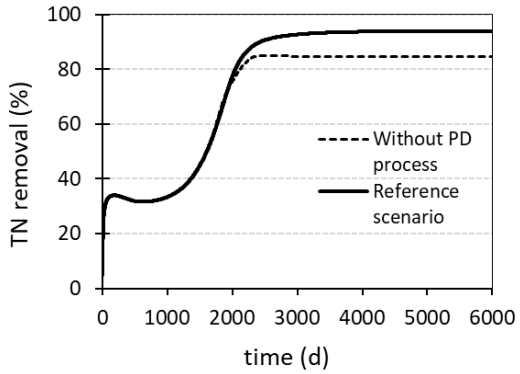

Figure A.4.2 Total nitrogen removal efficiency considering the reference scenario and the simulation without partial denitrification (deactivation of nitrate reduction to nitrite – see process 6, Table A.3.1 – Chapter 3)

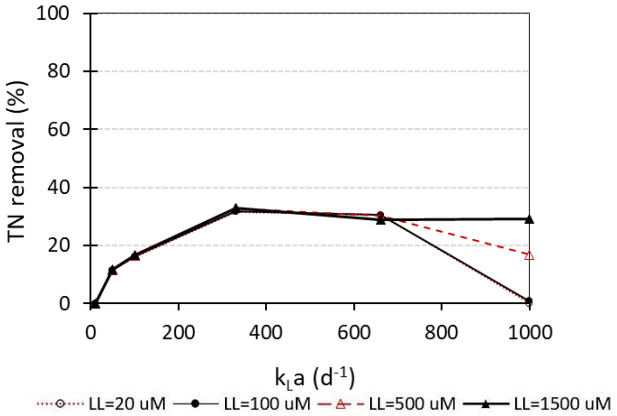

Figure A.4.3 Total nitrogen removal at 365 days of simulation, considering the interaction between k_La and L_L at a fixed L_F of 65 µm

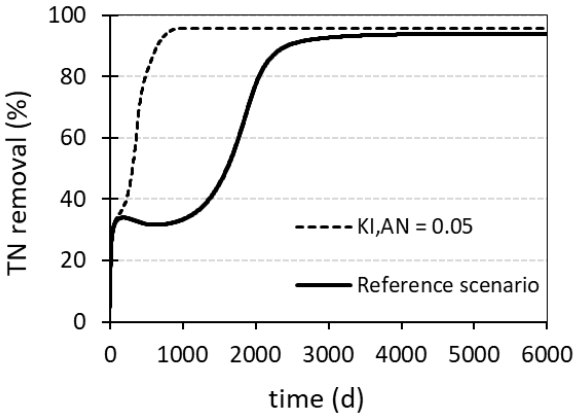

Figure A.4.4 Total nitrogen removal efficiency considering the reference scenario and the simulation with a reduced oxygen inhibition for anammox bacteria (i.e., increasing $K_{O2,AN}$ from 0.01 to 0.05 g O_2 m^{-3})

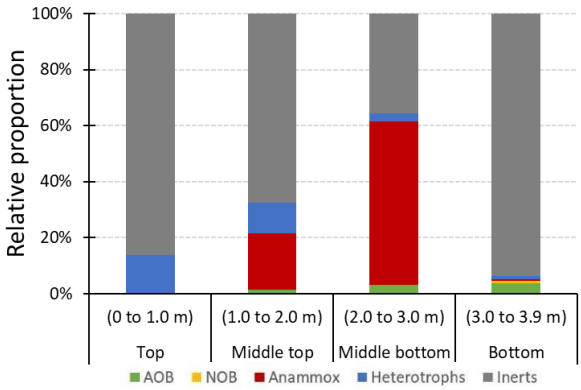

Figure A.4.5 Relative biomass proportion in each SBTF compartment at 3100 days for a C/N ratio of 3.0 g COD g N^{-1} (OLR = 0.84 kg COD m^{-3}_{sponge} d^{-1}). *Other parameters are retained as the reference condition*

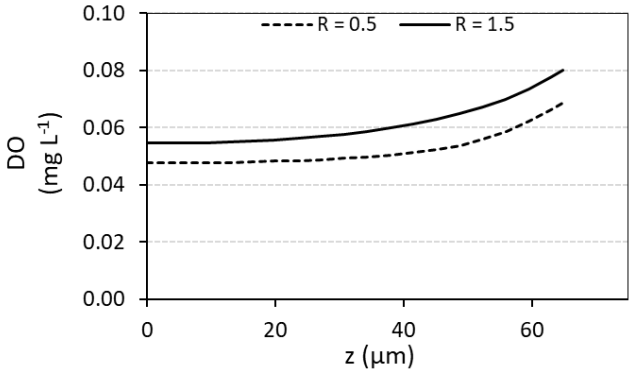

Figure A.4.6 Dissolved oxygen penetration in the biofilm considering the recirculation ratio of 0.5 and 1.5

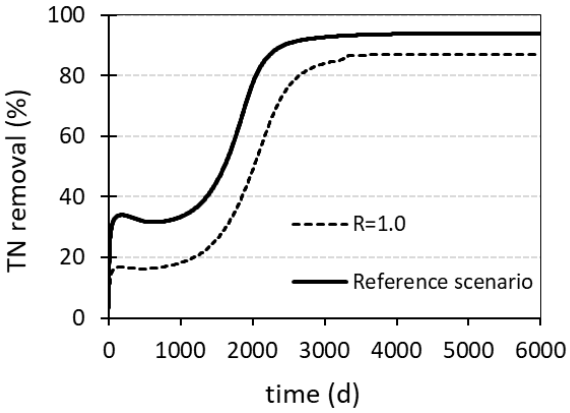

Figure A.4.7 Total nitrogen removal efficiency considering the reference scenario and the simulation with a recirculation ratio of 1, augmented with inorganic carbon (influent concentration set as 500 mg L^{-1})

Chapter 5

Long-term comparative study of sponge-bed trickling filters treating mainstream anaerobic effluents

5.0 Abstract

Post-treatment of anaerobic effluents in sponge-bed trickling filters (SBTFs) has already been demonstrated in full-scale installations. Those reactors were initially conceived to remove residual carbon and ammonium from the anaerobically treated sewage. Process configurations have been researched for enhancing total nitrogen removal performance via heterotrophic denitrification or partial nitritation-anammox. Only one full-scale long-term study is available considering effluent recirculation as a strategy to enhance denitrification. Some studies addressed ventilation strategies to limit oxygen transfer and promote partial nitritation-anammox in lab-scale SBTFs; none considered real sewage. In the present contribution, two demo-scale SBTFs were operated in parallel for 890 days following a UASB reactor treating real sewage. Effluent recirculation to the top compartment of the SBTF showed a rapid increase in total nitrogen removal efficiency. Nevertheless, further supplying organic carbon via sewage by-pass was detrimental to AOB activity. Stepwise ventilation strategies decreased volumetric ammonium conversion rates; however, nitrate remained the main end-product throughout the monitoring period, meaning NOB repression was ineffective. A mechanistic model was further used to gain process insight based on the observed experimental data. Results indicated that other compounds may have exerted oxygen demand, thus impairing AOB during restricted ventilation. Moreover, under the observed temperature range (15 – 30 ^{o}C), the long-term ingrowth of anammox bacteria was constrained.

5.1 Introduction

Technological options for reliable biological nitrogen removal from mainstream anaerobic sewage treatment are currently limited, and the post-treatment of anaerobic effluents using sponge-bed trickling filters (SBTFs) is restrained for ammonium removal so far, as addressed in **Chapter 1**. Regardless of possible process limitations concerning inorganic carbon for complete nitrification, as characterized in **Chapter 3**, effluent ammonium concentrations from SBTFs can meet less stringent discharge criteria that may be applicable for developing countries (e.g., < 20 N L^{-1}). Nevertheless, if the claimed potential of further removing total nitrogen is not fully demonstrated, broad adoption of those reactors can be compromised.

Two main nitrogen removal pathways have been explored in those reactors. Firstly, heterotrophic denitrification has been reported as a significant contributor in SBTFs following anaerobic sewage treatment. Biomass decay products related to typical high solids retention time (> 100 days) have been theoretically assumed as a carbon source for the biofilm retained in the sponge pore (Machdar et al., 2000). Microsensor measurements corroborated this theory, as anoxic niches were reported towards the inner sponge pore (Araki et al., 1999). The only full-scale experience reported so far reached 65% nitrogen removal efficiency, implementing effluent recirculation (Onodera et al., 2016). Improved total nitrogen removal performance (approximately 74%) was achieved considering sewage by-pass and effluent recirculation for an SBTF dealing with settled sewage (Bundy et al., 2017). From a practical point of view, there is still motivation to invest in enhancing heterotrophic denitrification in SBTFs following UASB reactors, namely: (i) no oxygen is required for assuring the previous required complete nitrification step; (ii) sludge production in SBTFs is reportedly low (Onodera et al., 2013), eventually sustaining the operation without secondary settlers (Bressani-Ribeiro et al., 2017). The only remaining drawback would be the need for exogenous organic carbon, which could be solved with sewage by-pass at the expense of lower energy potential in the previous anaerobic reactor.

Secondly, experimental evidence was reported on sustained partial nitritation (Chuang et al., 2007) and anammox activity (Sánchez-Guillén et al., 2015a) in lab-scale SBTFs fed with synthetic wastewater. There are also modelling indications of long-term anammox colonization in SBTFs, provided that the dissolved oxygen (DO)

concentration at the biofilm-liquid interface lies at an optimum level, as addressed in **Chapter 4**. However, demonstration with real anaerobic effluents is still lacking.

A long-term experiment (890 days) was conducted in two parallel demo-scale SBTFs (approximately 20 PE) following a UASB reactor. The aim was to realize one-stage partial nitritation-anammox (PN/A) and foster heterotrophic denitrification. To the best of our knowledge, this is the first study exploring the implementation of PN/A in SBTFs fed with real anaerobically treated effluents. To this end, oxygen-limiting (low DO) strategies were stepwise applied in the reactors, controlling natural ventilation. Moreover, effluent recirculation and raw sewage by-pass were tested based on prior simulation results (**Chapter 4**). Finally, the developed model (**Chapter 3**) was used to gain mechanist insights on process performance.

5.2 Methodology

5.2.1 Experimental set-up

Two identical sponge-bed trickling filters (Figure 5.1) were operated in parallel following the same UASB reactor treating real raw sewage. The main design characteristics for both SBTFs are the same as reported in **Chapter 3**, which are summarized in Table 5.1. The anaerobic effluent was distributed at the top of the SBTFs by rotary arms and trickled down to the bottom. No secondary settler was implemented, as previously motivated (**Chapter 2**). For oxygen supply, ventilation ports were provided along with the STBF depth. The area of each port was equivalent to the total required area for natural-draft trickling filters (Metcalf & Eddy, 2013).

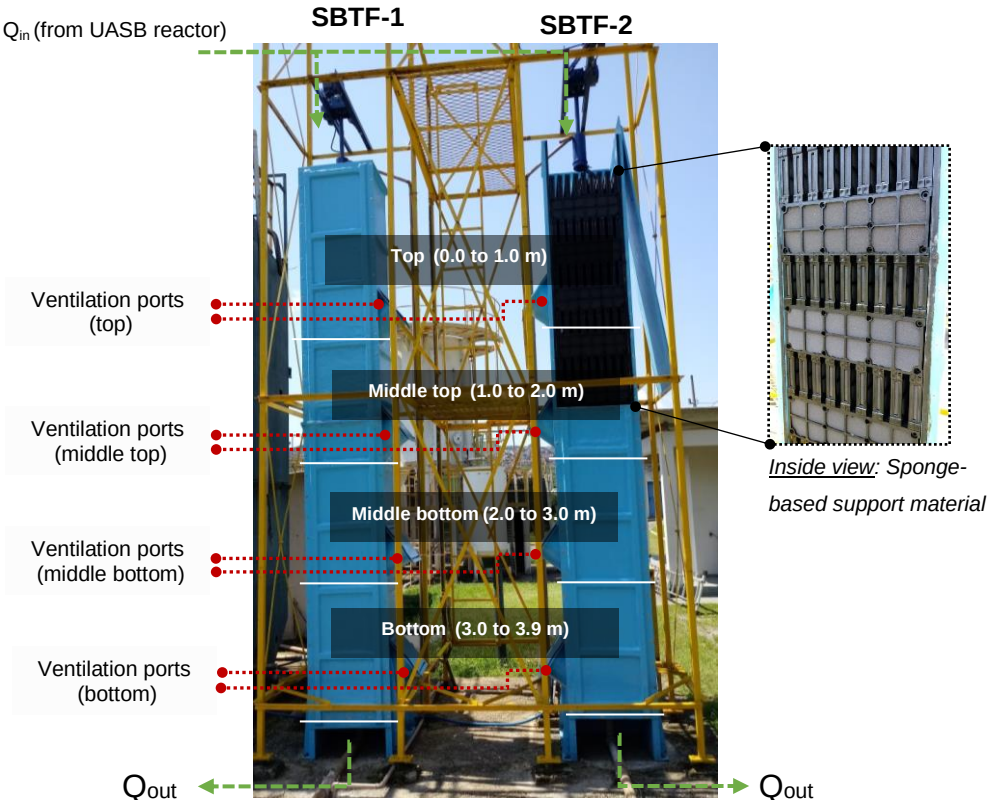

Figure 5.1 Sponge-bed trickling filters (SBTFs): schematic representation of the compartments and ventilation ports for natural ventilation in both reactors. *Fiberglass front cover removed from SBTF-2 only for illustrating the interior of the reactor*

Table 5.1 Summary of the main characteristics of both SBTFs investigated

Parameter	Value	Unit
Useful height (H)	3.91	m
Cross-section area (A)	0.25	m^2
Reactor volume (V)	0.98	m^3
Sponge filling ratio (FR)[a]	40	%
Total sponge volume (V_{sponge})	0.39	m^3
Specific surface area of the sponge (a_s)[b]	6,600	$m^2\ m^{-3}$

[a] Ratio between sponge volume and reactor volume; [b] Estimated as described in Chapter 3.

5.2.2 Operational phases and monitoring

A long-term monitoring period of 890 days was carried out for each SBTF, comprising three main operational phases as summarized in Table 5.2 and further detailed. No inoculum was used for the start-up of the reactors. As for SBTF-1, operational phases were mainly related to different ventilation control strategies, seeking to realize partial nitritation through DO control. Concerning SBTF-2, besides ventilation control, operational phases considered effluent recirculation and sewage by-pass to promote

heterotrophic denitrification. Those operational phases and sub-phases for each reactor are also schematically depicted in Figure 5.2. The reactors were fed with the same anaerobic effluent during the whole operational period. Influent samples were collected from the outlet of the UASB reactor that fed both SBTFs. Effluent samples were collected from each SBTF at the outlet of the reactors (bottom compartment – see Figure 5.1). The operational phases are detailed as follows:

- Phase I (conventional operation): the two monitored SBTFs were identically operated until stable nitrification performance was observed, indicated by the volumetric ammonium conversion rate.

- Phase II (ventilation control strategies): the SBTFs were operated as in Phase I, but different ventilation control strategies were implemented according to operational results. This means that DO concentration was not directly controlled, but the lateral openings of the monitored reactors were managed to prevent or increase oxygen transfer to the liquid phase. When the reactors were airtightly closed, a water seal was applied in the outlet to avoid air diffusion into the SBTF. On-site smoke tests were performed to ensure virtually hermetic conditions.

- Phase III (conventional operation vs. effluent recirculation): following a period of approximately 350 under oxygen-limited conditions, the SBTF-1 was then operated again as a conventional trickling filter (bottom ventilation port open). As for the SBTF-2, a typical ventilation strategy was also applied (bottom ventilation port open); however, effluent recirculation was used, followed by a period with raw sewage by-pass (i.e., part of the influent to the UASB reactor was directly diverted to the inlet of the SBTF-2). During Phase III for SBTF-2, the bottom ventilation port remained open in all cases.

Table 5.2 Overview of the main characteristics for each operational phase for both SBTFs

Reactor	Parameter (unit)	Phase								
		I – Conventional operation	II – Ventilation control					III – Conventional operation *vs.* effluent recirculation[a]		
			II – A	II – B	II – C	II – D	II – E	III – A	III – B	III – C
SBTF-1	Ventilation scheme[b]	Bottom open	Fully closed – not airtight	Bottom partially open	Fully closed – airtight	Fully closed – not airtight	Bottom open (top cover)	Bottom open		
	Period (days)	0 – 310	311 – 385	386 – 427	428 – 596	597 – 633	634 – 659	660 – 890		
	Duration (days)	310	75	42	169	37	26	231		
	Temperature (°C)	23 (3)	25 (1)	24 (1)	22 (2)	25 (4)	25 (3)	23 (2)		
	Flow rate ($m^3\ d^{-1}$)	2.5 (0.7)	2.5 (0.4)	2.6 (0.1)	2.3 (0.3)	2.5 (0.8)	2.4 (0.1)	2.4 (0.2)		
	Surface hydraulic loading rate - HLRs ($m^3\ m^{-2}\ d^{-1}$)[c]	10.2 (2.8)	10.0 (1.5)	10.4 (0.6)	9.0 (1.2)	10.0 (3.3)	9.6 (0.3)	9.6 (0.7)		
	Theoretical percolation time (h)[f]	3.8 (0.7)	3.8 (0.4)	3.7 (0.2)	4.3 (0.6)	3.8 (1.3)	4.0 (0.1)	4.0 (0.3)		
	Influent total COD ($mg\ L^{-1}$)	148 (59)	111 (23)	89 (29)	205 (49)	155 (37)	136 (13)	125 (44)		
	Influent DO ($mg\ L^{-1}$)	0.6 (0.5)	0.6 (0.4)	0.6 (0.4)	0.5 (0.1)	0.3 (0.1)	0.4 (0.0)	0.4 (0.2)		
	Influent TN ($mg\ L^{-1}$)	52 (10)	36 (6)	31 (7)	46 (6)	50 (3)	45 (2)	45 (5)		
	Influent NH_4^+-N ($mg\ L^{-1}$)	31 (8)	36 (6)	31 (7)	43 (6)	50 (3)	44 (2)	44 (5)		
	Influent pH	7.2 (0.2)	7.2 (0.0)	7.3 (0.0)	7.2 (0.2)	7.1 (0.1)	7.2 (0.1)	7.1 (0.6)		
SBTF-2	Ventilation scheme[b]	Bottom open	Bottom open[d]	Bottom and middle top open	Fully open	Fully closed – not airtight	Fully closed – airtight	Bottom open		
	Period (days)	0 – 304	317 – 391	392 – 464	465 – 596	597 – 659	660 – 685	686 – 776	777 – 818	819 – 890
	Duration (days)	304	75	73	132	63	26	91	42	72
	Temperature (°C)	23 (3)	25 (1)	23 (1)	22 (1)	25 (3)	23 (2)	25 (2)	23 (2)	21 (2)
	Flow rate ($m^3\ d^{-1}$)	2.5 (0.4)	2.2 (0.3)	2.5 (0.2)	2.2 (0.5)	2.4 (0.2)	2.4 (0.1)	2.4 (0.1)	2.4 (0.1)	2.5 (0.2)
	Surface hydraulic loading rate - HLRs ($m^3\ m^{-2}\ d^{-1}$)[c]	10.0 (1.6)	8.8 (1.4)	10.0 (1.3)	8.8 (2.2)	9.6 (0.6)	9.6 (0.4)	18.8 (0.4)	17.2 (0.1)	21.2 (0.9)
	Theoretical percolation time (h)[f]	3.8 (0.6)	4.4 (0.8)	3.8 (0.6)	4.4 (0.9)	4.0 (0.3)	4.0 (0.1)	2.0 (0.04)	2.2 (0.02)	1.8 (0.1)
	Influent total COD ($mg\ L^{-1}$)	151 (59)	107 (24)	114 (31)	205 (49)	152 (29)	125 (31)	113 (60)	156 (39)	133 (29)[e]
	Influent DO ($mg\ L^{-1}$)	0.6 (0.5)	0.6 (0.4)	0.5 (0.2)	0.5 (0.1)	0.4 (0.1)	0.4 (0.1)	0.4 (0.1)	0.3 (0.1)	0.4 (0.1)
	Influent TN ($mg\ L^{-1}$)	52 (10)	36 (6)	35 (9)	47 (5)	47 (3)	47 (7)	43 (4)	42 (4)	52 (4)
	Influent NH_4^+-N ($mg\ L^{-1}$)	31 (8)	36 (6)	35 (9)	42 (6)	46 (3)	45 (7)	42 (4)	42 (4)	50 (4)
	Influent pH	7.2 (0.2)	7.2 (0.0)	7.3 (0.2)	7.2 (0.2)	7.1 (0.1)	7.1 (0.1)	7.1 (1.0)	7.1 (0.0)	7.2 (0.0)
	Recirculation ratio	N.A.						1	0.8	1
	Sewage by-pass (%)	N.A.								10

N.A.: not applied; Median values. Standard deviations in brackets. [a] Phase III was only subdivided into phases A, B, and C for the operation of the SBTF-2; [b] See schematic representation in Figure 5.2; [c] HLRs = Q/A; [d] SBTF-2 was fully closed for 12 days (between days 305-316) before the start of Phase II-A; [e] Without considering organic addition from raw sewage addition. [f] Calculated as V_{sponge}/Q, assuming a saturated medium.

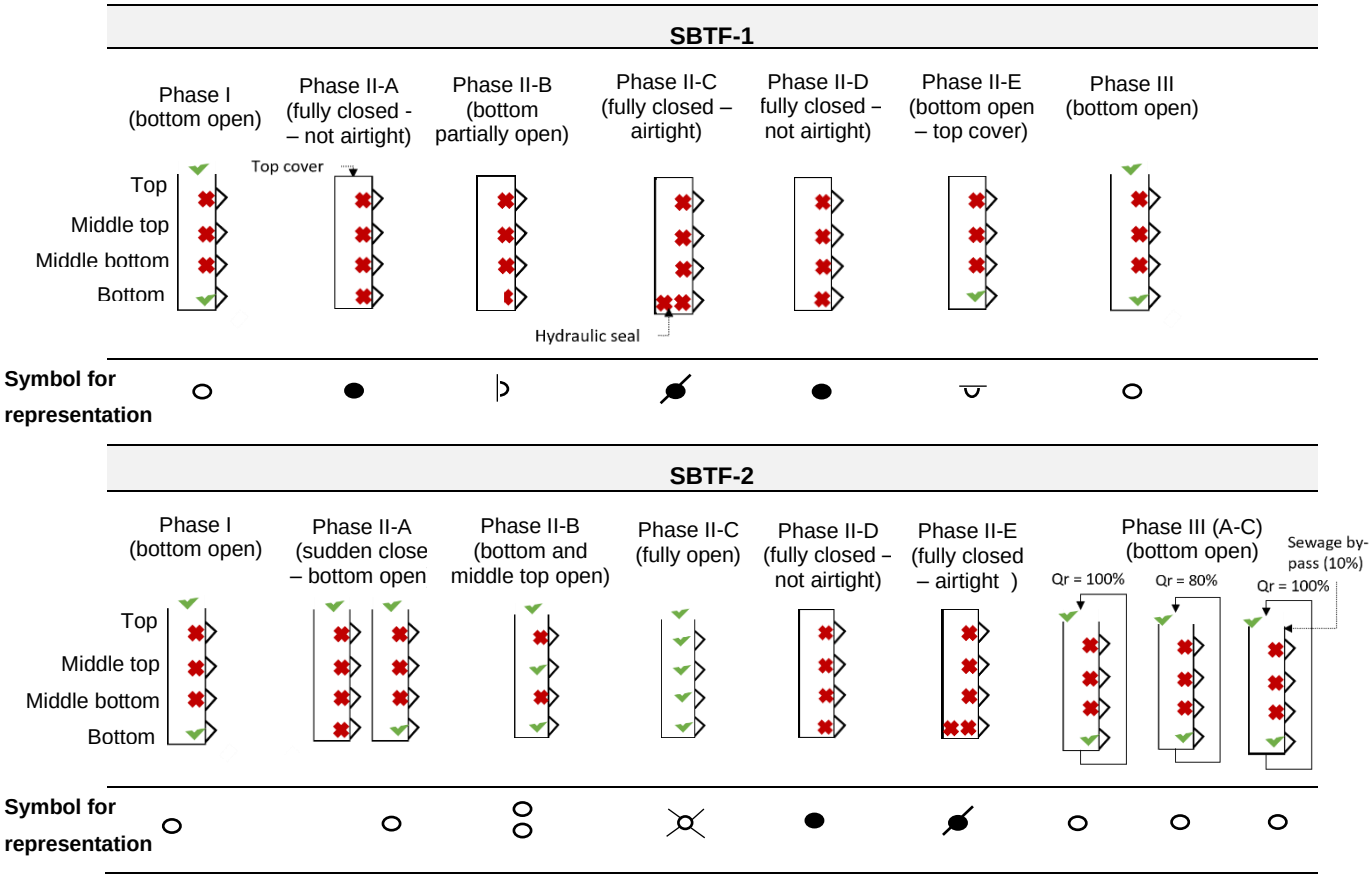

Figure 5.2 Schematic representation of the ventilation strategies adopted in each operational phase for both monitored SBTFs. *Red crosses represent lateral ventilation ports that remained closed during operation*. *Green signs represent lateral ventilation ports or top cover that remained open during operation. Additional symbols are provided to aid in the interpretation of results (e.g., Figure 5.3)*

5.2.3 Analytical methods

Grab samples were collected twice or thrice per week, and the following parameters were measured according to the Standard Methods for the Examination of Water and Wastewater (Baird and Bridgewater, 2017): COD_{total}, $COD_{filtered}$ (0.45 µm), TSS, bicarbonate alkalinity (as $CaCO_3$) and NH_4^+-N. Nitrite (NO_2^--N) and nitrate (NO_3^--N) were analysed using ion chromatography until operational day 219. Following that, nitrite was analysed as the colorimetric method (4500 NO_2 B) and nitrate via nitration of salicylic acid (Robarge et al., 1983). Total nitrogen was determined using a TOC/TN analyser (Shimadzu TOC-VCPH – TNM-1) till operational day 282. Following that, TKN measurement was implemented, and thus total nitrogen as the sum of TKN, nitrite, and nitrate. Field analysis of dissolved oxygen (DO), pH, and temperature measurements were performed using a multiparametric sensor (Hach HQ 40D).

5.2.4 Tracer tests

Tracer tests were performed in both reactors to assess possible hydraulic short-circuiting. A sodium chloride (NaCl) solution (35%) was used as a tracer. The goal was to raise the natural specific conductance of the influent to the SBTFs, exceeding the background values to trace fluid's passage through the reactor. A volume of 500 mL of NaCl was applied as a pulse injection at the rotary distributor arms of both SBTFs. Each test lasted around 7 h (approximately twofold the theoretical percolation time), and the sampling time step was set as 5 seconds. A multi-parameter probe (YSI 600XLM V2® - detection range from 0 to 100 mS cm^{-1}) with an internal data logger was used to monitor the specific conductance of the fluid at the outlet of both SBTFs. Specific conductance values were transformed into NaCl concentration using a calibration curve obtained from measurements of different tracer concentrations with the probe. Before applying the tracer, the background-specific conductance of the effluent of the SBTFs was characterized. Those values were deducted from the recorded outlet concentration during tracer tests.

The real mean percolation time (T_{perc}) was obtained from the curves of percolation time distribution at the outlet (t_i), considering NaCl concentrations at each time step (C_i) (Eq. 5.1).

$$T_{perc} = \frac{\int_0^\infty tCdt}{\int_0^\infty Cdt} \cong \frac{\sum_i t_i C_i \Delta t_i}{\sum_i C_i t_i} \quad [min] \qquad \text{Eq. 5.1}$$

The mass recovery time t10 was selected as a short-circuiting indicator. Such parameter refers to the arrival time of 10% of tracer mass injected at the inlet of the reactor. It is considered a suitable indicator for evaluating short-circuiting in wastewater treatment systems (Guo et al., 2015; Passos et al., 2020; Teixeira and Siqueira, 2008). The lower the t10, the higher the short-circuit (i.e., lower hydraulic performance).

As for SBTF1, 10 tests were carried out between operational days 743 and 828 (Phase III). Concerning SBTF2, a total of 8 tests were conducted between operational days 673 and 681 (Phase II-E) before effluent recirculation was implemented. Wilcoxon's matched pairs tests were performed to assure that neither influent composition (i.e., COD, N) nor temperature was statistically different between the tracer tests.

Differences were considered significant at a p-value below 0.05. Analyses were performed in SPSS Statistics software (IBM Corp., v27).

5.2.5 Simulation study

Experimental results indicated temperature impact on nitrogen conversions. To further gain mechanistic insight, the same model presented in **Chapter 3** was used. Biological conversion reactions were based on Mozumder et al. (2014), and inorganic bicarbonate was included as a limitation term in the kinetic expressions for the growth of autotrophs. The stoichiometric matrix, kinetic expressions, and model parameter values were retained as in **Chapter 3** (detailed in Appendix, Section A.3.1). Biological conversion reactions were adapted to describe the temperature dependency of specific maximum growth and decay rates for AOB, NOB, heterotrophs, and anammox bacteria, as reported by Wan et al. (2019). Temperature dependency of the diffusion coefficients was also considered (detailed in Appendix, section A.5.2).

A set of two simulations was performed. (i) First, the observed temperature variation along the monitored operational (15 – 30 ^{o}C) period was implemented in the model. Initial conditions and input variables were retained as the reference scenario in **Chapter 4**. The model was run for 2000 days; (ii) Second, a steady-state simulation was performed to mechanistically assess the observed experimental behaviour of the SBTF-1 operated under restricted ventilation during Phase II (from operational day 311 to 596; Phases II-A – II-C). In order to simulate oxygen-limited conditions, the volumetric oxygen transfer coefficient (k_La) was decreased such that the simulated effluent DO fit the measured data. Temperature was assumed constant for simplicity. Median measured influent values (Table 5.2) were considered for model input.

5.2.6 Statistical analyses

The non-parametric Wilcoxon's matched pairs test was selected for comparisons between the operational phases assessed. Differences were considered significant at a *p*-value below 0.05. Furthermore, a multivariate statistical method (i.e., principal component analysis) was used to provide independence for capturing the data variance during Phase III for SBTF-1. All computations were processed in SPSS Statistics software (IBM Corp., v27).

5.3 Results

5.3.1 Nitrogen conversions

The performance of both monitored SBTFs over the whole operational phases is summarized in Table 5.3. Figure 5.3 shows nitrogen concentration (a-b), total nitrogen removal performance (c-d), volumetric ammonium conversion rates (e-f), and dissolved oxygen concentrations (g-h) in the elapsed time.

5.3.1.1 Start-up period – conventional operation

Phase I is considered the start-up period, in which a conventional operation was implemented for both reactors (i.e., oxygen supply provided via natural ventilation through the bottom compartment). This period lasted approximately 300 days, in which effluent ammonium concentrations were systematically below 10 mg L^{-1} (Figure 5.3a-b). This corresponded to a median ammonium removal efficiency of approximately 80% for both SBTFs. Effluent nitrite concentrations were less than 1.0 mg L^{-1}, and nitrate production amounted to 0.6 g NO_3^--N g NH_4^+-$N_{removed}^{-1}$ for both reactors. Therefore, total nitrogen removal performance (Figure 5.3c-d) varied between 22 and 37 % (percentiles 25 – 75%) (median value of approximately 27%).

Despite the identical operational conditions and overall performance for nitrogen conversions of both reactors during Phase I, a faster nitrification process was noticed for the SBTF-2. Median volumetric conversion rates of ammonium for SBTF-2 (123 gNH_4^+-N m^{-3}_{sponge} d^{-1}) were approximately 40% higher than those observed for SBTF-1 (88 gNH_4^+-N m^{-3}_{sponge} d^{-1}) during the first 100 days of operation (Figure 5.3e-f). Nonetheless, median ammonium conversion rates all over the start-up period were similar for both reactors (approximately 150 gNH_4^+-N m^{-3}_{sponge} d^{-1}). Effluent dissolved oxygen concentrations remained systematically higher than 6 mg L^{-1} for both reactors (Figure 5.3g-h).

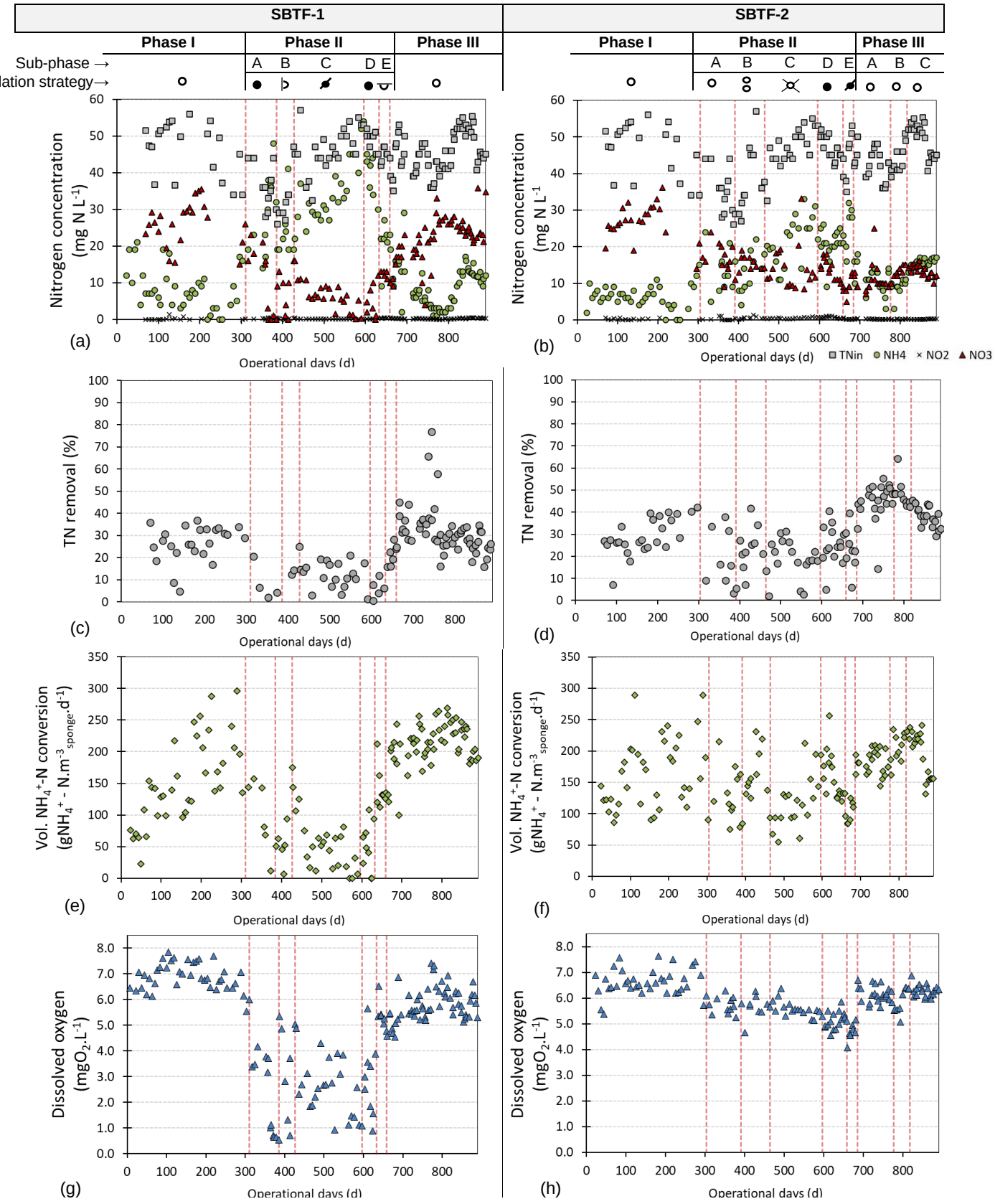

Figure 5.3 Evolution of (a-b) nitrogen concentrations (total nitrogen, ammonium, nitrite, and nitrate), (c-d) total nitrogen removal efficiency, (e-f) volumetric ammonium conversion rates, and (g-h) bulk liquid dissolved oxygen for SBTF-1 and SBTF-2 *Red dotted lines represent operational phases*

Table 5.3 Summary of the SBTFs performance for each operational period

Reactor	Variable (mg L^{-1})	Phase I	II					III		
			II-A	II-B	II-C	II-D	II-E			
SBTF-1	Effluent NH_4^+-N	7 (6)	27 (10)	24 (7)	33 (8)	32 (12)	15 (3)	9 (6)		
	Effluent NO_2^--N	0.1 (1.4)	0.3 (0.2)	0.1 (0.1)	0.1 (0.0)	0.2 (0.2)	0.2 (0.0)	0.2 (0.1)		
	Effluent NO_3^--N	26 (8)	9 (9)	10 (6)	6 (4)	4 (11)	13 (1)	23 (6)		
	Effluent DO	6.8 (0.5)	2.1 (1.5)	3.7 (1.8)	2.6 (1.1)	3.0 (1.4)	5.4 (0.5)	5.7 (0.7)		
	TN removal (%)	27 (11)	-7 (11)	-4 (16)	11 (8)	2 (5)	21 (5)	31 (13)		
	Effluent COD_{total}	63 (22)	51 (20)	61 (35)	69 (17)	57 (61)	53 (16)	41 (25)		
								III-A	III-B	III-C
SBTF2	Effluent NH_4^+-N	6 (3)	12 (6)	14 (5)	23 (6)	21 (4)	28 (6)	12 (4)	10 (2)	16 (1)
	Effluent NO_2^--N	0.2 (1.0)	0.0 (0.4)	0.5 (0.3)	0.5 (0.2)	0.7 (0.2)	0.2 (0.1)	0.2 (0.1)	0.2 (0.1)	0.2 (0.0)
	Effluent NO_3^--N	27 (8)	16 (4)	15 (2)	12 (6)	14 (3)	9 (3)	10 (4)	13 (2)	13 (2)
	Effluent DO	6.6 (0.5)	5.7 (0.3)	5.7 (0.4)	5.5 (0.3)	5.1 (0.3)	6.1 (0.3)	6.1 (0.3)	5.9 (0.5)	6.3 (0.2)
	TN removal	27 (11)	12 (16)	21 (10)	18 (10)	24 (9)	22 (10)	46 (9)	47 (6)	38 (5)
	Effluent COD_{total}	61 (30)	51 (6)	55 (10)	66 (26)	58 (33)	75 (25)	62 (24)	13 (1)	67 (22)

Median values. Standard deviations in brackets.

5.3.1.2 Ventilation control strategies

Phase II was implemented considering different strategies to control oxygen transfer to the monitored reactors. As for the SBTF-1, the reactor was completely closed but not airtight (Phase II-A). Effluent ammonium concentrations immediately soared, and nitrate formation was ceased by the end of such operational phase (Figure 5.3a). Total nitrogen removal was then severely impaired (Figure 5.3d). Dissolved oxygen concentrations immediately dropped from a median of 6.8 mg L^{-1} to 3.6 mg L^{-1} at the beginning of the operational phase, further decreasing to values lower than 1.0 mg L^{-1} (Figure 5.3g). To regain AOB activity, the ventilation port at the bottom compartment was partially open (Phase II-B). Dissolved oxygen concentrations strongly fluctuated between 0.7 and 5.0 mg L^{-1}. Median volumetric ammonium conversion was approximately 45 gNH_4^+-N m^{-3}_{sponge} d^{-1}, similar to that observed during the first 100 days after the reactor start-up. However, negative total nitrogen removal was noticed during this operational period (see Table 5.3), indicating biomass decay and, consequently, organic nitrogen release. No nitrite build-up was observed.

As nitrification was re-established, oxygen supply was further limited by airtightly closing the SBTF (Phase II-C). However, even after sealing off the reactor, oxygen levels in the bulk liquid remained higher than 2 mg L^{-1} for approximately 29 days (Figure 5.3g). DO in the anaerobic effluent fed to reactor was systematically below 0.5 mg L^{-1}

(see Table 5.2). Such operational phase was retained for 169 days to push for NOB out-selection. Nevertheless, nitrate remained the major end-product even under low bulk liquid DO concentrations. The following monitoring period allowed air to diffuse into the SBTF by removing the water seal at its outlet (Phase II-D). Nitrification was sharply regained (132 gNH_4^+-N m^{-3}_{sponge} d^{-1}; Figure 5.3e), and nitrate production amounted to 0.7 g NO_3^--N g NH_4^+-$N_{removed}^{-1}$ (median total nitrogen removal of 21%). DO varied between 4.8 and 6.5 mg L^{-1} (Figure 5.3g), stressing the hurdles of controlling oxygen transfer in SBTFs receiving anaerobic effluents. The bottom ventilation port was thus open (top cover kept), allowing more oxygen to be incorporated into the bulk liquid (Phase II-E). At that moment, sustained oxidation of half of the influent nitrogen was noticed. Nonetheless, the removed ammonium was further oxidized to nitrate, which accumulated in the effluent (Figure 5.3a). Total nitrogen removal performance varied between 20 and 30%, similar to Phase I, previous the disturbances.

Concerning the SBTF-2, a twelve-day operation with the reactor closed was applied at the beginning of Phase II. The reactor was then returned to a conventional mode of operation (Phase II-A). Nevertheless, the observed behaviour during Phase I was not regained even after 75 days of operation after the imposed constrained ventilation. The median volumetric ammonium conversion significantly decreased to approximately 125 gNH_4^+-N m^{-3}_{sponge} d^{-1} (Figure 5.3f) (17% lower than Phase I). Dissolved oxygen concentrations in the effluent were significantly lower (mostly below 6 mg L^{-1}) than in Phase I (Figure 5.3h), despite decreased influent total nitrogen concentration (Figure 5.3b). Hence, to improve AOB activity, the middle top ventilation port was open (Phase II-B). This increased ammonium conversion (147 gNH_4^+-N m^{-3}_{sponge} d^{-1}; median values) and consequently nitrate production, but oxygen levels remained low compared to Phase I.

The SBTF was further fully open to enhance oxygen transfer (Phase II-C). Nevertheless, DO concentrations remained low (5.5 mg L^{-1}), and the volumetric ammonium conversion rate worsened (122 gNH_4^+-N m^{-3}_{sponge} d^{-1}; median values). As for checking the seemingly counterintuitive oxygen behaviour, the SBTF was fully closed (Phase II-D). The median volumetric ammonium conversion rate rapidly increased (150 gNH_4^+-N m^{-3}_{sponge} d^{-1}), accompanied by a slight rise in total nitrogen removal (24%; see median values in Table 5.3). During this operational phase,

approximately half of the influent nitrogen was oxidized. However, the removed ammonium was fully converted to nitrate as observed at Phase II-E for the SBTF-1. Seeking nitrite accumulation, the SBTF-2 was airtightly sealed (Phase II-E). Nevertheless, the ammonium conversion rate was hampered (96 gNH_4^+-N m^{-3}_{sponge} d^{-1}; median values), and nitrate was still the end-product obtained. Overall, total nitrogen removal over Phase II for the SBTF-2 was unstable, and median efficiency stayed below 25%.

5.3.1.3 Conventional operation, effluent recirculation, and raw sewage by-pass

Phase III comprised the return of SBTF-1 to a conventional mode of operation (e.g., bottom ventilation; similarly to Phase I) after being subjected to a prolonged oxygen supply limitation (ventilation restriction). Such operational condition lasted 231 days and was marked by a steep decrease in ammonium concentrations at the first half of the monitoring period, followed by reduced AOB activity (a sharp increase of effluent ammonium concentrations) (See Figure 5.3a). Interestingly, during approximately 80 days (from operational day 736 to 814), ammonium was systematically lower than 5 mg NH_4^+-N L^{-1} in the effluent, accompanied by an unusually low level of effluent inorganic carbon (< 10 mg $CaCO_3$ L^{-1}) and relatively low pH (6.4 – 7.0; percentiles 25 – 75%) (Figure A.5.1) compared to results presented in **Chapter 3**.

A principal component analysis was performed to investigate further what parameters affected nitrogen conversions during this monitoring period. Figure 5.4 shows that effluent concentrations of ammonium were positive in principal component 1, whereas temperature had a negative score (arrow 1). Effluent DO concentrations and temperature also showed opposite trends along with the principal component 2 (arrow 2). Since nitrification is occurring, the clustering of effluent concentrations of ammonium, COD, and inorganic carbon would be expected in the opposite direction from effluent DO and nitrate concentrations. Worth noticing the distance and opposite behaviour between temperature and dissolved oxygen.

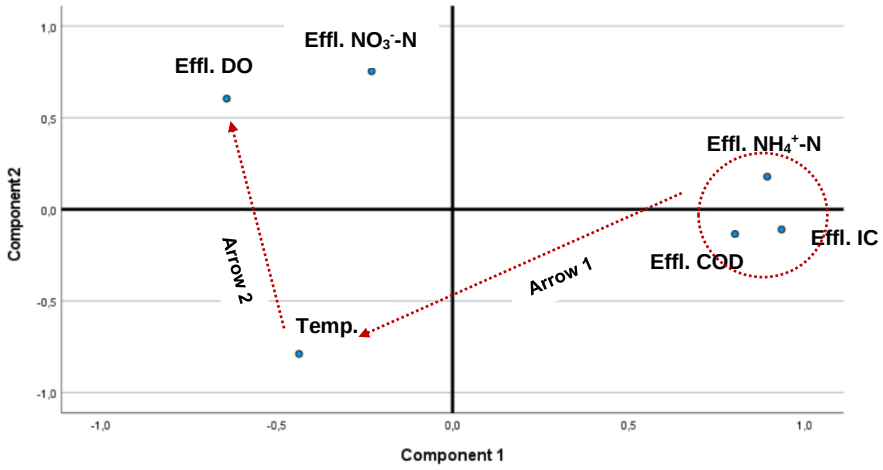

Figure 5.4 The plot of the principal component analysis considering effluent concentrations (ammonium, inorganic carbon, COD, nitrate, and DO) and air temperature during Phase III for the SBTF-1

As for SBTF-2, effluent recirculation was firstly implemented at a ratio I of 1 (i.e., 100% of the incoming flow rate was recirculated) (Phase III-A). Such a ratio was supported by theoretical calculations of the denitrification potential in the SBTF (detailed in Appendix, section A.5.3). A significant effect was noticed in nitrogen conversions. Median volumetric ammonium conversion rates increased to 181 gNH_4^+-N m^{-3}_{sponge} d^{-1} (Figure 5.3f), and nitrate concentrations were mainly below 11 mg L^{-1} (percentile 75%). Median nitrate production amounted to approximately 0.3 g NO_3^--N g NH_4^+-$N_{removed}^{-1}$, corresponding to a total nitrogen removal efficiency of 46% (maximum 55%). Based on indications of excessive dilution of the incoming inorganic carbon content (around 30% considering mixing at the inlet of SBTF), the recirculation ratio was decreased to 0.8 in the following operational step (Phase III-B). Volumetric ammonium conversion rates increased significantly (204 gNH_4^+-N m^{-3}_{sponge} d^{-1}); however, nitrate production slightly increased to 0.4 g NO_3^--N g NH_4^+-$N_{removed}^{-1}$. A final operational phase was motivated by the apparent lack of readily biodegradable organic carbon for heterotrophic denitrification. Thus, raw sewage was directly supplied at a flow rate equivalent to 10% of the incoming flow (Phase III-C). Effluent nitrate concentrations were not further reduced. Besides, the high volumetric ammonium conversion rate at the beginning of this operation phase (approximately 220 gNH_4^+-N m^{-3}_{sponge} d^{-1}) is likely explained by the increased influent total nitrogen (see Figure 5.3b). By the end of the monitoring period (from days 869 - 890), nitrification was hampered (155 gNH_4^+-N m^{-3}_{sponge} d^{-1}).

5.3.2 Outcome from tracer tests

Despite the identical experimental set-up, the degree of short-circuiting was lower in the SBTF-1 compared to STBF-2 (n = 10 for SBTF-1 tests; n = 8 for SBTF-2 tests). The average t_{10} value in SBTF-1 (42.9 ± 9.8 min) was about 140% higher than the t_{10} in SBTF-2 (18.0 ± 3.0 min) (Table A.5.1), which means a significantly lower short-circuiting degree in SBTF1.

The actual mean fluid percolation time in SBTF-1 (T_{perc} = 126 min) was about 16% higher in SBTF-2 (T_{perc} = 108 min), suggesting higher volumetric efficiency for SBTF-1 since the theoretical percolation time ($V_{sponge}/Q \approx 240$ min; see Table 5.2) was the same for both reactors during the period the tests were performed.

5.4 Discussion

5.4.1 Nitrogen conversions in SBTFs during restricted ventilation

Sponge-bed trickling filters following UASB reactors for sewage treatment lack operational flexibility for enriching AOB while inhibiting NOB. Strategies based on solids retention time (SRT) (Regmi et al., 2014) are unsuitable for SBTFs, as SRT cannot be controlled. Intermittent aeration to explore the lag time of NOB (Sun et al., 2017b) would demand mechanized ventilation rather than the natural draft SBTFs. Free ammonia (FA) or free nitrous acid-based (FNA) control strategies for NOB inhibition are technically unfeasible in the process flowsheet comprised of SBTFs preceded by UASB reactors. If secondary settlers are applied, the removed sludge is sent to thickening and digestion at the UASB reactor. Therefore, no side-stream line devoted to sludge treatment could generate a high-strength digestate to be used in FA-based sludge treatment (Wang et al., 2021). Out of the reported techniques, low DO setpoint control seems to remain the only feasible kinetic-based NOB out-selection mechanism to implement in SBTFs. This was thus pushed forward.

Overall, results showed that ammonium conversion was significantly impaired during imposed restricted ventilation even with relatively high dissolved oxygen concentrations in the bulk liquid (> 2 mg L^{-1}). DO was the main limiting factor for nitritation, which is indicated by the immediate regain of the volumetric ammonium conversion rates when the SBTF-1 was reopened (> 200 gNH_4^+-N m^{-3}_{sponge} d^{-1}; higher

than the typical median value of 188 gNH_4^+-N m^{-3}_{sponge} d^{-1} reported for SBTFs, as addressed in **Chapter 2**). Limited ventilation conditions promoted the partial oxidation of the influent nitrogen. Nevertheless, nitrate was always the end-product (i.e., the removed ammonium was practically fully converted to nitrate) besides the remaining non-oxidized ammonium accumulated in the effluent, meaning that anammox activity was likely not relevant. On the other hand, the absence of nitrite could also be related to a rapid depletion by a tiny contribution of anammox bacteria. A successful coupling between AOB and anammox activity in SBTFs strongly depends on the oxygen concentration at the biofilm-liquid interface, as pointed out in **Chapter 4**. The unstable bulk liquid DO throughout the monitoring period (markedly in SBTF-1) is one possible explanation for the out-selection of anammox bacteria. Furthermore, NOB adaptation to low DO (< 0.4 mg L^{-1}) after a relatively short period (3 months) was recently reported for an SBR treating effluent from a high-rate activated sludge plant (Wang et al., 2021).

Experimental (Laureni et al., 2019) and simulation studies (Pérez et al., 2020) reported that a stable partial nitritation-anammox process in the mainstream relies mainly on the operation at low DO (< 0.5 mg L^{-1}) and residual ammonium concentrations (between 2 and 6 mg NH_4^+-N L^{-1}). However, none of them has considered other reduced species besides ammonium (such as sulfide, methane, and residual COD) that can further lead to different DO setpoints to enable nitritation, which is the case of anaerobic effluents. The lower free energy change of ammonium oxidation compared to, e.g., sulfide and methane (Rittmann and McCarty, 2001) would possibly favour other aerobic microorganisms under low oxygen conditions. DO setpoints for stable partial nitrification considering the post-treatment of anaerobic effluents are not yet clear.

Interestingly, after an induced short-term ventilation limitation (12 days), the SBTF-2 did not recover the previously observed volumetric ammonium conversion capacity. Further opening ventilation ports did not contribute. Moreover, as for the operation of a completely open reactor, oxygen transfer to the bulk liquid and consequently increased ammonium turnover was not observed. During this monitoring period (Phase II-C for SBTF-2), the calculated natural draft based on temperature gradients was systematically higher than the estimated headloss (Figure A.5.2), which rules out convective mass transport limitations.

Fully open trickling filters (without side walls) were initially conceived to improve oxygen transfer (Vieira and von Sperling, 2012), based on the theoretical concept of increased gaseous flux for larger contact areas (Wik, 2003). Nevertheless, it was later postulated that the primary driver mechanism for air supply and further oxygen transfer refers to the pressure gradient between the external atmosphere and the internal reactor (Vieira, 2013). Such a gradient can possibly be augmented by the consumption and production of gases during biological reactions (e.g., O_2, CO_2), promoting an advective mass flow from outside towards the inner reactor. A fully open trickling filter would thus be prone to smaller pressure gradients, reducing convective air fluxes. This possibly explain the decreased bulk liquid DO concentration and impaired volumetric ammonium conversions observed in Phase II-C for SBTF-2.

Overall, a worse nitrification performance during Phase II for SBTF-2 was noticed compared to Phase I for both monitored reactors. A reasonable explanation can be attributable to the observed significantly higher hydraulic short-circuiting for SBTF-2. Despite the identical reactor configuration, clogging and fluid flow are dynamic processes in porous media, substantially relying on biomass decay and lysis processes combined with shear stress (Bottero et al., 2013). The observed high short-circuiting in SBTF-2 can indirectly lead to organic overload, as less sponge volume is used for the same influent flow. Fast-growing heterotrophs thus outcompete AOB.

5.4.2 Effect of effluent recirculation and raw sewage by-pass

Despite published evidence of NOB repression in lab-scale SBTFs, no nitrite accumulation was observed throughout the whole monitoring period for both monitored SBTFs fed with real anaerobically treated effluents. Under oxygen-limited conditions, ammonium removal was hampered, and nitrate was still being produced. Therefore, operational strategies to enhance the conventional nitrification-denitrification process were implemented rather than insisting on oxygen control for inducing partial nitritation.

Effluent recirculation promoted an increase in total nitrogen removal (from less than 30% to a median of 46%). Nevertheless, a further improvement in process performance was likely limited by two simultaneous aspects: first, the volumetric ammonium conversion rate remained low (< 200 gNH_4^+-N m^{-3}_{sponge} d^{-1}) compared to the high observed values in this study (up to 250 gNH_4^+-N m^{-3}_{sponge} d^{-1}). Dilution of the

available inorganic carbon content in the influent is a possible explanation, which can compromise AOB activity, as addressed in **Chapter 3**; and second, although nitrate consumption increased due to an apparent proper stoichiometric relation at the inlet of the reactor (approximately 3 g $COD_{filtered}$ g NO_3^--N^{-1}), the organic content is possibly most non-biodegradable, hampering heterotrophic denitrification. To address the first issue, the recirculation ratio was reduced (R=0.8), which led to a significant increase in the volumetric ammonium conversion rate. Nevertheless, better nitrification was counteracted by lower nitrate consumption so that total nitrogen removal remained the same as for operating at a recirculation ratio of 1.

To tackle the second observed issue, a carbon supply was provided to the inlet of the SBTF by feeding raw sewage, which increased the organic loading rate compared to the previous operational phases (Figure A.5.3). Nitrogen conversion dynamics throughout this operational period clearly showed a decreasing trend in terms of effluent nitrate concentrations, however, counterbalanced by increased effluent ammonium concentrations. Such a condition is typically related to overloaded SBTFs (Bressani Ribeiro et al., 2017), where organic loadings (>1.5 kgCOD m^{-3} $_{sponge}$ d^{-1}) were considered the main reason for low nitrification performance (Almeida et al., 2013; Tandukar et al., 2006b). Furthermore, simulation results from **Chapter 4** also showed that nitrogen-related microorganisms are pushed downwards in the SBTF under high organic loadings. That observation, combined with the previously discussed reduced sponge volume for biomass colonization (i.e., high hydraulic short-circuiting), likely explains AOB activity suppression due to space competition with heterotrophs. Complementary, providing sewage directly to the inlet of the SBTF might have negatively influenced nitrification due to the adsorption of particles onto the biofilm surface, increasing thickness and impairing mass transfer, as supported by experimental evidence on plastic-based trickling filters (Boller et al., 1990).

The sludge yield coefficient nearly tripled when effluent recirculation was implemented (from 0.16 to 0.42 kg TSS kg $COD_{removed}^{-1}$; median values). Such high solids production can be explained by the observed reduced COD load removed per volume of sponge (Figure A.5.4a) associated with the increased shear stress under high surface hydraulic loading rates, displacing retained particles in the sponge pores. Nevertheless, median effluent TSS concentrations remained lower than 25 mg L^{-1}

(Figure A.5.4b), even without secondary settlers following the SBTF. Moreover, such a high sludge yield is still significantly lower than conventional aerobic processes (e.g., activated sludge) following UASB reactors treating sewage (as presented in **Chapter 2**).

5.4.3 Further insights on SBTFs under limited oxygen supply

Although a partial ammonium conversion was noticed under limited oxygen supply, no nitrite accumulation was observed. However, this could not be predicted by the developed model (**Chapter 3**) by simply decreasing the volumetric oxygen transfer coefficient (k_La) (Figure A.5.5). In this case, oxygen concentrations higher than 2 mg L^{-1} can fully oxidize the influent ammonium. Nevertheless, the observed experimental data showed impaired volumetric ammonium conversion rates for SBTFs under limited oxygen supply. Hence, a hypothesis is raised that dissolved gases (methane and hydrogen sulfide – H_2S) are being stripped and back-diffused into the bulk liquid, enhancing oxygen competition between AOB and aerobic heterotrophs (i.e., ordinary heterotrophs, methanotrophs, and sulfide oxidizing bacteria). This is supported by experimental observations of a closed SBTF treating synthetic wastewater containing sulfide and methane, in which ammonium oxidation was hampered (Hatamoto et al., 2011). Since conversion dynamics of those gases are not included in the developed model, the behaviour of an SBTF under restricted ventilation fed with anaerobic effluents could not be predicted.

5.4.4 Insights on microbial adaptation and temperature effects

Reduced AOB activity under low temperatures is a well-known phenomenon (Ekama et al., 2020), which is counteracted by increasing solids retention time (SRT) in the activated sludge process. Even though the high SRT in the SBTF (> 100 days), temperature variations significantly impacted nitrification. This finding likely affects nitrogen conversion dynamics in SBTFs following UASB reactors in the long run. Based on such experimental indications, complementary simulations considering the observed temperature range (15 – 30 ^oC) were performed to gain process insight.

Less pronounced fluctuations in effluent ammonium concentrations were noticed from simulation (Figure A.5.6), compared to experimental data (Phase III for SBTF-1; see Figure 5.3a). A possible explanation is that the previously restricted ventilation

operation (Phase II) might have pushed the selection of AOB strains capable of up-regulating the CO_2 fixation pathway under limited substrate (inorganic carbon). Therefore, when the SBTF-1 was gradually reopened (Phases II-D; II-E and III), those selected strains grew fast. From a fundamental standpoint, AOB (i.e., *Nitrosomonas europaea*) can maintain some genes that would allow a quick recovery upon starvation (in the present case, caused by the lack of oxygen for ammonium oxidation) (Wei et al., 2006). An increased AOB activity after reopening the SBTF-1, temporarily not inhibited by inorganic carbon, also caused the observed temporary pH drop, which might have exerted negative feedback, hampering AOB activity. The influence of pH lower than 7.0 impairing AOB is well documented in the literature (Biesterfeld et al., 2003), although bias persists on the actual cause of the inhibition (low pH or lack of inorganic carbon). The model could not help to explain the possible extent of the observed dynamics besides temperature since those mechanisms (i.e., metabolism up-regulation and pH changes) are not included.

From the previously discussed results of a long-term simulation study (**Chapter 4**), the anammox process takes over nitrogen removal in SBTFs. Nonetheless, temperature variations were not considered in the simulated scenarios. The prevalence of the autotrophic pathway in the long term and the associated high total nitrogen removal (> 60%) (viz. **Chapter 4**) is undermined considering the operational temperature range between 15 and 30 ^{o}C (Figure A.5.6). Such behaviour could be expected considering the high sensitivity of μ_{max} of anammox bacteria (**Chapter 4**), which is thus washed out from the SBTF. Lotti et al. (2014) reported evidence of anammox growth in a temperature range between 10 and 20 ^{o}C. Nevertheless, nitrite was supplied, and oxygen was absent. Therefore, competition with NOB and oxygen inhibitory effects were excluded. The feasibility of the anammox process below 20 ^{o}C for treating anaerobic effluents in a lab-scale SBR was presented by Fernandes et al. (2018); however, the nitritation step was omitted. Stable partial nitritation-anammox under low temperatures was also demonstrated in lab-scale SBRs fed with carbon-free synthetic wastewater (Gilbert et al., 2014; Hu et al., 2013). A stepwise acclimatization procedure following an optimum process start-up (influent ammonium higher than 500 mg N L^{-1} and temperature of 30 ^{o}C) were critical characteristics for a successful operation. De Cocker et al. (2018) also suggested a controlled and gradual temperature decrease, while eliminating competition and enhancing anammox bacteria retention to ensure

high activity in the operation range of 10 – 30 ^{o}C. Nevertheless, those strategies are not straightforwardly upscaled for mainstream applications, especially in SBTFs where SRT cannot be directly controlled.

Low temperatures are also related to increased oxygen concentrations in the bulk liquid. Despite the high oxygen availability, nitrification rates are hampered by the temperature decrease. This is shown by the inverse correlation between ammonium concentrations and temperature from the performed principal component analysis. The reduced AOB activity potentially contributes to a deep oxygen penetration in the biofilm, inhibiting anammox bacteria, as also observed by Wang et al. (2019). In summary, decreasing temperature triggers a cascade of physical and biological events in the SBTF that eventually reduces the available anoxic niches for anammox bacteria.

5.5 Conclusions

A long-term operation of two parallel SBTFs fed with real anaerobically treated effluents was carried out. Different operational phases were implemented considering ventilation strategies, effluent recirculation, and raw sewage by-pass.

- Effluent recirculation was confirmed as the best strategy for improving total nitrogen removal in SBTFs. However, the maximum total nitrogen removal performance was limited due to nitrate build-up in the effluent.

- Carbon supply (i.e., raw sewage by-pass) to the top SBTF compartment decreased total nitrogen removal, as nitrification was impaired under a high organic loading rate. This could also be attributable to a high hydraulic short-circuiting, which indirectly increased the organic loading rate and pushed AOB out-selection.

- Sludge yield nearly tripled when effluent recirculation was implemented, but effluent TSS concentrations remained low (< 25 mg L^{-1}). Therefore, the possibility of operation without secondary settlers is evidenced even under increased shear stress conditions.

- The strategy of kinetic suppression of NOB by ventilation control in SBTFs proved impractical. Even though partial oxidation of the influent nitrogen was

achieved under limited oxygen supply, ammonium and nitrate build-up in the effluent.

- No indications of significant anammox activity were perceived in the long-term experiment. Dynamic simulations revealed that the oscillating operational temperature (15 – 30 ^{o}C) hampered anammox bacteria ingrowth.

Appendix

In this appendix, the parameter dependencies on temperature are given (Section A.5.1), considering the adaptation of the bioconversion model addressed in **Chapter 3**. The calculations that theoretically support the implementation of effluent recirculation are given in Section A.5.2. The following content brings supplementary experimental (Section A.5.3) and simulation (Section A.5.4) results.

A.5.1 Model bioconversions

To evaluate the effect of temperature on the reactor performance, parameter dependencies on temperature were explicitly included in the bioconversions of the model presented in **Chapter 3** (see A.3.1). The temperature (T, K) dependencies of maximum growth (μ_{max}) and decay rates (b) for AOB, NOB, anammox bacteria (AN), and heterotrophs (HET) were calculated with equation Eq. A.5.1.

$$K(T) = K(T_{ref})\exp\left(\frac{E_{act}(T - T_{ref})}{RTT_{ref}}\right) \quad \text{Eq. A.5.1}$$

where E_{act}^{AOB} = 68 kJ.mol^{-1}, E_{act}^{NOB} = 44 kJ.mol^{-1}, E_{act}^{AN} = 70 kJ.mol^{-1}, (Hao et al., 2002); E_{act}^{Het} = 48 kJ.mol^{-1} (calculated with maximum growth rate values at 283.15 K and 293.15 K according to Henze et al., 2006); R = 8.31 J mol^{-1} K^{-1}.

The temperature dependency of the diffusion coefficients was calculated with Eq. A.5.2.

$$D_i(T) = D_i(T_{ref})\frac{\mu(T_{ref})}{\mu(T)}\frac{T}{T_{ref}} \quad \text{Eq. A.5.2}$$

where $D_i(T_{ref})$ (m^2 d^{-1}) is the diffusion coefficient at the reference temperature; $D_i(T)$ (m^2 d^{-1}) is the effective diffusion coefficient at temperature T; $\mu(T)$ (Pa.s) and $\mu(T_{ref})$ (Pa.s) represent the viscosity of water at temperature (Venard and Street, 1975) T (K) and reference temperature T_{ref} (K), respectively.

A.5.2 Theoretical calculations of the denitrification potential in the SBTF

The theoretical determination of the heterotrophic denitrification potential (DP) over nitrate in the SBTF was performed based on the well-established calculation procedure

for the activated sludge process (Henze et al., 2008), considering the separate utilization of the readily biodegradable COD (RBCOD) (Eq. A.5.3) and the slowly biodegradable COD (SBCOD) (Eq. A.5.4). Therefore, combining those two equations gives the total denitrification potential of the system (i.e., the amount of nitrate that can stoichiometrically be denitrified considering the available electron donors). Kinetic limitations are assumed for denitrification on SBCOD.

$$\mathrm{DP(RBCOD)} = \frac{(1 - Y_H)}{2.86} * RBCOD \qquad \text{Eq. A.5.3}$$

$$\mathrm{DP(SBCOD)} = k_2 * f_x * Y_H * \frac{SRT}{(1 + b_H * SRT)} \qquad \text{Eq. A.5.4}$$

where *RBCOD* was considered as the typical COD_{total} from the UASB reactor (140 mg L^{-1}) and COD_{total} from the SBTF (60 mg L^{-1}) after mixing in the rotary distributor arm; Y_H the yield coefficient of heterotrophs (0.67 g COD $gCOD^{-1}$; see Table A3.3); 2.86 the stoichiometric amount of nitrate consumed per gram COD; k_2 is the specific denitrification rate (adopted as 0.1, according to Henze et al., 2008); f_x is the fraction of anoxic biomass (assumed as 0.6 in this study); b_h is the decay rate of heterotrophs (0.54 d^{-1}; see Table A3.3); and SRT is solids retention time (adopted as 100 d, according to Bressani-Ribeiro et al., 2017).

A.5.3 Supplementary experimental results

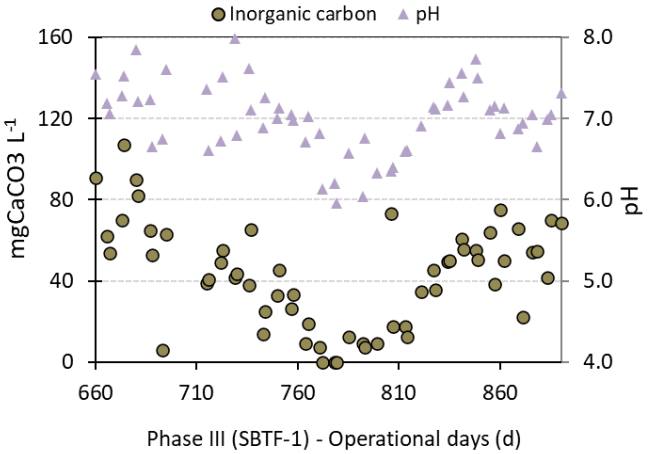

Figure A.5.1 Effluent pH and inorganic carbon concentrations for the SBTF-1 under Phase III (i.e., conventional operation after a prolonged ventilation restriction)

Phase II-C (SBTF 2): Fully open operation	
Temperature gradients (liquid-air)	Estimated draft and headloss[a]

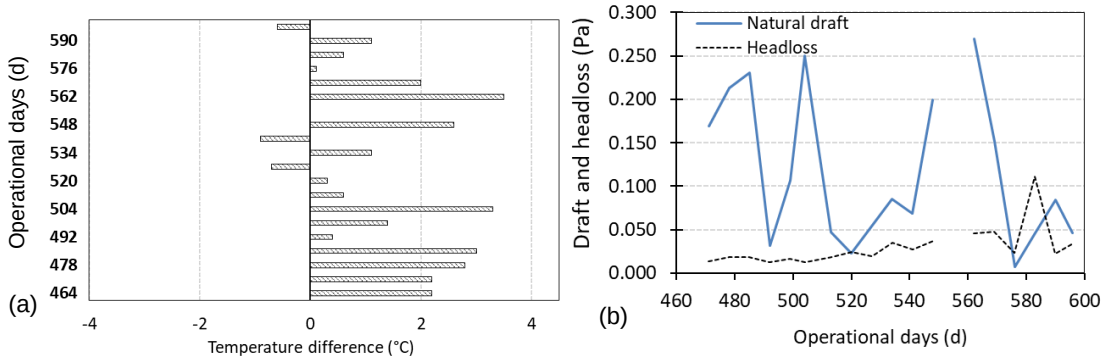

Figure A.5.2 Temperature gradients (a) and estimated draft and headloss (b) for the SBTF 2 during the operational Phase II-C (days 465-596; fully open) *[a]Estimated draft and headloss based on Metcalf & Eddy (2013). Oxygen transfer efficiency is assumed as 5%*

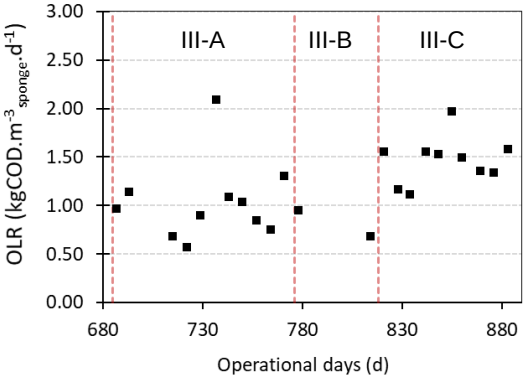

Figure A.5.3 Applied organic loading rates during Phase III for SBTF-2

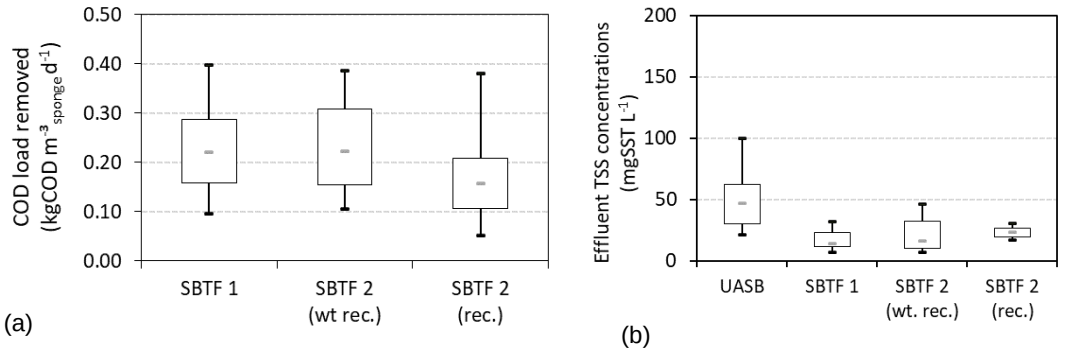

Figure A.5.4 COD load removed in both monitored SBTFs (a) and effluent TSS concentrations (b). *"wt. rec." stands for the operational period without effluent recirculation (Phases I and II). "rec." refers to the operational period with effluent recirculation (Phase III)*

Table A.5.1 Results from tracer tests performed in both SBTFs

SBTF-1	
Test date	T_{10} (minutes)
01/02/2021	30,77
04/02/2021	21,51
15/03/2021	40,30
09/04/2021	49,66
13/04/2021	48,34
14/04/2021	48,43
15/04/2021	43,75
16/04/2021	51,68
28/04/2021	50,51
29/04/2021	44,42
Mean	**42,94**
Standard deviation	**9,75**

SBTF-2	
Test date	T_{10} (minutes)
23/11/2020	16,31
25/11/2020	14,67
27/11/2020	13,84
30/11/2020	20,77
01/12/2020	21,18
02/12/2020	16,85
03/12/2020	20,70
04/12/2020	19,95
Mean	**18,03**
Standard deviation	**2,96**

A.5.4 Supplementary simulation results

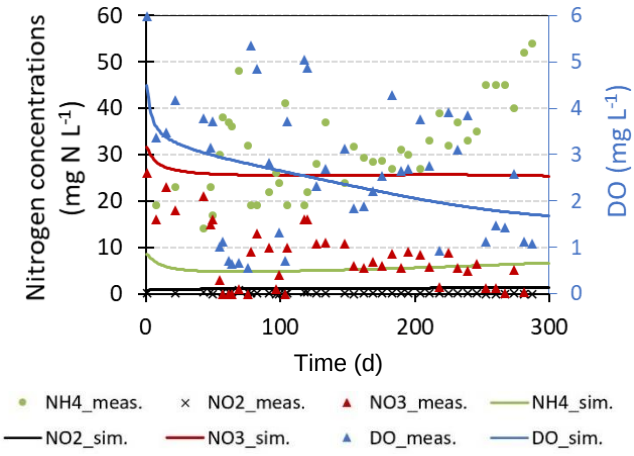

Figure A.5.5 Simulated and experimental data for effluent ammonium, nitrite, nitrate, and dissolved oxygen for the SBTF under limited oxygen supply. *Day 0 of simulation refers to the first operational day of Phase II-A (day 385)*

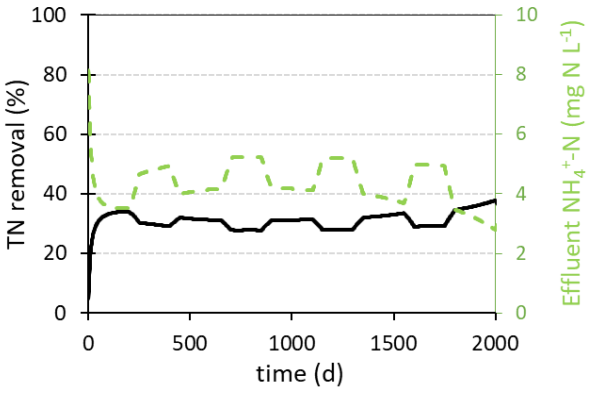

Figure A.5.6 Simulated results on effluent ammonium (green) and total nitrogen removal efficiency (black) considering the effect of temperature variation according to the experimentally observed range (15 – 30 ^{o}C)

Chapter 6

Fate of dissolved methane and H_2S during mainstream nitrogen conversions in sponge-bed trickling filters

6.0 Abstract

Anaerobic sewage treatment in UASB reactors is a consolidated technology due to its appealing low cost and operational complexity compared to conventional activated sludge, besides the energy recovery potential of biogas. Nonetheless, the residual organic carbon and nitrogen in the anaerobic effluent demand a further treatment step. Sponge-bed trickling filters (SBTF) have been successfully applied for such a purpose. However, the fate of dissolved methane and H_2S in the anaerobic effluent is often neglected in SBTFs. This chapter aimed to assess the relevance of dissolved gas stripping in SBTFs and the impact on nitrogen conversions. Therefore, a previously developed mathematical model was expanded considering stripping and biological conversion processes of dissolved methane and H_2S. Simulations showed that nearly all the dissolved gases were stripped from the anaerobic effluent. If a (partially) closed SBTF is applied, gas desorption is decreased, and practically all methane and H_2S were aerobically oxidized by methane oxidizing and sulfide oxidizing bacteria, respectively. Nevertheless, total nitrogen removal efficiencies were impaired. Dissolved methane and H_2S hampering nitrogen removal were related to competition for oxygen, which was generally lost by ammonium oxidizing bacteria. Consequently, methane oxidizing and sulfide oxidizing bacteria pushed nitrogen removal to the bottom compartments of the SBTF. Simulations also did not prove the occurrence of Denitrifying Anaerobic Methane Oxidation (DAMO) or Sulfide Based Denitrification (SBDN), often proposed for treatment of anaerobic effluents as these processes combine methane and H_2S removal with nitrogen removal, respectively. Further experimental tests with a closed SBTF fed with desorbed anaerobic effluents showed that nitrogen conversions are potentially better handled with methane and H_2S are removed upfront.

6.1 Introduction

Anaerobic sewage treatment in warm climate regions is mainly performed through UASB reactors, profiting from the well-known process simplicity and low operational costs, besides the potential for net energy generation (Chernicharo et al., 2015). As two critical by-products of anaerobic digestion, methane and hydrogen sulfide (H_2S) are present in the biogas. However, a significant amount of those gases remains dissolved or entrapped in the liquid phase, leaving the UASB reactor with the anaerobic effluent. The dissolved concentrations of methane and H_2S range from 10 to 25 mg L^{-1} and from 6 to 15 mg L^{-1}, respectively (Souza et al., 2012, 2011). If not adequately collected and treated, shortcomings related to greenhouse gas emission, odour nuisance, and corrosion arise.

Possible management options include physical and biological removal processes. As for physical units, the most straightforward technique is the stripping of those dissolved gases in the anaerobic effluent, which should then be further treated (Centeno-Mora et al., 2020). Concerning biological processes, the focus is often the aerobic oxidation of methane and H_2S (Hatamoto et al., 2011) by methane oxidizing bacteria (MOB) and sulfide oxidizing bacteria (SOB), respectively. More recently, attention has also been devoted to the simultaneous abatement of methane and H_2S coupled with autotrophic nitrogen removal processes. In the latter case, dissolved methane and H_2S are electron donors in the so-called denitrifying anaerobic methane oxidation (DAMO) and sulfide-based denitrification (SBDN), respectively. Silva-Teira et al. (2017) proposed an anaerobic membrane bioreactor with DAMO as a post-treatment system to couple nitrogen removal with dissolved methane removal. Although a high methane abatement was observed (80%), nitrogen removal was less than 50%. SBDN was reported to achieve nitrogen removal efficiencies as high as 99% in an aerobic/anoxic fixed bed reactor (Guerrero and Zaiat, 2018); however, H_2S was supplemented through gas injection. For typical anaerobically treated sewage with relatively low H_2S concentrations (< 20 mg L^{-1}), additional electron donor, e.g., in the form of organic carbon, is required to achieve complete nitrogen removal, thus combining SBDN and heterotrophic denitrification (van den Hove et al., 2020).

Reliable ammonium oxidation is achieved in SBTFs (Bressani-Ribeiro et al., 2017). Also, methane oxidation (Matsuura et al., 2015) and H_2S oxidation (Hatamoto et al.,

2011) have been demonstrated. Moreover, enrichment of DAMO organisms was successfully achieved in a sponge-bed trickling filter over long periods (Hatamoto et al., 2017). Nevertheless, combining an adequate nitrogen removal performance with efficient removal of dissolved methane and H_2S in an SBTF remains to be demonstrated. Many interactions are to be expected. For instance, there is a competition for oxygen between ammonium oxidizing bacteria (AOB), SOB, and MOB. Alternatively, methane and H_2S could be removed using nitrite or nitrate as an electron acceptor in the DAMO and SBDN process, respectively, potentially increasing total nitrogen removal but also causing microorganisms to compete for nitrogen substrates.

Modelling and simulation are ideal tools for studying complex microbial interactions and assessing the feasibility of novel processes. It was applied by Chen et al. (2016) to assess simultaneous ammonium, dissolved methane, and H_2S removal from anaerobic digestion liquid in a membrane biofilm reactor, which has implications related to the gas transfer to the biofilm compared to an SBTF. Heterotrophic growth and its interaction with methanotrophic growth were neglected by Chen et al. (2016), which was motivated by the fact that anaerobic effluents typically contain only low organic carbon concentrations. However, the heterotrophs grow on decay products, impacting process performance, as demonstrated for autotrophic nitrogen removal (Mozumder et al., 2014). The coupling between DAMO and anammox has already been researched in biofilm reactors through modelling (Fan et al., 2021; Liu et al., 2020). Nevertheless, MOB are often neglected, although they can grow at low oxygen concentrations and thus compete with DAMO for methane even in anoxic environments.

The fate of methane and H_2S during nitrogen conversions in SBTFs treating anaerobic effluents remains unclear. Therefore, a previously developed SBTF model (**Chapter 3**) was expanded to include stripping and biological conversions of dissolved methane and H_2S in the influent. The model was applied in simulation studies to quantify methane and H_2S stripping and assess the impact of these substances on nitrogen removal. Based on the simulation results and previous experimental evidence on the impact of dissolved gases on nitrogen conversions, an SBTF fed with desorbed anaerobic effluents (i.e., deprived of methane and H_2S) was further experimentally assessed.

6.2 Methodology

6.2.1 Modelling combined nitrogen, methane, and H_2S conversion in an SBTF

6.2.1.1 Bioconversion processes

The mathematical model described in **Chapter 3** was further expanded to account for the biological conversion processes of dissolved methane and H_2S. A complex network of microbial interdependencies and competition for products and substrates is observed (Table 6.1). Detailed process stoichiometry, rate expressions, and applied parameters are presented in Appendix (Section A.6.1).

Table 6.1 Interdependencies and competition for products (P) and substrates (S)

	Ss[a]	O_2	NO_2^-	NO_3^-	NH_4^+	N_2	CH_4	H_2S	SO_4^{2-}	S_0	CO_2
Aerobic											
Heterotrophs	S	S									P
AOB		S	P		S		(S)[b]				
NOB		S	S	P							
MOB		S			(S)[b]		S				P
SOB		S						S	P	P	
Anoxic											
Heterotrophs (NO_2^-)	S		S			P					P
Heterotrophs (NO_3^-)	S		P	S							P
Anammox			S	P	S	P					
DAMO-B			S			P	S				P
DAMO-A			P	S			S				P
SBDN (NO_3^-)			P	S				S	P	P	
SBDN (NO_2^-)			S			P		S	P	P	

[a] Ss represents soluble biodegradable organic carbon (substrate for heterotrophic organisms) [b] Cometabolic substrate that does not provide energy.

Methane conversion processes

Methanotrophic conversions were based on Daelman et al. (2014) and Winkler et al. (2015) for MOB and DAMO organisms, respectively. Ammonium was considered the sole nitrogen source for cell synthesis. Inhibition of methanotrophic activity due to ammonium was not considered because of the ambiguous effects of this compound. While ammonium serves as a nutrient sustaining methanotrophic growth, it is also a competitive inhibitor of methane monooxygenases (Stein and Klotz, 2011). A mixed culture of methanotrophs was considered; therefore, no distinction was made between type 1 and type 2 methanotrophs (Hanson and Hanson, 1996).

The contribution of MOB to nitritation, the so-called methanotrophic nitrification, was not considered in the model. The affinity of MOB for ammonium is generally lower than that of AOB. Furthermore, MOB lack cytochromes to transfer electrons to the quinone pool, meaning they cannot conserve energy from the ammonium oxidation (Mohammadi et al., 2017). Contributions of AOB for methane oxidation were also not included in the model. Even though some AOB species have similar affinities for methane as of MOB, their methane oxidation rates are five times lower (Bédard & Knowles,1989). Moreover, AOB are unable to grow on methane as a sole substrate.

DAMO organisms (bacteria and archaea) convert nitrate to nitrite and nitrite to N_2, respectively, both using methane as an electron donor (and as a carbon source for cell synthesis). They are inhibited by oxygen, which was incorporated into the kinetic rate expression (processes 10 and 11 – Table A.6.2) using Haldane kinetics, like the anammox process. DAMO-A were considered to use ammonium for biomass growth. DAMO-B can use ammonium and nitrite as nitrogen sources for biomass growth, but nitrite was chosen as the sole nitrogen source in this model, based on Winkler et al. (2015).

Half-saturation coefficients of methane for DAMO ($K_{S,CH4}^{Da/b}$) vary vastly in literature and play an important role in the coexistence of MOB and DAMO organisms (Castro-Barros et al., 2018). Those authors reported a half-saturation constant 30 times lower (higher affinity) than Chen et al. (2015), who did not include MOB. Since the present study assessed the role of MOB coupled with DAMO, the value of Castro-Barros et al. (2018) was adopted. Also, the nitrite half-saturation coefficient for DAMO B ($K_{S,NO2}^{Db}$) seemed to determine the successful colonization of this microbial community. Chen et al. (2015) favoured DAMO-B over anammox by assuming a lower value for $K_{S,NO2}^{Db}$. Conversely, Castro-Barros et al. (2018) assumed that anammox had a higher nitrite affinity than DAMO-B. The effect on anammox growth was minor but favouring DAMO-B did show increased levels of DAMO-B growth. For consistency, the value reported by Castro-Barros et al. (2018) was retained in this study.

Sulfide conversion processes

A two-step pathway for sulfide oxidation was implemented in the model, based on Jensen et al. (2009). Oxidation of H_2S yielding elemental sulfur (process 8 – Table

A.6.1) and oxidation of elemental sulfur yielding sulfate (process 9 – Table A.6.1). Most studies considering SOB or SBDN only include the first step to simulate the formation of elemental biogenic sulfur, often for recovery purposes (Chen et al., 2016; Cueto et al., 2021; Xu et al., 2013).

The main end-product (i.e., elemental sulfur or sulfate) depends on the oxygen-to-sulfide ratio (Janssen et al., 2009). Nevertheless, sulfide oxidizers are also known to acclimate to the main sulfur source present. Hydrogen sulfide has previously been identified as the preferred substrate, as elemental sulfur required a more extended acclimation period (An et al., 2010; Mora et al., 2016, 2015). Hence, the presence of H_2S in the system is expected to limit sulfur oxidation, which was reflected in the model by including a non-competitive inhibition term, as also done by Decru et al. (2021) (process 9 – Table A.6.2). This term expressed inhibition of the second oxidation step in the presence of H_2S.

Modelling sulfide-based denitrification was based on Decru et al. (2021). SBDN was split into four processes, distinguishing between electron donors (H_2S and S_0) and electron acceptors (NO_2^- and NO_3^-), based on previously observed intermediate products of SBDN (Campos et al., 2008). As such, the sequential reduction of nitrate to nitrite and finally to N_2, realizing denitrification, was explicitly considered. Each process was characterized by a specific growth rate, as determined by Mora et al. (2015).

Intracellular accumulation of elemental sulfur, as often observed with SOB and SBDN organisms (Mora et al., 2016), was not integrated into the model. Chemical sulfide oxidation was assumed insignificant compared to biological oxidation processes. In theory, this process can cause less sulfide to be available for the SOB and SBDN organisms, and not including it might lead to an overestimation of SOB and SBDN growth. However, the chemical oxidation of sulfides is much slower compared to biological oxidation, which is catalysed by enzymes (Mora et al., 2016). Therefore, chemical sulfide oxidation is often neglected in the presence of biological conversions (Xu et al., 2013). Another sulfur conversion pathway is the reduction by sulfate-reducing bacteria (SRB). Nonetheless, sulfate is not an appealing electron acceptor as it yields less energy than nitrite or nitrate (Madigan et al., 2011), which is why SRB were not included in the model. Sulfide inhibition was also not integrated into the

described kinetics because of (i) the relatively low concentrations of H_2S (11 g S m^{-3}) in the anaerobic effluent (see further); and (ii) the pH around neutrality of the anaerobic effluent, which causes less than 50% of the total sulfide being present in its undissociated, most toxic form.

Nitrite inhibition was neither included for biological reactions on sulfide nor methane. This is supported by previous experimental evidence of no nitrite accumulation in the long-term operation of SBTFs following UASB reactors (**Chapter 5**). Furthermore, MOB and SOB were assumed to be less affected by inorganic carbon limitation, as those bacteria were also reported to up-regulate their anabolism mixotrophically (Carere et al., 2017; Sun et al., 2019). Therefore, a similar kinetics approach was adopted based on NOB (i.e., Monod-type saturation with a low half-saturation constant value (1.2 mg $CaCO_3$ L^{-1})).

6.2.1.2 Biofilm model

Biofilm porosity was kept constant (ε_W = 0.80) as in **Chapter 3**. Initial fractions of particulate components were thus reset at $\varepsilon^{in}_{XMOB} = \varepsilon^{in}_{XDAMO\text{-}A} = \varepsilon^{in}_{XDAMO\text{-}B} = \varepsilon^{in}_{XSOB} = \varepsilon^{in}_{XSBDN} = \varepsilon^{in}_{XAN}$ = 0.005; ε^{in}_{XH} = 0.035, ε^{in}_{XAOB} = 0.09, ε^{in}_{XNOB} = 0.045.

6.2.1.3 Interphase mass transport

The description of stripping of dissolved methane and H_2S from the SBTF was similar to the description for oxygen diffusion adopted in **Chapter 3**. The volumetric rate transfers for methane and H_2S ($k_La_{,G}$) were adopted based on the relation between their diffusion constants and that of oxygen (Eq. 6.1), as performed by Castro-Barros et al. (2018). Additional gas stripping induced by liquid turbulence at the outlet of the rotary arm distributor was not taken into account in the model.

$$kLa_G = kLa_{O2}\left(\frac{DG}{D_{O2}}\right)^{1/2} \quad \text{Eq 6.1}$$

where *DG* is the diffusion coefficient for methane and H_2S in water. Equilibrium concentrations in the liquid (SG_{eq}) were calculated using Henry's law (Eq. 6.2).

$$SG_{eq} = k_h PG \quad \text{Eq 6.2}$$

where k_h the Henry constant for methane (Crovetto et al., 1982) and H_2S (Sander, 2015) ($1.4x10^{-5}$ and $1x10^{-3}$, respectively) and *PG* the partial pressures of methane and H_2S in the atmosphere. Atmospheric concentrations of both gases are extremely low (assumed as 1.8x10-4%v/v for methane (Blake et al., 1982) and $2x10^{-8}$% v/v for H_2S (Axelrod et al., 1969)). This means that once methane and H_2S are stripped from the trickling liquid, back-diffusion is negligible. Partial pressures are thus based on the ideal gas law (Eq. 6.3).

$$PG = \frac{nG}{n_{atm}} P_{atm} \qquad \text{Eq 6.3}$$

where the mole fraction n_G/n_{atm} refers to the atmospheric concentration of methane and H_2S and P_{atm} to the atmospheric pressure (H = 780 m and T = 25°C) of 92,558 Pa.

6.2.2 Simulation set-up and influent conditions

Simulations were performed according to three proposed scenarios, besides a reference case, as summarized in Table 6.2. The latter refers to the same reference scenario presented in **Chapter 4**, which does not comprise methane and H_2S conversion processes. Scenario 1 aimed to assess the extent of stripping dissolved gases (methane and H_2S) in SBTFs and the impact on nitrogen conversions. This first scenario resembles the operation of a conventional passively aerated SBTF post-UASB reactor, neglecting the management of dissolved gases in the anaerobic effluent (as in Phase I in **Chapter 5**). All parameters and operational conditions of the reference scenario (**Chapter 4)** were retained, and biological conversions of methane and H_2S were added. Scenario 2 aimed at mimicking the limited ventilation conditions in which an SBTF post-UASB reactor was previously operated (as in Phase II in **Chapter 5**). Such an approach is also analogous to the concept presented by Castro-Barros et al. (2018), in which aeration was minimized to reduce gas stripping (in an aerobic granular sludge reactor). To this end, a low value of the oxygen transfer coefficient was adopted (k_La = 5 d^{-1}) compared to the reference scenario (k_La = 330 d^{-1}). Finally, Scenario 3 aimed at assessing the effect of high dissolved methane and H_2S availability on nitrogen conversions in SBTFs. Such simulation scenario could be translated into the operation of a closed SBTF to avoid stripping of dissolved gases (i.e., the stripped fraction remains trapped in the reactor and diffuses back into the liquid, preserving equilibrium). Oxygen would therefore be mechanically supplied (forced ventilation).

This approach corresponds with the experimental set-up investigated by Hatamoto et al. (2011). The same input conditions for Scenario 1 were adopted, except for the exclusion of gaseous stripping.

Influent concentrations were assumed the same as for **Chapter 3**, except for the inclusion of methane (20 g CH_4 m^{-3}) and H_2S (11 g S m^{-3}) based on experimental data on the anaerobic effluent (median values).

Table 6.2 Overview of scenario analysis considering different operating conditions

Assessed scenarios	k_La (d^{-1})	Stripping of dissolved gases
Reference scenario (Chapter 4)	330	No
Scenario 1 *Stripping of methane and H_2S and impact on nitrogen conversions*	330	Yes
Scenario 2 *Effect of restricted ventilation on stripping of methane and H_2S and impact on nitrogen conversions*	5	Yes
Scenario 3 *Conversions of methane and H_2S in a closed SBTF and impact on nitrogen conversions*	330	No

6.2.3 Experimental set-up

An experimental study was planned based on the observed impacts of dissolved methane and H_2S on nitrogen removal in SBTFs derived from simulations. The main goal was to assess the behaviour of a closed SBTF when fed with desorbed anaerobic effluent (dissolved gases removed upfront the SBTF). Therefore, the previously described SBTF-1 (**Chapter 5**) was further assessed. For the sake of conciseness, the SBTF-1 is simply termed SBTF in the present Chapter. The SBTF was fed with the anaerobically treated sewage from the same UASB reactor that provided effluent from the previous long-term monitoring study (**Chapter 5**). However, prior to the SBTF, the anaerobic effluent was subjected to a desorption chamber designed to remove dissolved gases (methane and H_2S), as described by Glória et al. (2016). A schematic representation is shown in Figure 6.1. Two operational phases were conducted as follows:

- Phase I: the SBTF was operated as a conventional trickling filter post-UASB reactors (natural ventilation from open bottom), identically to the Phase III

described in **Chapter 5;** however, fed with desorbed anaerobic effluents. Such operational phase lasted 61 days to ensure stable nitrification was occurring.

- Phase II: the SBTF was fully closed, however not airtightly. The system was then monitored for 39 days.

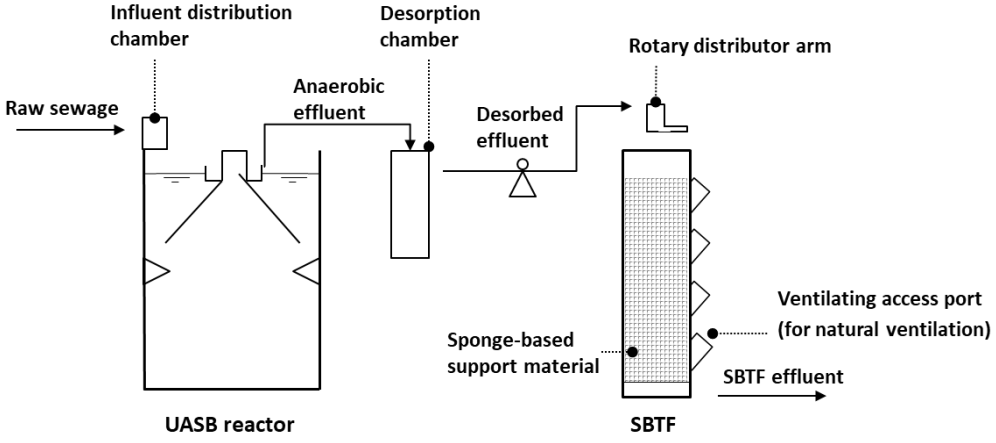

Figure 6.1 Schematic representation of the experimental UASB/SBTF set-up considering a desorption chamber (DC) for the anaerobic effluent prior to the SBTF. *Gases collected in the DC were conveyed for separate treatment (out of the scope of this Chapter)*

6.2.4 Analytical methods

Grab samples were collected thrice per week, and the following parameters were measured according to the Standard Methods for the Examination of Water and Wastewater (Baird and Bridgewater, 2017): TKN, NH_4^+-N, and NO_2^--N. NO_3^--N was analysed according to Robarge et al. (1983). Field analysis of dissolved oxygen (DO), pH, and temperature were carried out using a multiparametric sensor (Hach HQ 40D). As described by Souza et al. (2011), sampling and analysis of dissolved methane were performed based on headspace samples and gas chromatography. Dissolved H_2S sampling followed the recommendations from the Standard Methods for the Examination of Water and Wastewater (Baird and Bridgewater, 2017). Analytical determination was performed according to Plas et al. (1992).

6.3 Results and discussion

6.3.1 Conventional SBTF - with natural ventilation

The share of stripping and biological oxidation of methane and H_2S over the SBTF depth is displayed in Figure 6.2. Extensive stripping of methane (47%) and H_2S (25%) is noticed in the SBTF during simulations, primarily at the top compartment (Figure 6.2a). Experimental results on dissolved methane and H_2S concentrations confirmed that those gases are significantly stripped at the inlet of the SBTF (Figure A.6.3). Such a phenomenon would be expected to occur, as mass transfer resistance of those gases primarily relies upon the turbulence at the liquid phase (Perry and Chilton, 1973). The remaining dissolved gases in the liquid phase are mostly biologically oxidized at the same compartment top compartment of the SBTF (Figure 6.2b). Therefore, simultaneously stripping and biological oxidation thoroughly remove methane and H_2S at the upper layers of the SBTF (up to 2.0 m). H_2S is mainly converted into sulfate due to the high influent oxygen-to-sulfide ratio (i.e., 3.5; a ratio above 2 favours complete oxidation to sulfate (Janssen et al., 2009) (Figure A.6.1a).

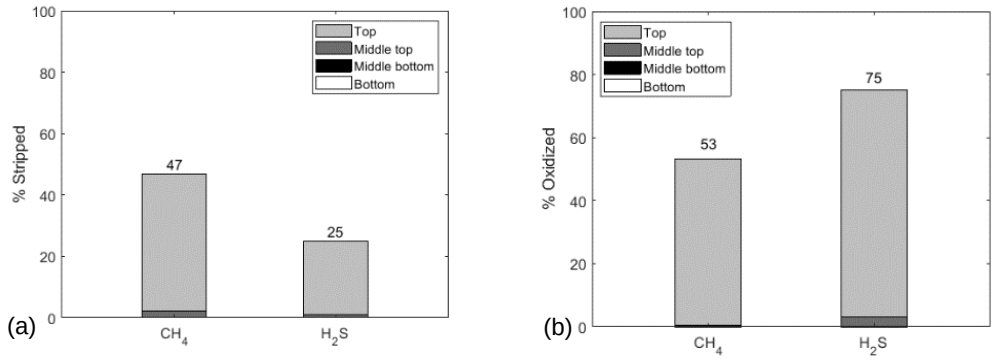

Figure 6.2 Percentage of stripping (a) and biological oxidation (b) of methane and H_2S over the SBTF depth (or compartments)

As dissolved gases are mainly stripped at the top compartment of the SBTF, low concentrations remain dissolved in the liquid phase to support biological activity. Figure 6.3a reveals the population dynamics along with the SBTF compartments. The top compartment of the reactor is mainly colonized by MOB and SOB, matching experimentally observed results of low evenness and the presence of dominant species (Hatamoto et al., 2018). Other bacteria (AOB, anammox, and heterotrophs) are pushed downwards in the reactor compared to the reference scenario (see

Chapter 4 – Figure 4.2). SOB were, as opposed to MOB, also present in the middle top compartment as these bacteria have a higher affinity for their substrate (H_2S) ($K_{S,H2S}^{SOB}$ = 0.00135 g S.m^{-3}), and the dissolved H_2S concentration still exceeded the half-saturation coefficient (Figure 6.3b). Prevailing sulfide oxidation at the upper compartments of a full-scale SBTF following a UASB reactor treating sewage was also noticed by Nomoto et al. (2018b). A possible explanation is that MOB and SOB have a high affinity for oxygen ($K_{S,O2}^{SOB, MOB, HET} \leq 0.2$ g O_2 m^{-3}), which is also the case for heterotrophs ($K_{S,O2}^{HET} \leq 0.2$ g O_2 m^{-3}). Nevertheless, the former are stronger competitors for their primary substrate (methane and H_2S, respectively), out-competing heterotrophs in the top compartment.

SOB also compete with AOB for oxygen in the middle top compartment, hampering the latter and, as such, pushing anammox bacteria deeper into the biofilm (Figure 6.3c). Conversely, AOB prevailed in the middle bottom compartment due to the absence of H_2S sustaining SOB growth. Anammox, therefore, grew close to the surface, right beneath a layer of heterotrophs (Figure 6.3d). A slight decrease (from 94% to 88%) in total nitrogen removal at steady-state (Figure A.6.2) is observed compared to the reference scenario (i.e., without methane and H_2S conversions - Chapter 4).

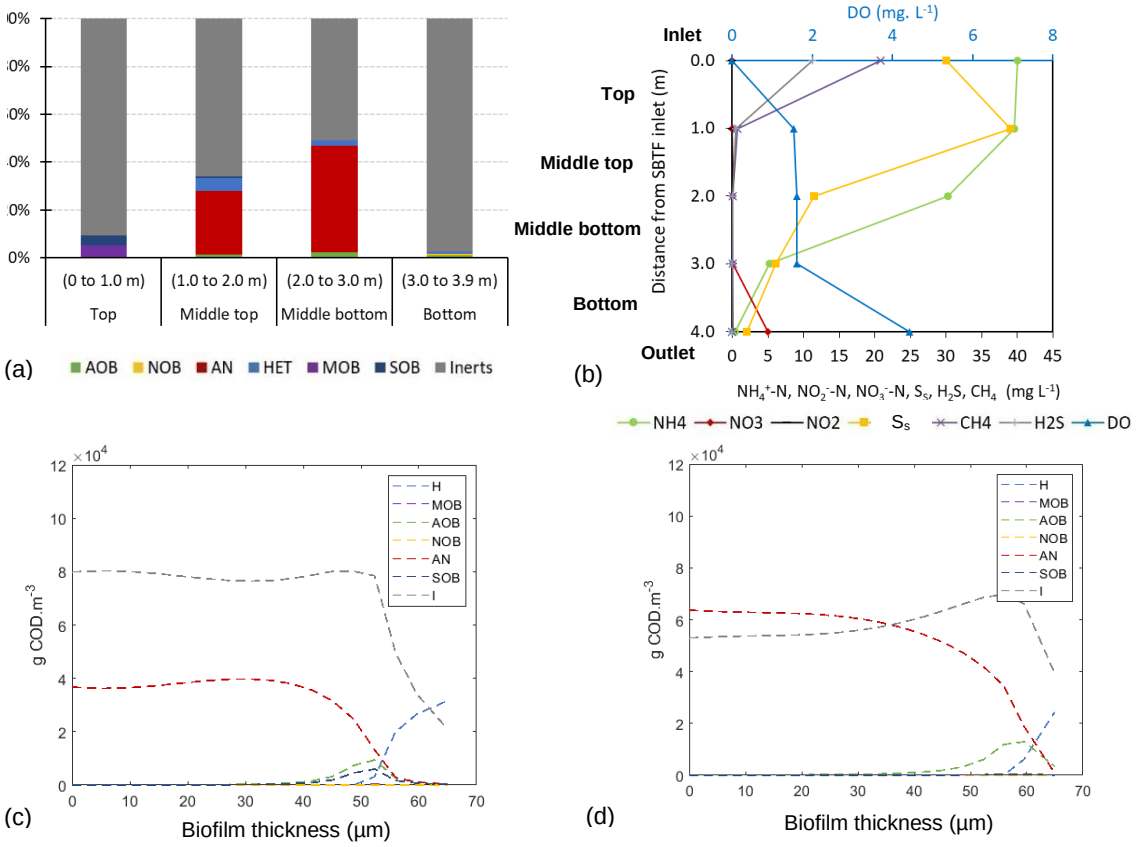

Figure 6.3 Relative biomass proportion in each SBTF compartment (a), substrate profiles over the SBTF compartments (b), biomass distribution profile in the biofilm at the middle top (c) and middle bottom (d) compartments at steady-state

The middle bottom compartment of the SBTF showed a more diverse microbial community coexisting in the biofilm. There, a combination of nitrification, heterotrophic denitrification, and anammox took place and jointly realized nitrogen removal, as also observed for the reference scenario (**Chapter 4**) and experimentally evidenced by Mac Conell et al. (2015) and Tanikawa et al. (2019). Nonetheless, anammox activity was pushed downwards along the depth of the SBTF compared to the reference scenario (**Chapter 4**). Therefore, the growth of SOB and MOB simultaneously caused a downward shift of nitrogen removing organisms, while SOB moreover pushed anammox deeper into the biofilm. However, the remaining low methane and H_2S concentrations in the liquid phase barely affected total nitrogen removal efficiency (6% decrease) compared to the reference scenario.

6.3.2 SBTF with restricted ventilation

The share of stripping and biological oxidation of methane and H_2S over the SBTF depth is depicted in Figure 6.4 (a-b). Even subjected to restricted ventilation (i.e., modelled assuming an extremely low k_La of 5 d^{-1}); still 68% and 12% of the dissolved methane and H_2S are stripped from the STBF, respectively. Despite the oxygen-limiting conditions (nearly null concentration all over the SBTF) (Figure 6.4(c)), up to 83% of the H_2S remaining in the liquid phase is biologically oxidized. Conversely, only 4% of the methane that remained dissolved is further removed by biological oxidation.

H_2S removal was mainly performed by SOB, which dominated the biofilm at steady-state from the top to the middle bottom compartment (Figure 6.4(d)). MOB was restrained to the bottom compartment of the SBTF and outgrow heterotrophs. AOB and consequently anammox bacteria are washed out from the SBTF, and the observed nitrogen removal is mainly ascribed to biomass incorporation. Hence, a significant impact on total nitrogen removal at steady-state (Figure A.6.2) is noticed, and influent ammonium leaves the reactor practically untreated (40 mg NH_4^+-N L^{-1}; see Figure 6.4(c)) compared to the simulation of a conventional SBTF under natural ventilation.

Under limiting oxygen conditions, it was shown that SOB referentially colonizes the SBTF. This is related to their high oxygen affinity, besides the substrate (H_2S) availability in the liquid phase (i.e., less stripped). Moreover, the low influent S_s concentration (30 g COD m^{-3}) restricts heterotrophic growth. Ordinary heterotrophs are also outcompeted by MOB at the bottom compartment of the SBTF. Despite their the same half-saturation coefficient for oxygen ($K_{S,O2}^{H/MOB}$ = 0.2 g O2 m^{-3}), theoretical calculations based on measured growth demonstrated that methanotrophs could outcompete heterotrophs at low oxygen concentrations (van Bodegom et al., 2001). Moreover, methane concentrations do not seem to influence the oxygen concentration at which methanotrophs win the competition, as the latter have a higher affinity for their substrate ($K_{S,CH4}^{MOB}$ = 0.06 g CH_4 m^{-3}) than heterotrophs for organic matter ($K_{S,COD}^{H}$ = 20 g COD m^{-3}). Therefore, organic carbon concentrations are essential. This possibly explains the difference in the oxidation sequence observed in the present simulation study (H_2S; methane; organic matter; ammonium) compared to the experimental report of an SBTF subjected to limited oxygen supply (H_2S; organic matter; methane; ammonium) (Hatamoto et al. (2011)). The influent S_s concentration was lower in the

present study (30 g COD m^{-3}) compared to Hatamoto et al. (2011) (approximately 60 g COD m^{-3}).

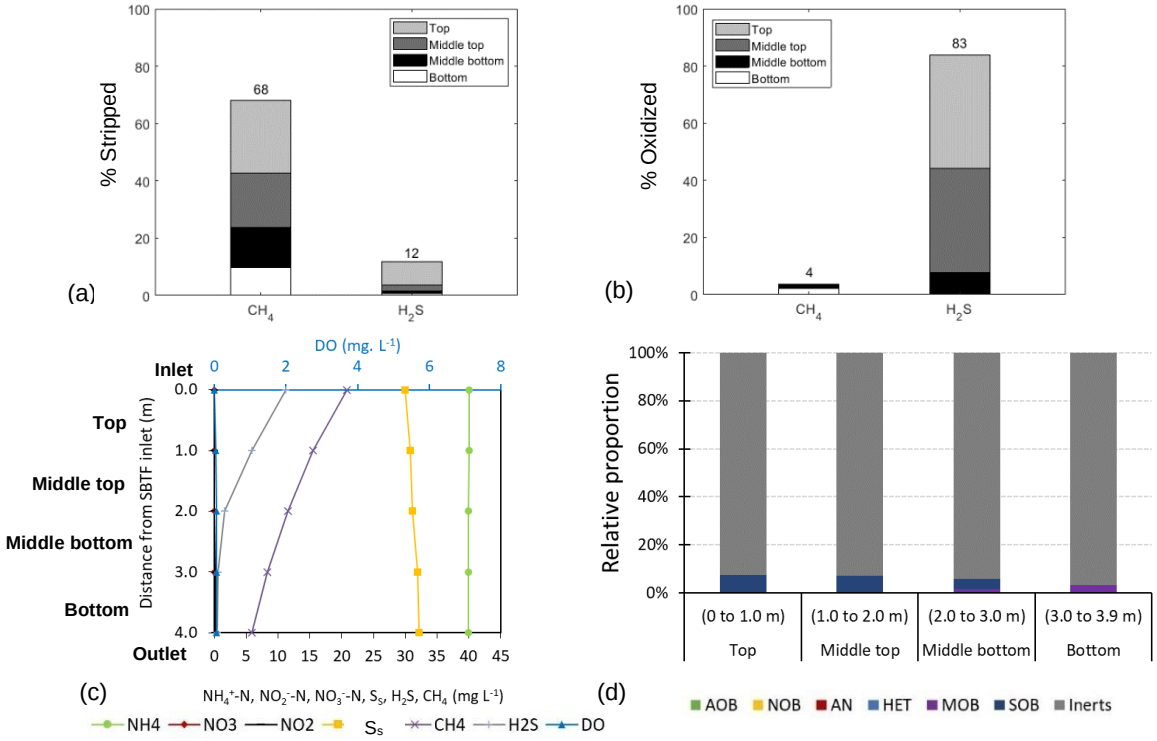

Figure 6.4 Methane and H_2S removal percentages by stripping (a) and biological oxidation (b); substrate profiles over the SBTF compartments (c), and relative biomass proportion in each SBTF compartment (d)

In any case, ammonium oxidation is disrupted prior to other oxidation reactions. AOB are weak competitors for oxygen, owing to their relatively low affinity for oxygen ($K_{,SO2}^{AOB}$ = 0.6 g O_2 m^{-3}) compared to SOB and MOB, besides the lower free energy change of ammonium oxidation compared to methane and sulfide oxidations, thus leading to a relatively lower maximum growth rate (Rittmann and McCarty, 2001). As such, no nitrite is supplied for further nitrogen removal processes, hampering process efficiency. Therefore, simply closing off the reactor is impractical for the combined abatement of dissolved gases (i.e., methane and H_2S) and total nitrogen removal in SBTFs following UASB reactors treating sewage. Those results confirm the hypothesis raised in **Chapter 5** that AOB activity is hampered even under high bulk liquid DO concentrations (> 4 mg L^{-1}) when dissolved gases are not prior removed from the anaerobic effluent, and the SBTF is (partially)closed.

6.3.3 Closed SBTF with mechanical aeration

The increased availability of methane and H_2S compared to the previously simulated condition (i.e., no stripping of dissolved gases was considered) leads to a significantly higher (approximately 60 %) oxygen demand compared to the simulation with a fully open reactor, which decreases bulk liquid DO concentrations (< 2 mg L^{-1}) along the SBTF (Figure 6.5a). H_2S is mainly converted to elemental sulfur in the top compartment of the SBTF (oxygen-to-sulfide ratio of 1.5, favouring elemental sulfur formation), while in the middle top compartment, sulfate formation prevailed (oxygen-to-sulfide ratio >> 2) (Figure A.6.1b). H_2S is thus practically fully removed at the upper layers (up to 2.0 depth) of the reactor. Methane is nearly fully oxidized at the top compartment.

Microbial population dynamics along the SBTF compartments are shown in Figure 6.5b. A further downward shift of anammox bacteria occurs to the middle bottom and bottom compartments compared to simulations with an open reactor (see Figure 6.3a). As the upper compartments are devoted to aerobically oxidizing sulfur and methane, AOB is displaced downwards, hence the niches for anammox bacteria. Although such a vertical migration along with the depth of the STBF, the anammox process remains the primary process responsible for total nitrogen removal at steady-state, with a small share of heterotrophic denitrification. The contribution of DAMO and SBDN processes to the simulated total nitrogen removal in SBTFs post-UASB reactors treating sewage was negligible.

A non-significative decrease (from 88% to 85%) in total nitrogen removal at steady-state (Figure A.6.2) is observed compared to the simulation of a fully open SBTF without proper control of diffuse methane and H_2S emissions from the anaerobic effluent.

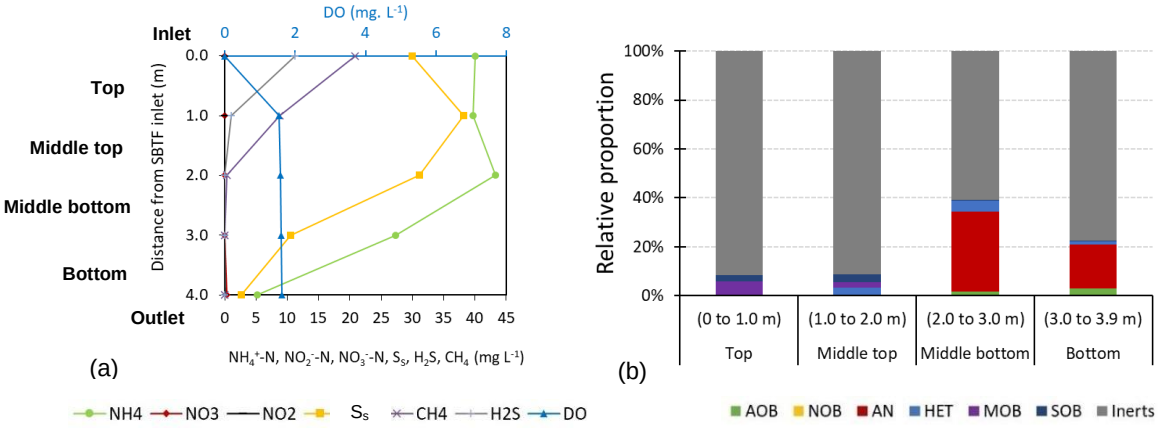

Figure 6.5 Substrate profiles over the SBTF compartments (a) and relative biomass proportion in each SBTF compartment (b)

As for the high availability of methane and H_2S, the theoretical oxygen requirement is increased compared to the previous scenarios, which led to significant oxygen depletion in all compartments of the SBTF. Analogously to the discussed condition of a reactor subjected to restricted ventilation, MOB and SOB outgrown AOB in the upper compartments due to competitive advantage for oxygen. Hence, autotrophic nitrogen removal over nitrite is disrupted, meaning that besides anammox, DAMO and SBDN organisms are negatively affected. As AOB could only form nitrite after most of the dissolved methane and H_2S have been oxidized by MOB and SOB, respectively, microbial niches comprising both sufficient methane, H_2S, and nitrite to sustain DAMO and SBDN organisms were absent from the SBTF.

Although the relatively higher substrate availability (i.e., no stripping of methane and H_2S) than a fully open SBTF, DAMO and SBDN organisms cannot colonize the simulated closed reactor. Worth noticing that DAMO-B is not outcompeted by anammox bacteria due to their lower affinity for nitrite, as observed by Winkler et al. (2015). Conversely, there is simply no substrate available since MOB consumes methane at the top compartment of the SBTF. A similar pattern is verified for interaction between SOB and SBDN. As the former resembles a K-strategist species, with a relatively high substrate affinity and low μ_{max} comparatively to the latter, H_2S is rapidly aerobically oxidized, even before ammonium does. The successful cultivation of DAMO organisms reported by Hatamoto et al. (2017) in a closed SBTF considered the addition of nitrite. Therefore, as partial nitratation in the same reactor was skipped, no

oxygen was allowed that could have triggered aerobic methanotrophs, thus hampering DAMO-B.

The results indicate that partially or totally closing the reactor to avoid diffuse methane and H_2S emissions would not be a solution for the combined abatement of dissolved gases and total nitrogen removal. Even though biological processes could practically completely convert those dissolved gases, this implies a reduced total nitrogen removal efficiency. Therefore, desorption of methane and H_2S prior to the SBTF is recommended. Simple techniques such as desorption chambers could serve this purpose.

6.3.4 Nitrogen conversions in an SBTF fed with desorbed effluents: experimental results

Based on the simulation results and previous experimental evidence (**Chapter 5**) on the extent of the impact of dissolved gases on nitrogen conversion, an SBTF fed with desorbed anaerobic effluents was further assessed. The experimental results of nitrogen conversions and bulk liquid dissolved oxygen concentrations are shown in Figure 6.6. After the indicative stable nitrification (Figure 6.6a), the reactor was entirely closed (Phase II). In approximately 5 days, bulk liquid DO concentrations dropped to values systematically below 6 mg L^{-1}. Median ammonium removal efficiency decreased from 68 to 58%. No nitrite accumulation was observed, and nitrate production amounted to 0.6 g NO_3^--N g NH_4^+-$N_{removed}^{-1}$ (25% median total nitrogen removal efficiency). Worth mentioning that the incoming concentration of dissolved gases in the anaerobic effluent significantly decreases due to the desorption chamber prior to the SBTF (Figure A.6.3). Approximately 58% and 76% of dissolved methane and H_2S are removed before the inlet (rotary distributor arm) of the reactor.

Under restricted ventilation, more stable control of the bulk liquid DO concentration was achieved, and consequently, the volumetric ammonium conversion rate was less variable than the experimental results presented in **Chapter 5**. This further testifies the hypothesis that dissolved gases in the aerobic effluent (i.e., methane and H_2S) hamper AOB activity in a (partially) closed SBTF. Regardless of the indication of better control over the extent of ammonium conversion, nitrate builds up in the effluent, meaning that NOB out-selection remains a major practical challenge. Nevertheless, the improved

robustness for handling nitrification rates through ventilation control justifies further tests restraining oxygen in SBTFs fed with desorbed anaerobic effluents. The gases removed in a previous step thus require separate treatment.

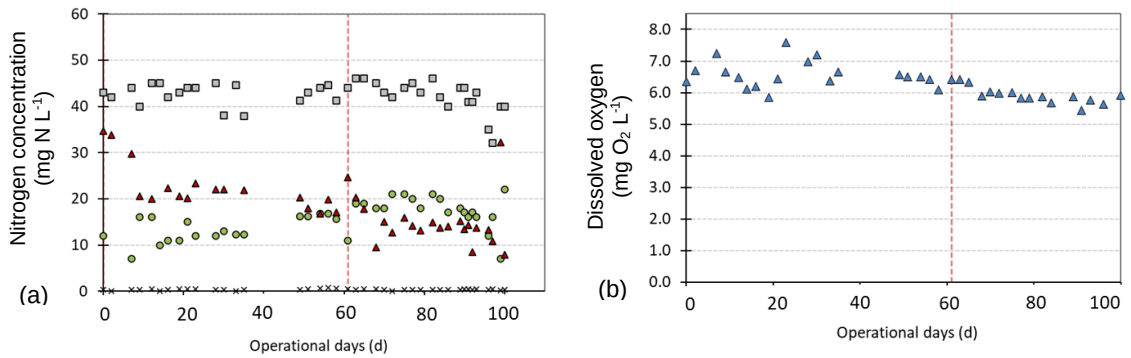

Figure 6.6 Behaviour of an SBTF fed with anaerobic effluent after a desorption chamber: (a) influent total nitrogen and effluent ammonium, nitrite, and nitrate concentrations, and (b) Efflu NH4 in NH4 NO2 NO3 olved oxygen concentrations. *Red dotted line represents operational phase change*

6.3.5 Implications for process design

Abating methane and H_2S simultaneously with nitrogen removal in SBTF might still be feasible, provided the stripped gases from a desorption chamber are injected at the bottom of the SBTF. The reference scenario (**Chapter 4**) indicated that nitrogen removal in the absence of dissolved methane and H_2S primarily occurred in the upper compartments (top and middle top). Hence, possibly introducing the gases at the bottom compartment should not hamper AOB activity. MOB and SOB could then colonize the bottommost reactor layers, profiting from aerobic conditions. To which extent biological oxidation would counteract stripping rates of the reintroduced gases remains a knowledge gap. However, a high gas to liquid flow ratio (between 3 and 5) is expected from desorption chambers (Centeno-Mora et al., 2020), likely triggering stripping when gases are reintroduced in the SBTF. Based on the presented simulation and experimental results, ventilation control should most likely be fine-tuned, which can reinstate the hurdles for MOB, SOB, and AOB coexistence in an oxygen-deprived environment. Nonetheless, from a theoretical standpoint, such design configuration would effectively use all SBTF compartments for biological conversions, performing treatment of the liquid phase at the top and the gas phase at the bottom without hampering total nitrogen removal.

6.4 Conclusions

A dedicated model was set up to describe the fate of dissolved methane and H_2S in a sponge-bed trickling filter (SBTF), besides the conversion of organic matter and nitrogen. The model was applied in simulation studies to quantify methane and H_2S stripping and assess the impact of these substances on nitrogen removal. Moreover, nitrogen conversions were experimentally assessed in a closed SBTF fed with desorbed anaerobic effluents (i.e., without dissolved methane and H_2S).

- Dissolved gases in the anaerobic effluent are extensively stripped, mainly at the top compartment of the SBTF if not removed upfront (e.g., in a desorption chamber).

- Closing the SBTF can decrease methane and H_2S stripping, and the dissolved gases are biologically oxidized. Nonetheless, this increases oxygen requirements up to 60% beyond the demand for organic carbon and ammonium conversions, thus hampering AOB activity and ultimately total nitrogen removal.

- Autotrophic nitrogen removal processes combining methane (DAMO) and H_2S oxidation (SBDN) are impracticable in SBTFs treating anaerobic effluents, mainly ascribed to the competition for substrate with MOB and SOB, respectively.

- Experiments with an SBTF fed with desorbed anaerobic effluents indicated better control over the extent of ammonium conversion. Nevertheless, nitrate builds up in the effluent, meaning NOB out-selection remains a major practical challenge.

Appendix

A.6.1 Stoichiometric matrix, kinetic expressions, and model parameter

Table A.6.1. Stoichiometric matrix and composition matrix

A_{ij} i component → / j process ↓	S_S [g COD m^{-3}]	S_{NH} [g N m^{-3}]	S_{ND} [gN m^{-3}]	S_{NO2} [g N m^{-3}]	S_{NO3} [g N m^{-3}]	S_{O2} [g O_2 m^{-3}]	S_{N2} [g N m^{-3}]	S_{CH4} [g CH_4 m^{-3}]	S_{HS} [g S m^{-3}]	S_{SO4} [g S m^{-3}]	S_{S0} [g S m^{-3}]	S_{IC}* [g $CaCO_3$ m^{-3}]	X_{AOB} [gCOD m^{-3}]	X_{NOB} [gCOD m^{-3}]	X_H [gCOD m^{-3}]	X_{AN} [gCOD m^{-3}]	X_{MOB} [gCOD m^{-3}]	X_{SOB} [gCOD m^{-3}]	X_{Da} [gCOD m^{-3}]	X_{SBDN} [gCOD m^{-3}]	X_{Db} [gCOD m^{-3}]	X_I [gCOD m^{-3}]
1. nitritation - growth of X_{AOB}		$-\frac{1}{Y_{AOB}}-i_{NXB}$		$\frac{1}{Y_{AOB}}$		$1-\frac{3.43}{Y_{AOB}}$						$\left(-\frac{i_{NXB}}{14}-\frac{1}{7Y_{AOB}}\right)50$	1									
2. nitratation - growth of X_{NOB}		$-i_{NXB}$		$-\frac{1}{Y_{NOB}}$	$\frac{1}{Y_{NOB}}$	$1-\frac{1.14}{Y_{NOB}}$						$\left(-\frac{i_{NXB}}{14}\right)50$		1								
3. anammox - growth of X_{AN}		$-\frac{1}{Y_{AN}}-i_{NXB}$	$-\left(\frac{1}{Y_{AN}}\right)-\left(\frac{1}{1.14}\right)$		$\frac{1}{1.14}$							$\left(-\frac{i_{NXB}}{14}\right)50$				1						
4. aerobic growth of heterotrophs (X_H)	$-\frac{1}{Y_H}$	$-i_{NXB}+\frac{i_{NSS}}{Y_H}$				$1-\frac{1}{Y_H}$						$\left(-\frac{i_{NXB}}{14}+\frac{i_{NSS}}{14Y_H}\right)50$			1							
5. denitritation - anoxic (on NO_2^-) growth of heterotrophs (X_H)	$-\frac{1}{Y_{H,NO_2}}$	$-i_{NXB}+\frac{i_{NSS}}{Y_{H,NO_2}}$		$-\frac{1-Y_{H,NO_2}}{1.71\,Y_{H,NO_2}}$			$\frac{1-Y_{H,NO_2}}{1.71\,Y_{H,NO_2}}$					$\left(-\frac{i_{NXB}}{14}+\frac{i_{NSS}}{14Y_{H,NO_2}}\right)+\left(\frac{1-Y_{H,NO_2}}{1.71\,Y_{H,NO_2}14}\right)50$			1							
6. denitrification - anoxic (on NO_3^-) growth of heterotrophs (X_H)	$-\frac{1}{Y_{H,NO_3}}$	$-i_{NXB}+\frac{i_{NSS}}{Y_{H,NO_3}}$		$\frac{1-Y_{H,NO_3}}{1.14\,Y_{H,NO_3}}$	$-\frac{1-Y_{H,NO_3}}{1.14\,Y_{H,NO_3}}$							$(\frac{i_{NXB}}{14}-\frac{i_{NSS}}{14Y_{H,NO_3}})50$			1							
7. aerobic growth of MOB (X_{MOB})		$-i_{NXB}$				$1-\frac{4}{Y_{MOB}}$		$\frac{-1}{Y_{MOB}}$				$\left(-\frac{i_{NXB}}{14}\right)50$					1					
8. aerobic growth of SOB ($X_{SOB,\ H2S}$)		$-i_{NXB}$				$1-\frac{0.5}{Y_{SOB}}$			$\frac{-1}{Y_{SOB}}$		$\frac{1}{Y_{SOB}}$	$\left(\frac{1}{32Y_{SOB}}-\frac{i_{NXB}}{14}\right)50$						1				
9. aerobic growth of SOB ($X_{SOB,\ S0}$)		$-i_{NXB}$				$1-\frac{1.5}{Y_{SOB}}$				$\frac{1}{Y_{SOB}}$	$\frac{-1}{Y_{SOB}}$	$\left(\frac{i_{NXB}}{14}-\frac{1}{16Y_{SOB}}\right)50$						1				
10. Anaerobic growth of DAMO A (X_{Da})		$-i_{NXB}$		$\frac{4-Y_{Da}}{1.14Y_{Da}}$	$\frac{Y_{Da}-4}{1.14Y_{Da}}$			$\frac{-1}{Y_{Da}}$				$\left(-\frac{i_{NXB}}{14}\right)50$							1			
11. Anaerobic growth of DAMO B (X_{Db})				$\frac{Y_{Db}-4}{1.71Y_{Db}}+i_{NXB}$			$-\frac{Y_{Db}-4}{1.71Y_{Db}}-2i_{NXB}$	$\frac{-1}{Y_{Db}}$				$\left(\frac{4-Y_{Db}}{1.71Y_{Db}14}+\frac{i_{NXB}}{14}\right)50$								1		
12. Anaerobic growth of SBDN ($X_{SBDN,\ H2S,\ NO2}$)		$-i_{NXB}$		$\frac{Y_{SBDN}-0.5}{1.71Y_{SBDN}}$			$\frac{0.5-Y_{SBDN}}{1.71Y_{SBDN}}$		$\frac{-1}{Y_{SBDN}}$			$\left(\frac{1}{32Y_{SBDN}}+\frac{0.5-Y_{SBDN}{}'}{1.71Y_{SBDN}14}-\frac{i_{NXB}}{14}\right)50$								1		
13. Anaerobic growth of SBDN ($X_{SBDN,\ S0,\ NO2}$)		$-i_{NXB}$		$\frac{Y_{SBDN}-1.5}{1.71Y_{SBDN}}$			$\frac{1.5-Y_{SBDN}}{1.71Y_{SBDN}}$			$\frac{1}{Y_{SBDN}}$	$\frac{-1}{Y_{SBDN}}$	$\left(\frac{1}{16Y_{SBDN}}+\frac{0.5-Y_{SBDN}{}'}{1.71Y_{SBDN}14}-\frac{i_{NXB}}{14}\right)50$								1		
14. Anaerobic growth of SBDN ($X_{SBDN,\ H2S,\ NO3}$)		$-i_{NXB}$		$\frac{0.5-Y_{SBDN}}{1.71Y_{SBDN}}$	$\frac{Y_{SBDN}-0.5}{1.14Y_{SBDN}}$				$\frac{-1}{Y_{SBDN}}$			$\left(\frac{1}{32Y_{SBDN}}-\frac{i_{NXB}}{14}\right)50$								1		
15. Anaerobic growth of SBDN ($X_{SBDN,\ S0,\ NO3}$)		$-i_{NXB}$		$\frac{1.5-Y_{SBDN}}{1.71Y_{SBDN}}$	$\frac{Y_{SBDN}-1.5}{1.14Y_{SBDN}}$					$\frac{1}{Y_{SBDN}}$	$\frac{-1}{Y_{SBDN}}$	$\left(\frac{-1}{16Y_{SOB}}-\frac{i_{NXB}}{14}\right)50$								1		
16. ammonification		1	-1									$\left(\frac{1}{1.14}\right)50$										
17. decay of X_{AOB}	1-f_I	i_{NXB} - f_I i_{NXI} – (1-f_I) i_{NSS}											-1									f_I
18. decay of X_{NOB}	1-f_I	i_{NXB} - f_I i_{NXI} – (1-f_I) i_{NSS}												-1								f_I
19. decay of X_{AN}	1-f_I	i_{NXB} - f_I i_{NXI} – (1-f_I) i_{NSS}														-1						f_I
20. decay of X_H	1-f_I	i_{NXB} - f_I i_{NXI} – (1-f_I) i_{NSS}													-1							f_I
21. decay of X_{MOB}	1-f	i_{NXB} - f_I i_{NXI} – (1-f_I) i_{NSS}															-1					f_I
22. decay of X_{SOB}	1-f	i_{NXB} - f_I i_{NXI} – (1-f_I) i_{NSS}																-1				f_I
23. decay of X_{Da}	1-f	i_{NXB} - f_I i_{NXI} – (1-f_I) i_{NSS}																	-1			f_I
24. Decay of X_{Db}	1-f	i_{NXB} - f_I i_{NXI} – (1-f_I) i_{NSS}																		-1		f_I
25. Decay of X_{SBDN}	1-f	i_{NXB} - f_I i_{NXI} – (1-f_I) i_{NSS}																			-1	f_I
gCOD/unit comp	1			-3.43	-4.57	-1	-1.71	4	2		1.5		1	1	1	1	1	1	1	1	1	1
gN/unit comp	i_{NSS}	1		1	1								i_{NXB}	i_{NXB}	i_{NXB}	i_{NXB}	i_{NXB}	i_{NXB}	i_{NXB}	i_{NXB}	i_{NXB}	i_{NXI}
Charge (mol$_{eq}$/unit comp)		1/14		-1/14	-1/14				-1/32	-1/16		-1/50										

*Coefficients for inorganic carbon (S_{IC}), expressed as mol equiv HCO_3 m^{-3}, were determined from the charge balance. Conversion of inorganic carbon expressed as calcium carbonate (g $CaCO_3$ m-, as experimentally measured) is performed taking into account a conversion factor of 50 g mol equiv^{-1}.

Table A.6.2 Kinetic rate expressions

j process ↓	Rate expression
1. nitritation - growth of XAOB	$\rho G,AOB = \mu_{max}^{AOB}.\frac{S_{O2}}{K_{O2}^{AOB}+S_{O2}}.\frac{S_{NH}}{K_{NH}^{AOB}+S_{NH}}.\frac{e^{(S_{IC}-k)/a}}{1+e^{(S_{IC}-k)/a}}.X_{AOB}$
2. nitratation - growth of X_{NOB}	$\rho G,NOB = \mu_{max}^{NOB}.\frac{S_{O2}}{K_{O2}^{NOB}+S_{O2}}.\frac{S_{NO2}}{K_{NO2}^{NOB}+S_{NO2}}.\frac{S_{NH}}{K_{NH}^{NOBH}+S_{NH}}.\frac{S_{IC}}{K_{IC}^{NOB}+S_{IC}}.X_{NOB}$
3. anammox - growth of X_{AN}	$\rho G,AN = \mu_{max}^{AN}.\frac{K_{O2}^{AN}}{K_{O2}^{AN}+S_{O2}}.\frac{S_{NH}}{K_{NH}^{AN}+S_{NH}}.\frac{S_{NO2}}{K_{NO2}^{AN}+S_{NO2}}.\frac{S_{IC}}{K_{IC}^{AN}+S_{IC}}.X_{AN}$
4. aerobic growth of X_H	$\rho G,H = \mu_{max}^{H}.\frac{S_S}{K_S^H+S_S}.\frac{S_{O2}}{K_{O2}^{H}+S_{O2}}.\frac{S_{NH}}{K_{NH}^{NOBH}+S_{NH}}.X_H$
5. denitritation - anoxic growth (on NO_2^-) of X_H	$\rho G,H^{NO2} = \mu_{max}^{H}.\eta_{NO2}.\frac{K_{O2}^{H}}{K_{O2}^{H}+S_{O2}}.\frac{S_{NO2}}{K_{NO2}^{H}+S_{NO2}}.\frac{S_{NO2}}{S_{NO2}+S_{NO3}}.\frac{S_S}{K_S^H+S_S}.\frac{S_{NH}}{K_{NH}^{NOBH}+S_{NH}}.X_H$
6. denitrification - anoxic growth (on NO_3^-) of X_H	$\rho G,H^{NO3} = \mu_{max}^{H}.\eta_{NO3}.\frac{K_{O2}^{H}}{K_{O2}^{H}+S_{O2}}.\frac{S_{NO3}}{K_{NO3}^{H}+S_{NO3}}.\frac{S_{NO3}}{S_{NO2}+S_{NO3}}.\frac{S_S}{K_S^H+S_S}.\frac{S_{NH}}{K_{NH}^{NOBH}+S_{NH}}.X_H$
7. aerobic growth of X_{MOB}	$\rho G,MOB = \mu_{max}^{MOB}.\frac{S_{O2}}{S_{O2}+K_{O2}^{MOB}}.\frac{S_{CH4}}{S_{CH4}+K_{CH4}^{MOB}}.\frac{S_{NH}}{S_{NH}+K_{NH}^{MOB}}.\frac{S_{IC}}{S_{IC}+K_{IC}^{MOB}}X_{MOB}$
8. aerobic growth of $X_{SOB,H2S}$	$\rho G,SOB = \mu_{max}^{SOB}.\frac{S_{O2}}{S_{O2}+K_{O2}^{SOB}}.\frac{S_{HS}}{S_{HS}+K_{HS}^{SOB}}.\frac{S_{NH}}{S_{NH}+K_{NH}^{SOB}}.\frac{S_{IC}}{S_{IC}+K_{IC}^{SOB}}.\frac{S_{HS}}{S_{S0}+S_{HS}}.X_{SOB}$
9. aerobic growth of $X_{SOB,S0}$	$\rho G,SOB = \mu_{max}^{SOB}.\frac{S_{O2}}{S_{O2}+K_{O2}^{SOB}}.\frac{S_{S0}}{S_{S0}+K_{S0}^{SOB}}.\frac{S_{NH}}{S_{NH}+K_{NH}^{SOB}}.\frac{S_{IC}}{S_{IC}+K_{IC}^{SOB}}.\frac{S_{S0}}{S_{S0}+S_{HS}}.\frac{K_{nc,H2S}^{SOB}}{K_{nc,H2S}^{SOB}+S_{HS}}X_{SOB}$
10. anaerobic growth of X_{Da}	$\rho G,Da = \mu_{max}^{Da}.\frac{K_{i,O2}^{Da}}{S_{O2}+K_{i,O2}^{Da}}.\frac{S_{CH4}}{S_{CH4}+K_{CH4}^{Da}}.\frac{S_{NH}}{S_{NH}+K_{NH}^{Da}}.\frac{S_{NO3}}{S_{NO3}+K_{NO3}^{Da}}X_{Da}$
11. anaerobic growth of X_{Db}	$\rho G,Db = \mu_{max}^{Db}.\frac{K_{i,O2}^{Db}}{S_{O2}+K_{i,O2}^{Db}}.\frac{S_{CH4}}{S_{CH4}+K_{CH4}^{Db}}.\frac{S_{NO2}}{S_{NO3}+K_{NO2}^{Db}}X_{Db}$
12. anaerobic growth of $X_{SBDN,H2S,NO2}$	$\rho G,SBDN = \mu_{max}^{SBDN,1}.\frac{K_{i,O2}^{SBDN}}{S_{O2}+K_{i,O2}^{\mathrm{SBDN}}}.\frac{S_{HS}}{S_{HS}+K_{HS}^{SBDN}}.\frac{S_{NH}}{S_{NH}+K_{NH}^{SBDN}}.\frac{S_{NO2}}{S_{NO2}+K_{NO2}^{SBDN}}.\frac{S_{HS}}{S_{S0}+S_{HS}}.\frac{S_{NO2}}{S_{NO3}+S_{NO2}}.X_{SBDN}$
13. anaerobic growth of $X_{SBDN,S0,NO2}$	$\rho G,SBDN = \mu_{max}^{SBDN,2}.\frac{K_{i,O2}^{SBDN}}{S_{O2}+K_{i,O2}^{\mathrm{SBDN}}}.\frac{S_{S0}}{S_{S0}+K_{S0}^{SBDN}}.\frac{S_{NH}}{S_{NH}+K_{NH}^{SBDN}}.\frac{S_{NO2}}{S_{NO2}+K_{NO2}^{SBDN}}.\frac{S_{S0}}{S_{S0}+S_{HS}}.\frac{S_{NO2}}{S_{NO3}+S_{NO2}}.\frac{K_{nc,H2S}^{SBDN}}{K_{nc,H2S}^{SBDN}+S_{HS}}X_{SBDN}$
14. anaerobic growth of $X_{SBDN,H2S,NO3}$	$\rho G,SBDN = \mu_{max}^{SBDN,3}.\frac{K_{i,O2}^{SBDN}}{S_{O2}+K_{i,O2}^{\mathrm{SBDN}}}.\frac{S_{HS}}{S_{HS}+K_{HS}^{SBDN}}.\frac{S_{NH}}{S_{NH}+K_{NH}^{SBDN}}.\frac{S_{NO3}}{S_{NO3}+K_{NO3}^{SBDN}}.\frac{S_{HS}}{S_{S0}+S_{HS}}.\frac{S_{NO3}}{S_{NO3}+S_{NO2}}.X_{SBDN}$
15. anaerobic growth of $X_{SBDN,S0,NO3}$	$\rho G,SBDN = \mu_{max}^{SBDN,2}.\frac{K_{i,O2}^{SBDN}}{S_{O2}+K_{i,O2}^{\mathrm{SBDN}}}.\frac{S_{S0}}{S_{S0}+K_{S0}^{SBDN}}.\frac{S_{NH}}{S_{NH}+K_{NH}^{SBDN}}.\frac{S_{NO3}}{S_{NO3}+K_{NO3}^{SBDN}}.\frac{S_{S0}}{S_{S0}+S_{HS}}.\frac{S_{NO3}}{S_{NO3}+S_{NO2}}.\frac{K_{nc,H2S}^{SBDN}}{K_{nc,H2S}^{SBDN}+S_{HS}}X_{SBDN}$
16. ammonification	$\rho a = k_a.S_{NH}.X_H$
17. decay of AOB	$\rho D,AOB = b_{AOB}.X_{AOB}$

j process ↓	Rate expression
18. decay of NOB	$\rho D, NOB = b_{NOB}.X_{NOB}$
19. decay of anammox	$\rho D, AN = b_{AN}.X_{AN}$
20. decay of heterotrophs	$\rho D, H = b_H.X_H$
21. decay of MOB	$\rho D, MOB = b_{MOB}.X_{MOB}$
22. decay of SOB	$\rho D, SOB = b_{SOB}.X_{SOB}$
23. decay of Da	$\rho D, Da = b_{Da}.X_{Da}$
24. decay of Db	$\rho D, Db = b_{Db}.X_{Db}$
25. decay of SBDN	$\rho D, SBDN = b_{SBDN}.X_{SBDN}$

Table A.6.3 Stoichiometric and kinetic parameter values. *Parameters estimated in this study are indicated in bold*

Parameter	Description	Value	Unit	Reference/Comments
Stoichiometric parameters				
Y_{AOB}	Yield coefficient of AOB	0.20	g COD g^{-1} N	Wiesmann, 1994[a]
Y_{NOB}	Yield coefficient of NOB	0.057	g COD g^{-1} N	Wiesmann, 1994[a]
Y_{AN}	Yield coefficient of AN	0.17	g COD g^{-1} N	Strous et al., 1998[b]
Y_H	Yield coefficient of heterotrophs (H)	0.67	g COD g^{-1} COD	Henze et al., 2006
$Y_{H,NO2}$	Yield coefficient of HNO_2	0.53	g COD g^{-1} COD	Muller et al., 2003
$Y_{H,NO3}$	Yield coefficient of HNO_3	0.53	g COD g^{-1} COD	Muller et al., 2003
Y_{MOB}	Yield coefficient of MOB	0.57	g COD g^{-1} CH_4	Arcangeli and Arvin, 1999
Y_{SOB1}	Yield coefficient of H_2S for SOB	0.128	g COD.g^{-1} S	Xu et al., 2013
Y_{SOB2}	Yield coefficient of S_0 for SOB	0.375	g COD.g^{-1} S	Buisman et al., 1991
Y_{Db}	Yield coefficient of DAMO B	2.2	g COD g^{-1} CH_4	Chen, 2017
Y_{Da}	Yield coefficient of DAMO A	0.284	g COD g^{-1} CH_4	Chen, 2017
Y_{SBDN1}	Yield coefficient of H_2S for SBDN organisms	0.065	g COD.g^{-1} S	Mora et al., 2014
Y_{SBDN2}	Yield coefficient of S_0 for SBDN organisms	0.40	g COD.g^{-1} S	Mora et al., 2014
i_{NXB}	N content of biomass	0.07	g N g^{-1} COD	Mozumder et al., 2014
i_{NXI}	N content of particulate inerts	0.07	g N g^{-1} COD	Mozumder et al., 2014
i_{NSS}	N content of soluble organic substrate	0.03	g N g^{-1} COD	Henze et al., 2006
f_I	Fraction of inert COD in biomass	0.08	g COD g^{-1} COD	Henze et al., 2006
Kinetic parameters (at 24.3°C)				
AOB				
μ_{max}^{AOB}	Growth rate of AOB	0.81	d^{-1}	Hellinga *et al.*, 1999[c]
b^{AOB}	Decay rate of AOB	0.054	d^{-1}	Assumed, such that ratio b^{AOB}: $\mu_{max}^{AOB} = b^H$: μ_{max}^{H} as proposed in Mozumder et al., 2014
$K_{O_2}^{AOB}$	DO half-saturation coefficient for AOB	0.6	g O_2 m^{-3}	Hao et al., 2002
K_{NH}^{AOB}	NH_4^+ half-saturation coefficient for AOB	1.1	g N m^{-3}	Wiesmann, 1994
k	**Inorganic carbon saturation coefficient for AOB (Sigmoidal kinetics)**	**31**	**g $CaCO_3$ m^{-3}**	**Chapter 3**
a	**Inorganic carbon sigmoidal kinetics non-dimensional parameter**	**5**	**Dimensionless**	**Chapter 3**
NOB				
μ_{max}^{NOB}	Growth rate of NOB	0.57	d^{-1}	Hellinga et al., 1999[c]
b^{NOB}	Decay rate of NOB	0.038	d^{-1}	Assumed, such that ratio b^{NOB}: $\mu_{max}^{NOB} = b^H$: μ_{max}^{H} as proposed in Mozumder et al., 2014
$K_{NO_2}^{NOB}$	NO_2^- half-saturation coefficient for NOB	0.51	g N m^{-3}	Wiesmann, 1994
$K_{O_2}^{NOB}$	DO half-saturation coefficient for NOB	1.1	g O_2 m^{-3}	Wiesmann, 1994
K_{NH}^{NOBH}	NH_4^+ half-saturation coefficient for NOB and heterotrophs	0.02	g N m^{-3}	Mozumder et al., 2014
K_{IC}^{NOB}	Inorganic carbon half-saturation coefficient for NOB	1.2	g $CaCO_3$ m^{-3}	Al-Omari et al., 2015
AN				
μ_{max}^{AN}	Growth rate of AN	0.03	d^{-1}	Strous *et al.*, 1998[c]

b^{AN}	Decay rate of AN	0.002	d^{-1}	Assumed, such that ratio b^{AN}: $\mu_{max}^{AN} = b^{H}$: μ_{max}^{H} as proposed in Mozumder et al., 2014
K_{NH}^{AN}	NH_4^+ half-saturation coefficient for AN	0.03	g N m^{-3}	Mozumder et al., 2014
$K_{O_2}^{AN}$	DO inhibition coefficient for AN	0.01	g O_2 m^{-3}	Strous et al., 1998
$K_{NO_2}^{AN}$	NO_2^- half-saturation coefficient for AN	0.005	g N m^{-3}	Mozumder et al., 2014
K_{IC}^{AN}	Inorganic carbon half-saturation coefficient for AN	1.2	g $CaCO_3$ m^{-3}	Kimura et al., 2011
Heterotrophs				
μ_{max}^{H}	Growth rate of heterotrophs	8.1	d^{-1}	Henze et al., 2006[d]
b^{H}	Decay rate of heterotrophs	0.54	d^{-1}	Hiatt and Grady, 2008[e]
$K_{NO_2}^{H}$	NO_2^- half-saturation coefficient for heterotrophs	0.3	g N m^{-3}	Alpkvist et al., 2006
$K_{NO_3}^{H}$	NO_3^- half-saturation coefficient for heterotrophs	0.3	g N m^{-3}	Alpkvist et al., 2006
K_S^H	COD half-saturation coefficient for heterotrophs	20	g COD m^{-3}	Henze et al., 2006
$K_{O_2}^{H}$	DO half-saturation coefficient for heterotrophs	0.2	g O_2 m^{-3}	Henze et al., 2006
$\eta_{NO2}=\eta_{NO3}$	Reduction factor for maximum growth rate under anoxic conditions	0.8	Dimensionless	Henze et al., 2006
k_a	Organic nitrogen hydrolysis rate constant	0.11	m^3COD (g d) $^{-1}$	Henze et al., 2006[d]
MOB				
μ_{max}^{MOB}	Growth rate of MOB	2.12	d^{-1}	Arcangeli and Arvin, 1999[c]
b^{MOB}	Decay rate of MOB	0.106	d^{-1}	$b^{MOB} = 0.05\ \mu_{max}^{MOB}$ as proposed in Castro-Barros et al., 2018[c]
$\boldsymbol{K_{Alk}^{MOB}}$	**Inorganic carbon half-saturation coefficient for MOB**	**1.2**	**g $CaCO_3$ m^{-3}**	**Assumed the same as NOB**
K_{CH4}^{MOB}	CH_4 half-saturation coefficient for MOB	0.06	g CH_4.m^{-3}	Arcangeli and Arvin, 1999
K_{O2}^{MOB}	O_2 half-saturation coefficient for MOB	0.2	g O_2.m^{-3}	Arcangeli and Arvin, 1999
K_{NH}^{MOB}	NH_4^+ half-saturation coefficient for MOB	1	g N.m^{-3}	Arcangeli and Arvin, 1999
SOB				
μ_{max}^{SOB1}	Growth rate of SOB on H_2S	6.03	d^{-1}	Sun et al., 2017a[g]
μ_{max}^{SOB2}	Growth rate of SOB on S_0	2.11	d^{-1}	Sun et al., 2017a[g]
b^{SOB}	Decay rate of SOB	0.054	d^{-1}	Huang et al., 2016[g]
$\boldsymbol{K_{Alk}^{SOB}}$	**Inorganic carbon half-saturation coefficient for SOB**	**1.2**	**g $CaCO_3$ m^{-3}**	**Assumed the same as NOB**
K_{H2S}^{SOB2}	H_2S half-saturation coefficient for SOB	0.00135	g S.m^{-3}	Jensen et al., 2009
K_{S0}^{SOB2}	S_0 half-saturation coefficient for SOB	0.9	g S.m^{-3}	Jensen et al., 2009
K_{O2}^{SOB1}	O_2 half-saturation coefficient for SOB	0.1	g O_2.m^{-3}	Jensen et al., 2009
K_{O2}^{SOB2}	O_2 half-saturation coefficient for SOB	0.45	g O_2.m^{-3}	Jensen et al., 2009
$\boldsymbol{K_{NH}^{SOB}}$	**NH_4^+ half-saturation coefficient for SOB**	**0.02**	**g N.m^{-3}**	**Assumed the same as NOB**
$K_{nc,H2S}^{SOB}$	Non-competitive inhibition constant of H_2S	0.455	g S.m^{-3}	Mora et al., 2016
DAMO B				
μ_{max}^{Db}	Growth rate of DAMO B	0.0459	d^{-1}	Ettwig et al., 2010
b^{Db}	Decay rate of DAMO B	0.0025	d^{-1}	$b^{Db} = 0.5\mu_{max}^{Db}$ as proposed by Castro-Barros et al., 2018
K_{CH4}^{Db}	CH_4 half-saturation coefficient	0.0475	g CH_4.m^{-3}	Castro-Barros et al., 2018
K_{NO2}^{Db}	NO_2 half-saturation coefficient	0.6	g N.m^{-3}	He et al., 2013
$K_{i,O2}^{Db}$	O_2 inhibition constant for DAMO B	0.01	g O_2.m^{-3}	Assumed equal to $K_{i,O2}^{AN}$ as proposed by Castro-Barros et al., 2018
DAMO A				
μ_{max}^{Da}	Growth rate of DAMO A	0.036	d^{-1}	Chen et al., 2014
b^{Da}	Decay rate of DAMO A	0.0018	d^{-1}	$b^{Da} = 0.5\mu_{max}^{Da}$ as proposed by Castro-Barros et al., 2018
K_{CH4}^{Da}	CH_4 half-saturation coefficient for DAMO A	0.0475	g CH_4.m^{-3}	Castro-Barros et al., 2018
K_{NO3}^{Da}	NO_3^- half-saturation coefficient for DAMO A	0.11	g N.m^{-3}	Chen et al., 2014
K_{NH}^{Da}	NH_4^+ half-saturation coefficient for DAMO A	0.02	g N.m^{-3}	Castro-Barros et al., 2018
$K_{i,O2}^{Da}$	O_2 inhibition coefficient for DAMO A	0.01	g O_2.m^{-3}	Assumed equal to $K_{i,O2}^{AN}$ as proposed by Castro-Barros et al., 2018

SBDN				
$\mu_{max}^{SBDN1,NO3}$	Growth rate of SBDN (H_2S) on NO_3^-	1.6	d^{-1}	Mora et al., 2014[g]
$\mu_{max}^{SBDN2,NO3}$	Growth rate of SBDN (S_0) on NO_3^-	2.8	d^{-1}	Mora et al., 2014[g]
$\mu_{max}^{SBDN1,NO2}$	Growth rate of SBDN (H_2S) on NO_2^-	2.4	d^{-1}	Mora et al., 2014[g]
$\mu_{max}^{SBDN2,NO2}$	Growth rate of SBDN (S_0) on NO_2^-	1.19	d^{-1}	Mora et al., 2014[g]
b^{SBDN}	Decay rate of SBDN	0.076	d^{-1}	Zeng and Zhang, 2005[g]
K_{H2S}^{SBDN}	H_2S half-saturation coefficient for SBDN	1.8	g S.m^{-3}	Jing et al., 2010
K_{S0}^{SBDN}	S_0 half-saturation coefficient for SBDN	16	g S.m^{-3}	Decru et al., 2021
K_{NO3}^{SBDN1}	NO_3^- half-saturation coefficient for SBDN (H_2S)	1.30	g N. m^{-3}	Mora et al., 2014
K_{NO3}^{SBDN2}	NO_3^- half-saturation coefficient for SBDN (S_0)	1.30	g N. m^{-3}	Mora et al., 2014
K_{NO2}^{SBDN1}	NO_2^- half-saturation coefficient for SBDN (H_2S)	0.43	g N. m^{-3}	Mora et al., 2014
K_{NO2}^{SBDN2}	NO_2^- half-saturation coefficient for SBDN (S_0)	0.43	g N.m^{-3}	Mora et al., 2014
$K_{nc,H2S}^{SBDN}$	Non-competitive inhibition constant for H_2S	0.455	g S.m^{-3}	Mora et al., 2014
Mass transfer				
D_{NH4}	NH_4^+ diffusion coefficient in water	$1.5x10^{-4}$	m^2 d^{-1}	Williamson and McCarty, 1976
D_{NO2}	NO_2^- diffusion coefficient in water	$1.4x10^{-4}$	m^2 d^{-1}	Williamson and McCarty, 1976
D_{NO3}	NO_3^- diffusion coefficient in water	$1.4x10^{-4}$	m^2 d^{-1}	Williamson and McCarty, 1976
D_{O2}	O_2 diffusion coefficient in water	$2.2x10^{-4}$	m^2 d^{-1}	Picioreanu et al., 1997
D_{N2}	N_2 diffusion coefficient in water	$2.2x10^{-4}$	m^2 d^{-1}	Williamson and McCarty, 1976
D_{IC}	Inorganic carbon (as bicarbonate) diffusion coefficient in water	$1.6x10^{-4}$	m^2 d^{-1}	Williamson and McCarty, 1976
D_S	COD diffusion coefficient in water	$1x10^{-4}$	m^2 d^{-1}	Hao and van Loosdrecht, 2004
D_{CH4}	CH_4 diffusion coefficient in water	$1.84x10^{-4}$	m^2 d^{-1}	Haynes, 2013
D_{H2S}	H_2S diffusion coefficient in water	$1.5x10^{-4}$	m^2 d^{-1}	Haynes, 2013
D_{SO4}	SO_4^{2-} diffusion coefficient in water	$9.2x10^{-5}$	m^2 d^{-1}	Haynes, 2013
D_{S0}	S_0 diffusion coefficient in water	$9.2x10^{-5}$	m^2 d^{-1}	Decru et al., 2021[f]
Df/Dw	Diffusion correction factor	0.8	Dimensionless	Eberl et al., 2006

[a] After unit conversion, using a typical biomass composition of $CH_{1.8}O_{0.5}N_{0.2}$, corresponding to 1.3659 g COD g^{-1} biomass

[b] After unit conversion, using an anammox biomass composition of $CH_2O_{0.5}N_{0.15}$ (Strous et al., 1998) corresponding to 36.4 g COD mol^{-1} or 1.51 g COD g^{-1} biomass

[c] Conversion of values given by Hellinga et al. (1999) at 35°C, by Strous et al. (1998) at 32.5°C and Arcangeli and Arvin (1999) at 20°C to 24.3°C using the following relationship (written for X_{AOB}, analogous for X_{NOB}, X_{AN}, and X_{MOB}) (Eq. A.6.1)

$$\mu_{\max}^{\mathrm{AOB}}(\mathrm{T}) = \mu_{\max}^{\mathrm{AOB}}(\mathrm{T_{ref}}) \exp\left(\frac{\mathrm{E_a^{AOB}}.(\mathrm{T}-\mathrm{T_{ref}})}{\mathrm{R.\ T.\ T_{ref}}}\right) \qquad \text{Eq. A.6.1}$$

with E_a^{AOB}= 68 kJ mol^{-1} ; E_a^{NOB}= 44 kJ mol^{-1}; E_a^{AN} = 70 kJ mol^{-1} (Strous et al., 1998); E_a^{MOB} = 58.1 kj.mol^{-1}; R = 8.31 J mol^{-1} K^{-1}.

[d] Conversion of ASM1-value (μ_{max}^{H}) given by Henze et al. (2006) at 10°C and 20°C to 24.3°C using the temperature relationship proposed by those authors (ASM3).

[e] Conversions of decay rate of heterotrophs at 20 °C to 24.3°C through the equation Eq. A.6.2.

$$\mathrm{b(T)} = \mathrm{b(T_{ref})} \exp\left(\frac{\mathrm{E_{act}(T - T_{ref})}}{\mathrm{RTT_{ref}}}\right) \qquad \text{Eq. A.6.2}$$

in which E_{act}^{Het} = 48 kJ mol^{-1} (calculated with maximum growth rate values at 283.15 K and 293.15 K according to Eq. A.6.2 (Henze et al., 2006))

[f] Decru et al. (2021) assumed the diffusivity of elemental sulfur (S_0) equal to the diffusivity of sulfate (SO_4^{2-}), as elemental sulfur is mainly present under the form of polysulfide (Steudel, 1996)

[g] For SOB and SBDN organisms, Arrhenius constants were used to convert maximum growth rates (μ_{max}) and decay rates (b) according to the reference temperature (30°C (Mora et al., 2015)) as follows (Eq. A.6.3)

$$\mu_{\max}\ (T) = \mu_{\max}\ (T_{ref})\theta^{T-T_{ref}} \qquad \text{Eq. A.6.3}$$

With θ^{SOB} and θ^{SBDN} respectively 1.100 (dimensionless) (Nielsen et al., 2006) and 1.116 (Di Capua et al., 2016). Θ^{SOB} was determined for the first step yielding elemental sulfur (μ_{max}^{SOB1}) but was also assumed to correct μ_{max}^{SOB2} for the second step yielding sulfate. θ^{SBDN} was originally determined for growth on thiosulfate ($S_2O_3^{2-}$) but was assumed to be the same for growth on H_2S (μ_{max}^{SBDN1}) and elemental sulfur (μ_{max}^{SBDN2}). The decay rate (b) for both SOB and SBDN organisms was corrected using the same Arrhenius constant as for autotrophic nitrifiers, that is 1.029 (Metcalf & Eddy, 2013).

A.6.2. Supplementary simulation results

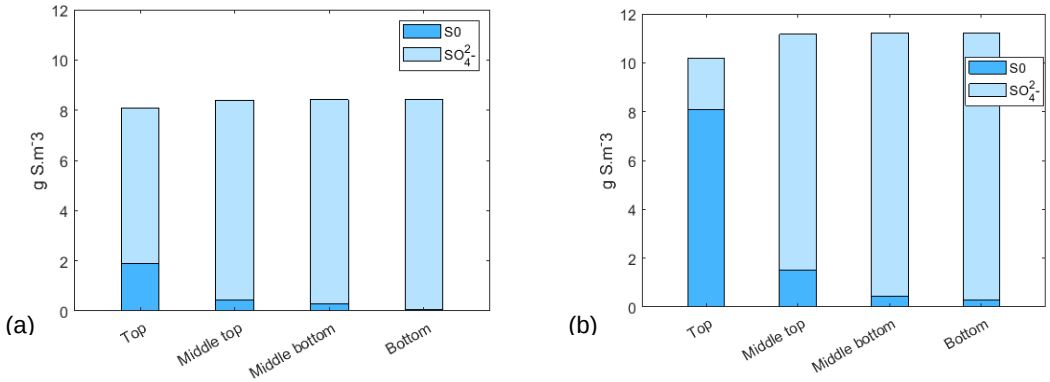

Figure A.6.1 Sulfur end-products over the SBTF depth for an open reactor (scenario I) (a) and closed reactor with mechanical ventilation (scenario III) (b). *Sulfate formation prevails over the SBTF compartments, except for the top layer for the closed configuration with forced ventilation*

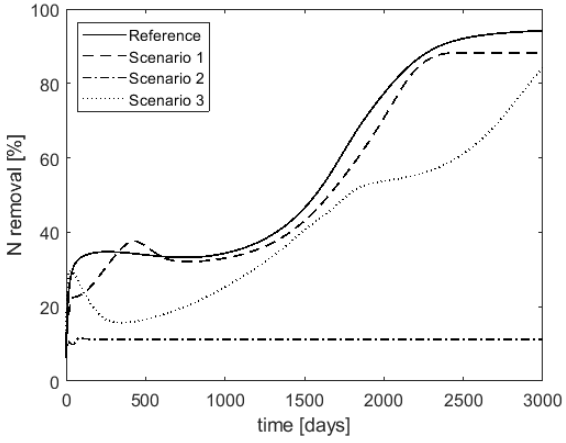

Figure A.6.2 Total nitrogen removal efficiencies for all simulated scenarios

A.6.3. Supplementary experimental data

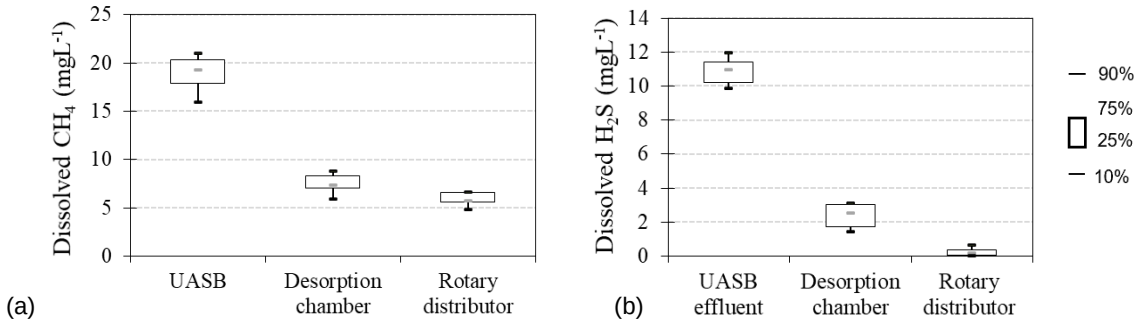

Figure A.6.3. Experimentally measured concentrations of dissolved methane (a) and H_2S (b) in the anaerobic effluent prior to and after the desorption chamber, as well as at the outlet of the rotary distributor of the SBTF (inlet of the system)

Chapter 7

General discussion, conclusions, and perspectives

This doctoral research work deals with the post-treatment of anaerobic effluents using sponge-bed trickling filters (SBTFs). The overall goal was to establish highly efficient nitrogen removal, dealing with residual organic carbon and integrated with the abatement of dissolved gases. To this end, demo-scale experimental studies were combined with modelling and simulation work. This chapter reviews the main findings of this thesis, which involve both mechanistic insights and practical experiences, as summarized in Table 7.1 and further discussed in section 7.1. Perspectives concerning practical implications and research needs are provided in section 7.2. Selected take-home messages conclude this chapter (section 7.3).

Table 7.1 Summary of the mechanistic insights and practical experiences on total nitrogen removal in SBTFs following UASB obtained in this doctoral research work

Chapter number and main methodology	TN removal efficiency (standard deviation)	Main mechanistic insights and practical experiences
2. Literature review	45% (14) / 70% (12)[a]	• Consolidated design approach for ammonium removal • Low biodegradability of the anaerobic effluent • Potential for PN/A or heterotrophic denitrification
3. Experimental data & modelling/simulation	26% (14)	• Lack of inorganic carbon hampered AOB activity • Limited total nitrogen removal efficiency
4 Simulation	93% (26)[b]	• PN/A in the long run • Kinetic and mass transfer parameters controlling DO at the biofilm-liquid interface • Operational strategies for optimizing process start-up: effluent recirculation and sewage by-pass
5. Experimental data	46% (9)	• Ventilation control suppressed AOB activity • Effluent recirculation improved heterotrophic denitrification • Temperature affected anammox growth in the long-term
6 Simulations	88% (23)[b]	• Dissolved methane and H_2S were mostly stripped at the top compartment of the SBTF • DAMO and SBDN processes outcompeted by MOB and SOB, respectively • Better control of ammonium oxidation with desorbed anaerobic effluent

Median values. Standard deviation in brackets. [a] Median and standard deviation for primarily heterotrophic and anammox pathways, respectively, from data presented in Table 2.8 (Chapter 2).
[b] Values considering a 3000-day simulation, where steady-state was reached after 2000 days.

7.1 Mechanistic insights and practical experiences

7.1.1 Nitrogen removal efficiency and prevailing pathways

Nitrogen removal in SBTFs has been primarily ascribed to the heterotrophic pathway (Tandukar et al., 2006; Onodera et al., 2016), and the implementation of partial nitritation-anammox was experimentally demonstrated with synthetic effluents (Sánchez-Guillén et al., 2015b). In this thesis, relatively high total nitrogen removal efficiencies (> 60%) were only observed through the partial nitritation-anammox pathway during simulations (as indicated in Table 7.1). **Chapter 2** reviewed the potential of this pathway. The primary rationale resides in the characteristics of the anaerobic effluent, i.e., low biodegradability of the residual COD and the possibility of controlling oxygen transfer to the SBTF (see Section 7.1.3). **Chapter 2** also pointed out the potential of heterotrophic denitrification, considering a possible carbon source from biomass decay products. The realization of those nitrogen removal pathways was further explored in the subsequent chapters through modelling and simulations, besides experiments.

Chapter 4 highlighted the potential of partial nitritation-anammox; however, the long start-up period jeopardizes the process. Partial denitrification was a less relevant mechanism supplying nitrite for the anammox process in the SBTF. Furthermore, decreasing oxygen transfer did not further benefit partial nitritation-anammox, as AOB activity was impaired.

Chapter 3 and **Chapter 5** showed that for conventional SBTFs post-UASB reactors, a limited total nitrogen removal efficiency is achieved (< 30%), mainly attributable to heterotrophic denitrification. Moreover, recirculation is currently the best strategy for fast-improving total nitrogen removal in SBTFs (see section 7.1.3). However, maximum process performance was limited to 55% due to effluent nitrate build-up, which was also verified in long-term simulations in **Chapter 4**.

Chapter 6 revealed that complementary autotrophic nitrogen removal processes combining methane (DAMO) and H_2S oxidation (SBDN) are impractical in SBTFs treating anaerobic effluents, mainly ascribed to the competition for substrate with MOB and SOB, respectively.

7.1.2 Modelling nitrogen removal from anaerobic mainstream effluent

The SBTF model was based on an existing model for a nitrifying biofilm reactor (Mozumder et al., 2014). However, with the latter model, the experimentally observed nitrogen conversions in the SBTF treating anaerobic mainstream effluent could only be reproduced using unrealistic kinetic parameter values for AOB (unlikely high affinity constant K_{NH} and unlikely low maximum growth rate). Using experimental evidence combined with simulations, inorganic carbon limitation was identified as the cause for this discrepancy and subsequently included in the rate expressions for autotrophic growth. Bicarbonate was implemented as the model state variable referring to inorganic carbon, as it was the dominant form at the prevailing neutral pH conditions (taking into account pK_{CO2} = 6.3 and pK_{HCO3^-} = 10.3 at 25 ^oC – Stumm and Morgan, 1996). The stoichiometric coefficient for bicarbonate was calculated from the charge balance (see Table A.3.1, **Chapter 3**), which was warranted because the pH was constant, so no shifts in chemical equilibria occurred. In this study, pH served as a model parameter, not a state variable.

In a more detailed model, both inorganic carbon and pH (H^+) would be included as state variables. Dynamic pH calculation is needed in case significant pH changes occur. The equilibrium forms of inorganic carbon, namely CO_2, HCO_3^- and CO_3^{2-} would then need to be calculated for every time step, depending on the prevailing pH. In case both inorganic carbon and pH are considered as state variables, the stoichiometric coefficient for total inorganic carbon would be determined from the carbon balance, and the produced protons would be calculated from the charge balance. Calculating the stoichiometric coefficient of total inorganic carbon from the carbon balance requires the knowledge of the carbon content of all model state variables (in terms of gC $gCOD^{-1}$ or gC gN^{-1}). While this is *a priori* not known, an assumption could be made (see, e.g., Volcke et al., 2006). However, since pH was about constant in this study, there was no need to include H^+ as a state variable. Therefore, a simplified model approach was decided for calculating the stoichiometric coefficient of bicarbonate from a charge balance.

Further reflections on research needs in terms of modelling improvements are addressed in section 7.2.2.

7.1.3 Design parameters and influent characteristics

The design of SBTFs following UASB reactors for sewage treatment should be based on the practical experiences of applied organic and hydraulic loading rates, as addressed in **Chapter 2**. Under proper loading criteria (< 1.0 kgCOD m^{-3}_{sponge} d^{-1}), process efficiency for ammonium removal is safely assured. Nevertheless, **Chapter 3** revealed intrinsic process limitations attributed to the lack of influent inorganic carbon. The modelling approach unlocked the crucial role of inorganic carbon for both buffering and inorganic carbon source in nitrogen conversions in SBTFs, rather than merely indicating pH changes. NOB activity was little affected by the inorganic carbon limitation, or at least less than AOB activity.

Design parameters for total nitrogen require more process understanding, as addressed in **Chapter 2**. Long-term simulations were thus performed in the scope of **Chapter 4**, following a sensitivity analysis that revealed key reactor-operation-specific parameters influencing nitrogen gas production in the long run of SBTFs, namely: the volumetric oxygen mass transfer coefficient (k_La), the maximum biofilm thickness (L_F), the specific surface area of the sponge media (a_s) and the external mass transfer boundary layer thickness (L_L). The simulation outputs from **Chapter 4** showed that the interaction of those reactor-operation-specific parameters ultimately dictates oxygen levels at the biofilm-liquid interface, which can favour anammox bacteria growth in the long run. Moreover, the anammox process seems to be resilient in the long term, even if high organic loading rates are applied. In this case, anammox bacteria are pushed to the bottom compartment of the reactor. Therefore, SBTFs should have at least 3.0 m depth to safely ensure high total nitrogen removal.

The aforementioned drawback of slow process start-up for PN/A could not be circumvented with biomass inoculation as a standalone strategy, as non-inhibiting oxygen levels at the biofilm-liquid interface are not guaranteed. Conversely, a fast start-up can be achieved via heterotrophic denitrification under high C/N, thin external mass transfer boundary layer, and high volumetric oxygen transfer, meaning that effluent recirculation coupled to sewage by-pass seems to be a relevant operational strategy. Therefore, this was experimentally assessed in **Chapter 5**, but nitrogen removal efficiency was hampered due to a decreased AOB activity. Such behaviour was attributed to the observed hydraulic short-circuiting, which indirectly increased the

organic loading rate (i.e., less sponge volume for the same influent flow) and pushed for AOB out-selection.

Chapter 5 also elucidated that the observed temperature ranges during experiments (15 – 30 ^{o}C) might change the prospect of having PN/A in the long run in SBTFs, as characterized in **Chapter 4**. Moreover, the observed bulk liquid DO fluctuations likely contributed to inhibiting anammox bacteria based on the relevance of dissolved oxygen control for realizing the PN/A. The need to assure non-inhibitory oxygen levels in the SBTFs has also motivated the experimental evaluation of several ventilation strategies (**Chapter 5**). Nevertheless, AOB activity was remarkably hampered even with a relatively high DO, and NOB was not washed out. Therefore, it was postulated that the dissolved gases in the anaerobic effluent might significantly affect nitrogen conversions in (partially) closed SBTFs if not handled upfront.

The interaction of dissolved gases (methane and H_2S) and nitrogen transformations was explored under **Chapter 6**. For a conventionally operated SBTF (bottom ventilation), simulations showed that dissolved methane and H_2S are mostly stripped at the top compartment of the reactor. Concerns can then be raised related to greenhouse emissions, odour nuisance, and corrosion. Nevertheless, total nitrogen removal is barely impacted, considering the remaining low methane and H_2S in the liquid phase. The figure completely changes when restricting the ventilation of an SBTF. As less gas strip takes place, dissolved methane and H_2S are fully biologically oxidized by methanotrophs and sulfide oxidizing bacteria, respectively. The increased oxygen requirements, up to 60% beyond the demand for organic carbon and ammonium conversions, hampers AOB activity and ultimately total nitrogen removal, thus confirming the observed trends for the closed SBTFs operated in **Chapter 5**.

Hence, a simple structure for desorbing dissolved gases was recommended prior to feeding an SBTF, which was also experimentally assessed in **Chapter 6**. The results indicated that better control over the extent of ammonium conversion was possible. Nevertheless, nitrate still accumulated in the effluent, meaning that NOB out-selection remained a major practical challenge.

7.2 Perspectives

7.2.1 Practical implications

Given the vast number of anaerobic (UASB) reactors treating sewage in Brazil, practical answers are urged to the increasing environmental pressure for nitrogen removal. This section briefly outlines the outcomes of this doctoral research work that may impact process design and operation of SBTF reactors for post-UASB nitrogen removal. First, reflections are provided for enhancing heterotrophic denitrification, followed by considerations on the partial nitritation-anammox.

Heterotrophic denitrification in SBTFs could be stimulated by effluent recirculation. Diverting part of the sewage from the anaerobic reactor (bypass) to the SBTF for carbon supply still requires more detailed process optimization such that AOB activity is not hampered by the competition with heterotrophs. Therefore, alternative feeding strategies such as supplying sewage at the middle bottom compartment or even submerging the bottom compartment of the STBF (Bundy et al., 2017) have yet to be better assessed. In any case, a comprehensive analysis should be performed between the possible trade-off of increasing total nitrogen removal at the expense of reduced energy potential at the anaerobic treatment step (less organic matter to be converted into biogas).

The results of a preliminary assessment on the impact of effluent recirculation and sewage by-pass are presented in Table 7.2. Two different scales for UASB + SBTF systems were considered, namely: a small-scale plant (PE 10.000) and a large-scale plant (PE 100.000). As for the first, electricity generation from biogas is economically unfeasible (Possetti et al., 2019). Hence, the biogas was conveyed for thermal energy recovery (e.g., sludge drying). The biogas of the large-scale plant was assumed to serve a combined heat and power (CHP) engine, with an electrical efficiency (η_{el}) of 35% (Possetti et al., 2019). Biogas flow was determined from a unitary biogas yield (Y_{biogas}) of 13.6 NL_{biogas} PE d^{-1}, containing 75% methane (Lobato et al., 2012). The lower calorific value of methane (LCV_{CH4}) was 9.9 KWh m^{-3} (Moran et al., 2014). The energy requirement for effluent recirculation was considered for both sewage treatment plants (small- and large-scale) based on a total pumping head of 5.0 m.

Table 7.2 Preliminary assessment of the impact of effluent recirculation in UASB + SBTF systems

	Small-scale plant (PE 10.000)	Large-scale plant (PE 100.000)
Electricity production potential (EP)[a] (kWh d^{-1})	N.A.	3,500
Electricity consumption (kWh d^{-1})[b]	40	400
Electricity balance (kWh d^{-1})	-40	3,100

[a] $EP = Y_{biogas} \times 0.75 \times PE \times \eta_{el} \times LCV_{CH4}$; [b] Pumping efficiency assumed as 60% and per capita sewage generation of 150 L PE d^{-1}; N.A.: not applicable

While electricity is not produced in the small-scale plant, the energy consumption is significantly lower than a similar conventional activated sludge plant with nitrification (0.9 MWh d^{-1}, assuming 0.65 KWh m^{-3} based on Metcalf & Eddy, 2013). Concerning the large-scale plant, the energy requirement is considerably outweighed by the energy potential from biogas recovery. In case a raw sewage by-pass is implemented, such energy potential would decrease proportionally. Nonetheless, even if 30% of the raw incoming sewage is diverted from the anaerobic reactor to the SBTF, the system remains energy autarchic.

As for promoting partial nitritation-anammox in a single SBTF, oxygen control proved hard to handle. There is no practical appeal in closing an SBTF if dissolved methane and H_2S in the anaerobic effluent are not removed upfront. These remaining gases in the liquid phase tend to impair AOB activity due to the competition for oxygen with SOB and MOB. Different technologies for collecting those dissolved gases are proposed by Centeno-Mora et al. (2020), some of them already implemented in full-scale UASB rectors (e.g., desorption chambers). A separate reactor is thus needed for the gas treatment, while integration in the SBTF still demands research (see section 7.2.2).

Feeding the SBTF with a desorbed anaerobic effluent can potentially facilitate the oxygen transfer control in the SBTF. Nevertheless, it remains unclear to which extent this will foster anammox activity while ensuring NOB out-selection. Overall, additional research is needed to improve the autotrophic nitrogen removal pathway in SBTFs (see section 7.2.2).

7.2.2 Research needs

The following research needs are drawn based on the identified remaining knowledge gaps and insights that emerged during this doctoral research work.

- The contribution of entrapped solids in the sponge pores as a carbon source for heterotrophic denitrification still requires clarification. The characterization of solids entrapment and further COD release could be included in a more detailed model. However, this would also lead to the need to assess flow paths in porous media, requiring a more detailed (at least 2-dimensional, as proposed by Bottero et al. (2013)) biofilm model, and consequently increase the computational burden.

- Microbial communities along the SBTF depth can be better engineered, which, however, demands further fundamental understanding; *(i)* Dissolved gases removed from the anaerobic effluent could be injected at the bottom of the SBTF (counter-current), fostering aerobic oxidation of methane and H_2S at the bottom without interfering in total nitrogen conversions at the top compartment. This could help better profit from the available sponge volume in different reactor compartments. Nevertheless, the gas transfer and stripping process should be better assessed to avoid new emissions and simultaneously preserve AOB activity; *(ii)* a closed SBTF equipped with mechanical aeration would allow for intermittent aeration. Therefore, NOB out-selection would be stimulated based on their growth lag time comparatively to AOB, besides better controlling the DO set-point (Sun et al., 2017b). Nonetheless, in the long run, NOB adaptation to low DO has been recently reported (Wang et al., 2021), which could pose a problem for SBTFs that generally lack other operational mechanisms to suppress NOB other than DO control.

- The integrated abatement of dissolved gases in the anaerobic effluent and nitrogen removal could be analysed considering the carbon footprint of different scenarios based on economically feasible technologies for small and large-scale anaerobic-based sewage treatment plants (Chernicharo et al., 2017). For a fair technical assessment, at least the management of the produced biogas should be considered.

- The chemical sulfide oxidation was assumed insignificant compared to biological oxidation processes, as often performed in modelling studies. Although the volumetric biochemical oxidation of sulfide was shown 2.5 times

faster than the chemical oxidation rate under microaerobic conditions (Pokorna-Krayzelova et al., 2018), this should be assessed for a further model improvement. Less available sulfide would decrease oxygen competition between SOB and AOB, but dissolved methane remains primarily responsible for increased oxygen requirements in the SBTF.

- The observed inorganic carbon limitation in SBTFs post-UASB reactors treating sewage may lead to increased N_2O emissions due to altering AOB metabolism, as observed by Ma et al. (2015) in a lab-scale nitritation-anammox reactor fed with synthetic wastewater. Nonetheless, the possible interaction with heterotrophic denitrification that further consumes N_2O can be a mitigation strategy (Wan et al., 2021), which is likely to occur in SBTFs due to high interaction between microbial groups over the SBTF depth.

- The process scheme (UASB followed by SBTFs) could be further evaluated concerning future challenges such as phosphorus removal or recovery. As biological phosphorus removal is inherently limited following anaerobic sewage treatment, most likely a physicochemical unit (e.g., precipitation tank) has to be considered after the SBTF. Furthermore, as far as micropollutants are concerned, the aerobic conditions and high SRT in SBTFs may be key factors for a good process performance (Brandt et al., 2013), which is nonetheless yet to be assessed.

- The environmental sustainability of using synthetic polyurethane-based sponge media for trickling filters could be evaluated using life cycle assessment. Based on the treatment target of removing residual organic carbon and ammonium from the anaerobic effluent, consolidated post-treatment options (e.g., activated sludge, submerged aerated biofilters, constructed wetlands) could be compared based on flows of raw materials, energy and sludge generated.

7.3 Take-home messages

- Empirical design approaches based on organic and hydraulic loading rates effectively ensure a high ammonium removal efficiency (> 70%) in SBTFs following UASB reactors, but are falling short in establishing total nitrogen removal.
- Full ammonium conversion in anaerobically treated sewage is hampered by inorganic carbon limitation.
- Effluent recirculation stimulates heterotrophic denitrification (up to 55%). However, achieving higher total nitrogen removal efficiencies requires more detailed process optimization, considering influent characteristics and kinetic and mass transfer parameters.
- Alternative nitrogen removal pathways based on partial ammonium conversion and/or anammox are hard to realize in naturally ventilated SBTFs.
- The presence of methane and H_2S in anaerobic effluents negatively affects nitrogen removal; these compounds should therefore preferentially be removed upfront.

Bibliography

Agrawal, L.K., Ohashi, Y., Mochida, E., Okui, H., Ueki, Y., Harada, H., Ohashi, A.,1997. Treatment of raw sewage in a temperate climate using a UASB reactor and the hanging sponge cubes process. Water Sci. Technol. 36, 433–440.

Aisse, M. M., PhD Thesis, 2002. Tratamento de efluentes de reatores anaeróbios (Treatment of anaerobic reactor effluents). Universidade de São Paulo. In Portuguese.

Almeida, P.G.S, Chernicharo, C. A. L., Souza, C. L., 2009. Development of compact UASB-TF systems for the treatment of domestic wastewater in small communities in Brazil. Water Sci. Technol. 59(7), 1431 – 1439.

Almeida, P.G.S., MSc dissertation, 2007. Efeito de diferentes tipos de meio suporte no desempenho de filtros biológicos percoladores aplicados ao pós-tratamento de efluentes de reatores UASB, com ênfase na nitrificação (Effect of different types of support media in trickling filters performance Applied to post-treat UASB reactors effluents, focusing on nitrification). Universidade Federal de Minas Gerais. In Portuguese.

Almeida, P.G.S., Chernicharo, C.A.L., Souza, C.L., 2009. Development of compact UASB/trickling filter systems for treating domestic wastewater in small communities in Brazil. Water Sci. Technol. 59, 1431–1439.

Almeida, P.G.S, Oliveira, S.C., Chernicharo, C. A. L., 2011. Operation of trickling filters post-UASB reactors without the secondary sedimentation stage. Eng. Sanit. e Ambit. 16(2), 1 – 10. In Portuguese.

Almeida, P.G.S., PhD Thesis, 2012. Remoção de matéria orgânica e nitrogênio em filtros biológicos percoladores aplicados ao pós-tratamento de efluentes de reatores UASB (Carbon and nitrogen removal in trickling filters post-UASB reactor). Universidade Federal de Minas Gerais. In Portuguese.

Almeida, P.G.S., Marcus, A.K., Rittmann, B.E., Chernicharo, C.A.L., 2013. Performance of plastic- and sponge-based trickling filters treating effluents from an UASB reactor. Water Sci. Technol. 67, 1034–1042.

Al-Omari, A., Wett, B., Nopens, I., De Clippeleir, H., Han, M., Regmi, P., Bott, C., Murthy, S., 2015. Model-based evaluation of mechanisms and benefits of mainstream shortcut nitrogen removal processes. Water Sci. Technol. 71, 840–847.

Alpkvist, E., Picioreanu, C., van Loosdrecht, M.C.M., Heyden, A., 2006. Three-dimensional biofilm model with individual cells and continuum EPS matrix. Biotechnol. Bioeng. 94, 961–979.

An, S., Tang, K., Nemati, M., 2010. Simultaneous biodesulphurization and denitrification using an oil reservoir microbial culture: Effects of sulphide loading rate and sulphide to nitrate loading ratio. Water Res. 44, 1531–1541.

ANA, Agência Nacional de Águas, 2020. ATLAS Esgotos: Despoluição de Bacias Hidrográficas. https://portal1.snirh.gov.br/ana/apps/webappviewer/index.html?id=6d866c5d54c64b17bd53af4bdcfb4b91 (accessed 1.2.21). In Portuguese.

Aquino, S.F., Gloria, R.M., Silva, S.Q., Chernicharo, C.A.L., 2009. Quantification of the Inert Chemical Oxygen Demand of Raw Wastewater and Evaluation of Soluble Microbial Product Production in Demo-Scale Upflow Anaerobic Sludge Blanket Reactors under Different Operational Conditions. Water Environ. Res. 81, 608–616.

Araki, N., Ohashi, A., Machdar, I., Harada, H., 1999. Behaviour of nitrifiers in a novel

biofilm reactor employing hanging sponge-cubes as attachment site. Water Sci. Technol. 39(7), 23-31.

Arcangeli, J.P., Arvin, E., 1999. Modelling the growth of a methanotrophic biofilm: Estimation of parameters and variability. Biodegradation 10, 177–191.

Axelrod, H.D., Cary, J.H., Bonelli, J.E., Lodge, J.P., 1969. Fluorescence Determination of Sub-Parts per Billion Hydrogen Sulfide in the Atmosphere. Anal. Chem. 41, 1856–1858.

Azevedo, L.S., Bressani-Ribeiro, T., Chernicharo, C.A.L., Araújo, J.C., 2021. Mainstream partial nitritation-anammox as post-treatment of anaerobic effluents under warm climate regions: a critical review of the reported drawbacks. Environ. Technol. Rev. 10, 143–160.

Baird, R., Bridgewater, L., 2017. Standard methods for the examination of water and wastewater, 23rd ed. American Public Health Association, Washington, D.C.

Bédard, C., Knowles, R., 1989. Physiology, biochemistry, and specific inhibitors of CH_4, NH_4^+, and CO oxidation by methanotrophs and nitrifiers. Microbiol. Mol. Biol. Rev., 53, 68–84.

Benthum, W.A.J. va., Loosdrecht, M.C.M. va., L.Tijhuis, J.J.Heijnen., 1995. Solids retention time in heterotrophic and nitrifying biofilms in a biofilm airlift suspension reactor. Water Sci. Technol. 32(8), 53-60..

Biesterfeld, S., Farmer, G., Russell, P., Figueroa, L., 2003. Effect of Alkalinity Type and Concentration on Nitrifying Biofilm Activity. Water Environ. Res. 75, 196–204.

Blake, D.R., Mayer, E.W., Tyler, S.C., 1982. ppmv from January to January 9, 477–480.

Bock, E., 1976. Growth of Nitrobacter in the presence of organic matter. Arch. Microbiol. 108, 305–312.

Boller, M., Gujer, W., Nyhuis, G., 1990. Tertiary rotating biological contactors for nitrification. Water Sci. Technol. 22, 89–100.

Boller, M., Gujer, W., Tschui, M., 1994. Parameters affecting nitrifying biofilm reactors. Water Sci. Technol. 29, 1–11.

Boltz, J.P., Morgenroth, E., Brockmann, D., Bott, C., Gellner, W.J., 2011. Vanrolleghem, P.A. Systematic evaluation of biofilm models for engineering practice: Components and critical assumptions. Water Sci. Technol. 64, 930–944.

Bottero, S., Storck, T., Heimovaara, T.J., van Loosdrecht, M.C.M., Enzien, M. V., Picioreanu, C., 2013. Biofilm development and the dynamics of preferential flow paths in porous media. Biofouling 29, 1069–1086.

Bressani-Ribeiro, T., MSc dissertation, 2015. Sistema UASB/FBP submetido a hidrograma típico de vazão: avaliação do meio suporte baseado em espuma de poliuretano e operação sem decantadores secundários (UASB/TF system submitted to a typical hydrograph flow: assessment of a sponge-based packing medium and operation without secondary settlers). Universidade Federal de Minas Gerais. In Portuguese.

Bressani-Ribeiro, T., Freire Brandt, E.M., Sertório de Almeida, P.G., Díaz Flórez, C.A., Chernicharo, C.A.L., 2017. Technological improvements in compact UASB/SBTF systems for decentralized sewage treatment in developing countries. Desalin. Water Treat. 91, 112–120.

Bressani-Ribeiro, T., Almeida, P.G.S., Volcke, E.I.P., Chernicharo, C.A.L., 2018. Trickling filters following anaerobic sewage treatment: state of the art and perspectives. Environ. Sci. Water Science and Technology 4, 1721–1738.

Bressani-Ribeiro, T., Almeida, P.G.S., Chernicharo, C.A.L., Volcke, E.I.P., 2021. Inorganic carbon limitation during nitrogen conversions in sponge-bed trickling

filters for mainstream treatment of anaerobic effluent. Water Res. 201, 117337.
Buisman, C.J.N., Jspeert, P.I., Hof, A., Janssen, A.J.H., Hagen, R. Ten, Lettinga, G., 1991. Kinetic parameters of a mixed culture oxidizing sulfide and sulfur with oxygen. Biotechnol. Bioeng. 38, 813–820.
Bundy, C.A., Wu, D., Jong, M.C., Edwards, S.R., Ahammad, Z.S., Graham, D.W., 2017. Enhanced denitrification in Downflow Hanging Sponge reactors for decentralised domestic wastewater treatment. Bioresour. Technol. 226, 1–8.
Campos, J.L., Carvalho, S., Portela, R., Mosquera-Corral, A., Méndez, R., 2008. Kinetics of denitrification using sulphur compounds: Effects of S/N ratio, endogenous and exogenous compounds. Bioresour. Technol. 99, 1293–1299.
Castro-Barros, C.M., Ho, L.T., Winkler, M.K.H., Volcke, E.I.P., 2018. Integration of methane removal in aerobic anammox-based granular sludge reactors. Environ. Technol. (United Kingdom) 39, 1615–1625.
Centeno-Mora, E., Fonseca, P.R., Andreão, W.L., Brandt, E.M.F., de Souza, C.L., de Lemos Chernicharo, C., 2020. Mitigation of diffuse CH4 and H2S emissions from the liquid phase of UASB-based sewage treatment plants: challenges, techniques, and perspectives. Environ. Sci. Pollut. Res. 27, 35979–35992.
Chan, Y.I., Chong, M.F., Law, C.L., Hassell, D.G., 2009. A review on anaerobic–aerobic treatment of industrial and municipal wastewater. Chem. Eng. J. 155, 1-18.
Chen, G., van Loosdrecht, M.C.M., Ekama, G.A., Brdjanovic, D., 2020. Wastewater treatment development, in: Chen, G., Loosdrecht, M.C.M. van, Ekama, G.A., Brdjanovic, D. (Eds.), Biological Wastewater Treatment: Principles, Modelling and Design. IWA Publishing, London.
Chen, X., Guo, J., Shi, Y., Hu, S., Yuan, Z., Ni, B.J., 2014. Modeling of simultaneous anaerobic methane and ammonium oxidation in a membrane biofilm reactor. Environ. Sci. Technol. 48, 9540–9547.
Chen, X., Guo, J., Xie, G.J., Liu, Y., Yuan, Z., Ni, B.J., 2015. A new approach to simultaneous ammonium and dissolved methane removal from anaerobic digestion liquor: A model-based investigation of feasibility. Water Res. 85, 295–303.
Chen, X., Liu, Y., Peng, L., Yuan, Z., Ni, B., 2016. Model-Based Feasibility Assessment of Membrane Biofilm Reactor to Achieve Simultaneous Ammonium , Dissolved Methane , and Sulfide Removal from Anaerobic Digestion Liquor. Nat. Publ. Gr. 1–13.
Chen, X., PhD Thesis, 2017. Understanding and Modeling the Microbial Interactions in a Novel Nitrogen Removal Process. University of Queensland, Australia.
Chernicharo. C.A.L. (coordinator)., 2001. Pós-tratamento de efluentes de reatores anaeróbios (Post-treatment of Anaerobic effluents). PROSAB/FINEP, 1ª ed. Rio de Janeiro: Segrac. 544 p. In Portuguese.
Chernicharo, C.A.L., 2006. Post-Treatment Options for the Anaerobic Treatment of Domestic Wastewater. Rev. Environ. Sci. Biotechnol. 5(1), 73-92.
Chernicharo, C.A.L. Lobato, L.C., Júnior, C.A.P., Barbosa, E.V., Souza, J.R., Silva, L.R., Judice, M.A.M., Moraes, O.J., Almeida, P.G., Gonçalves, T.C.F., 2014. Secondary sludge return for thickening and digestion in UASB reactors: Case study of ONÇA STP – Brazil. Proceedings of XI Taller y Simposio Latinoamericano de Digestión Anaerobia. Cuba.
Chernicharo, C.A.L., Almeida, P. G., 2011. Feasibility of UASB/trickling filter systems without final clarifiers for the treatment of domestic wastewater in small communities in Brazil. Water Sci. Technol. 64(6), 1347-54.

Chernicharo, C.A.L., Van Lier, J.B., Noyola, A., Bressani-Ribeiro, T., 2015. Anaerobic sewage treatment : state of the art, constraints and challenges. Rev. Environ. Sci. Biotechnol. 14(4), 649–679.

Chernicharo C.AL., Brandt E.M.F., Bressani-Ribeiro T., Melo V.R., Bianchetti F.J., Mota Filho C.R., McAdam, E., 2017. Development of a tool for improving the management of gaseous emissions in UASB-based sewage treatment plants. Water Pract. Technol., 12, 917–926.

Chernicharo, C.A.L., Bressani-Ribeiro, T., Garcia, G.B., Lermontov, A., Pereira, C.B., Platzer, C.J., Possetti, G.R.C., Leites, M.A.L., Rosseto, R., 2018. Panorama do tratamento de esgoto sanitário nas regiões Sul, Sudeste e Centro-Oeste do Brasil: tecnologias mais empregadas (Overview of sewage treatment in the South, Southeast and Midwest regions of Brazil: most used technologies). Revista DAE, 213 (66). In Portuguese.

Chernicharo, C.A.L., Bressani-Ribeiro, T., von Sperling, M., 2019. Introduction to anaerobic sewage treatment, in: Chernicharo, C.A.L., Bressani-Ribeiro, T. (Eds.), Anaerobic Reactors for Sewage Treatment: Design, Construction and Operation. IWA Publishing, London.

Chong, S., Sen, T.K., Kayaalp, A., Ang, H.M., 2012. The performance enhancements of upflow anaerobic sludge blanket (UASB) reactors for domestic sludge treatment-a state-of-the-art review. Water Res. 46(11), 3434-3470.

Chuang, H.P., Ohashi, A., Imachi, H., Tandukar, M., Harada, H., 2007. Effective partial nitrification to nitrite by down-flow hanging sponge reactor under limited oxygen condition. Water Res. 41, 295-302.

Chuang, H.P., Yamaguchi, T., Harada, H., Ohashi, A., 2008. Anoxic ammonium oxidation by application of a down-flow Hanging sponge (DHS) reactor. J. Environ. Eng. Manage. 18(6), 409-417.

Collivignarelli, C., Urbini, G., Farneti, A., Bassetti, A., Barbaresi, U., 1990. Anaerobic-Aerobic treatment of municipal wastewater with full-scale upflow anaerobic sludge blanket and attached biofilm reactors. Water Sci. Technol. 22(1-2), 475-482.

Crovetto, R., Fernández-Prini, R., Japas, M.L., 1982. Solubilities of inert gases and methane in H2O and in D 2O in the temperature range of 300 to 600 K. J. Chem. Phys. 76, 1077–1086.

Corbalá-Robles, L., Picioreanu, C., van Loosdrecht, M.C.M., Pérez, J., 2016. Analysing the effects of the aeration pattern and residual ammonium concentration in a partial nitritation-anammox process. Environ. Technol. (United Kingdom) 37, 694–702.

Cueto, D., Mora, M., Gabriel, D., 2021. Evaluating and modeling biological sulfur production in the treatment of sulfide-laden streams containing ammonium. J. Chem. Technol. Biotechnol. 96, 439–447.

Daelman, M.R.J., Van Eynde, T., van Loosdrecht, M.C.M., Volcke, E.I.P., 2014. Effect of process design and operating parameters on aerobic methane oxidation in municipal WWTPs. Water Res. 66, 308–319.

Daigger, G.T.; Boltz, J.P., 2011. Trickling filter and trickling filter-Suspended Growth Process Design and Operation: A State-of-the-Art Review. Water Environ. Res. 83(5), 388-404.

Daims, H., Nielsen, J.L., Nielsen, P.H., Schleifer, K.-H., Wagner, M., 2001. In Situ Characterization ofNitrospira-Like Nitrite-Oxidizing Bacteria Active in Wastewater Treatment Plants. Appl. Environ. Microbiol. 67, 5273–5284.

De Cocker, P., Bessiere, Y., Hernandez-Raquet, G., Dubos, S., Mozo, I., Gaval, G., Caligaris, M., Barillon, B., Vlaeminck, S.E., Sperandio, M., 2018. Enrichment and

adaptation yield high anammox conversion rates under low temperatures. Bioresour. Technol. 250, 505–512.

De Kreuk, M.K., Picioreanu, C., Hosseini, M., Xavier, J.B., van Loosdrecht, M.C.M., 2007. Kinetic model of a granular sludge SBR: Influences on nutrient removal. Biotechnol. Bioeng. 97, 801–815.

Decru, S.O., Baeten, J.E., Cui, Y.X., Wu, D., Chen, G.H., Volcke, E.I.P., 2021. Model-based analysis of sulfur-based denitrification in a moving bed biofilm reactor. Environ. Technol. (United Kingdom) 0, 1–8.

Denecke, M., Liebig, T., 2003. Effect of carbon dioxide on nitrification rates. Bioprocess Biosyst. Eng. 25, 249–253.

Di Capua, F., Ahoranta, S.H., Papirio, S., Lens, P.N.L., Esposito, G., 2016. Impacts of sulfur source and temperature on sulfur-driven denitrification by pure and mixed cultures of Thiobacillus. Process Biochem. 51, 1576–1584.

Eberl, H., Morgenroth, E., Noguera, D., Picioreanu, C., Rittmann, B.E., van Loosdrecht, M.C.M., Wanner, O., 2006. Mathematical Modeling of Biofilms. IWA Publishing, London.

Egli, K., Bosshard, F., Werlen, C., Lais, P., Siegrist, H., Zehnder, A.J.B., Van Der Meer, J.R., 2003. Microbial composition and structure of a rotating biological contactor biofilm treating ammonium-rich wastewater without organic carbon. Microb. Ecol. 45, 419–432.

Ekama, G.A., Wentzel, M.C., van Loosdrecht, M.C.M., 2020. Nitrogen removal, in: Chen, G., Ekama, G.A., Loosdrecht, M.C.M. van, Brdjanovic, D. (Eds.), Biological Wastewater Treatment: Principles, Modelling and Design. IWA Publishing, London.

Ettwig, K.F., Butler, M.K., Le Paslier, D., Pelletier, E., Mangenot, S., Kuypers, M.M.M., Schreiber, F., Dutilh, B.E., Zedelius, J., de Beer, D., Gloerich, J., Wessels, H.J.C.T., van Alen, T., Luesken, F., Wu, M.L., van de Pas-Schoonen, K.T., Op den Camp, H.J.M., Janssen-Megens, E.M., Francoijs, K.-J., Stunnenberg, H., Weissenbach, J., Jetten, M.S.M., Strous, M., 2010. Nitrite-driven anaerobic methane oxidation by oxygenic bacteria. Nature 464, 543–548.

Fan, S.Q., Xie, G.J., Lu, Y., Liu, B.F., Xing, D.F., Ding, J., Han, H.J., Ren, N.Q., 2021. Nitrate/nitrite dependent anaerobic methane oxidation coupling with anammox in membrane biotrickling filter for nitrogen removal. Environ. Res. 193, 110533.

Fernandes, A.L., Pereira, A.D., Leal, C.D., Davenport, R., Werner, D., Filho, C.R.M., Bressani-Ribeiro, T., de Lemos Chernicharo, C.A., de Araújo, J.C., 2018. Effect of temperature on microbial diversity and nitrogen removal performance of an anammox reactor treating anaerobically pretreated municipal wastewater. Bioresour. Technol. 258, 208–219.

Fonseca, M.F., MSc Dissertation, 2009. Remoção de nitrogênio amoniacal em filtro biológico percolador pós-tratando efluente de reator UASB (Ammoniun-N removal in a trickling filter post-treating UASB reactor effluent). Universidade Federal do Rio de Janeiro. In Portuguese.

Foresti, E., Zaiat, M., Vallero, M., 2006. Anaerobic processes as the core technology for sustainable domestic wastewater treatment: Consolidated applications, new trends, perspectives, and challenges. Rev. Environ. Sci. Biotechnol. 5, 3-19.

Frade, E.C., MSc Dissertation, 2003. Concepção e Avaliação de Desempenho de um Sistema Compacto Reator UASB/Filtro Biológico Percolador Utilizado para o Tratamento de Esgotos Sanitário (Design and evaluation of a compact UASB/TF system for sewage treatment). Universidade Federal de Minas Gerais. In Portuguese.

Gilbert, E.M., Agrawal, S., Karst, S.M., Horn, H., Nielsen, P.H., Lackner, S., 2014. Low temperature partial nitritation/anammox in a moving bed biofilm reactor treating low strength wastewater. Environ. Sci. Technol. 48, 8784–8792.

Glória, R.M., Motta, T.M., Silva, P.V.O., Da Costa, P., Brandt, E.M.F., Souza, C.L., Chernicharo, C.A.L., 2016. Stripping and dissipation techniques for the removal of dissolved gases from anaerobic effluents. Brazilian J. Chem. Eng. 33, 713–721.

Gonçalves, R.F., Araújo,V.L.D., Chernicharo, C.A.L., 1998. Association of a UASB reactor and a submerged aerated biofilter for domestic sewage treatment. Water Sci. Technol. 38(8–9), 189-195.

Gonçalves, R.F., Chernicharo, C.A.L., Andrade Neto, C.O., Alem Sobrinho, P., Kato, M.T., Costa, R.H.R., Aisse, M.M., Zaiat, M., 2001. Pós-tratamento de efluentes de reatores anaeróbios por reatores com biofilme (Post-treatment of Anaerobic effluents with bioflim reactors). In: Chernicharo, C.A.L. (coordenador). Pós-tratamento de efluentes de reatores anaeróbios. FINEP/PROSAB, Rio de Janeiro, Brasil. In Portuguese.

Grady, C.P.L., Daigger, G.T., Lim, H.D., 1999. Biological Wastewater Treatment, 2ed, revised and expanded, Marcel Dekker, New York.

Gruber-Dorninger, C., Pester, M., Kitzinger, K., Savio, D.F., Loy, A., Rattei, T., Wagner, M., Daims, H., 2015. Functionally relevant diversity of closely related Nitrospira in activated sludge. ISME J. 9, 643–655.

Guerrero, R.B.S., Zaiat, M., 2018. Wastewater post-treatment for simultaneous ammonium removal and elemental sulfur recovery using a novel horizontal mixed aerobic-anoxic fixed-bed reactor configuration. J. Environ. Manage. 215, 358–365.

Guisasola, A., Petzet, S., Baeza, J.A., Carrera, J., Lafuente, J., 2007. Inorganic carbon limitations on nitrification: Experimental assessment and modelling. Water Res. 41, 277–286.

Guo, C.Q., Dong, B., Liu, J.J., Liu, F.P., 2015. The best indicator of hydraulic short-circuiting and mixing of constructed wetlands. Water Pract. Technol. 10, 505–516.

Hanson, R.S., Hanson, T.E., 1996. Methanotrophic bacteria. Microbiol. Rev. 60, 439–471.

Hao, X., Heijnen, J.J., van Loosdrecht, M.C.M., 2002. Sensitivity analysis of a biofilm model describing a one-stage completely autotrophic nitrogen removal (CANON) process. Biotechnol. Bioeng. 77, 266–277.

Hao, X. Di, van Loosdrecht, M.C.M., 2004. Model-based evaluation of COD influence on a partial nitrification-Anammox biofilm (CANON) process. Water Sci. Technol. 49, 83–90.

Hatamoto, M., Miyauchi, T., Kindaichi, T., Ozaki, N., Ohashi, A., 2011. Dissolved methane oxidation and competition for oxygen in down-flow hanging sponge reactor for post-treatment of anaerobic wastewater treatment. Bioresour. Technol. 102, 10299–10304.

Hatamoto, M., Sato, T., Nemoto, S., Yamaguchi, T., 2017. Cultivation of denitrifying anaerobic methane-oxidizing microorganisms in a continuous-flow sponge bioreactor. Appl. Microbiol. Biotechnol. 101, 5881–5888.

Hatamoto, M., Okubo, T., Kubota, K., Yamaguchi, T., 2018. Characterization of downflow hanging sponge reactors with regard to structure, process function, and microbial community compositions. Appl. Microbiol. Biotechnol. 102, 10345–10352.

Haynes, W.M., 2013. CRC handbook of chemistry and physics : a ready-reference book of chemical and physical data. / editor-in-chief, W. M. Haynes ; associate Editors David R. Lide, Thomas J. Bruno

He, Z., Cai, C., Geng, S., Lou, L., Xu, X., Zheng, P., Hu, B., 2013. Modelling a nitrite-dependent anaerobic methane oxidation process: Parameters identification and model evaluation. Bioresour. Technol. 147, 315–320.

Hellinga, C., van Loosdrecht, M.C.M., Heijnen, J.J., 1999. Model Based Design of a Novel Process for Nitrogen Removal from Concentrated Flows. Math. Comput. Model. Dyn. Syst. 5, 351–371.

Hendrickx, T.L.G., Temmink, H., Elissen, H.J.H., Buisman, C.J.N., 2009. The effect of operating conditions on aquatic worms eating waste sludge. Water Res. 43(4), 943-950.

Henze, M., Gujer, W., Mino, T., van Loosedrecht, M.C.M., 2006. Activated Sludge Models ASM1, ASM2, ASM2d and ASM3. IWA Publishing, London.

Henze, M., van Loosdrecht, M.C.M., Ekama, G.A., Brdjanovic, D., 2008. Biological Wastewater Treatment: Principles, Modelling and Design. IWA Publishing.

Hiatt, W.C., Grady, C.P.L., 2008. An Updated Process Model for Carbon Oxidation, Nitrification, and Denitrification. Water Environ. Res. 80, 2145–2156.

Hu, Z., Lotti, T., de Kreuk, M., Kleerebezem, R., van Loosdrecht, M., Kruit, J., Jetten, M.S.M., Kartal, B., 2013. Nitrogen removal by a nitritation-anammox bioreactor at low temperature. Appl. Environ. Microbiol. 79, 2807–2812.

Huang, J., Ji, M., Xie, Y., Wang, S., He, Y., Ran, J., 2016. Global semi-arid climate change over last 60 years. Clim. Dyn. 46, 1131–1150.

Hubaux, N., Wells, G., Morgenroth, E., 2015. Impact of coexistence of flocs and biofilm on performance of combined nitritation-anammox granular sludge reactors. Water Res. 68, 127–139.

Ikeda, N., Natori, T., Okubo, T., Sugo, A., Aoki, M., Kimura, M., Yamaguchi, T, Harada, H, Ohashi, A., Uemura, S., 2013. Enhancement of denitrification in a DHS reactor by effluent recirculation. Water Sci. Technol. 8(3), 591-598.

Janssen, A.J.H., Lens, P.N.L., Stams, A.J.M., Plugge, C.M., Sorokin, D.Y., Muyzer, G., Dijkman, H., Van Zessen, E., Luimes, P., Buisman, C.J.N., 2009. Application of bacteria involved in the biological sulfur cycle for paper mill effluent purification. Sci. Total Environ. 407, 1333–1343.

Jensen, H.S., Nielsen, A.H., Hvitved-Jacobsen, T., Vollertsen, J., 2009. Modeling of Hydrogen Sulfide Oxidation in Concrete Corrosion Products from Sewer Pipes. Water Environ. Res. 81, 365–373.

Jia, M., Solon, K., Vandeplassche, D., Venugopal, H., Volcke, E.I.P., 2020. Model-based evaluation of an integrated high-rate activated sludge and mainstream anammox system. Chem. Eng. J. 382, 122878.

Jiang, D., Khunjar, W.O., Wett, B., Murthy, S.N., Chandran, K., 2015. Characterizing the metabolic trade-off in Nitrosomonas europaea in response to changes in inorganic carbon supply. Environ. Sci. Technol. 49, 2523–2531.

Jing, C., Ping, Z., Mahmood, Q., 2010. Influence of various nitrogenous electron acceptors on the anaerobic sulfide oxidation. Bioresour. Technol. 101, 2931–2937.

Jordão, E.P., Pessoa, C.A., 2005. Tratamento de Esgotos Domésticos (Domestic sewage treatment). 4ª. ed., Rio de Janeiro: Associação Brasileira de Engenharia Sanitária – ABES. In Portuguese.

Kassab, G., Halalsheh, M., Klapwijk, A., Fayyad, M., van Lier, J.B., 2010. Sequential anaerobic-aerobic treatment for domestic wastewater - a review. Bioresour. Technol. 101(10), 3299-310.

Khan, A. A., Gaur, R.Z., Tyagi, V.K., Khursheed, A., Lew, B., Mehrotra, I., Kazmi, A.A., 2011. Sustainable options of post-treatment of UASB effluent treating sewage: A review. Resources, Conservation and Recycling 55(12), 1232-1251.

Kimura, Y., Isaka, K., Kazama, F., 2011. Effects of inorganic carbon limitation on anaerobic ammonium oxidation (anammox) activity. Bioresour. Technol. 102, 4390–4394.

Kubota, K., Hayashi, M., Matsunaga, K., Iguchi, A., Ohashi, A, LI, Y., Yamaguchi, T., Harada, H., 2014. Microbial community composition of a down-flow hanging sponge (DHS) reactor combined with an up-flow anaerobic sludge blanket (UASB) reactor for the treatment of municipal sewage. Bioresour Technol. 151, 144-150.

Laureni, M., Weissbrodt, D.G., Villez, K., Robin, O., de Jonge, N., Rosenthal, A., Wells, G., Nielsen, J.L., Morgenroth, E., Joss, A., 2019. Biomass segregation between biofilm and flocs improves the control of nitrite-oxidizing bacteria in mainstream partial nitritation and anammox processes. Water Res. 154, 104–116.

Leal, C.D., Pereira, A.D., Nunes, F.T., Ferreira, L.O., Coelho, A.C., Bicalho, S.K., Mac Conell, E.F.A., Bressani-Ribeiro, T., Chernicharo, C.A.L., Araújo, J.C., 2016. Anammox for nitrogen removal from anaerobically pre-treated municipal wastewater: Effect of COD/N ratios on process performance and bacterial community structure. Bioresour Technol. 211, 257-266.

Liu, T., Guo, J., Hu, S., Yuan, Z., 2020. Model-based investigation of membrane biofilm reactors coupling anammox with nitrite/nitrate-dependent anaerobic methane oxidation. Environ. Int. 137, 105501.

Lobato, L.C.S, Cardoso, L.C., Divino, M.G., Silva, H., Chernicharo, C.A.L., 2011. Influência da rotina operacional de descarte do lodo excedente de reatores UASB na qualidade do efluente de uma estação de tratamento de esgoto (Influence of operational routine of excess UASB sludge discharge on effluent quality). In: Proceedings of 26º Congresso Brasileiro de Engenharia Sanitária e Ambiental. ABES, Porto Alegre - RS. In Portuguese.

Lobato, L.C.S., Chernicharo, C.A.L., Souza, C.L., 2012. Estimates of methane loss and energy recovery potential in anaerobic reactors treating domestic wastewater. Water Sci. Technol. 66, 2745–2753.

Logan, B.E., 1993. Oxygen Transfer in Trickling Filters. J. Environ. Eng. 119, 1059–1076.

Lücker, S., Schwarz, J., Gruber-Dorninger, C., Spieck, E., Wagner, M., Daims, H., 2015. Nitrotoga-like bacteria are previously unrecognized key nitrite oxidizers in full-scale wastewater treatment plants. ISME J. 9, 708–720.

Ma, Y., Sundar, S., Park, H., Chandran, K., 2015. The effect of inorganic carbon on microbial interactions in a biofilm nitritation-anammox process. Water Res. 70, 246–254.

Mac Conell, E.F., Almeida, P.G.S., Zerbini, A.M., Brandt, E.M.F., Araújo, J.C., Chernicharo, C.A.L., 2013. Diversity and dynamics of ammonia-oxidizing bacterial communities in a sponge-based trickling filter treating effluent from a UASB reactor. Water Sci. Technol. 68(3), 650-657.

Mac Conell, E.F.A., Almeida, P.G.S., Martins, K.E L., Araújo, J.C, Chernicharo, C.A.L., 2015. Bacterial community involved in the nitrogen cycle in a down-flow sponge-based trickling filter treating UASB effluent. Water Sci. Technol. 72(1), 116-122.

Machdar, I., Harada, H., Ohashi, A., Sekiguchi, Y., Okui, H., Ueki, K., 1997. A novel and cost-effective sewage treatment system consisting of UASB pre-treatment and aerobic post-treatment units for developing countries. Water Science and Technology 36(12), 189-197.

Machdar, I., Harada, H, Ohashi, A., Sekiguchi, Y., Okui, H., Ueki, K., 2000. Combination of UASB reactor and curtains type DHS (downflow hanging sponge) reactor as a cost effective sewage treatment system for developing countries.

Water Sci. Technol. 42(3-4), 83-88.
Madigan, M., Clark, D., Stah, D., Martinko, J., 2011. Brock biology of microorganisms, 13th ed. San Francisco. Benjamin Cummings.
Mahmoud, M., Tawfik, A., El-Gohary, F., 2010. Simultaneous organic and nutrient removal in a naturally ventilated biotower treating pre-settled municipal wastewater. J. Environ. Eng. 136, 301-307.
Mahmoud, M., Tawfik, A., El-Gohary, F., 2011. Use of down-flow hanging sponge (DHS) reactor as a promising post-treatment system for municipal wastewater. Chem. Eng. J., 2011, 168, 535–543.
Matsuura, N., Hatamoto, M., Sumino, H., Syutsubo, K., Yamaguchi, T., Ohashi, A., 2015. Recovery and biological oxidation of dissolved methane in effluent from UASB treatment of municipal sewage using a two-stage closed downflow hanging sponge system. J. Environ. Manage. 151, 200–209.
Mburu, N., Rousseau, D.P.L., Stein, O.R., Lens, P.N.L., 2014. Simulation of batch-operated experimental wetland mesocosms in AQUASIM bio ilm reactor compartment. J. Environ. Manage. 134, 100–108.
Mellbye, B.L., Giguere, A., Chaplen, F., Bottomley, P.J., Sayavedra-Soto, L.A., 2016. Steady-state growth under inorganic carbon limitation conditions increases energy consumption for maintenance and enhances nitrous oxide production in Nitrosomonas europaea. Appl. Environ. Microbiol. 82, 3310–3318.
Metcalf & Eddy, I., 2013. Wastewater engineering: treatment and reuse. 5th ed. New York, NY: McGraw-Hill.
Mohammadi, S.S., Pol, A., van Alen, T., Jetten, M.S.M., Op den Camp, H.J.M., 2017. Ammonia oxidation and nitrite reduction in the Verrucomicrobial Methanotroph *Methylacidiphilum fumariolicum* SolV. Front. microbiol., 8, 1901.
Moon, C., Lee, E.Y., Park, S., 2010. Biodegradation of gas-phase styrene in a high-performance biotrickling filter using porous polyurethane foam as a packing medium. Biotechnol. Bioprocess Eng. 15, 512–519.
Mora, M., Fernández, M., Manuel Gómez, J., Cantero, D., Lafuente, J., Gamisans, X., Gabriel, D., 2015. Kinetic and stoichiometric characterization of anoxic sulfide oxidation by SO-NR mixed cultures from anoxic biotrickling filters. Appl. Microbiol. Biotechnol. 99, 77–87.
Mora, M., López, L.R., Lafuente, J., Pérez, J., Kleerebezem, R., van Loosdrecht, M.C.M., Gamisans, X., Gabriel, D., 2016. Respirometric characterization of aerobic sulfide, thiosulfate and elemental sulfur oxidation by S-oxidizing biomass. Water Res. 89, 282–292.
Moraes, O.J.S., Souza, J.R., Silva, L.R., Azevedo, S.G., Chernicharo, C.A.L., Lobato, L.C.S., Silva, R.V., 2011. Long term performance of the largest Brazilian combined anaerobic/aerobic treatment plant (PE = 1 million inhabitants). In: Proceedings of the X DAAL - Latin American Workshop and Symposium on Anaerobic Digestion. Ouro Preto.
Morais, N.W.S., Santos, A.B., 2019. Análise dos padrões de lançamento de efluentes em corpos hídricos e de reúso de águas residuárias de diversos estados do Brasil. Rev. DAE 67, 40–55. In Portuguese.
Moran, M.J., Shapiro, H.N., Boettner, D.D., Bailey, M.B., 2014. Fundamentals of Engineering Thermodynamics, 8th ed. Wiley, New Jersey.
Mozumder, M.S.I., Picioreanu, C., van Loosdrecht, M.C.M., Volcke, E.I.P., 2014. Effect of heterotrophic growth on autotrophic nitrogen removal in a granular sludge reactor. Environ. Technol. (United Kingdom) 35, 1027–1037.
Muller, A., Wentzel, M.C., Loewenthal, R.E., Ekama, G.A., 2003. Heterotroph anoxic

yield in anoxic aerobic activated sludge systems treating municipal wastewater. Water Res. 37, 2435–2441.

Nash, J.E., Sutcliffe, J. V., 1970. River flow forecasting through conceptual models part I - A discussion of principles. J. Hydrol. 10, 282–290.

Ni, S.Q., Zhang, J., 2013. Anaerobic ammonium oxidation: From laboratory to full-scale application. Biomed Res. Int. 2013.

Nielsen, A.H., Vollertsen, J., Hvitved-Jacobsen, T., 2006. Kinetics and Stoichiometry of Aerobic Sulfide Oxidation in Wastewater from Sewers—Effects of pH and Temperature. Water Environ. Res. 78, 275–283.

Nomoto, N., Hatamoto, M., Hirakata, Y., Ali, M., Jayaswal, K., Iguchi, A., Okubo, T., Takahashi, M., Kubota, K., Tagawa, T., Uemura, S., Yamaguchi, T., Harada, H., 2018. Defining microbial community composition and seasonal variation in a sewage treatment plant in India using a down-flow hanging sponge reactor. Appl. Microbiol. Biotechnol. 102, 4381–4392.

Okubo, T., Onodera, T., Uemura, S., Yamaguchi, T., Ohashi, A., Harada, H., 2015 On-site evaluation of the performance of a full-scale down-flow hanging sponge reactor as a post-treatment process of an up-flow anaerobic sludge blanket reactor for treating sewage in India. Bioresour. Technol. 194, 156-164.

Okubo, T., Kubota, K., Yamaguchi, T., Uemura, S., Harada, H., 2016. Development of a new non-aeration-based sewage treatment technology: Performance evaluation of a full-scale down-flow hanging sponge reactor employing third-generation sponge carriers. Water Res. 102, 138-146.

Onodera, T., Matsunaga, K., Kubota, K., Taniguchi, R., Harada, H., Syutsubo, K., Okubo, T., Uemura, S., Araki, N., Yamada, M., Yamauchi, M., Yamaguchi, T., 2013. Characterization of the retained sludge in a down-flow hanging sponge (DHS) reactor with emphasis on its low excess sludge production. Bioresour. Technol. 136, 169–175.

Onodera, T., Tandukar, M., Sugiyana, D., Uemura, S., Ohashi, A., Harada, H., 2014. Development of a sixth-generation down-flow hanging sponge (DHS) reactor using rigid sponge media for post-treatment of UASB treating municipal sewage. Bioresour. Technol. 152, 93–100.

Onodera, T., Syutsubo, K., Yoochatchaval, W., Sumino, H., Mizuochi, M., Harada, H., 2015. Protection of biomass from snail overgrazing in a trickling filter using sponge media as a biomass carrier: down-flow hanging sponge system. Water Sci. Technol. 71(4), 518-523.

Onodera, T., Okubo, T., Uemura, S., Yamaguchi, T., Ohashi, A., Harada, H., 2016. Long-term performance evaluation of down-flow hanging sponge reactor regarding nitrification in a full-scale experiment in India. Bioresour. Technol. 204, 177–184.

Passos, R.G., Dias, D.F.C., von Sperling, M., 2020. Simple mid-depth transverse baffles to improve bacterial disinfection in a shallow maturation pond–performance evaluation and CFD simulation. Environ. Technol. (United Kingdom) 0, 1–9.

Pearce, P., Jarvis, S., 2011. Operational experiences with structured plastic media filters: 10 years on. Water Environ. J. 25(2), 200-207.

Pérez, J., Laureni, M., van Loosdrecht, M.C.M., Persson, F., Gustavsson, D.J.I., 2020. The role of the external mass transfer resistance in nitrite oxidizing bacteria repression in biofilm-based partial nitritation/anammox reactors. Water Res. 186.

Pérez, J., Lotti, T., Kleerebezem, R., Picioreanu, C., van Loosdrecht, M.C.M., 2014. Outcompeting nitrite-oxidizing bacteria in single-stage nitrogen removal in sewage treatment plants: A model-based study. Water Res. 66, 208–218.

Perry, R.H., Chilton, C., 1973. Chemical engineers' handbook. NY: McGraw-Hill.

Petropoulos E., Dolfing J., Davenport R.J., Bowen E.J., Curtis T.P., 2017. Developing cold-adapted biomass for the anaerobic treatment of domestic wastewater at low temperatures (4, 8 and 15°C) with inocula from cold environments. Water Res.112, 100-109.

Picioreanu, C., van Loosdrecht, M.C.M., Heijnen, J.J., 1997. Modelling the effect of oxygen concentration on nitrite accumulation in a biofilm airlift suspension reactor. Water Sci. Technol. 36(1), 147-156.

Plas, C., Harant, H., Danner, H., Jelinek, E., Wimmer, K., Holubar, P., Braun, R., 1992. Ratio of biological and chemical oxidation during the aerobic elimination of sulphide by colourless sulphur bacteria. Appl. Microbiol. Biotechnol. 36, 817–822.

Pokorna-Krayzelova, L., Vejmelková, D., Selan, L., Jenicek, P., Volcke, E.I.P., Bartacek, J., 2018. Final products and kinetics of biochemical and chemical sulfide oxidation under microaerobic conditions. Water Sci. Technol., 78, 1916–1924.

Pontes, P.P., Chernicharo, C.A.L., 2011. Characterization and removal of specific organic constituents in an UASB-trickling filter system treating domestic wastewater. Environ. Technol. 32(3), 281-287.

Possetti, G.R.C., Rietow, J.C., Cabral, C.B.G., Moreira, H.C., Platzer, C., Bressani-Ribeiro, T., Chernicharo, C.A.L., 2019. Energy recovery from biogas in UASB reactors treating sewage, in: Chernicharo, C.A.L., Bressani-Ribeiro, T. (Eds.), Anaerobic Reactors for Sewage Treatment: Design, Construction and Operation. IWA Publishing, London.

Preisner, M., Neverova-Dziopak, E., Kowalewski, Z., 2020. An Analytical Review of Different Approaches to Wastewater Discharge Standards with Particular Emphasis on Nutrients. Environ. Manage. 66, 694–708.

Regmi, P., Miller, M.W., Holgate, B., Bunce, R., Park, H., Chandran, K., Wett, B., Murthy, S., Bott, C.B., 2014. Control of aeration, aerobic SRT and COD input for mainstream nitritation/denitritation. Water Res. 57, 162–171.

Reichert, P., 1995. Design techniques of a computer program for the identification of processes and the simulation of water quality in aquatic systems. Environ. Softw. 10, 199–210.

Ren, Y.-X., Yang, L., Liang, X., 2014. The characteristics of a novel heterotrophic nitrifying and aerobic denitrifying bacterium, Acinetobacter junii YB. Bioresour. Technol. 171, 1–9.

Rieger, L., Gillot, S., Langergraber, G., Ohtsuki, T., Shaw, A., Tak´cs, I., Winkler, S., 2012. Guidelines for Using Activated Sludge Models. IWA Publishing, London.

Rittmann, B.E., McCarty, P.L., 2001. Environmental Biotechnology: Principles and Applications. McGraw-Hill Professional, Boston.

Robarge, W.P., Edwards, A., Johnson, B., 1983. Water and wastewater analysis for nitrate via nitration of salicylic acid. Commun. Soil Sci. Plant Anal. 14, 1207–1215.

Sánchez-Guillén J.A., Guardado, P.R.C., Vazquez, C.M.L., Cruz L.C.M., Brdjanovic D., van Lier, J.B., 2015a. Anammox cultivation in a closed sponge-bed trickling filter. Bioresour. Technol. 186, 252-260.

Sánchez-Guillén, J.A., Jayawardana, L.K.M.C.B., Lopez Vazquez, C.M., Oliveira Cruz, L.M., Brdjanovic, D., van Lier, J.B., 2015b. Autotrophic nitrogen removal over nitrite in a sponge-bed trickling filter. Bioresource Technol. 187, 314-325.

Sander, R., 2015. Compilation of Henry's law constants (version 4.0) for water as solvent. Atmos. Chem. Phys. 15, 4399–4981.

Seuntjens, D., Han, M., Kerckhof, F.-M., Boon, N., Al-Omari, A., Takacs, I., Meerburg, F., De Mulder, C., Wett, B., Bott, C., Murthy, S., Carvajal Arroyo, J.M., De

Clippeleir, H., Vlaeminck, S.E., 2018. Pinpointing wastewater and process parameters controlling the AOB to NOB activity ratio in sewage treatment plants. Water Res. 138, 37–46.

Siegrist, H., Gujer, W.,1987. Demonstration of mass transfer and pH effects in a nitrifying biofilm. Water Res. 21, 1481–1487.

Silva-Teira, A., Sánchez, A., Buntner, D., Rodríguez-Hernández, L., Garrido, J.M. 2017. Removal of dissolved methane and nitrogen from anaerobically treated effluents at low temperature by MBR post-treatment. Chem. Eng. J. 326, 970–979.

Sin, G., Kaelin, D., Kampschreur, M.J., Takács, I., Wett, B., Gernaey, K. V., Rieger, L., Siegrist, H., van Loosdrecht, M.C.M., 2008. Modelling nitrite in wastewater treatment systems: A discussion of different modelling concepts. Water Sci. Technol. 58, 1155–1171.

SNIS - Sistema Nacional de Informações sobre Saneamento: Diagnóstico dos Serviços de Água e Esgotos – 2018 (Diagnosis of water and sanitation services – 2018), http://www.snis.gov.br/diagnostico-anual-agua-e-esgotos/diagnostico-dos-servicos-de-agua-e-esgotos-2018 (accessed 12.5.19). In Portuguese.

Souza, C.L., Chernicharo, C.A.L., Aquino, S.F., 2011. Quantification of dissolved methane in UASB reactors treating domestic wastewater under different operating conditions. Water Sci. Technol. 64, 2259–2264.

Souza, C.L., Chernicharo, C.A.L., Melo, G.C.B., 2012. Methane and hydrogen sulfide emissions in UASB reactors treating domestic wastewater. Water Sci. Technol. 65, 1229–1237.

Stein, L.Y., Klotz, M.G., 2011. Nitrifying and denitrifying pathways of methanotrophic bacteria. Biochem. Soc. Trans. 39, 1826–1831.

Steudel, R., 1996. Mechanism for the Formation of Elemental Sulfur from Aqueous Sulfide in Chemical and Microbiological Desulfurization Processes. Ind. Eng. Chem. Res. 35, 1417–1423.

Strous, M., Heijnen, J.J., Kuenen, J.G., Jetten, M.S.M., 1998. The sequencing batch reactor as a powerful tool for the study of slowly growing anaerobic ammonium-oxidizing microorganisms. Appl. Microbiol. Biotechnol. 50, 589–596.

Stumm, W., Morgan, J.J., 1996. Aquatic chemistry. Environmental science and technology.Wiley-Interscience.

Sun, J., Dai, X., Liu, Y., Peng, L., Ni, B.J., 2017a. Sulfide removal and sulfur production in a membrane aerated biofilm reactor: Model evaluation. Chem. Eng. J. 309, 454–462.

Sun, Y., Guan, Y., Pan, M., Zhan, X., Hu, Z., Wu, G., 2017b. Enhanced biological nitrogen removal and N_2O emission characteristics of the intermittent aeration activated sludge process. Rev. Environ. Sci. Biotechnol. 16, 761–780.

Sun, Z., Pang, B., Xi, J., Hu, H.Y., 2019. Screening and characterization of mixotrophic sulfide oxidizing bacteria for odorous surface water bioremediation. Bioresour. Technol. 290, 121721.

Takahashi, M., Ohya, A., Kawakami, S., Yoneyama, Y., Onodera, T., Syutsubo, K., Yamazaki, S., Araki, N., Ohashi, A., Harada, H., Yamaguchi, T., 2011. Evaluation of treatment characteristics and sludge properties in a UASB reactor treating municipal sewage at ambient temperature. Int. J. Environ. Res. 5(4), 821-826.

Tanaka, H., Takahashi, M., Yoneyama, Y., Syutsubo, K., Kato, K., Nagano, A., Yamaguchi, T., Harada, H., 2012. Energy saving system with high effluent quality for municipal sewage treatment by UASB–DHS. Water Sci. Technol. 66(6), 1186-1194.

Tandukar, M., Uemura, S., Machdar, I., Ohashi, A., Harada, H., 2005. A low-cost

municipal sewage treatment system with a combination of UASB and the “fourth-generation” downflow hanging sponge reactors. Water Sci. Technol. 52(1-2), 323-329.

Tandukar, M., Machdar, I., Uemura, S., Ohashi, A., Harada, H., 2006a. Potential of a Combination of UASB and DHS Reactors a Novel Sewage Treatment System for Developing Countries: Long-Term Evaluation. Water Sci Technol. 53(3), 209-218.

Tandukar, M., Uemura, S., Ohashi, A., Harada, H., 2006b. Combining UASB and the “fourth generation” down-flow hanging sponge reactor for municipal wastewater treatment. J. Environ. Eng. 132(2), 166-172.

Tandukar, M., Ohashi, A., Harada, H., 2007. Performance comparison of a pilot-scale UASB and DHS system and activated sludge process for the treatment of municipal wastewater. Water Res. 41(12), 2697-705.

Tanikawa, D., Yamashita, S., Kataoka, T., Sonaka, H., Hirakata, Y., Hatamoto, M., Yamaguchi, T., 2019. Non-aerated single-stage nitrogen removal using a down-flow hanging sponge reactor as post-treatment for nitrogen-rich wastewater treatment. Chemosphere 233, 645–651.

Tawfik, A., El-Gohary, F., Ohashi, A., Harada, H., 2006a. The influence of physical–chemical and biological factors on the removal of faecal coliform through down-flow hanging sponge (DHS) system treating UASB reactor effluent. Water Res. 40, 1877-1883.

Tawfik, A., Ohashi, A., Harada, H., 2006b. Sewage treatment in a combined up-flow anaerobic sludge blanket (UASB)-down-flow hanging sponge (DHS) system. Biochem. Eng. J. 29, 210–219.

Tawfik, A., Ohashi, A., Harada, H., 2008. Effect of sponge volume on the performance of down-flow hanging sponge system treating UASB reactor effluent. Water Sci Technol. 58(1), 185-194.

Tawfik, A., El-Gohary, F., Ohashi, A., Harada, H., 2010. Optimization of the performance of an integrated anaerobic–aerobic system for domestic wastewater treatment. Bioprocess Biosyst Eng 33, 779-785.

Tawfik, A., Wahab, R.A., Al-Asmer, A., Matary, F., 2011. Effect of hydraulic retention time on the performance of down-flow hanging sponge system treating grey wastewater. Bioprocess Biosyst Eng. 34, 767-776.

Teixeira, E.C., do Nascimento Siqueira, R., 2008. Performance Assessment of Hydraulic Efficiency Indexes. J. Environ. Eng. 134, 851–859.

Trojanowicz, K., Plaza, E., Trela, J., 2019. Model extension, calibration and validation of partial nitritation–anammox process in moving bed biofilm reactor (MBBR) for reject and mainstream wastewater. Environ. Technol. 40, 1079–1100.

Uemura S., Harada, H., 2010. Application of UASB technology for sewage treatment with a novel post-treatment process. In: (eds.) Fang, H.H.P. Environmental Anaerobic Technology; Applications and New Developments. Imperial College Press, Londres.

Uemura S., Suzuki, S., Matuyama, Y., Harada, H., 2012. Direct treatment of settled sewage by DHS reactors with different sizes of sponge support media. Int. J. Environ. Res. 6(1), 25-32.

Uemura, S., Okubo, T., Maeno, Takahashi, M., Kubota, K., Harada, H., 2016. Evaluation of Water Distribution and Oxygen Mass Transfer in Sponge Support Media for a Down-flow Hanging Sponge Reactor. Int. J. Environ. Res 10, 265–272.

UNEP, 2016. A Snapshot of the World ’ s Water Quality : Towards a global assessment, United Nations Environment Programme.

United Nations, 2021. The United Nations World Water Development Report 2021:

Valuing Water. UNESCO, Paris.
van Bodegom, P., Stams, F., Mollema, L., Boeke, S., Leffelaar, P., 2001. Methane Oxidation and the Competition for Oxygen in the Rice Rhizosphere. Appl. Environ. Microbiol. 67, 3586–3597.
van den Hove, A., Baeten, J.E., Decru, S.O., Volcke, E.I.P., 2020. Potential of sulfide-based denitrification for municipal wastewater treatment. J. Water Process Eng., 35, 101206.
van der Star, W.R.L., Abma, W.R., Blommers, D., Mulder, J.W., Tokutomi, T., Strous, M., Picioreanu, C., van Loosdrecht, M.C.M., 2007. Startup of reactors for anoxic ammonium oxidation: Experiences from the first full-scale anammox reactor in Rotterdam. Water Res. 41, 4149–4163.
van Loosdrecht, Mark C.M.; Henze, M., 1999. Maintenance, endogeneous respiration, lysis, decay and predation. Water Sci. Technol. 39(1), 107-117.
Vannecke, T.P.W., Volcke, E.I.P., 2015. Modelling microbial competition in nitrifying biofilm reactors. Biotechnol. Bioeng. 112, 2550–2561.
Venard, J.K., Street, R.L.,1975. Elementary Fluid Mechanics, 5th ed. ed. Wiley, New York.
Victoria, J.A.R., PhD Thesis, 2006. Filtro biológico aeróbio-anóxico para remoção de nitrogênio de efluentes de reatores UASB (Aerobic-anoxic biofilter for nitrogen removal from UASB reactor effluents). Universidade de São Paulo. In Portuguese.
Vieira, P.C., von Sperling, M., 2012. Open trickling filter: An innovative, cheap and simple form of post-treatment of sanitary effluents from anaerobic reactors in small communities. J. Water Sanit. Hyg. Dev. 2, 59–67.
Vieira, P.C., PhD Thesis, 2013. Estudo do comportamento de um filtro biologico percolador com laterais abertas aplicado ao pós-tratamento de efluente de reator UASB (Study of the behavior of a trickling filter with open walls applied to the post-treatment of UASB reactor effluent). Universidade Federal de Minas Gerais, Belo Horizonte, 2013. In Portuguese.
Volcke, E.I.P., van Loosdrecht, M.C.M.,Vanrolleghem, P.A., 2010. Continuity-based model interfacing for plant-wide simulation: a general approach. Water Res. 40, 2817-2828.
Volcke, E.I.P., Picioreanu, C., de Baets, B., van Loosdrecht, M.C.M., 2010. Effect of granule size on autotrophic nitrogen removal in a granular sludge reactor. Environ. Technol. 31, 1271–1280.
von Sperling, M., Chernicharo, C.A.L. 2005. Biological Wastewater Treatment in Warm Climate Regions. IWA Publishing, London.
von Sperling, M., Almeida, P.G.S., Bressani-Ribeiro, T., Chernicharo, C.A.L. 2019. Post-treatment of anaerobic effluents, in: Chernicharo, C.A.L., Bressani-Ribeiro, T. (Eds.), Anaerobic Reactors for Sewage Treatment: Design, Construction and Operation. IWA Publishing, London.
Wan, X., Baeten, J.E., Volcke, E.I.P., 2019. Effect of operating conditions on N2O emissions from one-stage partial nitritation-anammox reactors. Biochem. Eng. J. 143, 24–33.
Wan, X., Laureni, M., Jia, M., Volcke, E.I.P., 2021. Impact of organics, aeration and flocs on N2O emissions during granular-based partial nitritation-anammox. Sci. Total Environ. 797, 149092.
Wang, W., Wang, Y., Wang, X., Zhang, Y., Yan, Y., 2019. Dissolved oxygen microelectrode measurements to develop a more sophisticated intermittent aeration regime control strategy for biofilm-based CANON systems. Chem. Eng. J. 365, 165–174.

Wang, Z., Zheng, M., Hu, Z., Duan, H., De Clippeleir, H., Al-Omari, A., Hu, S., Yuan, Z., 2021. Unravelling adaptation of nitrite-oxidizing bacteria in mainstream PN/A process: Mechanisms and counter-strategies. Water Res. 200, 117239.

Watari, T., Vazquez, C.L., Hatamoto, M., Yamaguchi, T., van Lier, J.B., 2020. Development of a single-stage mainstream anammox process using a sponge-bed trickling filter. Environ. Technol. 1–12.

WEF, Water Environment Federation, 1992. Design of Municipal Wastewater Treatment Plants (WEF manual of practice). American Society of Civil Engineers.

WEF, Water Environment Federation, 1996. Operation of municipal wastewater treatment plants. Manual of Practice nº 11. Alexandria, VA.: Water Environment Federation.

WEF, Water Environment Federation, 2000. Aerobic Fixed-Growth Reactors: a special publication. Alexandria, VA.: Water Environment Federation.

WEF, Water Environment Federation, 2010. Design of Municipal Wastewater Treatment Plants (WEF Manual of Practice Nº. 8: ASCE Manuals and Reports on Engineering Practice Nº. 76), 5th ed. McGraw-Hill Education.

Wei, X., Yan, T., Hommes, N.G., Liu, X., Wu, L., McAlvin, C., Klotz, M.G., Sayavedra-Soto, L.A., Zhou, J., Arp, D.J., 2006. Transcript profiles of Nitrosomonas europaea during growth and upon deprivation of ammonia and carbonate. FEMS Microbiol. Lett. 257, 76–83.

Wett, B., Rauch, W., 2003. The role of inorganic carbon limitation in biological nitrogen removal of extremely ammonia concentrated wastewater. Water Res. 37, 1100–1110.

Wiesmann, U., 1994. Biological nitrogen removal from wastewater. Adv Biochem Eng Biotechnol. 51,113-54.

Wik, T., 2003. Trickling filters and biofilm reactor modelling. Rev. Environ. Sci. Biotechnol. 2, 193–212.

Williamson, K., McCarty, P.L., 1976. Verification studies of the biofilm model for bacterial substrate utilization. J. Water Pollut. Control Fed. 48, 281–296.

Winkler, M.K.H., Ettwig, K.F., Vannecke, T.P.W., Stultiens, K., Bogdan, A., Kartal, B., Volcke, E.I.P., 2015. Modelling simultaneous anaerobic methane and ammonium removal in a granular sludge reactor. Water Res. 73, 323–331.

Xu, X., Chen, C., Lee, D.J., Wang, A., Guo, W., Zhou, X., Guo, H., Yuan, Y., Ren, N., Chang, J.S., 2013. Sulfate-reduction, sulfide-oxidation and elemental sulfur bioreduction process: Modeling and experimental validation. Bioresour. Technol. 147, 202–211.

Yoochatchaval, W., Onodera, T., Sumino, H., Yamaguchi, T., Mizuochi, M., Okadera, T, Syutsubo., 2014. Development of a down-flow hanging sponge reactor for the treatment of low strength sewage. Water Sci. Technol. 70(4), 656-663.

Zeng, H., Zhang, T.C., 2005. Evaluation of kinetic parameters of a sulfur–limestone autotrophic denitrification biofilm process. Water Res. 39, 4941–4952.

Zhang, T.C., Bishop, P.L., 1996. Evaluation of substrate and pH effects in a nitrifying biofilm. Water Environ. Res. 68, 1107–1115.

Zhang, X., Yu, B., Zhang, N., Zhang, Haojing, Wang, C., Zhang, Hongzhong., 2016. Effect of inorganic carbon on nitrogen removal and microbial communities of CANON process in a membrane bioreactor. Bioresour. Technol. 202, 113–118.